**DOCTOR OF PHILOSOPHY**

**Mechanism underlying linkage-selective polyubiquitin recognition**

Kristariyanto, Yosua Adi

*Award date:*
2017

[Link to publication](#)

# Mechanism underlying linkage-selective polyubiquitin recognition

## Yosua Adi Kristariyanto

A thesis submitted for the degree of Doctor of Philosophy

MRC Protein Phosphorylation and Ubiquitylation Unit

University of Dundee

January 2017

# Declaration

I hereby declare that the following thesis is based on the results of investigations conducted by myself, and that this thesis is of my own composition. Work other than my own is clearly indicated in the text by reference to the researchers or their publications. This thesis has not in whole or in part been previously presented for a higher degree.

Yosua Adi Kristariyanto

I certify that Yosua Adi Kristariyanto has spent the equivalent of at least nine terms in research work in the School of Life Sciences, University of Dundee and that he has fulfilled the conditions of the Ordinance General No. 14 of the University of Dundee and is qualified to submit the accompanying thesis in application for the degree of Doctor of Philosophy.

Dr Yogesh Kulathu

*"Rarely affirm, seldom deny, always distinguish"*

*Thomas Aquinas*

# Acknowledgement

Three and a half years went into the making of this thesis. During this time, I received countless help and supports from various individuals without whom I would not be able to compose this work. First and foremost, I would like to thank my mentor and PhD supervisor, Dr Yogesh Kulathu for getting me so deep in love with Ubiquitin research and for constantly challenging me to ask the right questions and to look at the bigger picture. I would also like to thank Dr Syed Arif Abdul Rehman for all of his help and expertise in the crystallisation projects. I am so blessed and honoured to be able to work alongside with him in so many projects. I would like to thank my thesis committee, Professor John Rouse and Professor Anton Gartner, for their constant support and advice on my projects as well as my future career. I am greatly in debt towards all members of DSTT. In particular, Dr Simone Weidlich and Dr Rachel Toth for generating DNA clones used in this study and Mark Dorward for taking care of crystallisation screens. I am thankful for Dr Axel Knebel, Clare Johnson and Dr Richard Ewan for milligrams of Ub and purified enzymes, as well as constructive discussion about protein purification. I would also like to thank Dr Ruben Julio Martínez-Torres, Teresa Cardote and Dr Carles Galdeano for guidance and help with ITC experiments. I thank Dr David Campbell and Dr Nicolas Morrice for PRM analyses. I thank Dr Satpal Virdee and Dr Mathew Stanley for discussion about enzyme kinetics and polyubiquitin chain assembly. I would not be able to complete my PhD without the technical supports from Alison Bridges, Hannah Kendall, Judith Hare, Rachel Naismith and Alison Hart. I would like to thank all members of Kulathu laboratory: Soo, Pawel, Arif, Jay, Dominika, Sven, Marjorie, Steve and Deepika as well as the past members: Lambert and Bret. Thank you for making work in the lab fun and productive! Special thanks to Arif and Marjorie who read my thesis in detail and suggest constructive feedbacks.

# Table of Contents

# List of Figures

# List of Tables

# List of Publications

**Kristariyanto Y.A.**, Abdul Rehman S.A., Weidlich S., Knebel A., and Kulathu Y. (2016) A single MIU motif of MINDY-1 recognizes K48-linked polyubiquitin chains. EMBO Rep. EMBO Rep. 18: 392–402

Huguenin-Dezot N., De Cesare V., Peltier J., Knebel A., **Kristariyanto Y.A.**, Rogerson D.T., Kulathu Y., Trost M., and Chin J.W. (2016) Synthesis of Isomeric Phosphoubiquitin Chains Reveals that Phosphorylation Controls Deubiquitinase Activity and Specificity. Cell Rep *16*: 1180–1193

Abdul Rehman S.A.*, **Kristariyanto Y.A.***, Choi S.Y.*, Nkosi P.J., Weidlich S., Labib K., Hofmann K., and Kulathu Y. (2016) MINDY-1 Is a Member of an Evolutionarily Conserved and Structurally Distinct New Family of Deubiquitinating Enzymes. Mol Cell *63*: 146–155
* Co-first author

**Kristariyanto Y.A.**, Abdul Rehman S.A., Campbell D.G., Morrice N.A., Johnson C., Toth R., and Kulathu Y. (2015) K29-selective ubiquitin binding domain reveals structural basis of specificity and heterotypic nature of K29 polyubiquitin. Mol Cell *58*: 83–94

**Kristariyanto Y.A.**, Choi S.Y., Abdul Rehman S.A., Ritorto M.S., Campbell D.G., Morrice N.A., Toth R., and Kulathu Y. (2015) Assembly and structure of Lys33-linked polyubiquitin reveals distinct conformations. Biochem. J. *467*: 345–352

# Abbreviations

| | |
|---|---|
| $\Delta G$ | Gibbs energy |
| $\Delta H$ | enthalpy |
| $\Delta S$ | entropy |
| ABP | activity-based probes |
| ACN | acetonitrile |
| ADP | adenosine 5′-diphosphate |
| APC/C | anaphase promoting complex/cyclosome |
| AREL1 | apoptosis-resistant E3 ubiquitin protein ligase 1 |
| ASU | asymmetric unit |
| ATG8 | autophagy-related gene 8 |
| ATP | adenosine 5'-triphosphate |
| BSA | Bovine serum albumin |
| CRL | Cullin-RING ligase |
| CUE | coupling of ubiquitin to ERAD |
| CV | column volume |
| ddH$_2$O | double-distilled H$_2$O |
| diUb | di-ubiquitin |
| DLS | Diamond Light Source |
| DMEM | Dulbecco's modified eagle medium |
| DMSO | dimethyl sulphoxide |
| DNA | dexoxribonucleic acid |
| DTT | dithiothreitol |
| DUB | deubiquitylating enzyme |
| DUF544 | domain of unknown function 544 |
| E1 | ubiquitin-activating enzyme |
| E2 | ubiquitin-conjugating enzyme |
| E3 | ubiquitin-ligating enzyme |
| ECL | enhance chemiluminescence |
| EDTA | sodium ethylenediaminetetraacetic acid |
| EGTA | sodium ethylene glycol tetra acetic acid |
| ERAD | endoplasmic reticulum associated degradation |
| ESCRT | endosomal sorting complex required for transport |
| ESRF | European Synchrotron Radiation Facility |
| FA | formic acid |
| FAT10 | HLA-F adjacent transcript 10 |
| FBS | fetal bovine serum |
| GAT | GGA and TOM1 |
| GFC | gel filtration column |

| | |
|---|---|
| GLUE | GRAM-like ubiquitin-binding in Eap45 |
| GST | glutathione S-transferase |
| h | hour |
| HA | hemagglutinin |
| HD | Huntington's disease |
| HECT | homologous to E6AP |
| HEK293 | human embryonic kidney 293 |
| HEPES | 4-(2-Hydroxyethyl)piperazine-1-ethanesulfonic acid |
| HERC | HECT and RCC1-like domain |
| HOIL-1L | haem-oxidised IRP2 ubiquitin ligase-1 |
| HOIP | HOIL-1L-interacting protein |
| HPLC | high performance liquid chromatography |
| IEC | ion-exchange chromatography |
| IPTG | isopropyl β-D- 1-thiogalactopyranoside |
| ISG15 | interferon-stimulated gene 15 |
| ITC | isothermal titration calorimetry |
| JAMM | JAB1/MPN/MOV34 |
| $k_{cat}$ | turnover rate |
| $K_d$ | dissociation constant |
| $k_i$ | inhibition constant |
| $K_m$ | Michaelis constant |
| $k_{off}$ | binding off-rate |
| $k_{on}$ | binding on-rate |
| LC-MS | liquid chromatography mass spectrometry |
| LDD | linear ubiquitin determining region |
| LDS | lithium dodecyl sulphate |
| LUBAC | linear ubiquitin assembly complex |
| min | minute |
| MINDY | MIU-containing novel DUB family |
| MIU | motif interacting with ubiquitin |
| monoUb | mono-ubiquitin |
| MRC PPU | Medical Research Council Protein Phosphorylation and Ubiquitylation Unit |
| MS | mass spectrometry |
| MS1 | precursor ions |
| MS2 | daughter ions |
| NEDD4 | neural precursor cell-expressed developmentally downregulated gene 4 |
| NEDD8 | neural precursor cell-expressed, developmentally downregulated protein 8 |
| NEMO | nuclear factor κB essential modulator |

| | |
|---|---|
| NF-κB | Nuclear factor κB |
| NP40 | Nonidet P40 |
| NZF | Npl zinc finger |
| OTU | ovarian tumor proteases |
| PAGE | polyacrylamide gel electrophoresis |
| PBS | phosphate buffered saline |
| PDB | protein data bank |
| PEG | polyethylene glycol |
| PEI | polyethylenimine |
| pentaUb | penta-ubiquitin |
| PH | plekstrin homology |
| polyUb | polyubiquitin |
| PPAD | protein production and assay development |
| PRM | parallel reaction monitoring |
| Pru | pleckstrin-like receptor for ubiquitin |
| PTM | post-translational modification |
| PVDF | polyvinylidene fluoride |
| RBR | RING-between-RING |
| RCC1 | regulator of chromosome condensation 1 |
| ResQ | Resource Q |
| ResS | Resource S |
| RIG-1 | retinoic acid-inducible gene 1 |
| RING | really interesting new gene |
| RLD | RCC1-like domain |
| RMSD | root-mean-quare deviation |
| SDS | sodium dodecyl sulphate |
| sec | second |
| SEC | size-exclusion chromatography |
| SUMO | small Ub-like modifier |
| TAB | TAK1-binding protein |
| TAK1 | transforming growth factor β-activated kinase 1 |
| TBK1 | TANK-binding kinase 1 |
| TBS | tris-buffered saline |
| TBST | tris-buffered saline with Tween 20 |
| TCEP | tris (2- carboxyethyl) phosphine |
| TCR | T cell antigen receptor |
| tetraUb | tetra-ubiquitin |
| TFA | trifluoroacetic acid |
| TNF | tumor necrosis factor |
| triUb | tri-ubiquitin |

| | |
|---|---|
| TUBE | tandem ubiquitin-binding entity |
| Ub | ubiquitin |
| UBA | ubiquitin associated |
| UBAN | ubiquitin binding in ABIN and NEMO |
| UBD | ubiquitin binding domain |
| UBL | ubiquitin-like protein |
| UCH | ubiquitin C-terminal hydrolyses |
| UFD | ubiquitin fold domain |
| UFD | ubiquitin fusion degradation |
| UFM-1 | ubiquitin-fold modifier 1 |
| UIM | ubiquitin-interacting motif |
| USP | ubiquitin specific proteases |
| UV | ultra-violet |
| $V_0$ | initial velocity |
| VHS | Vps27/Hrs/STAM |
| $V_{max}$ | maximum velocity |
| YUH | yeast protease ubiquitin hydrolase |
| ZnF | zinc finger |

# Amino Acid Code

| Amino acid | Three letter code | One letter code |
| --- | --- | --- |
| Alanine | Ala | A |
| Arginine | Arg | R |
| Asparagine | Asn | N |
| Aspartic acid | Asp | D |
| Cysteine | Cys | C |
| Glutamic acid | Glu | E |
| Glutamine | Gln | Q |
| Glycine | Gly | G |
| Histidine | His | H |
| Isoleucine | Ile | I |
| Leucine | Leu | L |
| Lysine | Lys | K |
| Methionine | Met | M |
| Phenylalanine | Phe | F |
| Proline | Pro | P |
| Serine | Ser | S |
| Threonine | Thr | T |
| Tryptophan | Trp | W |
| Tyrosine | Tyr | Y |
| Valine | Val | V |
| Any amino acid | Xaa | X |

# Thesis Summary

Ubiquitylation is a post-translational modification that conjugates ubiquitin (Ub) onto proteins. When Ub itself is ubiquitylated, eight types of polyubiquitin (polyUb) chains can be formed: M1, K6, K11, K27, K29, K33, K48 and K63. Each one of these different chain types can couple modified proteins to diverse cellular signalling pathways. For example, proteins modified with K48 polyUb chains are targeted for proteasomal degradation. In contrast, modification with K63 polyUb chains has non-proteolytic roles in DNA damage response and immune signalling pathway. However, the cellular roles of K29 and K33 polyUb were poorly understood. Central to the myriad of polyUb signalling are Ub-binding domains (UBDs). Some UBDs can differentiate between types of polyUb chains and thus, are essential for the specificity of Ub signalling, but these mechanisms of linkage-selective polyUb recognition are less known. The work presented in my thesis centres on understanding the mechanisms underlying linkage-selective polyUb recognition by UBDs.

I started this study by developing methods to enzymatically assemble large quantity of K29 and K33 polyUb chains *in vitro*. These allowed me to obtain milligram amounts of K29 and K33 chains, which were instrumental in characterising these chain types biochemically and biophysically. I identified the first NZF domain (NZF1) of TRABID as a UBD that selectively binds to K29 and K33 chains. To understand the molecular basis for TRABID NZF1 specific binding, I determined the crystal structure of K29 diUb in complex with TRABID NZF1. I found that TRABID NZF1 binds to the hydrophobic patch only on the distal Ub. Binding to K29 polyUb is achieved by additional interactions of the NZF with the unique surface on the proximal Ub moiety and explains the linkage-selective binding of TRABID NZF1 to K29 and K33 chains. Furthermore, I established methods to isolate K29 chains from cells using TRABID NZF1. I discovered that K29 chains may be present in heterotypic chains, containing other linkage types such as K48.

I was then interested in identifying other small UBDs that can selectively bind to other polyUb chains. During this endeavour, I discovered an uncharacterised protein FAM63A containing a tandem MIU (motif interacting with Ub) that selectively binds to K48 chains. I discovered that the linkage-selective binding is mediated by the second MIU (MIU2) motif in FAM63A. The crystal structure of tMIU in complex with K48-linked polyUb chains reveals the mechanism of linkage-selective binding. FAM63A MIU2 contains three distinct surfaces that bind to polyUb in a conformation that only K48-linked triUb can accommodate.

Our laboratory recently discovered that in addition to tMIU, FAM63A also contains a catalytic domain of deubiquitylating enzymes (DUBs) that is highly specific in cleaving K48 chains. DUBs regulates Ub signalling by removing Ub from the modified proteins. In the last chapter of my thesis, I characterised the DUB activity of FAM63A beyond its selectivity in cleaving K48 chains. I discovered that FAM63A acts as a chain-trimming enzyme that cleaves polyUb chains from the distal end.

The work described in this thesis covers three key areas of polyUb signalling: assembly, recognition and disassembly. In spite of this, the overarching theme of my work is to understand how UBDs selectively recognise polyUb chains. In addition to the mechanistic insights, the linkage-selective UBDs characterised in this study can be further exploited as tools to delineate the functional cellular roles of different polyUb signals.

# 1 Introduction

## 1.1 Ubiquitin

In 1975, a group of researchers isolated a ~8500 Da polypeptide from calf thymus, which was also detected in animal cells, yeast and higher plants with high degree of sequence conservations (Goldstein *et al*, 1975). Due to its ubiquitous presence in all eukaryotes, the polypeptide was named ubiquitin (Ub). Ub was initially described as an inducer of B-cells and T-cells differentiation (Goldstein *et al*, 1975). In a parallel study, another group of researchers isolated a ~9000 Da heat-resistant polypeptide from reticulocytes (Ciehanover *et al*, 1978). This polypeptide is a crucial component for an ATP-dependent proteolysis and thus it was named ATP-dependent proteolysis factor 1 (APF-1) (Ciechanover *et al*, 1980). Sequence comparison revealed that both Ub and APF-1 are the same protein (Hershko *et al*, 1980; Wilkinson *et al*, 1980). Therefore, this was the first link between Ub and ATP-dependent proteolysis. Four decades later since its discovery, it is evident that Ub is involved not only in protein degradation, but also in a vast number of other cellular processes (Chapter 1.5.1).

In humans, Ub is encoded by four different genes, namely UBB, UBC, UBA52 and RPS27. These genes contain varying copies of the Ub coding sequence. Human UBB and UBC encode four and nine copies of Ub, respectively (Wiborg et al, 1985). UBA52 and RPS27A encode a single Ub as a fusion protein with ribosomal proteins (Redman & Rechsteiner, 1989; Finley et al, 1989). The translation products of these different Ub genes are called proubiquitin that are either in the form of head-to-tail polyubiquitin (polyUb) or Ub-ribosomal protein fusions. Proubiquitin is further processed by deubiquitylating enzymes (DUBs) that produce single Ub molecules. The cellular homeostasis of Ub is maintained both at the transcriptional and post-translational level, and deregulation is implicated in many diseases (Kimura & Tanaka, 2010).

24

## 1.2 Structural view of Ubiquitin

Ub is composed of 76 amino acids that organise into a highly compact globular structure of a β-grasp fold (Figure 1.1). This is characterised by a 3.5-turn α-helix, a short $3_{10}$-helix and a mixed β-sheet composed of five β-strands (Vijay-Kumar *et al*, 1987). A hydrophobic core and extensive networks of hydrogen bonds stabilise the compact Ub structure. Therefore, Ub is highly stable in a wide range of pH, temperature and even denaturing agents (Lenkinski *et al*, 1977). The C-terminal portion of Ub does not make any significant intramolecular contacts and thus, is highly flexible (Lange *et al*, 2008). This flexible tail is crucial for Ub signalling cascades.



***Figure 1.1 Structure of ubiquitin***
*Three orientations of Ub coloured according to the secondary structures: red, α-helices; yellow, β-strands; green, loops. N- and C-terminal ends are indicated. PDB ID: 1UBQ (Vijay-Kumar* et al*, 1987).*

### 1.2.1 Interaction hotspots on Ubiquitin

The solvent exposed hydrophobic residues on Ub form patches that are crucial for interactions with binding proteins. I44-patch (L8, I44, H68 and V70) and F4-patch (Q2, F4, T12 and T14) are located on the two opposite sides of the β-sheet, whereas I36-patch (I36, L71, L73) is at the C-terminal end of Ub (Figure 1.2) (Kulathu & Komander, 2012). In addition to this, the polar D58-patch (R54, T55, S57 and D58) and the TEK box (K6,

K11, T12, T14 and E34) have also been observed in making crucial hydrogen bonds with binding proteins. Among these different patches, I44- and I36-patches are the two most commonly found to be involved in interactions with binding partners. Mutations of Ub residues forming these interaction patches severely retards yeast growth (Roscoe *et al*, 2013), highlighting the importance of these surface residues of Ub.
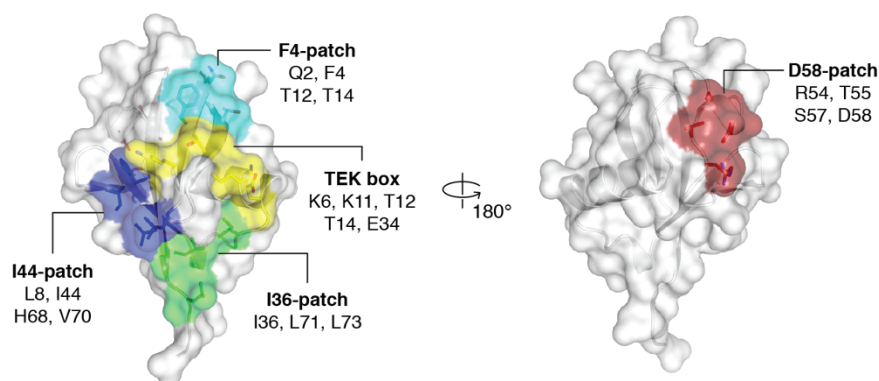


***Figure 1.2 Interaction hotspots on Ubiquitin***
*Two orientations of Ub in cartoon and semi-transparent surface representation. Highlighted are surface patches that mediate interactions with binding proteins, including DUBs and UBDs. PDB ID: 1UBQ (Vijay-Kumar* et al*, 1987).*

## 1.2.2 Ubiquitin-like proteins

Many proteins share structural homology with Ub, characterised by the β-grasp fold (Figure 1.3). These proteins are called Ub-like proteins (UBLs). UBLs can be classified into two sub-groups based on the nature of the proteins. Proteins belong to UBL class I exclusively contain the UBL fold. Consequently, they can be conjugated to target proteins through an enzymatic cascade akin to Ub (Chapter 1.2.2). These proteins include SUMO (small Ub-like modifier), NEDD8 (neural precursor cell-expressed, developmentally downregulated protein 8), ISG15 (interferon-stimulated gene 15), FAT10 (HLA-F

adjacent transcript 10), ATG8 (autophagy-related gene 8) and UFM1 (Ub-fold modifier 1) (van der Veen & Ploegh, 2012).

On the other hand, type II UBLs are present in multi-domain proteins and therefore cannot be conjugated to any protein substrates. For instance, type II UBLs can be found in many proteasome-shuttle proteins (Grice & Nathan, 2016), where the UBL interacts with Ub-receptors on the proteasome thus mediating the recruitment of these shuttling proteins to the proteasome. Many protein-protein interactions can be facilitated by the hydrophobic patches on the UBL fold. Thus, in some proteins, UBL type II mediate crucial intra- or inter-molecular interactions important for function. An example is the intramolecular interaction of the UBL domain of Parkin which inhibits its E3 ligase activity (Chaugule *et al*, 2011).
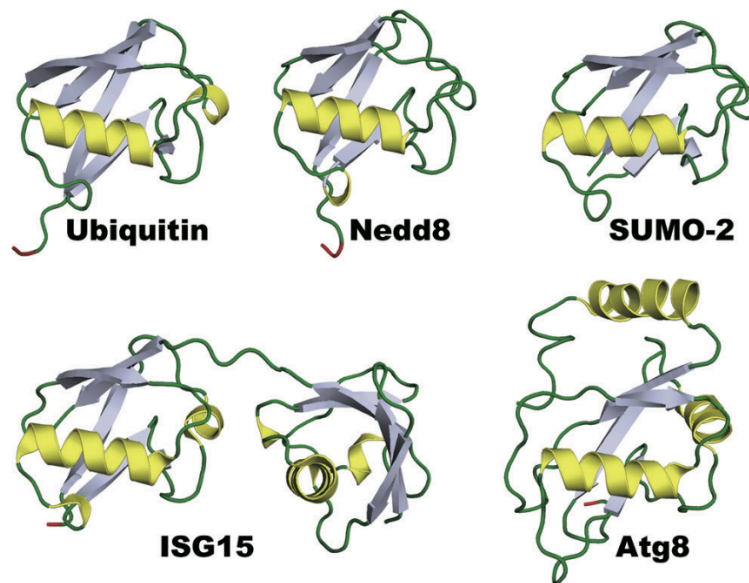


***Figure 1.3 Structural comparisons between Ubiquitin and Ub-like proteins***
*Structures of Ub and UBLs are in cartoon representation. α-helices are in yellow, β-strands are in grey and loops are in green. Figure was reproduced as a whole from (Ronau* et al*, 2016).*

## 1.3 Ubiquitin conjugation cascade

Ubiquitylation is the covalent conjugation of Ub onto protein substrates, which is mediated through a three-step enzymatic cascade (Figure 1.4). Three classes of enzymes are involved in this cascade: ubiquitin-activating (E1) enzymes, Ub-conjugating (E2) enzymes and ubiquitin-ligating (E3) enzymes. In a nutshell, Ub is initially activated by E1 in an ATP-dependent process, followed by Ub transfer to the catalytic Cys of E2s (Chapter 1.3.1) (Schulman & Harper, 2009; Stewart *et al*, 2016). Then, E3s catalyse the transfer of Ub from the Ub-loaded E2s onto substrate protein (Chapter 1.3.2) (Berndsen & Wolberger, 2014; Buetow & Huang, 2016). The G76 of Ub is conjugated to $\varepsilon$-NH$_2$ of Lys residue of substrates, forming isopeptide bond. Ub itself contains seven Lys residues, which each can be a conjugation site for another Ub molecule (Figure 1.5). Alternatively, Ub can be conjugated to the $\alpha$-NH$_2$ of Met of Ub, forming a peptide bond. These polymers of Ub are called polyubiquitin (polyUb) chains (Chapter 1.5).
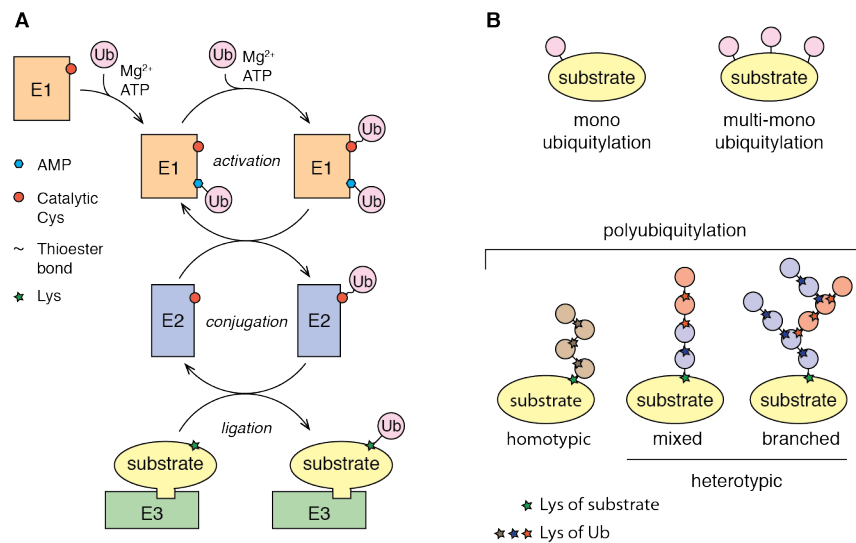
**Figure 1.4 The Ubiquitin conjugation system**

*(A) A schematic diagram illustrates three-step cascade of Ub conjugation. Initially, Ub-activating (E1) enzyme binds to Ub and Mg²⁺•ATP and catalyses adenylation of Ub, forming Ub-AMP (blue circle). Then, this Ub is covalently linked to the catalytic Cys of E1 (red circle) via thioester bond. Following this step, E1 can bind to another Ub and Mg²⁺•ATP for the formation of the second Ub-AMP. At the next step, the fully loaded E1 binds to Ub-conjugating (E2) enzyme and Ub is transferred from the catalytic Cys of E1 to the catalytic Cys of E2. At the final step, Ub-ligating (E3) enzyme binds to the Ub-loaded E2 and a substrate. Then, E3 catalyses Ub conjugation to a Lys residue of the substrate. (B) Schematic diagrams illustrate products of Ub conjugation. Ub can be conjugated to a single or multiple Lys residues on a substrate, forming mono- or multi-monoubiquitylation, respectively (top). Alternatively, Ub can be conjugated to Lys or Met residue of other Ub moieties, forming polyubiquitin chains (bottom). In homotypic chains, only one type of Lys/Met residue is used as conjugation sites. In heterotypic more than one types of Lys/Met are used for conjugating sites.*
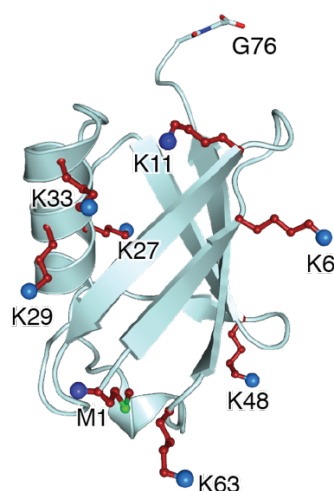
***Figure 1.5 Ubiquitin and its eight conjugation sites***
*Ub is in cartoon representation coloured in pink. Seven Lys and Met1 residues are shown in red sticks. The ε-NH₂ of Lys and the α-NH₂ of Met1 residues are shown as blue spheres. Sulfur atom on Met1 is coloured green. PDB ID: 1UBQ (Vijay-Kumar* et al*, 1987).*

### 1.3.1   Preparing Ub for conjugation: E1 and E2 in action

There are two Ub-activating (E1) enzymes in vertebrates, namely UBA1 and UBA6 (Ciechanover *et al*, 1981; Jin *et al*, 2007; Chiu *et al*, 2007).  Whereas UBA1 is specific for Ub, UBA6 functions as an E1 for both Ub and FAT10 (Chiu *et al*, 2007). UBA1 and UBA6 are characterised by a 110-120 kDa homodimer globular protein with multiple domains: an adenylation domain, a catalytic domain and a C-terminal Ub-fold domain. The first two domains catalyse the ATP-dependent Ub activation in a three-step reaction (Ciehanover *et al*, 1978; Ciechanover *et al*, 1981; Haas *et al*, 1982). At first, adenylation domain of E1 binds to Ub and $Mg^{2+}$•ATP, and catalyses the adenylation of Ub, forming Ub-AMP and pyrophosphate. Once Ub-AMP is formed, pyrophosphate is released and there is a structural modification on the E1 that allows the catalytic Cys domain to approach the adenylation domain (Olsen *et al*, 2010). Then the catalytic Cys of E1 attacks the Ub-AMP, forming a thioester bond between Ub G76 and the Cys sulphydryl of E1. This reaction frees the adenylation domain of E1 to catalyse the formation of a second

Ub-AMP (Huang *et al*, 2007). This results in E1 loaded with two Ub molecules: one Ub is conjugated to the catalytic Cys of E1 via a thioester bond, and the other Ub is bound at the E1 adenylation site as Ub-AMP. This fully loaded E1 has a dramatic increase in affinity for recruiting E2, which is crucial for the next step of Ub transfer to E2 (Haas *et al*, 1988).

The family of Ub-conjugating E2 enzymes consists of ~40 enzymes characterised by a core catalytic UBC domain of ~150 residues (Stewart *et al*, 2016). This domain adopts an α/β-fold composed of four α-helices and a four-stranded antiparallel β-sheet. The Ub-fold domain (UFD) of E1 binds to the region on E2 formed by the α1-helix and loop regions. The flexible linker of UFD allows a structural change on E1 that brings the catalytic Cys of E2 closer to the catalytic Cys of E1 where the Ub is bound (Lee & Schindelin, 2008; Olsen & Lima, 2013). Then, the catalytic Cys of E2 carries nucleophilic attack on the thioester bond of E1~Ub in transthiolation forming E2~Ub ('~' is used to refer to thioester bond from here on). This reaction reduces binding affinity of E2~Ub for E1, but increases the affinity of E2~Ub to bind to E3. Therefore, this allows the Ub conjugation cascade to progress to the final step, namely the transfer of Ub from the charged E2 to substrate, which is catalysed by E3 enzymes (Buetow & Huang, 2016).

### 1.3.2   Ub conjugation by E3: Three classes, one objective

Ub E3s can be classified into three classes based on the mechanism by which they catalyse Ub conjugation to substrate proteins. These are RING (really interesting new gene) E3s, HECT (homologous to E6AP) E3s and RBR (RING-between-RING) E3s (Figure 1.6). RING E3 ligases bind to both Ub-loaded E2 and substrates and catalyse the direct transfer of Ub onto substrates. On the other hand, Ub conjugation by HECT and RBR E3s involves a two-step conjugation process. First, Ub is transferred from the E2 to the catalytic Cys of HECT and RBR E3s, resulting in a thioester E3~Ub intermediate.

The Ub is subsequently transferred to substrate. The mechanisms of Ub conjugation by these different classes of E3 ligases are detailed in the sections below.
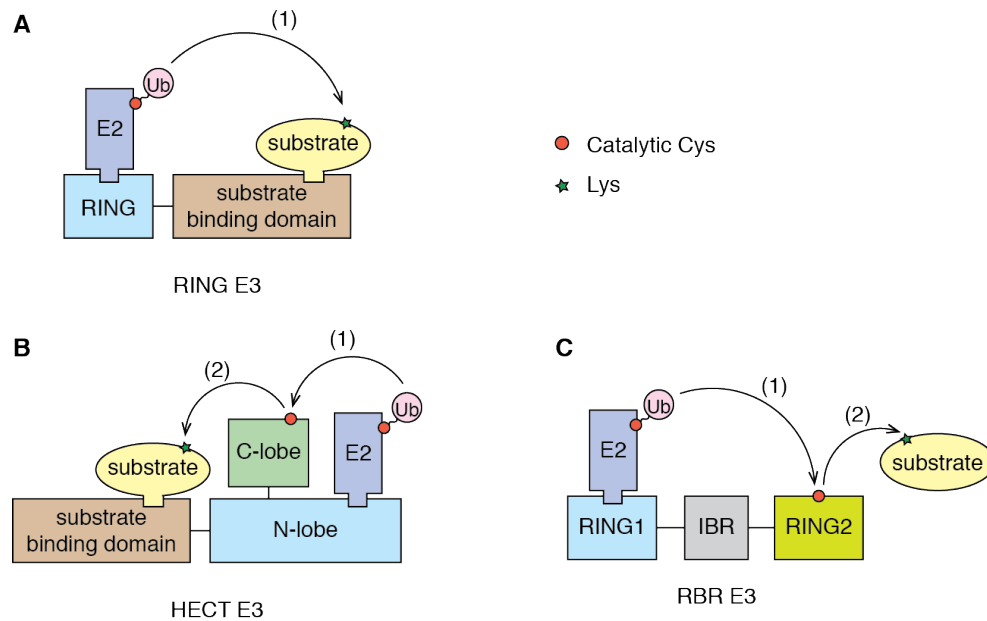


**Figure 1.6 Mechanisms of Ub conjugation by three classes of Ub-ligating enzymes**
*Schematic diagrams illustrate Ub conjugation catalysed by RING E3, HECT E3 and RBR E3. **(A)** RING domain of RING E3 binds to Ub-loaded E2 whereas its substrate-binding domain binds to substrate. Ub is conjugated in one-step reaction to a Lys residue of the substrate. On the other hand, HECT E3 and RBR E3 catalyse Ub conjugation in two-step reaction. **(B)** N-lobe of HECT E3 binds to Ub-loaded E2 and Ub is transferred to the catalytic Cys on the C-lobe of the HECT domain. Then, Ub is conjugated to a Lys of the bound substrate. **(C)** In RBR E3, RING1 interacts with Ub-loaded E2 and Ub is transferred to the catalytic Cys on RING2. Then, Ub is conjugated to a Lys residue on a substrate.*

### 1.3.2.1   RING E3

RING E3s are characterised by the presence of a RING domain, which is a zinc finger domain that binds to two zinc ions coordinated by Cys and His residues arranged in a cross-braced configuration. Zinc coordination is essential for proper folding of the RING domain (Buetow & Huang, 2016). Some RING E3s function as monomers (for example CBL), and other RINGs work as oligomers, for example homodimers of cIAP2 and the heterodimeric RING of BRCA1/BARD1 (Buetow & Huang, 2016). In addition to this,

some RING E3s function in multi-subunit complexes, such as Cullin-RING Ligases (CRLs) and anaphase promoting complex/cyclosome (APC/C) (Lydeard *et al*, 2013; Chang & Barford, 2014). Although different from the rest of RING E3s, U-box proteins are also classified as RING E3s based on a domain that resembles a RING domain in structure and function. However, the U-box domain lacks the key residues present in RING domains that coordinate zinc ions. These zinc-coordinating residues are replaced by polar residues, which mediate hydrogen interactions at the core of the protein and thus, hold the domain together (Ohi *et al*, 2003).

RING E3s bind to E2~Ub, which stabilises and primes the E2~Ub in a closed conformation. In this conformation, the closed E2~Ub is more reactive for Ub transfer to substrate (Plechanovová *et al*, 2012; Dou *et al*, 2012; Pruneda *et al*, 2012). In this primed state, both I44- and I36-patches of Ub are in contact with the E2 and E3, respectively, thereby orienting the C-terminus of Ub in a position optimal for nucleophilic attack by the incoming substrate Lys (Branigan *et al*, 2015).

### 1.3.2.2  HECT E3

HECT E3 ligases are characterised by a catalytic HECT domain of ~350 residues, which is located at the C terminus of the containing protein (Huibregtse *et al*, 1995). This HECT domain is composed of two lobes, a larger N-lobe that binds to E2 and a smaller C-lobe that contains the catalytic Cys (Huang *et al*, 1999). The flexible linker connecting the two lobes is crucial in the Ub transfer process from E2 to E3 (Verdecia *et al*, 2003).

Whilst there is high similarity in the C-terminal region that harbours the catalytic HECT domain, the N-terminal regions highly vary between HECT E3s. These N-terminal regions constitute protein-protein interaction domains that are essential for substrate recognition or for regulation of E3 activity (Kee & Huibregtse, 2007). There are 28 HECT E3s known to date that can be classified into three sub-classes based on the architecture of the N-terminal regions: NEDD4 (neural precursor cell-expressed developmentally

downregulated gene 4), HERC (HECT and RCC1-like domain) and "other" HECT E3s (Scheffner & Kumar, 2014). The NEDD4 family is the best-studied of the HECT E3s and comprises nine proteins: NEDD4-1, NEDD4L (NEDD4-2), SMURF1, SMURF2, ITCH, WWP1, WWP2, NEDL1 and NEDL2. These proteins contain a C2 domain and three to four WW domains, which are all involved in protein-protein interactions. Six HECT ligases belong to the HERC family that contain regulator of chromosome condensation 1 (RCC1)-like domains (RLDs), which are not well characterised (Sánchez-Tena *et al*, 2016). The remaining 13 proteins, including E6AP/UBE3A the founding member of HECT E3 ligases, fall into the class of "other" HECT E3s, and these do not share a common N-terminal domain architecture.

There are two steps involved in the Ub-conjugation process catalysed by HECT E3s: (1) Ub transfer from the E2 to the catalytic Cys of HECT E3 and (2) Ub transfer from E3 onto substrate (Figure 1.6B). The process is initiated and regulated by the N-lobe of the HECT domain that binds to the E2~Ub (Huang *et al*, 1999; Kamadurai *et al*, 2009). This interaction is selective and determines functional cooperation between the HECT E3 and its cognate E2s for Ub conjugation (Kumar *et al*, 1997; Nuber & Scheffner, 1999; Schwarz *et al*, 1998). There is a high degree of variation in the relative positioning of the N-lobe and the catalytic Cys-containing C-lobe owing to the flexible linker between the two lobes (Verdecia *et al*, 2003). When E2 is bound, the distance between the catalytic Cys of E2 and the HECT C-lobe are ~16 to 41 Å, which is too far for the transthiolation reaction to occur (Huang *et al*, 1999; Verdecia *et al*, 2003). When Ub-loaded E2 is bound, there is a structural modification on the HECT domain that bring the E2~Ub closer to the catalytic Cys of the HECT C-lobe. This allows nucleophilic attack that results in the thioester intermediate E3~Ub (Kamadurai *et al*, 2009). In the NEDD4 family, the E2~Ub/E3 conformation is further stabilised through additional interfaces, which facilitates transthiolation reaction (Kamadurai *et al*, 2009). Hydrophobic surface on the

C-lobe of NEDD4 interacts with the I36-patch of E2-bound Ub. However, the residues forming the hydrophobic patch on the C-lobe are not conserved in other classes of HECT E3s, suggesting distinct mechanisms in different HECT E3s.

When Ub is covalently conjugated to HECT E3s, the C-terminal tail of the loaded Ub is orientated in an extended conformation through a network of hydrogen interactions, forming an additional β-strand on the Ub C-terminal tail that extends the β-sheet of the HECT C-lobe (Maspero *et al*, 2013; Kamadurai *et al*, 2013). Then the Ub-loaded C-lobe rotates by ~130° to bring the thioester in close proximity to the substrate Lys. In addition to this, the N-lobe also has an additional Ub binding domain (Maspero *et al*, 2013), which possibly serves as a platform for the acceptor Ub in polyUb chains assembly.

### 1.3.2.3   RBR E3

RBR E3s are considered hybrid E3s as they contain features of both RING and HECT ligases. RBRs are characterised by the presence of RING1-IBR (in-between RING)-RING2 domains that are important for Ub conjugation. RBR E3s catalyse Ub conjugation in two-step reaction (Figure 1.6C) (Buetow & Huang, 2016). Initially, the RING1 domain of RBR binds to E2~Ub akin to the RING domain of RING E3s. Instead of direct conjugation of Ub from E2~Ub to the substrate, Ub is first transferred to the catalytic Cys residue on the RING2 domain of RBR, forming an E3~Ub thioester intermediate. Then, Ub is conjugated to Lys residue of substrate. This two-step Ub conjugation resembles the mechanism of HECT E3s. A remarkable feature for RBR E3s is that they are tightly regulated by intramolecular interaction with auto-inhibitory domains (Smit *et al*, 2012; Stieglitz *et al*, 2012; Duda *et al*, 2013; Chaugule *et al*, 2011).

## 1.4   Monoubiquitylation

The simplest outcome of protein ubiquitylation is when a Ub molecule is conjugated to the ε-amino group of single or multiple Lys of substrate proteins, which is known as

monoubiquitylation or multi-monoubiquitylation, respectively (Figure 1.4B). Despite this simplicity, monoubiquitylation regulates diverse cellular signalling pathways, including gene expression (Nakagawa & Nakayama, 2015), DNA damage response (Ulrich & Walden, 2010; Meas & Mao, 2015) and cellular trafficking (Haglund *et al*, 2003). In HEK293 cells, monoubiquitylation accounts for more than 60% of the total Ub, further supporting wide prevalence of this modification and diverse functional roles (Kaiser *et al*, 2011).

Several E2 enzymes are specialised to catalyse only monoubiquitylation onto Lys residues of substrate. These E2s include UBE2T that works together with the RING E3 FANCL to monoubiquitylate FANCD2 (Alpi *et al*, 2008). This monoubiquitylation of FANCD2 is essential for the Fanconi Anemia DNA repair pathway. Similarly, UBE2W activity is strictly limited to conjugate only single Ub moiety to the N-terminal $\alpha$-amino group of proteins (Tatham *et al*, 2013; Scaglione *et al*, 2013). A recent study reveals the molecular mechanism underlying the strict monoubiquitylating activity of UBE2W (Vittal *et al*, 2015). UBE2W has an unusual UBC domain that has a disordered C-terminal region. This region recognises and interacts with the backbone atoms of unstructured N-terminal region of substrates regardless of amino acid sequence (Vittal *et al*, 2015). Since the N terminus of Ub is highly structured, this explains why UBE2W cannot ubiquitylate Ub and thus, restricts its activity to monoubiquitylation. It is proposed that E2s specialised only for monoubiquitylation lack non-covalent Ub-binding site, which is essential for the chain-elongation process. Indeed, mutating the non-covalent Ub-binding site on chain-elongating E2 UBE2D3 abolishes its ability to assemble polyUb chains (Brzovic *et al*, 2006).

In contrast to monoubiquitylating E2s, chain-building E2s may use Ub conjugated on a substrate as a template for polyUb chain elongation. For example, during mitosis, multi-subunit RING E3 APC/C assembles K11 chains on its substrate using two different

E2s: UBE2C and UBE2S (Williamson *et al*, 2009). UBE2C primes APC/C substrate with monoUb, which serves as template for UBE2S to assemble K11 chains (Williamson *et al*, 2009; Wu *et al*, 2010). Similarly, K63-linked polyUb chains are conjugated to the RING E3 TRIM5α in autoubiquitylation reactions that require two E2s: UBE2W and UBE2N-UBE2V2 (Fletcher *et al*, 2015). UBE2W monoubiquitylates TRIM5α on its Lys residues, from which UBE2N-UBE2V2 elongates with K63 chains. This process is necessary for subsequent inhibition of retroviral reverse transcription. Collectively, these suggest close relationships between monoubiquitylation and polyubiquitylation in cellular Ub signalling.

## 1.5  Polyubiquitylation

Each of the seven Lys residues of Ub (K6, K11, K27, K29, K33, K48 and K63) can be the acceptor site for another Ub molecule, thus forming polyubiquitin chains (Figure 1.5). In addition to this, the main amide group of the N-terminal Met of Ub can become a conjugation point for ubiquitylation forming head-to-tail polyUb chains or simply M1 linkage type. Ub can be conjugated continuously using a single Lys/Met residue in a homogenous polyUb chain (Figure 1.4B). Alternatively, polyUb chains can be assembled where Ub moieties within the chain are conjugated at two or more Lys/Met residues. These chains are known as heterotypic polyUb. The topology of heterotypic polyUb chains is more complex, which includes mixed and branched chains. In mixed chains more than one linkage types may be present within a chain in an alternating arrangement, whereas in a branched architecture, more than one Lys/Met residues within a Ub moiety are used as a conjugation point (Figure 1.4B).

Mass spectrometry analyses have detected the presence of eight types of polyUb chains in yeast and mammalian cells (Peng *et al*, 2003; Xu *et al*, 2009; Dammer *et al*, 2011). Conjugation of each one of these polyUb chains onto substrates can signal distinct

outcomes and therefore, their abundance in cells is tightly regulated. Among the eight types of polyUb chains, K48 and K63 are the most well studied and thus, are called the typical type of polyUb chains. Although very little is known, the cellular pathways that the remaining atypical chain types i.e. M1, K6, K11, K27, K29 and K33 are involved in are starting to emerge (Kulathu & Komander, 2012).

### 1.5.1 Diverse roles of polyUb chains in cellular signalling

K48-linked polyUb chain type is well known for its role in mediating proteasomal degradation of the modified proteins (Chau *et al*, 1989). Consistent with this, upon proteasome inhibition, the intracellular levels of K48-linked polyUb increase (Xu *et al*, 2009). Proteins modified with K48-linked polyUb are targeted to the proteasome for degradation (Finley, 2009; Weissman *et al*, 2011). Compromising the integrity of E3s that conjugate K48 linkage type stabilises the substrate proteins, and in contrast, inhibiting DUBs that hydrolyse this linkage type results in increased turnover of the substrate proteins.

In contrast to K48 chain type, K63-linked polyUb are associated with non-proteolytic functions in signalling, which includes DNA damage response (Al-Hakim *et al*, 2010), NF-κB signalling (Skaug *et al*, 2009), kinase and phosphatase activation (Yang *et al*, 2010), cellular trafficking (Lauwers *et al*, 2009; Erpapazoglou *et al*, 2014) and oxidative stress response (Silva *et al*, 2015). Nevertheless, a role for K63 chains in proteasomal degradation has been observed. In yeast, the HECT E3 ligase Rsp5 catalyses the conjugation of K63-linked polyUb on Mga-p120, which results in proteasome binding and subsequent proteasomal degradation (Saeki *et al*, 2009).

Our understanding of the cellular role of M1 linkage type has dramatically increased in the past few years. The level of M1-linked polyUb is undetectable under basal conditions, but it is rapidly synthesized upon the activation of inflammatory

signalling cascade (Tokunaga *et al*, 2009). The assembly of this linkage type is mediated by a large protein complex called LUBAC (linear ubiquitin assembly complex), which is comprised of HOIP, HOIL-1L and Sharpin (Tokunaga *et al*, 2009; Gerlach *et al*, 2011; Tokunaga *et al*, 2011; Ikeda *et al*, 2011). In addition to NF-κB activation, M1-linked polyUb chain type is also involved in the regulation of type I interferon production (Inn *et al*, 2011) and Wnt signalling in angiogenesis (Rivkin *et al*, 2013).

K11-linked polyubiquitin is widely associated with the regulation of cell cycle progression. The abundance of K11-linked polyUb chains dramatically increases when cells are in mitosis or in early G1 (Matsumoto *et al*, 2010). K11 linkage type has been demonstrated to have proteolytic roles in cell-cycle progression as APC/C substrates conjugated with K11-linked polyUb chains are degraded by proteasome (Jin *et al*, 2008; Song & Rape, 2010; Song *et al*, 2014; Min *et al*, 2015). However, the homotypic K11-linked polyUb chains are poor signals for proteasomal degradation (Grice *et al*, 2015). To produce an efficient proteasomal targeting signal, K11 chains are present in heterotypic chains with K48 linkage type (Meyer & Rape, 2014). Although it is less understood, K11 linkage type may also be involved in pathways other than cell cycle regulation, for example in the regulation of HIF-1α (Bremm *et al*, 2014) and innate anti-viral immune response (Qin *et al*, 2014).

A role for K6 linkages has been associated primarily with DNA damage response. The heterodimeric RING E3s BRCA1/BARD1 mainly assemble K6 linkages *in vitro* and *in vivo* upon DNA damage response (Morris & Solomon, 2004). A recent Ub proteomics study revealed that K6 is the most upregulated of all chain types following UV damage, strongly supporting roles for K6 in DNA damage response (Elia *et al*, 2015). However, the identity of the proteins modified with K6 linkages following UV irradiation is unknown. K6 chains have also been reported to have roles in other pathways. For example, K6 polyUb have been shown to inhibit proteasomal degradation (Cripps *et al*,

2006; Shang *et al*, 2005) and modulate enzyme activity (Ben-Saadon *et al*, 2006). Recently, studies analysing the abundance of different linkages have observed that the abundance of K6 changes upon mitochondrial damage. Thus, it was proposed that K6 is involved in mitochondrial biogenesis and mitochondria-specific autophagy (Ordureau *et al*, 2014; Durcan *et al*, 2014; Cunningham *et al*, 2015).

Very little is known about K27-linked polyUb chains. K27 is situated in the central helix of Ub and is slightly buried raising the question of whether K27 chains can even be enzymatically assembled. Chemical approaches have succeeded in assembling K27 chains. However, all the DUBs analysed do not show any activity towards K27 linkages (Ritorto *et al*, 2014; Castañeda *et al*, 2016b). Sparse data however have linked this linkage type to DNA damage response (Gatti *et al*, 2015), lysosomal degradation (Ikeda & Kerppola, 2008), cellular trafficking (Palicharla & Maddika, 2015) and the regulation of immune signalling (Peng *et al*, 2011; Liu *et al*, 2014a).

K29-linked polyUb chains have been associated with proteolytic and non-proteolytic signalling. Initial studies suggested a role for K29 linkages in the ubiquitin-fusion degradation (UFD) pathway in yeast where it is assembled as heterotypic chains with K48 linkages (Johnson *et al*, 1995; Koegl *et al*, 1999). In mammalian cells, K29 chains are associated with lysosomal degradation. Deltex, NEMO and p65 are all conjugated with K29-linked polyUb chains, which results in their lysosomal degradation (Chastagner *et al*, 2006; Zotti *et al*, 2011). In contrast, the non-proteolytic functions of K29 linkage type are in the regulation of kinase activity and protein stability. Polyubiquitylation of AMPK-related kinases with K29 and K33 linkage types does not result in proteasomal degradation but inhibition of their kinase activity (Al-Hakim *et al*, 2008). The polyubiquitylation of β-catenin with K29 linkage type results in the stabilisation of the modified protein (Hay-Koren *et al*, 2011).

K33 chains may not be linked to proteasomal degradation, as the level of K33 linkage types do not increase following proteasome inhibition (Xu *et al*, 2009). Non-proteolytic roles of K33 have been observed in T-cell regulation, cellular trafficking, kinase activity regulation and immune signalling. T cell antigen receptor (TCR) activation is negatively regulated in a proteolysis independent manner by K33-linked polyUb (Huang *et al*, 2010). Similarly, non-proteolytic roles of K33 linkage type is involved in the activation of CD8$^+$ T cells (Yang *et al*, 2015) and the regulation of post-Golgi trafficking (Yuan *et al*, 2014). K33 chains protect TBK1 from being modified by K48 chains and thus, positively regulates type I interferon signalling pathway (Lin *et al*, 2016). However, many of these studies assigning linkage types of polyUb to specific pathways relied heavily on overexpression of Ub mutants and thus, should be interpreted with caution.

Most of the function of polyUb chains described above have been investigated assuming that polyUb is formed as homotypic chains in cells. However, the cellular topology of polyUb may be more complex than having just one linkage type within a polyUb chain. PolyUb chains that are assembled using two or more Lys/Met types are known as heterotypic chains. Recently, several studies reported the presence of heterotypic chains in different signalling pathways. During the progression of mitosis, APC/C conjugates branched K11/K48 chains onto its substrates, which results in a far more efficient proteasomal degradation signal (Meyer & Rape, 2014; Grice *et al*, 2015). Branched polyUb chains are also involved in non-proteolytic pathways, such as cellular surface receptor internalisation. Viral E3 ligases assemble branched K11/K63 chains that are important for endocytosis of host receptors (Boname *et al*, 2010). Non-proteolytic roles of heterotypic chains is also observed in the innate immune signalling. Upon IL-1 receptor activation, mixed chains of K63/M1 linkages are assembled for efficient NF-κB

activation (Emmerich *et al*, 2013; 2016). Collectively, whether in homotypic or heterotypic, polyUb chains are involved in regulating various cellular processes.

### 1.5.2 Specificity in polyUb conjugation

In the previous section, I discussed how different types of polyUb chains signal for distinct cellular outcomes. Therefore, assembling specific linkage types on specific proteins at the right time and place is key to precise Ub signalling (Grabbe *et al*, 2011). This task is mediated by E2 and E3 enzymes. Different strategies have been adopted by these enzymes for achieving linkage selective polyUb conjugation. In the following section, I will detail what is known about linkage specificity in polyUb conjugation by E3 ligases and several chain-elongating E2 enzymes.

M1-linked polyUb chain is synthesised by a multi-subunit E3 ligase LUBAC, which contains two RBR E3 ligases, HOIL-1L and HOIP (Kirisako *et al*, 2006). The catalytic core E3 HOIP contains the RBR domains, which synthesise M1-linked polyUb chains. A minimal domain of HOIP containing RING2 and LDD (linear Ub chain determining region) is sufficient to assemble M1-linked polyUb chains (Smit *et al*, 2012). The crystal structure of RING2-LDD in complex with a Ub moiety captures a snapshot of an event right before the conjugation process, where acceptor and donor Ub moieties are bound, and thus, suggests specificity determinants in conjugation  (Stieglitz *et al*, 2013). In this structure, the acceptor Ub is bound to two α-helices and a zinc-finger, which position the amino group of M1 close to the catalytic Cys of HOIP RING2. The donor Ub, which was obtained from crystal contact with the symmetry related molecule, has its C-terminal tail (71-76) stretch towards the catalytic Cys of HOIP by interactions with the β-hairpin from the LDD domain and the β-sheet of the RING2 domain. These interactions allow only the α-amino group of M1 to attack the thioester bonded HOIP~Ub, thus explaining why only M1 chains are assembled by LUBAC.

The formation of K63-linked polyUb chains depends on the heterodimeric E2: UBE2N-UBE2V1 (Ubc13-Mms2) (Deng *et al*, 2000). Whereas UBE2N has the catalytic Cys residue, UBE2V1 lacks key catalytic residues. UBE2V1 plays important non-catalytic roles by functioning as a binding platform for the acceptor Ub. The specificity for K63-linked polyUb chains conjugation is achieved by UBE2V1 binding to the I44-patch of Ub, which positions the K63 residue of the acceptor Ub in an optimal orientation to attack the thioester bond between the catalytic Cys of Ubc13 and G76 of the donor Ub (Branigan *et al*, 2015; Eddins *et al*, 2006).

Similar to the E2 UBE2N-UBE2V1 that can assemble K63 chains by itself, specificity in K11 chain assembly is dictated by the E2 UBE2S. During mitosis, K11-linked polyUb chains are assembled by a large multi-subunit E3 APC/C, which works with two E2 enzymes, UBE2C and UBE2S, in two sequential reactions (Williamson *et al*, 2009). APC/C and UBE2C catalyse monoubiquitylation of substrate, which is rapidly extended by APC/C and UBE2S into long polyUb linked via K11 linkage type. UBE2S is able to assemble K11 chain types *in* vitro in the absence of APC11, the RING E3 subunit of APC/C (Wu *et al*, 2010). This specificity comes from the close thioester-intermediate UBE2S~Ub stabilisation through UBE2S binding to I44-patch of donor Ub, and a substrate-assisted transthioesterification reaction through the orientation of the acceptor Ub on UBE2S (Wickliffe *et al*, 2011). UBE2S transiently binds to the TEK-motif on the acceptor Ub and orients its K11 and E34 in the close proximity with the thioester bond between UBE2S and the donor Ub. This allows E34 to lower the $pK_a$ of the acceptor K11 to be more nucleophilic to attack the thioester bond, ensuring the specificity of chain assembly by UBE2S.

Similarly, several other chain-elongating E2s are capable of assembling K48-linked polyubiquitin chains in the absence of their cognate RING E3s. These include Cdc34/UBE2R1, UBE2K and UBE2G2. Both UBE2R1 and UBE2K act as monomers,

where the E2 by itself can simultaneously bind to both donor and acceptor Ub (Chong *et al*, 2014; Middleton & Day, 2015). In contrast, homo-dimerization of UBE2G2 is absolutely essential for polyUb synthesis as the two protomers of UBE2G2 serve as a platform for binding to acceptor and donor Ub, respectively (Liu *et al*, 2014b). Despite this variation, the K48-specific E2s recognise E51-Y59 loop of the acceptor Ub, which is essential to orient the K48 residue of the acceptor Ub to attack the thioester bond between the donor Ub and the catalytic Cys of the E2 (Chong *et al*, 2014; Middleton & Day, 2015; Liu *et al*, 2014b). Interestingly, replacing E51 with the opposite charge residue alters the linkage type assembled by UBE2G2 from K48 to K63 type (Liu *et al*, 2014b). Another feature of K48-specific E2s is the insertion of ~12 residues to the proximal of the E2 active site. It is hypothesised, that this region lowers the $pK_a$ of the incoming K48 and thus, assists the transthiolation reaction (Ziemba *et al*, 2013).

### 1.5.3   Structure of polyUb chains: few snapshots out of many conformations

The distribution of Met1 and the seven Lys residues on the surface of Ub and the flexible nature of the C-terminal tail of Ub (Lange *et al*, 2008) account for various conformations polyUb chains can adopt. Several studies, including work done in this thesis, have tried to observe the variation in the structures of different types of polyUb. This can shed light into how components of the Ub system differentiate between chain types. These investigations, which focus on diUb, the minimal constituent of polyUb, classify conformations of polyUb into two groups: more compact 'closed' or more extended 'open' conformation (Figure 1.7).

K48-diUb was the first diUb structure to be solved and it shows a tight interaction between I44-patches of the two Ub moieties and thus, is in 'closed' conformation (Figure 1.7B) (Cook *et al*, 1992). Although similar 'closed' conformations are also observed for K6- and K11-diUb, the interface between the two Ub moieties vary. The interface in K6-diUb is formed between the I36- and I44-patches of the distal and proximal, respectively,

whereas in K11-diUb, both I36-pathces of the two Ub moieties form the interface (Figure 1.7C-D) (Virdee *et al*, 2010; Matsumoto *et al*, 2010). In contrast, there is no interface formed between the two Ub moieties linked via M1 or K63 and thus, both M1- and K63-diUb are in 'open' conformations (Figure 1.7E-F) (Komander *et al*, 2009b). M1 and K63 are located at the opposite ends of the C-terminal tail of Ub and due to steric hindrance, these two chain types may not adopt 'closed' conformations (Figure 1.5).
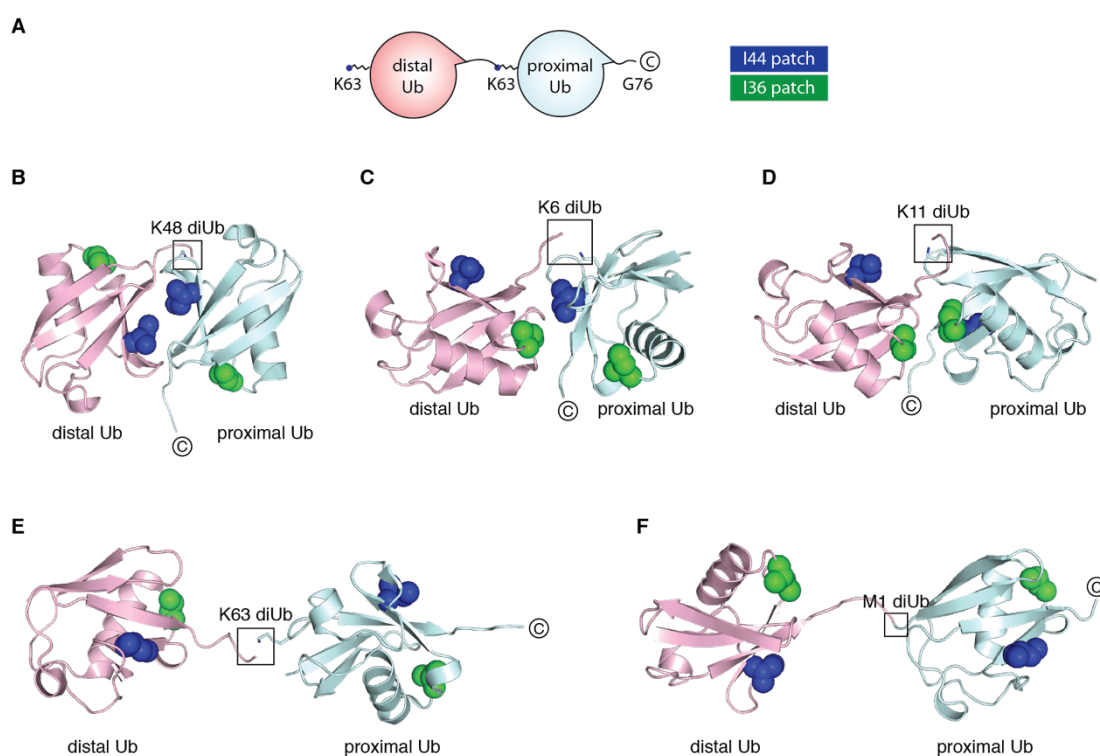


***Figure 1.7 Structures of diUb chains***
*(A) A schematic diagram illustrates diUb. Proximal Ub refers to Ub moiety that has a free C-terminal carboxylate in unanchored chains or the one that is closer to substrates. Distal Ub refers to the final Ub moiety within polyUb chains that all of its Lys and Met residues are free. (B-D) K48-diUb, K6-diUb and K11-diUb chains in 'closed' conformations. The two Ub moieties form interface through their hydrophobic surface. (E-F) K63-diUb and M1-diUb chains in 'open' conformation. There is no interface formed between two Ub moieties. Distal Ub (pink) and proximal Ub (light cyan) are in cartoon representation. Isopeptide or peptide bond is indicated. C-terminal end of diUb chains is indicated. For simplification, only I44 and I36 residues are shown as spheres to represent the hydrophobic I44- and I36-patches, respectively. PDB ID: 1AAR (Cook* et al*, 1992), 2XK5 (Virdee* et al*, 2010), 3NOB (Matsumoto* et al*, 2010), 2JF5 and 2W9N (Komander* et al*, 2009b).*

The conformations of the diUb described above are often cited as the conformation adopted by these chains in a cellular setting. However, increasing evidence shows that these 'canonical' conformations only capture a snap shot of many conformations that polyUb chains can adopt in a cellular context. For example, other structures have also observed K48-diUb in 'open' conformations, where I44-patch of Ub moieties do not form any interface (Hirano *et al*, 2011). These different conformations of polyUb chains are in dynamic equilibrium as there is rapid interchange between 'open' and 'closed' conformations in solution (Vijay-Kumar *et al*, 1987; Hirano *et al*, 2011; Lai *et al*, 2012; Ryabov & Fushman, 2006). Moreover, more 'open' K11-diUb and more 'closed' K63- and M1-diUb conformations have also been observed (Bremm *et al*, 2010; Datta *et al*, 2009; Liu *et al*, 2015; Rohaim *et al*, 2012). In addition to this, when bound to UBDs and DUBs, these diUb chains adopt different conformations, highlighting the flexible nature of polyUb chains (Ye *et al*, 2012).

When I started this study, there was no crystal structure available for K27, K29 and K33 diUb. Molecular dynamics and modelling predicted that K27 chains adopt a 'closed' conformation, whereas K29 and K33 chain adopt 'open' conformations (Fushman & Walker, 2010). Validation of this model is challenging as we still lacked methods to assemble sufficient amount of K27, K29 and K33-linked polyUb (Chapter 1.9).

## 1.6 Deubiquitylating enzymes

Analogous to any PTMs, the robustness of ubiquitylation lies within the precision of its conjugation and deconjugation, which ensure that the appropriate signal is delivered at the right duration and timing. Deubiquitylating enzymes (DUBs) remove Ub or polyUb modification by catalysing the hydrolysis of (iso)peptide bonds between Ub and substrates or between Ub moieties within polyUb chains. Bioinformatics analysis estimates that human genome encodes ~90 Ub-specific DUBs (Clague *et al*, 2013).

Based on their catalytic mechanism, DUBs are classified into two main groups: Cys protease DUBs and metallo-protease DUBs (Komander *et al*, 2009a). Cys protease DUBs are characterised by their active site, which contain a catalytic triad composed of a nucleophilic Cys, a basic His and an acidic residue. The acidic residue functions to lower the $pK_a$ of the His to polarise and deprotonate the catalytic Cys for it to carry out a nucleophilic attack on the carbonyl of the scissile (iso)peptide bond. In contrast, metallo-protease DUBs are characterised by a zinc ion and a water molecule at the active site, which are coordinated by conserved residues. During catalysis, the zinc ion deprotonates and polarises water to carry out a nucleophilic attack. Some DUBs, however, have unproductive active site for efficient catalysis (Wolberger, 2014). This may be because the residues forming the catalytic triad are not well aligned or the entry to active site is occluded by intramolecular domain. These suggest that conformational changes are required to reorient the catalytic centre for efficient activity of DUBs.

### 1.6.1    Classification of DUBs

Based on their structural folds, DUBs can be classified into five main families: Ub C-terminal hydrolyses (UCH), Ub-specific proteases (USP), ovarian tumour proteases (OTU), Josephins and JAB1/MPN/MOV34 (JAMM) family. UCH, USP, OTU and Josephins are Cys-protease DUBs whereas JAMM is a zinc metallo-protease DUB.

### 1.6.1.1    UCH

In humans, the UCH family is made up of four members: UCH-L1, UCH-L3, UCH-L5/UCH37 and BAP1, which all have a ~230-residue catalytic domain. The structure of the UCH DUB family was first characterised in UCH-L3. The catalytic domain is organised in a bilobal structure (Johnston *et al*, 1997). The catalytic triad is located in the active-site cleft located between the two lobes. In the absence of Ub substrate, a disordered 'cross-over' loop masks the active-site cleft. Upon binding to Ub substrate,

this loop becomes ordered and circle around the active site, which provide additional binding site to the Ub (Johnston *et al*, 1999). In such a conformation, the C-terminal portion of ubiquitylated substrate has to thread through the loop to reach the active site to release monoUb and therefore, prevents the binding of large, folded Ub conjugates. UCH-L1 and UCH-L3 have shorter 'cross-over' loop and consequently, they cleave only small Ub conjugates (Larsen *et al*, 1998). It was observed in *in vitro* reactions that engineered UCH-L3 with longer 'cross-over' loop has an increased activity in cleaving polyUb chains (Popp *et al*, 2009). However, UCH-L5 and BAP1 that naturally have longer 'cross-over' loops in comparison to UCH-L1 and UCH-L3 remain inefficient in cleaving polyUb chains (Yao *et al*, 2006; Scheuermann *et al*, 2010). These demonstrate that the size of the 'cross-over' loop of UCH family does not explain their poor activity in cleaving polyUb chains. Interestingly, a recent study found that UCH-L3, UCH-L5 and BAP1 are efficient at cleaving isopeptide or peptide bonds between Ub and structured proteins, but not between polyUb chains (Bett *et al*, 2015). Thus, it was proposed that the 'cross-over' loop may be flexible and binding to polyUb may fix this loop in 'closed' conformation and thus, prevent polyUb to access the UCH-L3 active site.

### 1.6.1.2   USP

The USPs form the largest family of DUBs with ~56 USP members in human identified so far (Ye *et al*, 2009). The catalytic domains of USP members vary in size between 295 and 850 residues due to various insertions in-between conserved motifs. These insertions often fold into UBLs and UBDs, which potentially regulate the catalytic activity (Ye *et al*, 2009). Despite this variation, the catalytic domain of the USP family adopts a distinct fold characterised by three subdomains that resemble thumb, palm and fingers of a hand (Hu *et al*, 2002). The catalytic triad is located at the intersection of the thumb and palm domain, whereas the distal Ub binding site is formed by the fingers domain. For some USPs, in the absence of substrate, their catalytic triads are not in a productive state.

Binding to Ub substrate induces conformational changes on the active site of USP7 that brings the catalytic triad together for catalysis (Hu *et al*, 2002). In contrast, although the catalytic triad of USP14 is constitutively in its active conformation, a surface loop located in the palm domain blocks the active site, which is displaced by Ub binding (Hu *et al*, 2005). In addition, N terminus UBL domain mediates USP14 interaction with proteasome, which increases DUB activity by ~500-fold (Hu *et al*, 2005). Study of 12 USP DUBs reveal that intramolecular domains affect DUB activity of USPs, either affecting the catalytic turnover or Ub substrate binding or both (Faesen *et al*, 2011). It was also observed that USP DUBs are largely linkage promiscuous and will cleave polyUb chains of multiple linkage types. It is therefore thought that USPs catalyse removal of Ub from substrates.

### 1.6.1.3 OTU

In contrast to USP DUBs, OTU family DUBs display a high degree of specificity in hydrolysing polyUb chains of specific linkage types. Based on sequence conservation of the catalytic domain, 18 OTU DUBs can be classified into four sub-families: the Otubains (OTUB1 and OTUB2), the OTUDs (OTUD1, OTUD2, OTUD3, OTUD4, ALG13, OTUD5, OTUD6A and OTUD6B), A20-like OTUs (A20, VCPIP, OTUD7A, OTUD7B and TRABID) and the OTULINs (OTULIN and FAM105A) (Mevissen *et al*, 2013). The Otubains and the OTUs have a smaller catalytic domain of approximately 130-220 residues, whereas A20-like OTUs have a larger catalytic domain of 300-350 residues. OTU DUBs display high degree of specificity in hydrolysing polyUb chains *in vitro*, which has been observed in OTUB1 (K48) (Wang *et al*, 2009), OTUB2 (K48 and K63) (Edelmann *et al*, 2009), A20 (K48) (Komander & Barford, 2008), Cezanne (K11) (Bremm *et al*, 2010) and TRABID (K29 and K33) (Licchesi *et al*, 2011). However at higher concentration, the isolated catalytic domain of some of these DUBs becomes less linkage specific (Ritorto *et al*, 2014).

### 1.6.1.4 Josephin

In humans, there are four proteins that belong to the Josephin family of DUBs: Ataxin-3, Ataxin-3L, Josephin-1 and Josephin-2. They are characterised by the ~180-residue Josephin domain. Among these proteins, the catalytic Josephin domain is best studied in Ataxin-3. In addition to the catalytic domain, Ataxin-3 contains two UIMs, a stretch of polyGlu repeats, followed by a third UIM depending on the splice variants. The expansion of polyGlu repeats in Ataxin-3 leads to the neurodegenerative disorder Machado-Joseph Disease (Matos *et al*, 2011). Full-length Ataxin-3 preferentially cleaves K63 chains. However, when the MIU motifs were mutated or deleted, Ataxin-3 cleaves both K48 and K63 chains (Winborn *et al*, 2008; Nicastro *et al*, 2010). This suggests that Ataxin-3 linkage selectivity is somehow influenced by the UBDs. Solution structures reveals two distinct structures of Josephin domain in which an extended helical arm is proposed to regulate polyUb access to the active site (Mao *et al*, 2005; Nicastro *et al*, 2005).

### 1.6.1.5 JAMM

In humans, the single family of metalloprotease DUBs is made up of seven functional JAMM members. They are characterised by a catalytic domain that contains an active site composed of two histidines, an aspartate and a glutamate. These residues are key to coordinating a zinc ion and water molecule for hydrolysis. JAMM proteins are commonly part of large multimeric complexes. For example, RPN11/POH1 is part of the 19S proteasome (Yao & Cohen, 2002), CSN5 is part of the COP9 signalosome (Cope *et al*, 2002), and AMSH is in the endocytic ESCRT machinery (McCullough *et al*, 2004). BRCC36 is part of the BRISC complex which is involved in DNA repair (Cooper *et al*, 2009). Intriguingly most JAMM family DUBs, BRCC36, AMSH and AMSH-LP, are highly selective in cleaving K63-linked polyUb chains (McCullough *et al*, 2004; Cooper *et al*, 2009; Ritorto *et al*, 2014).

### 1.6.2 Ub-binding surfaces on DUBs

DUBs have distinct binding surfaces on their catalytic domain that mediate non-covalent interactions with Ub or polyUb chain substrates. The naming of these binding sites are based on the binding sites nomenclature on papain protease (Schechter & Berger, 1967). In this nomenclature, binding sites at the distal position of the active site is called S1, S2, etc whereas binding sites at the proximal position is called S1', S2', etc (Figure 1.8).
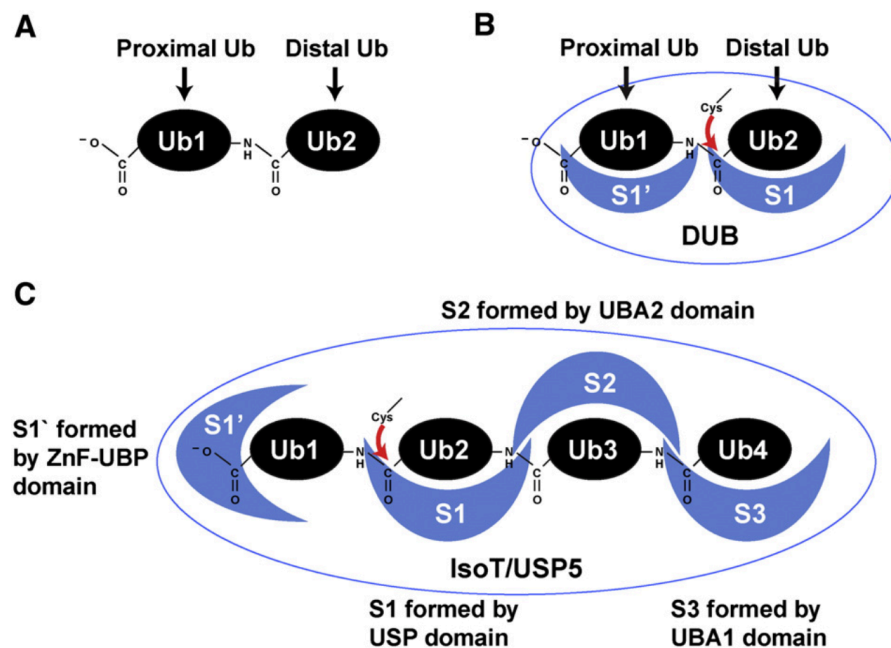


***Figure 1.8 Ubiquitin binding surfaces on DUBs***
*(A) A schematic diagram of diUb as in Figure 1.7A. (B) A general scenario of a Cys protease DUB cleaving diUb. Nomenclature of Ub-binding surfaces on DUBs is adapted from the actives site of Ser protease papain. Binding site at the distal position of the active site is called S1, whereas the binding site at the proximal position is called S1'. (C) Schematic diagram illustrates four Ub-binding sites on IsoT/USP5. Three of these are formed by Ub-binding domains: S1' site is formed by ZnF_UBP whereas S2 and S3 are formed by UBA domains. Figure is reproduced as a whole from (Eletr & Wilkinson, 2014).*

### 1.6.3   Exo-DUB and Endo-DUB

DUBs display various modes of action depending on the type of binding surfaces they contain. In general, DUBs can cleave polyUb from within chains and such DUBs are called endo-DUBs. In contrast, other DUBs can only cleave from either end of the chains, and such DUBs are called exo-DUBs (Figure 1.9).

Endo-DUBs position diUb on their S1' and S1 sites, stretching and stabilising the isopeptide bond across the active site. In addition to these S1-S1' sites, some endo-DUBs contains additional Ub-binding sites. For example, OTUD2 and Sars PLpro have been characterised to have additional S2 site, which allow them to cleave within polyUb chains releasing blocks of diUb (Békés *et al*, 2016; Flierman *et al*, 2016; Mevissen *et al*, 2013). Variations of endo-DUBs are ones that can cleave either monoUb or polyUb from substrates *en bloc*. These DUBs may bind Ub on their S1 site and lack the Ub-binding site on S1'. Instead, this S1' site can be occupied by substrate and thus, results in substrate-specific Ub cleavage.

Exo-DUBs may sense the position of Ub moieties within chains using their S1 or S1' site. One well-studied exo-DUB is IsoT/USP5 that cleaves polyUb from the proximal end of the chain (Figure 1.8C) (Wilkinson *et al*, 1995). A UBD called ZnF_UBP forms IsoT S1' site (Reyes-Turcu *et al*, 2006). ZnF_UBP specifically binds to the C-terminal tail of Ub (Figure 1.11D) and thus, senses the proximal end of the chain. Another example of an exo-DUB is USP14, which cleaves K48-linked polyUb from the distal end of the chain (Hu *et al*, 2005). Its S1 binding site senses the distal end of the chain by making contact with K48, which is available only at the distal end of the K48-linked chain.
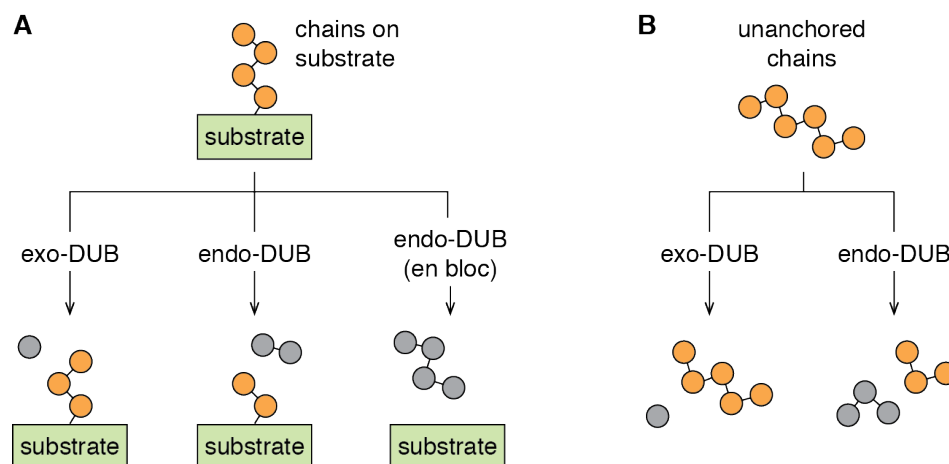
**Figure 1.9 Exo- and endo-DUB**
*(A-B) Schematic diagrams illustrate how exo-DUB and endo-DUB process polyUb chains conjugated on a substrate (A) or unanchored polyUb chain (B).*

### 1.6.4 Linkage selective DUB activity

Comprehensive analyses of linkage selective hydrolysis by DUBs have recently been made possible by the availability of diUb of all eight linkage types (see Chapter 1.9). Recent development of DUB assays coupled with MALDI-TOF MS analyses has enabled wide screening of linkage selectivity in DUBs (Ritorto *et al*, 2014). This study confirms that DUBs of the USP family cleave most of the diUb chains tested and do not have any linkage preference (Faesen *et al*, 2011). In addition to this, it confirms the linkage specific hydrolysis of some DUBs of the OTU family: OTULIN (M1) (Keusekotten *et al*, 2013), OTUB1 (K48) (Wang *et al*, 2009), Cezanne (K11) (Bremm *et al*, 2010), TRABID (K29, K33 and K63) (Licchesi *et al*, 2011; Virdee *et al*, 2010). This study also observed and confirmed the selective cleavage of K63 chains by DUBs of JAMM family: AMSH, AMSH-LP and BRCC36 (McCullough *et al*, 2004; *Sato et al*, 2008; Cooper *et al*, 2009).

In recent years several crystal structures of the DUB catalytic domain in complex with diUb have been determined (Sato *et al*, 2008; Keusekotten *et al*, 2013; Sato *et al*, 2015; Juang *et al*, 2012; Mevissen *et al*, 2016). These structures propose mechanisms of

how DUBs differentiate between linkage types. An emerging theme is that how proximal Ub is bound determines linkage-selective hydrolysis by DUB. Such a mechanism was first described for AMSH-LP, when the crystal structure of AMSH-LP in complex with K63 diUb was determined. There are two insertions within the core JAMM domain of AMSH-LP, and these insertions are conserved amongst all AMSH family members (Sato *et al*, 2008). Insertion 1 (S1) and Insertion 2 (S1') bind to distal and proximal Ub respectively. Mutating the S1' binding site does not affect K63-diUb binding, which means S1 is the primary site for diUb binding. Therefore, all type of diUb chains may come in contact with the catalytic domain of AMSH-LP as what has been observed in BRRC36, another JAMM DUB (Cooper *et al*, 2010). DiUb cleavage occurs only when S1' binds to K63 of proximal Ub and its surrounding residues, which stabilises the scissile isopeptide bond for hydrolysis.

Ub binding to S1' dictates M1 chain specific hydrolysis by OTULIN through a different mechanism (Keusekotten *et al*, 2013). In the absence of substrate, the active site of OTULIN is in an unproductive state. When M1-diUb binds, E16 and N2 residues of the proximal Ub (on the S1' site) induce rearrangement of the active site into a productive one. Recent crystal structure of Cezanne in complex to K11-diUb reveal another distinct mechanism (Mevissen *et al*, 2016). In the absence of substrate, Cezanne only has S1 site. When distal Ub binds, there is structural reorganisation that transiently forms S1' site. Efficient catalysis occurs only when K33 of the proximal Ub is in contact with E157 of the S1' site. This interaction can only occur when the diUb is linked via K11. This explain the preference of Cezanne to cleave K11 over K48 and K63, which all bind to Cezanne with similar binding affinity.

Molecular mechanisms of how DUBs differentiate and selectively cleave atypical Ub chains are yet to be determined. For example, how TRABID preferentially cleaves K29 and K33 chains over K63 chains remains to be elucidated (Licchesi *et al*, 2011;

Virdee *et al*, 2010). These mechanistic insights into how DUBs recognize polyUb highlight the value of polyUb chains in the biochemical and structural characterization of DUBs.

## 1.7 Ubiquitin binding domains

Once conjugated, Ub signals have to be coupled to specific cellular pathways and downstream signalling, which is mediated by proteins containing ubiquitin-binding domains (UBDs). There are several types of UBDs annotated to date and all these different domains bind to Ub to translate the ubiquitin signal.

Proteins with Ub-binding property was first described in S5a/Rpn10, a subunit of the 26S proteasome (Deveraux *et al*, 1994). It was discovered that this Ub-binding property is located within two conserved motifs, which was later termed as Ub-interacting motifs (UIMs) (Young *et al*, 1998; Hofmann & Falquet, 2001). Bioinformatics, biochemistry and biophysics analyses have expanded our knowledge and understanding of how UBDs work. For example, the Ub-associated (UBA) domain was initially identified as sequence motifs present in multiple proteins in the ubiquitylation pathway (Hofmann & Bucher, 1996). Later it was discovered that UBA-containing proteins are able to bind to Ub and polyUb chains (Bertolaet *et al*, 2001; Wilkinson *et al*, 2001). Nearly two decades after the discovery of the first two UBDs, now there are approximately 21 families of UBDs reported, which vary in size, structure and mode of binding to Ub. Based on their secondary structure, these UBDs can be classified into five groups: single or multiple α-helices, zinc fingers, plekstrin-homology (PH) fold, ubiquitin-conjugating-like, and other structures (Husnjak & Dikic, 2012).

## 1.7.1 Classification

### 1.7.1.1 Single or multiple alpha-helices

The simplest class of UBDs are characterised by the presence of one or more α-helices, which include UIM, MIU, UBA, CUE, GAT, UBAN and VHS domains. These α-helices form an interface that bind to the I44-patch of Ub (Figure 1.10).

UIM (Ub-interacting motif) and MIU (motif interacting with Ub) are the smallest among UBDs, composed of a single α-helix of ~20 residues (Hofmann & Falquet, 2001; Penengo *et al*, 2006). The palindromic nomenclature of UIM and MIU was chosen due to their conserved sequence motifs, which are the inverse of one another: xx##xxLxxALxΦSxx for UIM and xxDΦxLAxxLxx###x for MIU (Φ, hydrophobic; #, acidic; x, any residue) (Penengo *et al*, 2006). Although the residues of these motifs may vary, the central Ala is conserved in all UIM and MIU motifs. The interaction with Ub is centred on this key Ala, which when in complex with Ub is buried deep within the I44-patch of Ub. UIM and MIU both have a similar mode of binding to Ub although in an inverted orientation, which is explained by their inverted signature motifs. UIM-containing proteins are commonly involved in protein trafficking through their ability to bind to ubiquitylated cargoes, such as Epsin proteins (Shih *et al*, 2002).

UBA (Ub-associated), CUE (coupling of Ub to ERAD) and GAT (GGA and TOM1) are globular domains composed of three α-helices. The arrangement of the helices of UBA and CUE are similar, in which α1 and α3 helices bind to Ub I44-patch (Kang *et al*, 2003; Ohno *et al*, 2005). The three helices in GAT are longer than the one in UBA and CUE, and the binding interface with Ub I44-patch is formed by GAT α1 and α2 (Prag *et al*, 2005). UBA domains are found in various proteins involved in diverse Ub signalling (Hofmann & Bucher, 1996). For example in the two proteasomal shuttling factors Ubiquilin (hPLIC) and hHR23A (Kleijnen *et al*, 2000; Raasi *et al*, 2004).

The VHS (Vps27/Hrs/STAM) domain is a superhelical structure composed of eight α-helices, in which α2 and α4 bind to I44-patch of Ub (Ren & Hurley, 2010). VHS and GAT domains are commonly found in proteins that are involved in cellular trafficking pathways (Shields & Piper, 2011).

UBAN (Ub-binding in ABIN and NEMO) domain is composed of a parallel coiled-coil dimer, which has four Ub-binding sites (Rahighi *et al*, 2009). These allow UBAN to bind selectively to M1-linked polyUb chains (Figure 1.15). UBAN was found in ABIN and NEMO and the Ub binding properties of the UBAN domain is essential for NF-κB signalling.
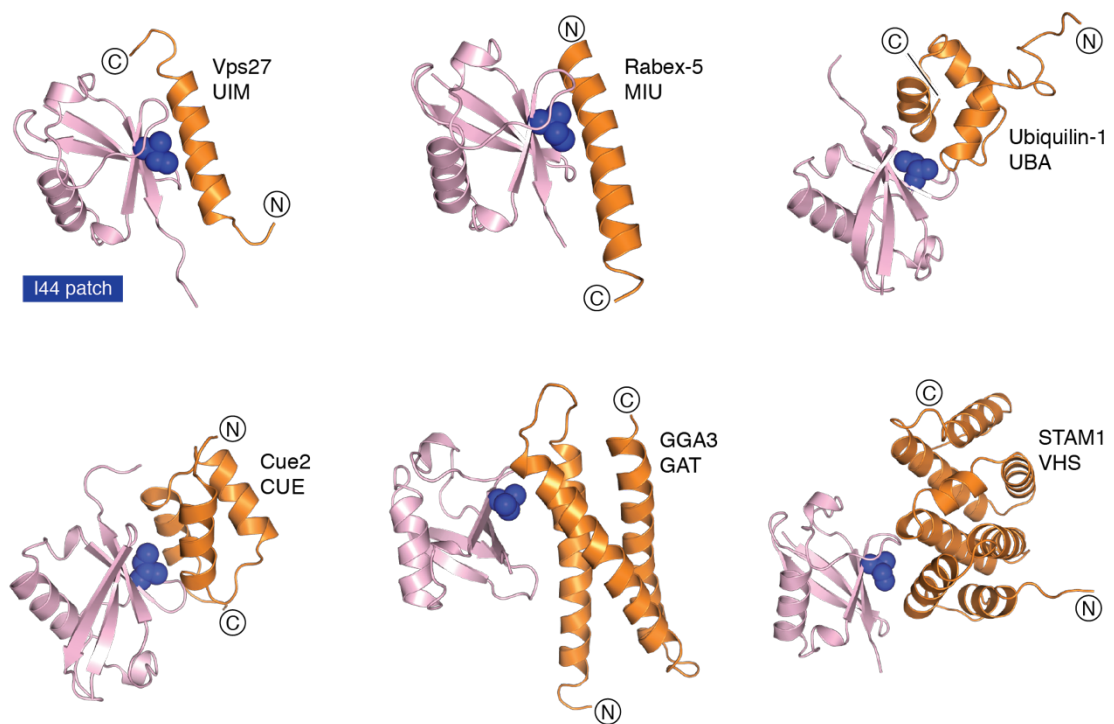


***Figure 1.10 Alpha-helical Ub-binding domains***
*Six members of alpha helical UBDs are shown in orange cartoon representation. N- and C-terminal ends are indicated. Ub is in pink cartoon. For simplicity, only I44 of Ub is shown as blue sphere to represent I44-patch (see also Figure 1.2). PDB ID: 1Q0W (Swanson* et al*, 2003), 2C7N (Penengo* et al*, 2006), 2JY6 (Zhang* et al*, 2008), 1OTR (Kang* et al*, 2003), 1YD8 (Prag* et al*, 2005) and 3LDZ (Ren & Hurley, 2010).*

### 1.7.1.2 Zinc fingers

The UBZ domain was first identified in the Y-family DNA polymerases η and κ, which are involved in translesion synthesis crucial for DNA replication bypassing DNA lesions (Bienko *et al*, 2005). It adopts a $C_2H_2$ zinc-finger structure with a C-terminal antiparallel β-sheet of two short β-strands and an N-terminal α-helix. The domain is stabilised by hydrophobic core interactions and a zinc ion coordinated by two Cys residues that sit on the β1-β2-loop and two His residues on the α-helix (Bomar *et al*, 2007). UBZ domain of Rad18 interacts with I44 patch of Ub with the α-helix and strand β1 (Figure 1.11A) (Rizzo *et al*, 2014).

A20-type ZnF (A20_ZnF) was first identified in A20 as a novel class of Ub ligases (Wertz *et al*, 2004). Not until later the Ub-binding property of A20_ZnF was observed in Rabex-5 (Mattera *et al*, 2006; Lee *et al*, 2006; Penengo *et al*, 2006). A20_ZnF is a $C_2C_2$ zinc-finger and structurally characterised by a C-terminal three-turn α-helix and an N-terminal region that lacks any secondary structure elements. Despite of this, intricate networks of hydrogen bonds stabilise the structure and coordinates the four conserved Cys residue to bind to Zn. The canonical interaction of A20_ZnF to Ub is entirely polar between the N-terminal portion of A20_ZnF and D58-patch of Ub (Figure 1.11B). In addition to this Ub-binding site, the fourth A20_ZnF on A20 (A20_ZnF4) has two additional Ub-binding sites that facilitate binding to K63-linked polyUb chains (Figure 1.14D) (Bosanac *et al*, 2010).
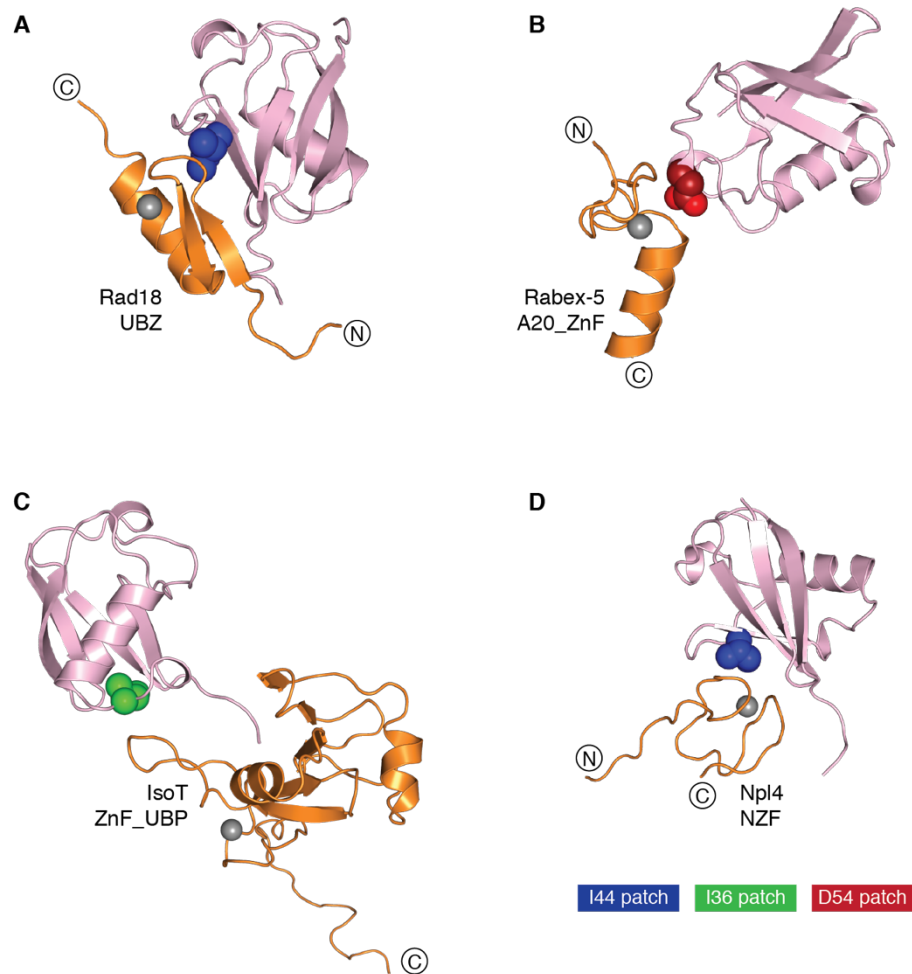
***Figure 1.11 Zinc finger Ub-binding domains***

*Four members of zinc finger UBDs are shown in orange cartoon representation. N- and C-terminal ends are indicated. Ub is in pink cartoon. For simplicity only one residue is displayed in spheres to represent hydrophobic patch on Ub: I44 (blue) for I44-patch, I36 (green) for I36-patch, and D58 (red) for D58-patch (see also Figure 1.2). PDB ID: 2MRE (Rizzo et al, 2014), 2C7N (Penengo et al, 2006), 2G45 (Reyes-Turcu et al, 2006) and 1Q5W (Alam et al, 2004).*

ZnF_UBP (Ub carboxyl-terminal hydrolase-like zinc-finger) domain was initially annotated for a region conserved in the USP family of DUBs and its ability to bind to unanchored monoUb and polyUb was first studied in cellular deacetylase MHAD6 (Seigneurin-Berny *et al*, 2001; Hook *et al*, 2002). Structurally, ZnF_UBP is characterised by a globular-fold structure composed of five anti-parallel β-strands and two α-helices (Reyes-Turcu *et al*, 2006). The conformation of the β-sheets and the α-1 helix forms a deep cleft that accommodates the C-terminal tail of Ub. In addition to this, β2-α1 loop,

which is stabilised by the interaction with zinc ion, interacts with I36 of Ub (Figure 1.11C). These contacts ensure selective binding of the UBD to unanchored Ub or polyUb that have their C terminus free and available for binding.

NZF (Npl4 zinc finger), first characterized in the VCP component Npl4, is a ~30 residue-domain characterised by two zinc-knuckle folds that coordinate a zinc ion (Alam *et al*, 2004). In addition to the four zinc-binding Cys residues, the NZF domain also contains a conserved TF-Φ motif, which forms the canonical binding surface that contact the I44-patch of Ub (Figure 1.11D). NZF domains of TAB2 and HOIL-1L highly selective in binding to K63 and M1 chains, respectively (Kanayama *et al*, 2004; Haas *et al*, 2009). These binding properties are essential for the activation of NF-κB signalling. Crystal structure reveals that these two linkage-selective UBDs possess additional binding surfaces in addition to the conserved NZF TF-Φ motif (Figure 1.14A-B) (Kulathu *et al*, 2009; Sato *et al*, 2009b; 2011). This underlying mechanism of selective binding will be discussed later in this section.

### 1.7.1.3   Plekstrin-homology (PH) fold

GLUE (GRAM-like ubiquitin-binding in EAP45) domain was first identified in EAP45 as a ubiquitin binding domain with a predicted secondary structure similar to phosphoinositide-binding GRAM and PH domains (Slagsvold *et al*, 2005). GLUE binds to the I44 patch of Ub through one edge of the beta-sheet, which is distinct from the proposed phosphoinositide-binding site (Figure 1.12) (Alam *et al*, 2006; Hirano *et al*, 2006b).

Another UBD that has a PH fold is Pru (pleckstrin-like receptor for ubiquitin) domain. Pru domain was first identified in Rpn13 through yeast two-hybrid screen using Ub lacking the last two glycines as bait (Husnjak *et al*, 2008). Rpn13 Pru domain is composed of four-stranded twisted antiparallel beta-sheet that packs almost orthogonally against a second triple-stranded beta-sheet, which is capped with an α-helix at the C-

terminal end (Schreiner *et al*, 2008). Unlike most of other UBDs, Rpn13 Pru binds to the I44 patch of Ub using an interface composed entirely of loops rather than ordered secondary structural elements (Figure 1.12). Rpn13 Pru domain also directly contacts the K48 linkage, thereby increasing the Pru-binding surface for K48-linked diUb chains as well as explaining the preference of Rpn13 in binding to the proximal Ub of K48-linked chains (Schreiner *et al*, 2008).
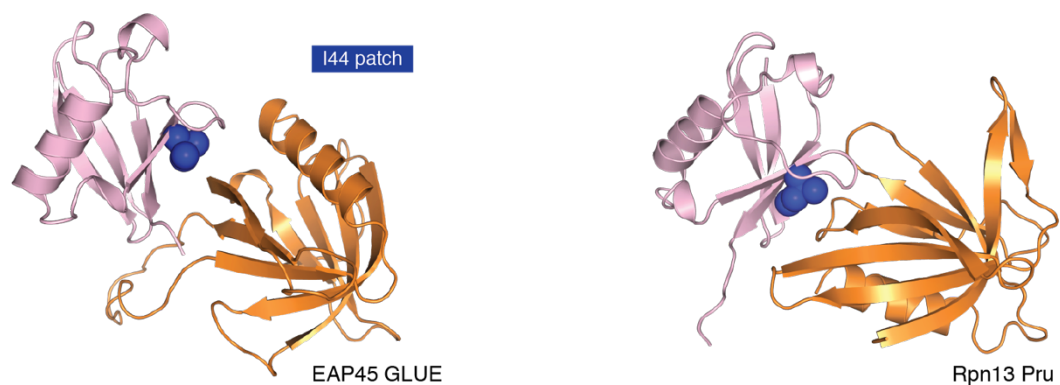


***Figure 1.12 Plekstrin homology fold Ub-binding domains***
*Two members of PH fold UBDs are shown in orange cartoon representation. Ub is in pink cartoon. For simplicity, only I44 residue is shown as blue spheres to represent I44-patch of Ub (see also Figure 1.2). PDB ID: 2HTH (Alam* et al*, 2006) and 2Z59 (Schreiner* et al*, 2008).*

### 1.7.1.4 Ubiquitin-conjugating-like

A region within the core α/β-fold domain of type I UBC, which is distinct from the catalytic active site, has been described in UBE2D3 E2 (also known as UbcH5c) to bind to monoUb (Brzovic *et al*, 2006). Here, the β-sheet region of UBE2D engages I44-patch of Ub (Figure 1.13A). Interestingly, this region is not conserved in all type I UBC and its composition defines its Ub-binding property. For example, UBE2L3 (also known as UbcH7) has an Arg at the position of UBE2D3 S22, which is buried deep in the interface. Consequently, UBE2L3 cannot bind to monoUb. The intact UBC-UBD domain is dispensable for monoubiquitylation, but is crucial for subsequent polyubiquitylation.

61

UBE2D3 S22R mutant that fails bind to Ub can no longer assemble polyUb chains (Brzovic *et al*, 2006).

Similarly, E2 variant (UEV) has also been described to bind to monoUb. UEV domain resembles UBC domain, but lacks the catalytic Cys. The UEV-UBD of TSG101 interacts with I44-patch of Ub primarily using a distinctive 'β-tongue', which is the loop of the extended β1-β2 strands (Figure 1.13B) (Sundquist *et al*, 2004). UEV domain of Vps23 also binds to monoUb using the canonical β-tongue structure (Teo *et al*, 2004). In contrast, the UEV domain of UBE2V1 (also known as Mms2) binds to monoUb using a β-sheet region, which is similar mode of binding as UBC-UBD (Figure 1.13C) (Eddins *et al*, 2006; Branigan *et al*, 2015). MonoUb binding property of UBE2V1 is crucial to orient K63 of the acceptor Ub to the catalytic Cys of UBE2N that leads to selective polyUb conjugation of K63 chain type.
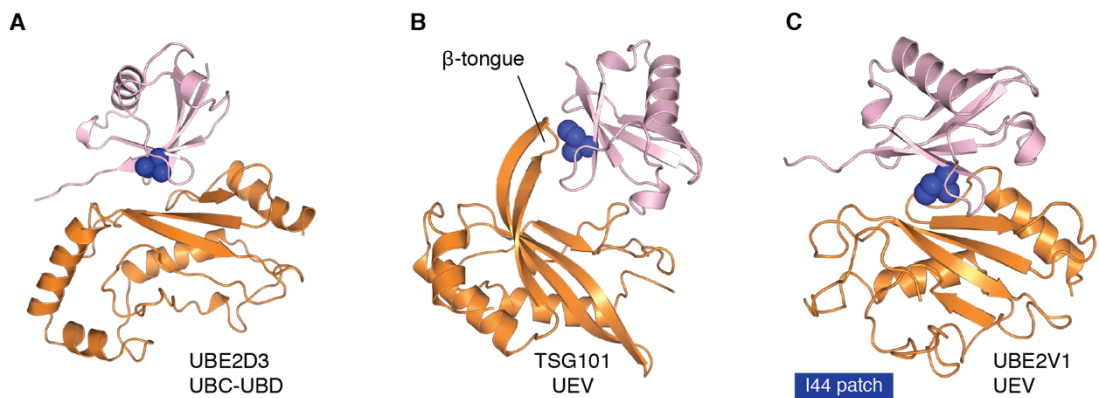


***Figure 1.13 Ub-conjugating like Ub-binding domains***
*Ub-conjugating like UBDs in UbcH5c (A), TSG101 (B) and Mms2 (C) are shown in orange cartoon representation. Ub is in pink cartoon. For simplicity, only I44 residue is shown as blue spheres to represent I44-patch of Ub (see also Figure 1.2). PDB ID: 2FUH (Brzovic* et al*, 2006), 1S1Q (Sundquist* et al*, 2004) and 2GMI (Eddins* et al*, 2006).*

### 1.7.1.5 Other structural classes

There are several UBDs that adopt secondary elements and folds that are distinct and cannot be classified into the four main classes described above. These UBDs include UBM (Bomar *et al*, 2010), PFU (Fu *et al*, 2009), Jab1/MPN (Bellare *et al*, 2006), WD40 repeat β-propeller (Pashkova *et al*, 2010) and SH3 domains (Stamenova *et al*, 2007; He *et al*, 2007).

### 1.7.2 Cooperative Ub binding by multiple UBDs

Binding affinities of individual UBDs to Ub are generally low with dissociation constants typically in the high micromolar range (Hurley *et al*, 2006). This mechanism may have evolved to prevent UBDs from randomly associating with Ub as the cellular concentration of Ub can be as high as ~85 μM (Kaiser *et al*, 2011). To compensate for this low binding affinity for UBDs, UBD-containing proteins are commonly found with multiple copies of UBDs (Husnjak & Dikic, 2012). For example, yeast Vps27 contains two UIM motifs arranged in tandem that are required for efficient binding to multi-monoubiquitylated sorting cargoes (Swanson *et al*, 2003). Similarly, Rabex-5 contains A20_ZnF and MIU motif that bind to two different patches on Ub, increasing its affinity for Ub (Penengo *et al*, 2006; Lee *et al*, 2006). Multiple UBDs also provide high binding avidity for polyUb chains. For example, the proteins STAM1 and STAM2 bind to polyUb proteins through tandem VHS domains and UIM motifs (Mizuno *et al*, 2003). Multiple VHS domains in ESCRT-0 are crucial for high-avidity binding to polyubiquitylated cargo (Ren & Hurley, 2010). In addition to this, UBD-containing proteins can oligomerize to form a protein complex, which cooperatively bind Ub and polyUb with higher binding affinity. This is observed in many UIM-containing proteins involved in protein trafficking. They have been shown to interact with each other, forming large protein complexes with multiple UBDs in the close proximity (Bache *et al*, 2003; Chen *et al*, 1998; Asao *et al*, 1997).

### 1.7.3   Specificity in polyubiquitin recognition by UBDs

Monoubiquitylation and polyubiquitylation signal to different cellular processes and UBDs-containing effector proteins have to be able to distinguish one from another. Some UBDs, for example IsoT ZnF_UBP, are able to bind both unanchored mono and polyUb chains of various linkage types (Figure 1.11C) (Reyes-Turcu *et al*, 2006). However, polyubiquitylation itself has many different flavours in cellular signalling and therefore, UBDs have to be able to distinguish between chain types, despite all types of polyUb chains being assembled from the same building block, Ub.

One factor that defines the linkage selective binding of UBDs is the flexible nature of polyUb chains (Chapter 1.5.3). Although they are all made from the same building block, the conformations of polyUb chains offer different orientations of binding patches that are uniquely recognised by UBDs (Figure 1.2 and Figure 1.7).

The other determining factor is the length of polyUb chains in cells, which is a big unanswered question in the field. For instance, it was first proposed that K48-tetraUb is the minimal signal for protein degradation (Thrower *et al*, 2000). However, a recent study suggests otherwise that multiple diUb across a protein is a more efficient degradation signal than a long polyUb chain on a single Lys (Lu *et al*, 2015). These observations suggest that there may be multiple mechanisms of how the length of polyUb chains are recognised. Furthermore, it was reported that unanchored K63 chains composed of minimally three Ub moieties can activate retinoic acid-inducible gene 1 (RIG-1) (Zeng *et al*, 2010). Indeed, some isolated UBDs bind to longer polyUb chains with relatively higher affinity than shorter chains (Raasi *et al*, 2004; Young *et al*, 1998; Rahighi *et al*, 2016; Burnett *et al*, 2003). Collectively, UBDs may have properties that allow them to distinguish between chain types and linkage types. Understanding these would be essential in decoding Ub signalling.

Despite these variations in properties offered by polyUb chains of different linkage types, the final determinant in selective polyUb binding lies within the UBDs themselves. The relatively weak affinity of UBDs to bind to a single Ub moiety requires them to bind to multiple Ub moieties within the same polyUb chain in order to achieve high-avidity interaction. This can be achieved by multiple Ub-binding sites present within a single UBD, in multiple repeats of UBD or a network of UBD-containing proteins.

Multi-sided UBDs have additional Ub-binding sites other than the conventional Ub-binding site, which defines the linkage selective binding to polyUb chains. This is best illustrated in the NZF domains of TAB2 and HOIL-1L. Although belong to the same type of zinc-finger UBDs, the NZF domains of TAB2 and HOIL-1L bind to two different chain types: K63 and M1, respectively (Sato *et al*, 2009b; Kulathu *et al*, 2009; Sato *et al*, 2011). These two NZF domains bind to distal Ub using an identical surface, namely the conserved TF-Φ motif (Figure 1.14A-B). The specificity lies in the different positioning of the proximal Ub on the second Ub-binding surface of NZF domains. Such binding orients K63 and M1 of the proximal Ub close to the C-terminal end of the distal Ub bound to TAB2 NZF and HOIL-1 NZF, respectively. The difference in the proximal Ub-binding sites of the two NZF domains allow binding to one type of polyUb chains, but not the other due to steric hindrance of C-terminal tail of Ub. Similarly, UBA2 of hHR23A binds to K48-diUb using two binding sites, and A20_ZnF4 binds to K63-triUb using three binding sites (Figure 1.14C-D) (Varadan *et al*, 2005; Bosanac *et al*, 2010).
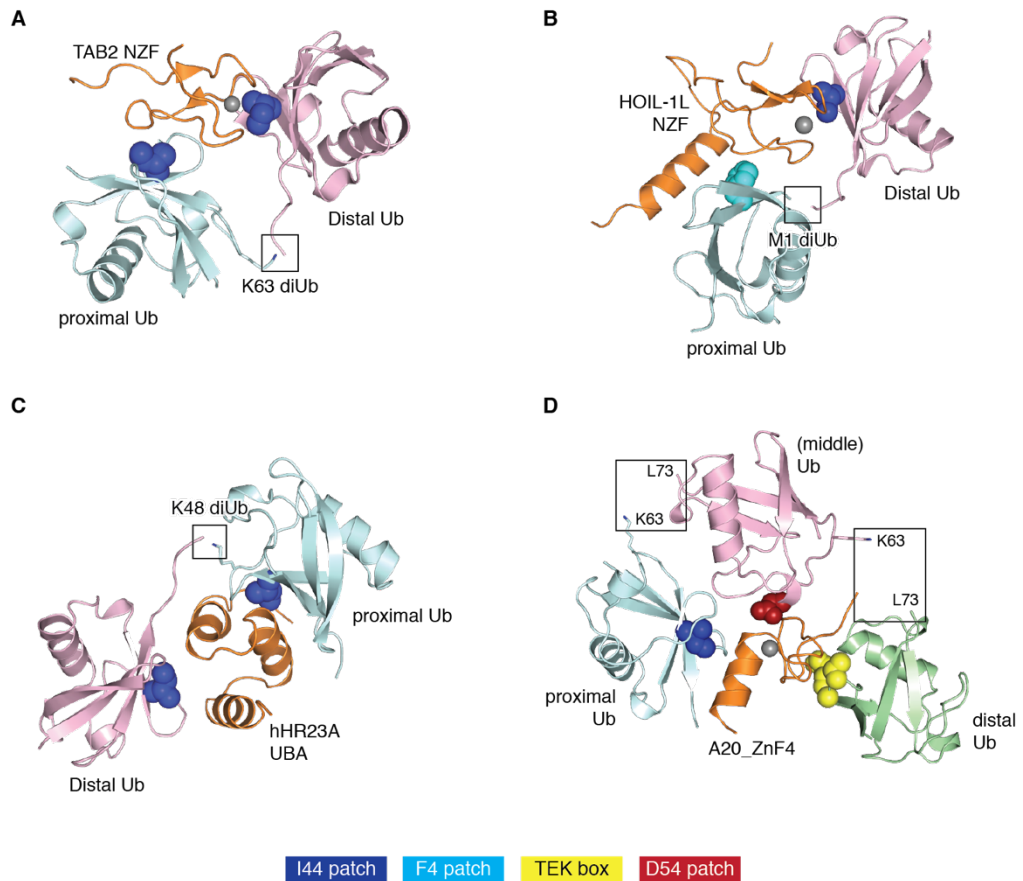
**Figure 1.14 Multiple Ub-binding sites on Ub-binding domains**
*(A) TAB2 NZF in complex with K63-diUb. (B) HOIL-1L NZF in complex with M1-diUb.
(C) hHR23A UBA2 in complex with K48-diUb. (D) A20_ZnF4 in complex with three Ub
moieties. L73 of the distal Ub is pointing towards K63 of the proximal Ub, indicating
K63 isopeptide bonds (box). UBDs (orange), distal Ub (pink) and proximal Ub (light
cyan) are in cartoon representation. For simplicity only one residue is displayed in
spheres to represent one hydrophobic patch on Ub: I44 (blue) for I44-patch, F4 (cyan)
for F4-patch, and D58 (red) for D58-patch. TEK box is indicated as yellow spheres (see
also Figure 1.2). PDB ID: 2WWZ (Kulathu et al, 2009), 3B08 (Sato et al, 2011), 1ZO6
(Varadan et al, 2005) and 3OJ3 (Bosanac et al, 2010).*

Similarly, the selective binding to M1-linked polyUb chains by the UBAN domain

of NEMO is mediated by multiple binding sites (Figure 1.15B). The parallel coiled-coil

dimer of UBAN forms four Ub-binding sites that accommodate two molecules of M1-

diUb on either side of the coiled-coil dimer (Rahighi *et al*, 2009). UBAN binds to the I44

patch of the distal Ub and F4 patch of the proximal Ub. In addition to this, linker region

between two Ub moieties was also engaged, ensuring exclusive binding to M1-linked polyUb chains.
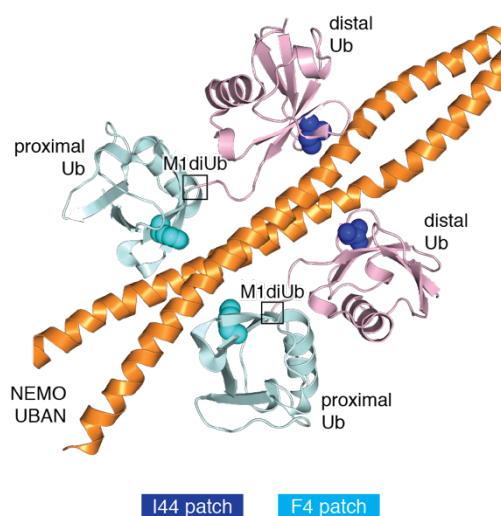


***Figure 1.15 M1-linkage selective binding by NEMO UBAN domain***
*NEMO UBAN (orange), distal Ub (pink) and proximal Ub (light cyan) are in cartoon representation. For simplicity, only I44 (blue) and F4 (cyan) are shown in spheres to represent I44- and F4-patches of Ub, respectively (see also Figure 1.2). PDB ID: 2ZVO (Rahighi* et al*, 2009).*

In some UBDs, multiple Ub-binding sites are provided from two UBDs arranged in tandem. These are observed in S5a tUIM binding to K48-diUb and in Rap80 tUIM binding to K63-diUb (Figure 1.16) (Zhang *et al*, 2009; Sato *et al*, 2009a). Each UIM binds to the I44-patch of Ub using the canonical binding mode. The linker in between two UIMs determine the orientation of Ub-binding surfaces so that only certain conformations of polyUb chains can bind. Whilst the linker region of Rap80 tUIM forms a continuous helical structure, the linker separating two UIM motifs in S5a adopts distinct region of extra loops and an α-helix (Figure 1.16). Consequently, the orientation of the two UIMs of S5a is flexible to engage more conformations of polyUb chains. Indeed, S5a tUIM can also bind to K63-diUb (Wang *et al*, 2005). In contrast, Rap80 tUIM is highly specific in binding to K63 chains (Sims & Cohen, 2009; Sato *et al*, 2009a). Altering the orientation of the two Ub-binding sites by increasing or decreasing the length of the linker in Rap80

tUIM, compromise the tMIU linkage-selective binding to polyUb. These examples highlight the strategies that UBDs have evolved to recognize the different ubiquitin signals and provide insights into how the same molecule Ub can function in so many different biological pathways.
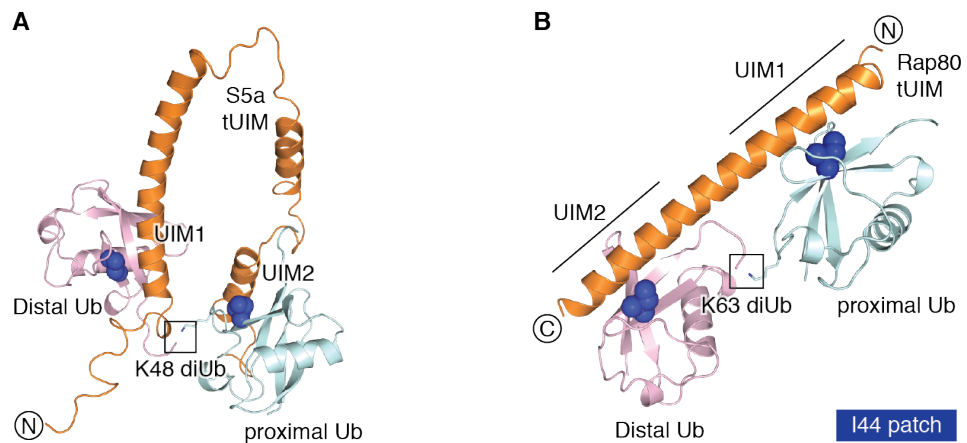


**Figure 1.16 Multiple Ub-binding sites in tandem UIMs**
*(A) S5a tUIM in complex with K48-diUb. (B) Rap80 tUIM in complex with K63-diUb. UBDs (orange), distal Ub (pink) and proximal Ub (light cyan) are in cartoon representation. For simplicity only I44 residue is shown as blue spheres to represent I44-patch of Ub (see also Figure 1.2). PDB ID: 2KDE (Zhang et al, 2009) and 3A1Q (Sato et al, 2009a)*

## 1.8   UBDs as tools to study Ub signalling

Linkage-specific Ub antibodies are valuable tools to study cellular signalling (Newton *et al*, 2008; Matsumoto *et al*, 2010; 2012). However, making these antibodies are challenging and not widely available for all types of polyUb chains. Enriching polyubiquitylated proteins by pulldown is very effective to study Ub signalling. For this purpose, UBDs that have high binding affinity for monoUb have been used to enrich both monoUb and polyUb chains from cells (Bennett *et al*, 2007; Kaiser *et al*, 2011). In contrast, linkage-selective UBDs have been essential to isolate particular chain types from cells (Emmerich *et al*, 2013). Being used as affinity reagents to capture cellular

polyUb is only one of many application of UBDs (Scott *et al*, 2014), which are discussed in the following section.

To increase their affinity for polyUb chains, UBDs can be used in multiple copies in tandem, and such synthetic domain fusions are called tandem ubiquitin-binding entities (TUBEs) (Hjerpe *et al*, 2009). TUBEs based on multiple copies of hHR23A UBA or Ubiquilin-1 (UQ1) UBA have 100- to 1000-fold higher affinity binding to K48 and K63 tetraUb in comparison to the single UBA domain. Alternatively, UBDs can be used as a single entity to isolate cellular Ub. UBDs such as UBA of Ubiquilin-1 (Zhang *et al*, 2008), ZnF_UBP of IsoT (Reyes-Turcu *et al*, 2006), UBAN domain of NEMO (Rahighi *et al*, 2009) and NZF domain of TAB2 (Kulathu *et al*, 2009) intrinsically have high affinity for Ub or polyUb chains and can be used as single entity Ub binders.

TUBEs or UBDs have been used in various studies to understand Ub signalling. For instance, Ubiquilin-2 (UQ2) UBA was used to capture Ub chains from Huntington's disease (HD) models and patients samples to dissect Ub system in HD pathology (Bennett *et al*, 2007). UQ2 UBA and IsoT ZnF_UBP in combination with MS-analyses were used to quantify levels of polyUb and Ub in various tissues and cells (Kaiser *et al*, 2011). Linkage selective NEMO UBAN (M1) and TAB2 NZF (K63) were used to investigate the role of hybrid M1/K63 polyUb chains in NF-κB activation (Emmerich *et al*, 2013).

In addition to being used as affinity reagents of polyUb, TUBEs or UBDs have been used as molecular sensors for polyUb chains in vivo. Here, a fluorescent tag is fused to linkage selective UBDs such as TAB2 NZF and Rap80 tUIM for the detection of K63 chains and NEMO UBAN for the detection of M1 chains (van Wijk *et al*, 2012; Sims *et al*, 2012). They are expressed in cells and used to monitor localisation and accumulation of specific types of polyUb chains in response to different cell stimuli. These sensors were used to confirm the role of K63-linked polyUb chains in DNA damage response

following DNA double-strand breaks, and in mitochondrial-specific autophagy (van Wijk *et al*, 2012).

One consequence of expressing exogenous UBD sensors in cells is that they may sequester and protect polyUb chains from deconjugation or degradation, thereby function as dominant negative inhibitors (Hjerpe *et al*, 2009; Sims *et al*, 2012; van Wijk *et al*, 2012). The inhibitory effect of linkage-selective UBDs have been exploited to study the role of certain types of polyUb chains in cellular signalling. The expression of the M1-specific NEMO UBAN based-sensor inhibited nuclear accumulation of p65 (RelA) after 15 min of TNFα stimulation whereas the expression of K63-specific TAB2 NZF based-sensor did not (van Wijk *et al*, 2012). These suggest that M1 but not K63 chains are essential in TNFα-mediated NF-κB signalling. Thus, UBD-based sensors can be applied to selectively inhibit and thus dissect Ub-dependent signalling.

## 1.9   Methods for enzymatic assembly of polyUb chains

Polyubiquitin chains come in many flavours that vary in linkage types and lengths to regulate various cellular processes. To understand such complexity, many researchers are trying to characterise the biochemical and biophysical properties of polyUb chains. For example, how they are selectively recognised by UBDs and cleaved by DUBs; what are the structural properties of different chains. To address these questions, we need large quantities of polyUb chains of defined lengths and linkage types. These can be achieved by chemical or enzymatic approaches. Classically, enzymatic approaches were used by Cecile Pickart and co-workers to generate large amounts of K48 and K63-linked chains (Cook *et al*, 1992; Hofmann & Pickart, 2001). Such established methods accelerated our understanding of K48 and K63 linkages. In contrast, for some time, enzyme systems capable of assembling the other linkage types were unknown and hence studying the property of other chain types was challenging.

70

To pioneer progress, several laboratories have established chemical biology approaches to make diUb of all linkage types. In general, chemical methods to assemble polyUb chains involve preparation of reactive Ub precursors, which are ligated by native chemical ligation (Hemantha & Brik, 2013). Using chemical methods, diUb of all linkage types were assembled (Virdee *et al*, 2010; Kumar *et al*, 2010; Virdee *et al*, 2011). Despite this success, several challenges limit chemical synthesis of polyUb chains and are therefore not widely accessible to all researchers. Synthesis of the Ub building blocks generally require special treatment. Moreover, to generate isopeptide bonds of interest, exceptional chemical tools are required (Hemantha & Brik, 2013). Furthermore, it is challenging to prepare long polyUb chains that involves several rounds of chemical reactions. Collectively, chemical synthesis of polyUb chains may be expensive, laborious and may not be easily applied in many laboratories.

An attractive alternative to chemical synthesis is enzymatic conjugation of polyUb chains. This method utilises natural enzymatic Ub conjugation cascades involving Ub, E1 and E2 or E2-E3. An E1 activates donor Ub in the presence of ATP and the specific E2 or E2-E3 catalyses Ub conjugation to specific Lys of the acceptor Ub (Chapter 1.3). Enzymatic synthesis was pioneered by Pickart and co-workers that used chain selective E2-25K to generate K48-linked polyUb chains (Cook *et al*, 1992). Similar methods were applied for the assembly of K63 chains using UBE2N-UBE2V1 E2 pairs (Hofmann & Pickart, 2001). The discovery of linkage-selective E2s and E3s have been exploited to assemble other chain types, including K6 and K11 (Lin *et al*, 2010; Baboshina & Haas, 1996; Hospenthal *et al*, 2013; Castañeda *et al*, 2013; Bremm *et al*, 2010; Dong *et al*, 2011). The enzymatic assembly methods can be divided into two, based on the precursor Ub molecules: mutant Ub and wildtype Ub.

### 1.9.1   Enzymatic conjugation using mutant Ub

The advantage of using Ub mutants is that polyUb chain can be assembled in a controlled manner. This is beneficial when only a particular length of polyUb chain is required. Furthermore, precise control of assembly allows isotope labelling of Ub in specific position within the chains (Varadan *et al*, 2002; Castañeda *et al*, 2013; Hospenthal *et al*, 2013). In addition to this, by using the precise controlled reaction, mutations can also be introduced to any specific Ub within the chain (Reyes-Turcu *et al*, 2008).

To control the product of polyUb chain synthesis, two different Ub mutants were used: Ub$^{D77}$ as acceptor Ub, and Ub$^{K48C}$ as donor Ub (Pickart & Raasi, 2005). The acceptor Ub$^{D77}$ has an Asp capping the C-terminal tail of Ub. As G76 is crucial for Ub activation by E1, masking this residue by an Asp prevents this Ub$^{D77}$ mutant to enter Ub conjugation cascade. Therefore, this mutant serves as an acceptor Ub that provides its Lys residue for the conjugation site. On the other hand, the donor Ub$^{K48C}$ has K48 mutated to a Cys and therefore, this Ub cannot be used as conjugation site in K48 chain assembly. The donor Ub mutant is tailored based on the linkage type of polyUb chains is to be assembled. For example, when K63 chains are assembled, the donor Ub$^{K63C}$ mutant is used. In the end of the enzymatic reaction, a uniform diUb is produced: diUb$^{UbD77-UbK48C}$.

In the next process, the produced diUb is deblocked that will yield wildtype diUb product. Removing D77 from the proximal Ub is necessary for the next reaction when diUb is used for making longer chains. This is done by treating the diUb with the yeast protease Ub hydrolase-1 (YUH1). YUH1 is a yeast DUB of UCH family that cleaves small adducts like Asp from C-terminal end of Ub. To deblock K48C of the distal Ub, the chain is treated with ethyleneimine. This chemical reacts with the Cys residue and converts C48 to form a S-aminoethylcysteine, which mimic a lysine residue and reacts as distally deblocked moiety. The result of such deblocking reactions enable further reactions to assemble longer polyUb chains.

By varying the enzyme components of the assembly reaction, various chain types can be generated. UBE2S was used to assemble K11 chains (Castañeda *et al*, 2013) whereas UBE2L3 and HECT E3 NleL were used to assemble K6 chains (Hospenthal *et al*, 2013). UBE2S produces K48 in addition to K11 and thus, to obtain pure K11 chains, K48R mutation was introduced to both acceptor and donor Ub. Similarly, K63R mutation was introduced to obtain pure K6 chains from UBE2L3-NleL conjugation reaction.

There are several disadvantages of using Ub mutants. It is a laborious process involving expression of various Ub mutants and deblocking treatments. Ub chains are rather sticky, and therefore it is prone to lose sample in each step of purification. Moreover, mutations introduced to Ub may have some yet undescribed effect on the properties of the chains.

### 1.9.2   Enzymatic conjugation using wildtype Ub

The main difference in polyUb conjugation when wildtype Ub is used as main precursor is the outcome of the conjugation reaction. Whilst a reaction containing acceptor and donor Ub mutants produces a uniform chain length, a reaction containing wildtype Ub produces polyUb chains of varying lengths. These chains of different lengths can be separated using ion exchange and size exclusion chromatography.

As described above, some E2 or E2-E3 pair also produces unwanted or contaminating chains types. Several studies have applied linkage selective DUBs to remove these chains. The contaminating K63 chains produced by UBE2S were cleaved by including AMSH in the reaction, producing pure K11 chains (Bremm *et al*, 2010). Similarly, OTUB1 was included to cleave K48 chains assembled by NleL and UBE2L3 to produce pure K6 chains (Hospenthal *et al*, 2013).

The advantage of using wildtype Ub is that chains of various lengths can be generated at ease. These longer Ub chains are valuable tools to study binding affinity of UBD to polyUb chains of different length (Chapter 4). In addition, they can be used to

study DUB activity in cleaving chains of varying length (Chapter 5). Another advantage is that cheap commercially available Ub can be used to produce milligram quantities of polyUb. However, there are also some disadvantages to this method. Since Ub chains assembly cannot be controlled, we cannot label or mutate Ub at specific positions within the chains. In addition to this, chains longer than tetraUb may be difficult to separate due to limits in the resolution of cation exchange chromatography.

Both enzymatic conjugation methods rely on specific E2 or E2-E3 pairs that target Lys residue in the conjugation process. Methods to enzymatically assemble M1, K6, K11, K48 and K63 have been developed as enzymes used for their assembly are well characterised. When I started the studies presented in this thesis, there were no methods available to enzymatically assemble K29 and K33 chains.

## 1.10 Research questions and aim of the thesis

Polyubiquitylation is a versatile post-translational modification that regulates diverse cellular processes. Among the eight types of polyUb chains that can be assembled, K48 and K63 are the most well studied chain types. Proteins modified with K48 polyUb chains are targeted for proteasomal degradation whereas K63 polyUb chains are non-proteolytic signal in DNA damage response and immune signalling pathway. In contrast, the cellular roles of K29 and K33 remain poorly understood.

The study of these atypical chain types is hampered by the lack of method to assemble large quantities of K29 and K33 chains for biochemical and biophysical characterisation. When I started this study, there were no crystal structures available for K29 and K33 chains and how these chains are selectively recognised by UBDs was unknown. Therefore, I began this study aiming to develop methods to assemble K29 and K33 chains enzymatically. Having been able to assemble large quantity of pure chains, I then aimed to characterise UBDs that can selectively bind to K29 and K33 chains. I

identified TRABID NZF1 as a K29 and K33-linkage selective UBD. To understand the underlying mechanisms of linkage-selective binding, I aimed to determine the crystal structure of K29 in complex with TRABID NZF1. In addition, I also aimed to determine the crystal structure of K29-diUb and K33-diUb in the absence of binding protein. Finally, I aimed to use TRABID NZF1 to enrich K29-linked polyUb chains from mammalian cells. This work is presented in Chapter 3.

When investigating other small UBDs, our laboratory discovered that the tandem MIU motifs (tMIU) of an uncharacterised protein FAM63A selectively binds to K48 chains and not to other linkage types. MIU binding to monoUb has been characterised but the molecular mechanism underlying how MIU binds to and distinguishes between different polyUb chain types is poorly understood. Therefore, I aimed to get a mechanistic understanding of how FAM63A tMIU selectively binds to K48 chains (Chapter 4).

In addition to tMIU, FAM63A also contains an uncharacterised domain that cleaves K48 chains. Sequence and structural analysis of this domain reveal a novel fold architecture distinct from other known families of DUBs. Thus, our lab classified FAM63A as a novel DUB family called MINDY (MIU-containing novel DUB family). At the time of the discovery, the catalytic property of FAM63A MINDY DUB was elusive. Therefore, it was my aim to biochemically characterise the DUB activity of FAM63A (Chapter 5).

# 2 Materials and Methods

## 2.1 Reagents

### 2.1.1 Chemicals and consumables

Ethanol, glycerol, glycine, 4-(2-Hydroxyethyl)piperazine-1-ethanesulfonic acid (HEPES), isopropanol, methanol, β-mercaptoethanol (β-ME), sodium chloride (NaCl), sodium ethylenediaminetetraacetic acid (EDTA), magnesium acetate, magnesium chloride (MgCl), sodium ethylene glycol tetra acetic acid (EGTA), sodium fluoride, sodium 2-glycerophosphate, sodium orthovanadate, adenosine 5'-triphosphate sodium salt (ATP), ammonium bicarbonate, ammonium persulphate (APS), bovine serum albumin (BSA), dimethyl sulphoxide (DMSO), iodoacetamide, phenylmethanesulphonylfluoride (PMSF), benzamidine, Ponceau S, sodium dodecyl sulphate (SDS), sodium tetraborate, tetramethylethylenediamine (TEMED), Triton-X-100, Tween-20, Nonidet P40 (NP40) substitute, Bovine serum albumin (BSA), ampicillin, kanamycin, dithiothreitol (DTT), isopropyl β-D-1-thiogalactopyranoside (IPTG), MG132, sodium azide, chicken egg lysozyme, tris(2-carboxyethyl)phosphine (TCEP), Ubiquitin from Bovine, Flag-M2 resins were from Sigma-Aldrich (Poole, UK). InstantBlue coomassie stain was from Expedeon (Cambridge, UK). HaloLink resin was from Promega (Wisonsin, USA). PreScision Plus protein markers and Bradford reagent were from BioRad (Herts, US). 40% (w/v) 29:1 Acrylamide: Bis-Acrylamide solution was from Flowgen Bioscience (Humberside, UK). Glutathione Sepharose 4B resins, Talon resins, PD-10 Desalting Columns (Sephadex G-25), Enhanced chemiluminescence (ECL) kit and Hyperfilm MP and were purchased from GE Healthcare (Piscataway, USA). X-ray films were from Konica (Japan). Dulbecco's modified eagle medium (DMEM), Opti-MEM reduced serum media, Dulbecco's phosphate buffered saline

(PBS), Trypsin/EDTA solution, sodium pyruvate, L-glutamine, non-essential amino acids and HEPES buffer, Precast NuPAGE Novex SDS polyacrylamide 4-12% Bis-Tris gels and NuPAGE MES running buffer (20X) were from Invitrogen (Paisley, UK). Cell culture dishes and flasks, cryovials and Spin-X columns were from Corning (NY, USA). Cell scrapers were from Costar (Cambridge, USA). Polyethylenimine (PEI) was from Polysciences (Warrington, PA). Skimmed milk (Marvel) was from Premier Beverages (Stafford, UK). Plasmid Maxiprep kits were from Qiagen Ltd (Crawley, UK). Acetonitrile (HPLC grade) was from Rathburn Chemicals (Walkerburn, UK). Trypsin (mass spectrometry grade) was from Promega (Southampton, UK). SnakeSkin Dialysis Tubing (3.5 kDa MWCO), Slide-A-Lyzer Dialysis Cassette (3.5 and 10 kDa), Silver-staining kit were from was from Thermo-Scientific (Essex, UK). Amicon concentrators 4 ml and 15 ml with MWCO of 4 and 10 kDa were from Merck Millipore (Darmstadt, Germany). IRDye® 800CW Maleimide was from LiCOR Biosciences (Cambridge, UK). Luria Bertani broth (LB), LB agar plates and 2xTY media were provided by the Central Technical Services team, University of Dundee.

### 2.1.2 Antibodies

Anti-Ub used to detect recombinant Ub in *in vitro* assays (U5379) and anti-Flag (F3165) were purchased from SIGMA. Anti-Ub used to detect Ub captured from mammalian cells was from DAKO (Z0458). Anti-HA was from Cell Signalling Technology (#3724).

### 2.1.3  Buffers

General buffers used in this study and their composition are listed in Table 2.1.

*Table 2.1 Composition of buffers used in this study*

| Buffer | Composition |
|---|---|
| Competent *E. coli* cells | |
| TB buffer | 250 mM KCl, 15 mM CaCl$_2$, 55 mM MnCl$_2$ and 10 mM PIPES pH 6.8 |
| TBD buffer | 7% (v/v) DMSO in TB buffer |
| GST-tagged protein purification | |
| GST lysis buffer | 50 mM Tris-HCl pH 7.5, 300 mM NaCl, 10% glycerol, 0.075% 2-mercaptoethanol, 1 mM benzamidine, 1 mM AEBSF, 100 µg/ml lysozyme and protease inhibitor cocktail |
| GST high salt buffer | 25 mM Tris-HCl pH 7.5, 500 mM NaCl and 1 mM DTT |
| GST low salt buffer | 25 mM Tris-HCl pH 7.5, 150 mM NaCl, 10% glycerol and 1 mM DTT |
| His-tagged protein purification | |
| His lysis buffer | 25 mM Tris-HCl pH 7.5, 300 mM NaCl, 1 mM AEBSF, 10 mM imidazole, 100 µg/ml lysozyme, 500 µM TCEP and protease inhibitor cocktail |
| His wash buffer | 25 mM Tris-HCl pH 7.5, 300 mM NaCl and 10 mM imidazole |
| His elution buffer | 25 mM Tris-HCl pH 7.5, 300 mM NaCl and 200 mM imidazole |
| In-vitro assays | |
| Ub reaction buffer | 50 mM Tris-HCl pH 7.5, 10 mM MgCl$_2$, 0.6 mM DTT and 10 mM ATP |
| Pulse buffer | 50 mM Tris-HCl pH 7.5, 10 mM MgCl$_2$, 0.6 mM DTT and 3 mM ATP |
| Chase buffer | 50 mM Tris-HCl pH 7.5, 10 mM MgCl$_2$ and 0.6 mM DTT |
| DUB buffer | 50 mM Tris-HCl pH 7.5, 50 mM NaCl and 10 mM DTT |
| Chromatography | |
| GFC buffer | 50 mM Tris, 150 mM NaCl and 2 mM DTT |
| ResS buffer A | 50 mM sodium acetate pH 4.5 |
| ResS buffer B | 50 mM sodium acetate pH 4.5 and 1 M NaCl |
| ResS buffer C | 10 mM ammonium acetate pH 4.5 |
| ResS buffer D | 10 mM ammonium acetate pH 4.5 and 1 M NaCl |
| ResQ buffer A | 50 mM Tris-HCl pH 8.5 |
| ResQ buffer B | 50 mM Tris-HCl pH 8.5 and 1 M NaCl |
| Mammalian lysis | |
| Freeze-thaw lysis buffer | 20 mM HEPES pH 7.5, 110 mM potassium acetate, 2 mM magnesium acetate, 1 mM EGTA, 1 mM sodium ortho-vanadate, 1 mM NaF, 0.1% NP-40, 1 mM AEBSF, 25 mM iodoacetamide, 0.02% benzonase and protease inhibitor cocktail |
| MRC lysis buffer | 50 mM Tris-HCl pH 7.5, 1 mM EDTA, 1 mM EGTA, 50 mM sodium fluoride, 5 mM sodium pyrophosphate, 10 mM sodium 2-glycerophosphate, 1 mM sodium orthovanadate, 0.27 M sucrose, 1% (v/v) Triton X-100, 1 mM PMSF, 1 mM benzamidine, protease inhibitor cocktail and 25 mM iodoacetamide |
| Halo-tag coupling | |
| Halo coupling buffer | 50 mM Tris-HCl pH 7.5, 150 mM NaCl, 0.05% NP-40 substitute and 1 mM DTT |
| Halo pulldown buffer | 50 mM Tris-HCl pH 7.5, 150 mM NaCl, 0.1% NP-40, 1 mM DTT and 0.5 mg/ml BSA |
| Halo wash buffer | 50 mM Tris-HCl pH 7.5, 250 mM NaCl, 0.2% NP-40 and 1 mM DTT |
| SDS-PAGE and Immunoblotting | |
| Stacking gel (4%) | 125 mM Tris-HCl pH 6.8, 0.1% (w/v) SDS, 4% (w/v) acrylamide (w/v), 0.1% ammonium persulfate (APS) and 0.1% (v/v) TEMED |

| Resolving gel (8-15%) | 375 mM Tris-HCl pH 8.6, 0.1% (w/v) SDS, 8-15% (w/v) acrylamide (w/v), 0.1% ammonium persulfate (APS) and 0.1% (v/v) TEMED |
|---|---|
| Tris-glycine SDS-PAGE running buffer | 25 mM Tris-HCl pH 8.3, 192 mM glycine and 0.1% (w/v) SDS |
| Tris-glycine transfer buffer | 25 mM Tris-HCl pH 8.3, 192 mM glycine and 20% (v/v) methanol |
| Denaturing buffer | 25 mM Tris-HCl pH 7.5, 6 M guanidium chloride and 1 mM DTT |
| TBS-Tween (TBST) | 20 mM Tris-HCl pH 7.6, 140 mM NaCl and 0.2% (v/v) Tween-20 |
| Others | |
| ITC buffer | 50 mM Hepes pH 7.5, 150 mM NaCl and 250 μM TCEP |

### 2.1.4 Crystallisation screens

Morpheus was from Molecular Dimension (Suffolk, UK). Index Screen, Crystal Screen I & II, PEG/Ion, Salt Rx, ProPlex were purchased from Hampton Research (Aliso Viejo, CA). Pi Minimal and JCSG ++ were from Jena Bioscience (Germany).

## 2.2 Equipment

Bacterial incubators were from Infors (Reigate, UK). Centrifuge tubes, rotors and centrifuges were from Beckmann Coulter (Palo Alto, USA). The digital sonicator was from Branson (Danbury, CT). ÄKTA pure chromatography system, Superdex 200 10/300, Superdex 75 16/600, Resource S 6 ml, Mono S 1 ml, Resource Q 1 ml and MicroCal iTC$_{200}$ were from GE Healthcare (Piscataway, NJ). MicroCal PEAQ-ITC was from Malvern Instruments (Worcestershire, UK). The BioPhotometer spectrophotometer, Thermomixer IP shakers and bench-top centrifuge were purchased from Eppendorf (Cambridge, UK). SpeedVacs were from CHRIST (Osterode, Germany). HPLC system components were obtained from Dionex (Camberley, UK). pH meters and electrodes were from Horiba (Kyoto, Japan). Power packs for electrophoresis, Trans-Blot Cells and automatic western blot processors were from BioRad (Herts, UK). Mini gel talk electrophoresis system was from Atto (Tokyo, Japan). X-Cell SureLock Mini-cell electrophoresis systems and X-Cell II Blot modules were from Invitrogen (Paisley, UK).

The Konica automatic film processor was from Konica Corporation (Japan). The LiCOR odyssey infrared imaging system was from LiCOR Biosciences (Cambridge, UK). The 96- well Versamax plate reader was from Molecular Devices (Wokingham, UK). The NanoDrop was from Thermo Scientific (Essex, UK). CO2 incubators were from Mackay and Lynn (Dundee, UK). Tissue culture class II safety cabinets were from Medical Air Technology (Oldham, UK). The Mosquito Crystal, Dragonfly liquid handling robot and consumables were from TTP Labtech (Herts, UK).

## 2.3 Molecular biology

### 2.3.1 Preparation of competent *E. coli* cells (performed by Dr Thomas Macartney and Andrew Davies)

*E. coli* strain DH5α (Invitrogen) was used for DNA cloning and BL21(DE)pLysS (Promega) was used for recombinant protein expression. Transformation-competent *E. coli* cells were prepared using Inoue method (Sambrook & Russell, 2010). Commercial DH5α or BL21 cells were streaked on an LB plate and incubated overnight at 37 °C. A single colony was inoculated into 4 ml LB medium and grown overnight at 30 °C. This culture was then transferred into 500 ml LB medium and grown at 30 °C until the culture reaches $OD_{600}$ of 0.35-0.45. Cells were harvested in 8 × 50-ml Falcon tube by centrifugation at 2000 *g* for 8 min at 4 °C. Supernatant was carefully removed and each cell pellet was re-suspended in 10 ml pre-chilled sterile *TB buffer*. Cells were collected by centrifugation at 2000 *g* for 8 min at 4 °C. After supernatant had been removed, each cell pellet was re-suspended in 10 ml pre-chilled sterile *TBD buffer*. Cells were aliquoted in 1.5-ml tubes, snap-frozen and stored in -80 °C.

### 2.3.2 Plasmid DNA transformation into competent *E. coli* cells

For each transformation, 100-200 ng of plasmid DNA was mixed with 50 µl of competent DH5α or BL21 cells (Chapter 2.3.1), which has been thawed on ice. Cells were incubated on ice for 10 min and heat-shocked at 42 °C for 45 sec. After 2-min recovery on ice, cells were streaked on LB plate containing 100 µg/ml ampicillin or 50 µg/ml kanamycin and incubated at 37 °C overnight.

### 2.3.3 Plasmid DNA amplification and isolation

To amplify plasmid DNA, a single colony of the transformed DH5α (Chapter 2.3.2) was inoculated into 200 ml of LB media containing 100 µg/ml ampicillin or 50 µg/ml kanamycin. Cell culture was grown overnight at 37 °C with a constant agitation at 180 rpm. Cells were then, harvested by centrifugation at 3400 *g* for 30 min at 4 °C and the plasmid DNA was isolated using Qiagen DNA Midi or Maxi kit according to the manufacturer's instructions. The concentration of isolated plasmid was quantified using a NanoDrop spectrophotometer at an absorbance of 260 nm.

### 2.3.4 DNA cloning (performed by molecular DNA cloning team in DSTT)

Most of the recombinant plasmid DNA constructs used in this study were generated by Dr Simone Weidlich and Dr Rachel Toth. Some DNA constructs were generated by Dr Nicola Wood, Dr Melaine Wightman, Dr Mark Peggie and Dr Thomas Macartney. All recombinant DNA procedures, restriction digests and ligations were performed using standard protocols. All PCR reactions were carried out using KOD Hot Start DNA polymerase (Novagen). To insert or delete large portion of gene, Q5 Site-Directed Mutagenesis Kit (NEB) was used. Sequences of all DNA constructs are verified by the DNA Sequencing Service (School of Life Sciences, University of Dundee). All DNA constructs encode human sequence unless indicated.

For recombinant protein expression in bacteria, DNA constructs were made in backbones of the following expression vectors: pGEX6P for GST-tagged protein, pET28 for 6His-tagged protein and pET15b for the untagged Ub constructs (Table 2.2). For insect cells expression, 6His-tagged UBE1 was made in pFB-HTB vector and GST-tagged UBE3C constructs was made in pFastBac vectors (Table 2.3). All mammalian expression constructs were made in pcDNA5/FRT/TO vector backbone (Table 2.4).

***Table 2.2 DNA constructs for protein expression in bacteria***
*All recombinant GST-tagged proteins were cleaved off from the tag, except those indicated with asterisks. Alias indicates how the construct may be referred in the thesis. The sources of purified proteins are indicated. PPAD, Protein production and assay development team.*

| Protein | Expressed | Alias | DU number | Protein purification |
|---|---|---|---|---|
| UBE3C | GST UBE3C 691-1083 | | 45901 | This study |
| UBE3C | GST UBE3C 636-1083 | | 45902 | This study |
| UBE3C | GST UBE3C 716-1083 | | 45317 | This study |
| UBE3C | GST HA UBE3C 691-1083 | | 49092 | This study |
| UBE3C | GST HA UBE3C 716-1083 | | 49093 | This study |
| UBE3C | GST HA UBE3C 636-1083 (C1051A) | | 49096 | This study |
| | | | | |
| UBE2D1 | 6His UBE2D1 | UbcH5a | 4315 | PPAD |
| UBE2D2 | 6His UBE2D2 | UbcH5b | 20184 | PPAD |
| UBE2D3 | 6His UBE2D3 | UbcH5c | 15703 | PPAD |
| UBE2L3 | 6His UBE2L3 | UbcH7 | 12798 | PPAD |
| UBE2R1 | 6His UBE2R1 | Cdc34 | 4317 | PPAD |
| UBE2S | GST UBE2S (2-195) + IsoT ZnF UBP (173-289) | UBE2S-UBP | 20647 | This study |
| | | | | |
| Ubiquitin | Ubiquitin | Ub WT | 51721 | PPAD |
| Ubiquitin | Ubiquitin K6R | Ub K6R | 23830 | PPAD |
| Ubiquitin | Ubiquitin K11R | Ub K11R | 23831 | PPAD |
| Ubiquitin | Ubiquitin K27R | Ub K27R | 23832 | PPAD |
| Ubiquitin | Ubiquitin K29R | Ub K29R | 23833 | PPAD |
| Ubiquitin | Ubiquitin K33R | Ub K33R | 23834 | PPAD |
| Ubiquitin | Ubiquitin K48R | Ub K48R | 20042 | PPAD |
| Ubiquitin | Ubiquitin K63R | Ub K63R | 20029 | PPAD |
| Ubiquitin | Ubiquitin K29only | Ub K29only | 24369 | PPAD |
| | | | | |
| ITCH* | GST ITCH M1-E862 (full length) | | 11097 | PPAD |
| AREL1 | GST KIAA0317 E437-L823 | | 45348 | This study |
| SMURF1* | GST SMURF1 M1-E754 (full length) | | 19628 | PPAD |
| SMURF2* | GST SMURF2 M1-E748 (full length) | | 19879 | PPAD |
| HECW1 | GST HECW1 Y1223-E1606 | | 45771 | PPAD |
| HUWE1* | GST HUWE1 S3760-A4374 | | 43501 | PPAD |
| WWP1* | GST WWP1 A2-E921 (full length) | | 19746 | PPAD |
| WWP2* | GST WWP2 M1-E870 | | 19786 | PPAD |
| NleL | GST NleL S170-R782 | | 45299 | This study |
| HOIP | GST HOIP Q697-K1072 | HOIP RBR-LDD | 22629 | PPAD |
| Cezanne | GST Cezanne N124-S438 | | 45327 | This study |
| Cezanne | GST Cezanne N124-S438 E287K E288K | Cezanne EK | 45353 | This study |
| TRABID | 6His TRABID L245-S697 | | 22468 | PPAD |
| OTUB1 | GST OTUB1 M1-K271 (full length) | | 19741 | PPAD |
| vOTU | GST vOTU M1-S183 | | 45351 | This study |

| | | | | |
|---|---|---|---|---|
| OTULIN | GST OTULIN | | 43487 | PPAD |
| AMSH | GST AMSH | | 44746 | This study |
| OTUB2* | GST OTUB2 | | 32795 | PPAD |
| USP2 | GST USP2(Rat) 271-618 6His | | 35832 | This study |
| | | | | |
| hHR23B | GST Halo hHR23B T186-D407 | hHR23B UBA1-2 | 49626 | This study |
| hPLIC1 | GST Halo Ubiquilin-1 Q539-Q587 | hPLIC1 UBA | 49634 | This study |
| Rap80 | GST Halo Rap80 Q78-D125 | Rap80 tUIM | 55032 | This study |
| Epsin-15 | GST Halo EPS15 S851-E895 | Epsin-15 tUIM | 49822 | This study |
| TRABID | GST TRABID G3-S33 | TRABID NZF1 | 23225 | This study |
| TRABID | GST Halo TRABID E3-N178 | TRABID NZF1-3 | 24214 | This study |
| TRABID | GST Halo TRABID E3-Q110 | TRABID NZF1-2 | 49556 | This study |
| TRABID | GST Halo TRABID M82-E187 | TRABID NZF2-3 | 24485 | This study |
| TRABID | GST Halo TRABID E139-E187 | TRABID NZF1 | 24486 | This study |
| TRABID | GST Halo TRABID M82-T113 | TRABID NZF2 | 24487 | This study |
| TRABID | GST Halo TRABID E139-E187 | TRABID NZF3 | 24486 | This study |
| Npl4 | GST Halo TAB2 D663-F693 | Npl4 NZF | 49635 | This study |
| TAB2 | GST Halo TAB2 D663-F693 | TAB2 NZF | 49635 | This study |
| | | | | |
| HOIL-1L | GST Halo HOIL-1L 192-222 | | 47212 | Syed Arif |
| Neil3 | GST Halo Neil3 316-346 | | 47173 | Syed Arif |
| RNF31 | GST Halo RNF31 349-379 | RNF31 1o2 | 47261 | Syed Arif |
| RNF31 | GST Halo RNF31 408-438 | RNF31 2o2 | 47185 | Syed Arif |
| RYBP | GST Halo RYBP 20-50 | | 47187 | Syed Arif |
| SHARPIN | GST Halo Sharpin 347-377 | | 47213 | Syed Arif |
| SOLH | GST Halo SOLH 2-32 | SOLH 1o5 | 47170 | Syed Arif |
| SOLH | GST Halo SOLH 43-73 | SOLH 2o5 | 47214 | Syed Arif |
| SOLH | GST Halo SOLH 142-172 | SOLH 3o5 | 47215 | Syed Arif |
| SOLH | GST Halo SOLH 339-369 | SOLH 4o5 | 47183 | Syed Arif |
| SOLH | GST Halo SOLH 411-441 | SOLH 5o5 | 47269 | Syed Arif |
| YAF2 | GST Halo YAF2 18-48 | | 47165 | Syed Arif |
| ZRAB2 | GST Halo ZRAB2 9-40 | ZRAB2 1o2 | 47175 | Syed Arif |
| ZRAB2 | GST Halo ZRAB2 65-95 | ZRAB2 2o2 | 47176 | Syed Arif |
| RANBP2 | GST Halo RANBP2 1351-1381 | RANBP2 1o2 | 47172 | Syed Arif |
| RANBP2 | GST Halo RANBP2 1414-1444 | RANBP2 2o2 | 47174 | Syed Arif |
| NUP153 | GST Halo NUP153 657-687 | | 47171 | Syed Arif |
| MDM4 | GST Halo MDM4 300-330 | | 47262 | Syed Arif |
| | | | | |
| FAM63A | GST Halo FAM63A Q388-Q426 | FAM63A tMIU | 47443 | This study |
| FAM63A | GST Halo FAM63A Q388-Q426 A416G | FAM63A tMIU A416G | 47712 | This study |
| FAM63A | GST Halo FAM63A Q388-Q426 A396G | FAM63A tMIU A396G | 47985 | This study |
| FAM63A | GST Halo FAM63A Q388-Q403 | FAM63A MIU1 | 55039 | This study |
| FAM63A | GST Halo FAM63A G406-Q426 | FAM63A MIU2 | 47422 | This study |
| FAM63A | GST Halo FAM63A G406-Q426 A416G | FAM63A MIU2 A416G | 47512 | This study |
| | | | | |
| FAM63A | GST Halo FAM63A Q388-Q403 + linker (QSQEINWEQIPE) + FAM63A G409-Q426 | FAM63A tMIU (linker QSQEINWEQIPE) | 48000 | This study |
| FAM63A | GST Halo FAM63A Q388-Q403 + linker (SGSGS) + FAM63A G409-Q426 | FAM63A tMIU (linker SGSGS) | 55001 | This study |
| FAM63A | GST Halo FAM63A Q388-Q426 P404A P407A | FAM63A tMIU (linker ARGAL) | 55020 | This study |
| FAM63A | GST Halo FAM63A Q388-Q403 + linker (AAAAA) + FAM63A G409-Q426 | FAM63A tMIU (linker AAAAA) | 55044 | This study |
| | | | | |
| FAM63A | GST Halo FAM63A Q388-Q426 L408A | FAM63A tMIU L408A | 55225 | This study |
| FAM63A | GST Halo FAM63A Q388-Q426 T411A | FAM63A tMIU T411A | 55241 | This study |
| FAM63A | GST Halo FAM63A Q388-Q426 D412A | FAM63A tMIU D412A | 55259 | This study |
| FAM63A | GST Halo FAM63A Q388-Q426 L413A | FAM63A tMIU L413A | 47703 | This study |
| FAM63A | GST Halo FAM63A Q388-Q426 E414A | FAM63A tMIU E414A | 55226 | This study |
| FAM63A | GST Halo FAM63A Q388-Q426 L415A | FAM63A tMIU L415A | 47711 | This study |
| FAM63A | GST Halo FAM63A Q388-Q426 A416G | FAM63A tMIU A416G | 47712 | This study |
| FAM63A | GST Halo FAM63A Q388-Q426 A416S | FAM63A tMIU A416S | 47762 | This study |

83

| | | | | | |
|---|---|---|---|---|---|
| FAM63A | GST Halo FAM63A Q388-Q426 A416D | FAM63A tMIU A416D | 55396 | This study |
| FAM63A | GST Halo FAM63A Q388-Q426 Q418A | FAM63A tMIU Q418A | 55227 | This study |
| FAM63A | GST Halo FAM63A Q388-Q426 Q418K | FAM63A tMIU Q418K | 55358 | This study |
| FAM63A | GST Halo FAM63A Q388-Q426 L419A | FAM63A tMIU L419A | 47708 | This study |
| FAM63A | GST Halo FAM63A Q388-Q426 Q420A | FAM63A tMIU Q420A | 55242 | This study |
| FAM63A | GST Halo FAM63A Q388-Q426 Q421E | FAM63A tMIU Q421E | 47827 | This study |
| FAM63A | GST Halo FAM63A Q388-Q426 Q421R | FAM63A tMIU Q421R | 47828 | This study |
| FAM63A | GST Halo FAM63A Q388-Q426 E422A | FAM63A tMIU E422A | 55395 | This study |
| FAM63A | GST Halo FAM63A Q388-Q426 E423A | FAM63A tMIU E423A | 55243 | This study |
| FAM63A | GST Halo FAM63A Q388-Q426 Y424A | FAM63A tMIU Y424A | 47721 | This study |
| FAM63A | GST Halo FAM63A Q388-Q426 Y424D | FAM63A tMIU Y424D | 47767 | This study |
| FAM63A | GST Halo FAM63A Q388-Q426 Y424E | FAM63A tMIU Y424E | 47759 | This study |
| FAM63A | GST Halo FAM63A Q388-Q426 Y424F | FAM63A tMIU Y424F | 47760 | This study |
| FAM63A | GST Halo FAM63A Q388-Q426 Y424W | FAM63A tMIU Y424W | 47768 | This study |
| | | | | |
| FAM63A | GST Halo FAM63A Q408-Q426 L408A | FAM63A MIU2 L408A | 55463 | This study |
| FAM63A | GST Halo FAM63A Q408-Q426 T411A | FAM63A MIU2 T411A | 28668 | This study |
| FAM63A | GST Halo FAM63A Q408-Q426 L415G | FAM63A MIU2 L415G | 47513 | This study |
| FAM63A | GST Halo FAM63A Q408-Q426 Q418A | FAM63A MIU2 Q418A | 55428 | This study |
| FAM63A | GST Halo FAM63A Q408-Q426 Q421A | FAM63A MIU2 Q421A | 55429 | This study |
| FAM63A | GST Halo FAM63A Q408-Q426 E422A | FAM63A MIU2 E422A | 55430 | This study |
| FAM63A | GST Halo FAM63A Q408-Q426 L419A | FAM63A MIU2 L419A | 47583 | This study |
| | | | | |
| FAM63A | GST FAM63A Q388-Q426 | FAM63A tMIU | 49555 | This study |
| FAM63A | GST FAM63A Q386-Q406 | FAM63A MIU1 | 47865 | This study |
| FAM63A | GST FAM63A G406-Q426 | FAM63A MIU2 | 47848 | This study |
| | | | | |
| FAM63A | GST Halo FAM63A Q388-Q426 (ΔE423) | FAM63A tMIU (-1) | 55221 | This study |
| FAM63A | GST Halo FAM63A Q388-Q426 E423 + A + Y423 | FAM63A tMIU (+1) | 55295 | This study |
| FAM63A | GST Halo FAM63A Q388-Q426 E423 + AAA + Y424 | FAM63A tMIU (+3) | 55222 | This study |
| FAM63A | GST Halo FAM63A Q388-Q426 E423 + AAAAAA + Y424 | FAM63A tMIU (+6) | 55223 | This study |
| FAM63A | GST Halo FAM63A Q388-Q426 E423 + AAAAAAA + Y424 | FAM63A tMIU (+7) | 55224 | This study |
| | | | | |
| FAM63B | GST Halo FAM63B G507-Q559 | FAM63B tMIU | 47515 | This study |
| FAM63B | GST Halo FAM63B G507-Q559 A546G | FAM63B tMIU A546G | 47758 | This study |
| FAM63B | GST Halo FAM63B G507-Q559 A519G | FAM63B tMIU A519G | 55074 | This study |
| FAM63B | GST Halo FAM63B G507-Q526 | FAM63B MIU1 | 55019 | This study |
| FAM63B | GST Halo FAM63B Q535-Q559 | FAM63B MIU2 | 47542 | This study |
| FAM63A/ FAM63B (hybrid) | GST Halo FAM63A G409-Q426 + linker (PRGPL) + FAM63A G409-Q426 | FAM63A MIU2 + FAM63A MIU2 (linker PRGPL) | 55043 | This study |
| FAM63A/ FAM63B (hybrid) | GST Halo FAM63B G507-Q526 + linker (PRGPL) + FAM63A G409-Q426 | FAM63B MIU1 + FAM63A MIU2 (linker PRGPL) | 55040 | This study |
| FAM63A | GST FAM63A 1-469 | FAM63A FL | 49563 | This study |
| FAM63A | GST FAM63A 110-380 | FAM63A cat | 47257 | This study |
| YPL191C | GST YPL191C 1-360 | YPL191C FL | 47420 | This study |
| Ubiquitin | GST Cys-Ubiquitin K48R | Cys-Ubiquitin K48R | 47729 | This study |
| Ubiquitin | GST Cys-Ubiquitin 1-75 | Cys-Ubiquitin 1-75 | 47779 | This study |
| Ubiquitin | GST Ubiquitin G75A/G76A | Ubiquitin G75A/G76A | 49488 | This study |
| Ubiquitin | GST Cys-Ubiquitin K48R | Cys-Ubiquitin K48R | 47729 | This study |
| Ubiquitin | GST Cys-Ubiquitin 1-75 | Cys-Ubiquitin 1-75 | 47779 | This study |

*Table 2.3 cDNA constructs for protein expression in insect cells*

| Protein | Expressed | DU number | Protein purification |
|---|---|---|---|
| UBE1 | 6His UBE1 | 32888 | PPAD |
| UBE3C | GST UBE3C Q641-S1083 | 45301 | PPAD |

*Table 2.4 cDNA constructs for protein expression in mammalian cells*

| Protein | Expressed | Alias | DU number |
|---------|-----------|-------|-----------|
| TRABID | 3XFlag TRABID WT | TRABID FL-WT | 49067 |
| TRABID | 3xFlag TRABID C443A | TRABID FL-C443A | 49089 |
| TRABID | 3XFLAG TRABID 1-187 | TRABID NZF1-3 | 24389 |
| TRABID | 3XFlag TRABID 1-245 | TRABID NZF1-3+ | 49140 |
| TRABID | 3XFlag TRABID 1-113 | TRABID NZF1-2 | 24391 |
| TRABID | 3XFlag TRABID 82-187 | TRABID NZF2-3 | 24390 |
| TRABID | 3XFlag TRABID 1-33 | TRABID NZF1 | 24394 |
| TRABID | 3XFlag TRABID 82-113 | TRABID NZF2 | 24393 |
| TRABID | 3XFlag TRABID 139-187 | TRABID NZF3 | 24392 |

## 2.4 Recombinant protein expression and purification

### 2.4.1 General recombinant protein expression in *BL21 E. coli* cells

Plasmid DNA was transformed in *E. coli* BL21 and the cells were streaked on LB plate containing 100 µg/ml ampicillin or 50 µg/ml kanamycin as describe in Chapter 2.3.2. A single colony was inoculated in 50 ml 2xTY media and grown overnight at 37 °C. From this culture, 10 ml was transferred to 1000 ml 2xTY media and the cells were grown at 37 °C until the culture reached $OD_{600}$ of 0.6-0.8. Protein expression was then induced by adding IPTG to a final concentration of 300 µM and the culture was incubated at 16 °C for 16 h. When zinc-binding proteins like NZF domain were expressed, protein expression in bacterial culture was supplemented with 200 µM $ZnCl_2$. Bacterial culture was then centrifuged at 3400 *g* for 15 min at 4 °C and the supernatant was discarded. The cell pellet was re-suspended in lysis buffer according to the protein-tag (Chapter 2.4.4 and 2.4.3). Alternatively, the cell pellet was frozen and stored at -80 °C for future use. To freeze cells, the cell pellet was re-suspended in PBS, transferred to 50-ml Falcon tube and centrifuged at 3500 *g* for 30 min. Supernatant was then discarded and the cell pellet was snap frozen in liquid nitrogen and stored at -80 °C.

### 2.4.2 General recombinant protein expression in Sf21 insect cells (completed by Clare Johnson)

For protein expression in insect cells, recombinant GST-fusion UBE3C (641-1083) was expressed in Sf21 cells using Bac-to-Bac baculovirus expression system (Invitrogen). Sf21 cells cultured at 27 °C in Insect Xpress medium (Lonza) supplemented with Antibiotic-Antimycotic (Invitrogen) were infected with P1 virus stocks and harvested 60 h later. Cells were lysed in Lysis Buffer (50 mM Tris-HCl pH 7.5, 5% glycerol, 0.1 M EDTA, 0.1 mM EGTA, 1 mM DTT, 1 mM Pefabloc and 20 µg/ml Leupeptin) using Dounce homogenizer, then centrifuged to remove insoluble material. Cell lysates were processed as described below (Chapter 2.4.3 and 2.4.4).

### 2.4.3 General GST-tagged protein purification

Cell pellets of bacteria expressing recombinant GST-tagged proteins (Chapter 2.4.1) were re-suspended in *GST lysis buffer* and incubated on ice for 15 min. Cells were lysed by sonication and cell lysate was clarified by centrifugation at 30000 *g* for 30 min at 4 °C. GST-tagged protein was captured by incubating cell lysate with pre-equilibrated Glutathione Sepharose 4B resin (750 µl settled resins/1 L cell culture) for 2 h at 4 °C. Resin was then washed with 100 column-volume (CV) of *GST high salt buffer*, followed by 50 CV of *GST low salt buffer*. Recombinant protein was eluted by incubating the resin with *GST low salt buffer* containing PreScission C3 protease that cleaves between the GST-tag and the recombinant protein. Alternatively, GST-tagged recombinant protein was eluted by incubating the resins with freshly prepared 30 mM L-glutathione that competes the binding of the GST-tagged protein to the resins. Eluted recombinant proteins (tag cleaved or GST-tagged) were then concentrated, snap-frozen and stored at -80 °C.

### 2.4.4 General His-tagged protein purification

For His-tag recombinant protein purification, cells were lysed in *His lysis buffer* and processed through a similar procedure as in Chapter 2.4.3. The only difference is in the lysis buffer and affinity resin used. His-tagged protein was captured by incubating the clarified cell lysate with pre-equilibrated Talon resin (750 µl settled resins/1 L cell culture) for 2 h at 4 °C. Resin was washed with 100 CV of His wash buffer. His-tagged protein was eluted by incubating the resin with His elution buffer, which contains high concentration of imidazole that competes for binding to Talon resins. Eluted His-tagged protein was then buffer exchanged to storage buffer, concentrated, snap-frozen and stored at -80 °C.

### 2.4.5 Purification of NZF domains and MIU motifs for ITC measurements and crystallography

GST-tagged TRABID NZF or GST-tagged MIU motif (without Halo tag) was expressed in BL21 cells and purified as described above (Chapter 2.4.3). After final wash with *GST low salt buffer*, GST-tagged NZF or MIU bound on resins was washed with 50 CV of *ResQ buffer A*. NZF or MIU was eluted by incubating resins with *ResQ buffer A* containing PreScission C3 protease. NZF or MIU was purified further using Resource Q 1 ml column and Superdex 75 26/600 column in ÄKTA pure chromatography system. Eluted NZF or MIU was loaded onto a Resource Q 1 ml column that had been equilibrated with *ResQ buffer A*. MIU was eluted in a gradient of *ResQ buffer B*. After being analysed on SDS-PAGE, peak chromatography fractions containing NZF or MIU were pooled, concentrated and loaded onto Superdex 75 26/600 column equilibrated with *GFC buffer*.

### 2.4.6 Untagged ubiquitin expression and purification (performed by Axel Knebel and Clare Johnson)

Plasmid DNA encoding untagged Ub wild-type or mutant was transformed as described in Chapter 2.3.2. A single colony was inoculated into 50 ml 2xTY media containing 50 µg/ml kanamycin and grown overnight at 37 °C. From this culture, 10 ml was transferred to 1000 ml 2xTY media containing 50 µg/ml kanamycin and grown until the culture reached an $OD_{600}$ of 0.6. To induce protein expression, 1 mM IPTG was added into the culture and the reaction was incubated for another 4 h at 37 °C.

Cells were harvested by centrifugation at 3400 $g$ for 30 min. Supernatant was removed and cells were re-suspended in 30 ml in $ddH_2O$ containing 1 mM EDTA and 1 mM EGTA. Cell suspension was transferred to 50-ml Falcon tube, snap-frozen and thawed in a 30 °C-water bath. Cells were lysed by sonication and the cell lysate was clarified by centrifugation at 30000 $g$ for 30 min at 4 °C. The cell lysate was diluted with 150 ml $ddH_2O$ and then 7% perchloric acid was slowly added with gentle stirring until a final pH 4.5. This low-pH cell lysate was incubated at room temperature overnight, which precipitates most proteins but not Ub (Lenkinski *et al*, 1977). Cell lysate was centrifuged at 30000 $g$ for 30 min at 4 °C and the supernatant was passed through a 0.45-µm membrane filter.

Recombinant Ub was purified using Resource S 6 ml column in the ÄKTA pure chromatography system. Filtered cell lysate was loaded onto a Resource S 6 ml column that has been equilibrated with *ResS buffer C*. Protein was eluted in gradient with *ResS buffer D*. Ub elutes at conductivity of 15-20 mS/cm. Fractions collected from the chromatography were analysed in SDS-PAGE. Fractions corresponding to Ub were pooled, buffer exchanged to 20 mM Tris-HCl pH 7.5, snap-frozen and stored in -80 °C.

## 2.5 Polyubiquitin chain assembly and purification

### 2.5.1 PolyUb chain assembly

PolyUb chains were assembled in enzymatic reactions that vary depending on the linkage type of polyUb. The limitation of the method is that the reaction efficiency may vary depending on the batch of enzymes used. Therefore, prior to large scale assemblies, I carried out pilot assembly reactions (~10 µl reaction volume) to determine the optimal time point of polyUb chains assembly for that batch of enzymes. The time points given below have been optimised for this study.

#### 2.5.1.1 M1 linkage

M1-linked polyUb chains were assembled in *Ub reaction buffer* containing 1500 µM Ub, 1 µM UBE1, 10 µM UBE2L3 and 10 µM HOIP (Stieglitz *et al*, 2012). The reaction was incubated for 2 h at 30 °C.

#### 2.5.1.2 K6 linkage

K6-linked polyUb chains were assembled in *Ub reaction buffer* containing 1500 µM Ub, 0.5 µM UBE1, 9.5 µM UBE2L3, 12.40 µM NleL (170-782) and 5 µM OTUB1 (Hospenthal *et al*, 2013). The reaction was incubated for 3 h at 30 °C.

#### 2.5.1.3 K11 linkage

K11-linked polyUb chains were assembled in *Ub reaction buffer* containing 1500 µM Ub, 1 µM UBE1, 40 µM UBE2S-UBP and 2 µM AMSH (Bremm *et al*, 2010). The reaction was incubated for 6 h at 30 °C. Fresh DUB and 5 µM of DTT were then added and the reaction was incubated further for 16 h.

#### 2.5.1.4 K29 linkage

K29-linked polyUb chains were assembled in *Ub reaction buffer* containing 1500 µM Ub, 0.64 µM UBE1, 9.5 µM UBE2D3 and 3 µM UBE3C (Kristariyanto *et al*, 2015a).

Reaction was incubated for 6 h at 30 °C. Then, a total of 5 μM DTT and 2 μM vOTU were added. The reaction was incubated for overnight.

### 2.5.1.5 K33 linkage

K33-linked polyUb chains were assembled in *Ub reaction buffer* containing 1500 μM Ub, 0.5 μM UBE1, 9 μM UBE2D1 and 6.3 μM AREL1 (Kristariyanto *et al*, 2015b). Reaction was incubated for 6 h at 30 °C. Then, a total of 5 μM DTT, 5 μM OTUB1 and 20 μM Cezanne E287K/E288K were added. The reaction was incubated for overnight.

### 2.5.1.6 K48 linkage

K48-linked polyUb chains were assembled in *Ub reaction buffer* containing 1500 μM Ub, 1 μM UBE1 and 25 μM UBE2R1 (Komander *et al*, 2008). The reaction was incubated for 6 h at 30 °C.

### 2.5.1.7 K63 linkage

K63-linked polyUb chains were assembled in *Ub reaction buffer* containing 1500 μM Ub, 1 μM UBE1, 10 μM UBE2N and 20 μM UBE2V1 (Komander *et al*, 2008). Reaction was incubated for 6 h at 30 °C.

### 2.5.2 Purification and isolation of polyUb of defined chain lengths

At the end of the polyUb assembly reaction, the reaction mixture was diluted in a total volume of 50 ml of 50 mM sodium acetate pH 4.5 (*ResS buffer A*). Conjugation enzymes precipitate at this low pH, but not polyUb chains (Lenkinski *et al*, 1977). After at least 3 h incubation at 4 °C, polyUb solution was passed through 0.45-μm filter. The theoretical isoelectric point of Ub is 6.56 and thus, at pH 4.5 Ub is positively charged. The strength of positive charge of polyUb chain is directly proportional to the number of Ub moieties within the chain. Therefore, longer polyUb chains bind stronger to cation exchange column. Exploiting this property, diUb, triUb, tetraUb and pentaUb chains were purified

using Resource S 6 ml column in ÄKTA pure chromatography system. Filtered polyUb solution was loaded onto Resource S 6 ml that has been equilibrated with *ResS buffer A*. PolyUb chains were eluted in a gradient with *ResS buffer B*. Typical elution chromatogram for polyUb chains is as in Figure 3.5C and Figure 3.13B. Peak fractions containing di-, tri-, tetra- and pentaUb chains were concentrated and buffer-exchanged to 20 mM Tris-HCl pH 7.5.

## 2.6   Synthesis of fluorescent dye-labelled polyUb chains

### 2.6.1   Assembly of K48-diUb$^{\text{distal-Cys}}$

K48-diUb$^{\text{distal-Cys}}$ has a Cys residue at the distal Ub, which serves as a conjugation site for the fluorescent dye through thiol-maleimide reaction. To assemble this diUb, two Ub mutants were used: Ub G75A/G76A (Ub$^{\text{G75A/G76A}}$), which serves as the acceptor Ub and a Cys-containing Ub K48R mutant (Ub$^{\text{Cys-K48R}}$), which serves as the donor Ub. Ub$^{\text{Cys-K48R}}$ has Cys at the N-terminal end, upstream of M1. The assembly reaction was carried out for 1 h at 30 °C in 1 ml *Ub reaction buffer* containing 1 mM Ub$^{\text{G75A/G76A}}$, 1 mM Ub$^{\text{Cys-K48R}}$, 0.5 µM UBE1 and 15 µM UBE2R1. K48-diUb$^{\text{distal-Cys}}$ was purified as described in Chapter 2.5.2. To prevent disulphide bond formation between diUb chains, all purification buffers were supplemented with 2 mM DTT.

### 2.6.2   Assembly of K48-triUb$^{\text{distal-Cys}}$

To assemble K48-triUb$^{\text{distal-Cys}}$, pre-formed K48-diUb (Chapter 2.5.1.6) was capped by Ub$^{\text{Cys-K48R}}$. The assembly reaction was carried out for 2 h at 30 °C in 1 ml *Ub reaction buffer* containing 250 µM K48-diUb, 1.25 mM Ub$^{\text{Cys-K48R}}$, 0.5 µM UBE1 and 15 µM UBE2R1. K48-triUb$^{\text{distal-Cys}}$ was purified as described in Chapter 2.5.2 with all buffers supplemented with 2 mM DTT.

### 2.6.3   Assembly of K48-pentaUb$^{\text{proximal-Cys}}$

To assemble K48-pentaUb$^{\text{proximal-Cys}}$, pre-formed K48-diUb was used to extend Ub$^{\text{Cys-}\Delta76}$ mutant. This Ub$^{\text{Cys-}\Delta76}$ mutant lacks G76 and therefore can only act as an acceptor Ub. In addition, it has a Cys residue at the N-terminal end, upstream of M1. The assembly reaction was carried out for 1.5 h at 30 °C in 1 ml *Ub reaction buffer* containing 250 μM K48-diUb, 1.25 mM Ub$^{\text{Cys-}\Delta76}$, 0.5 μM UBE1 and 15 μM UBE2R1. This reaction produced K48-triUb$^{\text{proximal-Cys}}$ and a smaller quantity of K48-pentaUb$^{\text{proximal-Cys}}$, which were purified as described in Chapter 2.5.2. All buffers were supplemented with 2 mM DTT.

### 2.6.4   Fluorescence labelling

The infrared dye, IRDye 800CW Maleimide, was conjugated to Cys-containing polyUb chains through thiol-maleimide 'click' chemistry. K48-linked polyUb chains were diluted in 20 mM Tris-HCl pH 7.5 and 500 μM TCEP to a final concentration of 50-100 μM. Protein sample was purged with argon and kept at room temperature for 30 min. In the meantime, IRDye 800CW Maleimide was dissolved in DMSO to prepare a 5 mM stock. Four-fold excess of IRDye 800CW Maleimide was added to the polyUb sample. The reaction was purged with argon and incubated at room temperature for 2 h in the dark. The completion of the coupling reaction was monitored by LC-MS. To stop the reaction, excess amount of 2-mercaptoethanol was added. Labelled K48-polyUb chains were separated from the unreacted IRDye 800CW using PD-10 (Sephadex G-25) Desalting Column as per manufacturer's manual. Proteins were eluted in aliquots of 50-100 μl and only fractions containing less noise-to-signal ratio were collected.

To quantify labelling efficiency, labelled proteins were analysed in LC-MS. Molecular weight of IRDye 800CW Maleimide is approximately 1190 Da and thus, proteins that have been labelled with have molecular weight shift by 1190 Da. The ratio of modified and unmodified proteins was used to determine the labelling efficiency.

## 2.7 Mammalian cell culture

### 2.7.1 General cell culture

All procedures were carried out under aseptic conditions that meets biological safety requirements. Cells were cultured in growth media at 37 °C and incubated in a 5% $CO_2$ humidified atmosphere. Human embryonic kidney (HEK) 293 cell line used in this study was maintained in growth media composed of DMEM supplemented with 10% (v/v) FBS, 2 mM L-glutamine, 100 units/ml penicillin and 0.1 mg/ml streptomycin.

### 2.7.2 Cell passaging

Cells were grown to 80-90% confluency in a 10- or 15-cm cell culture dish. The media was aspirated from the dish and cells were washed with PBS. To detach cells from the dish, cells were incubated with Trypsin/0.05% EDTA for 1-2 min. Cells were then re-suspended in fresh growth medium, which was used to seed a new cell culture.

### 2.7.3 Cell freezing and thawing

Confluent cells grown in a 15-well culture dish were detached by trypsination and re-suspended in growth media (Chapter 2.7.2). Cell suspension was centrifuged at 500 $g$ for 5 min and the supernatant was removed. Cells were then re-suspended in 2 ml of fresh growth. To this cell suspension, 2 ml of freezing solution (80% FBS and 20% DMSO) was added drop-wise with constant gentle stirring. Cell suspension was transferred in 1 ml-aliquots to cryovials. Cells were frozen in Mr Frosty Freezing Container at -80 °C for 24 h. Cells in cryovials were transferred to liquid nitrogen for long term storage. Cells were thawed by incubating cryovials in 37 °C water-bath. Cell suspension was then transferred to fresh growth media in 10-cm culture dish. After overnight incubation, growth media was replaced with fresh media.

### 2.7.4 DNA transfection into HEK293 cells using PEI

Polyethylenimine (PEI) was dissolved in cell culture-grade 20 mM HEPES pH 7.5 to make 1 mg/ml concentration. The pH of PEI solution is adjusted to 7.5. PEI solution was passed through a 0.22 μm filter to sterilise, aliquoted in sterile 1.5-ml tubes and stored at -80 °C. A day prior to transfection, $6 \times 10^6$ of HEK293 cells were seeded in 10-cm culture dish containing growth media in the absence of antibiotics. On the following day, growth media of the 30-40% confluent cells was replaced to Opti-MEM containing 1% FBS. To prepare transfection mix, 10 μg DNA was diluted in 1 ml Opti-MEM and briefly vortexed. PEI was then added to a final concentration of 30 μg/ml and then briefly vortexed. Transfection mix was incubated at room temperature for 15 min and transferred drop-wise to cell culture. After 24 h, the transfection media was replaced with growth media containing antibiotics. Cells were grown for an additional 24 h before being harvested.

### 2.7.5 Mammalian cell lysis

To harvest cells, growth media was aspirated from culture dish. Ice-cold PBS was then added and cells were gently scrapped and re-suspended. Cell suspension was centrifuged at 500 *g* for 5 min at 4 °C. PBS was removed and cell pellet was snap-frozen and stored at -80 °C for future use.

Cells were lysed using freeze-thaw method. Cell pellet was thawed in *Freeze-thaw lysis buffer* and cell suspension was incubated for 30 min at 4 °C in dark. Cell suspension was transferred to 1.5-ml tube, snap-frozen and thawed at 30 °C. After one additional freeze-thaw cycle, a final concentration of 150 mM NaCl and 5% glycerol was added. Cell lysate was centrifuged at 14000 *g* for 20 min at 4 °C and the supernatant was collected. Protein concentration was measured by Bradford method.

Alternatively, cells were lysed directly in lysis buffer. Cell pellet was thawed in *MRC lysis buffer* and cell lysate was incubated for 30 min at 4 °C. Cell lysate was centrifuged at 14000 $g$ for 20 min at 4 °C and the supernatant was collected. Protein concentration was measured by Bradford method.

## 2.8 In-vitro assays

### 2.8.1 Autoubiquitylation assays

Analytical assays were carried out in 20 μl *Ub reaction buffer* containing 125 nM UBE1, 2.25 μM E2, 1.56 μM E3 and 57 μM Ub. The reaction was incubated at 30 °C for the indicated time. Wherever indicated DUBs were added and the reaction was incubated further for 1 h. Reaction was stopped by adding reducing LDS sample buffer.

### 2.8.2 Pulse-chase assays

In pulse reaction, E2 was loaded with Ub in a 20 μl *Pulse buffer* containing 57 μM Ub, 125 nM UBE1 and 5 μM UBE2D3. Reaction was incubated for 15 min at 37 °C. Pulse reaction was stopped by depleting ATP by adding a total of 4.5 U/ml apyrase, followed by incubation on ice for 15 min. In the chase reaction, Ub-loaded UBE2D3 in pulse reaction was diluted to 1.4 μM in a total volume of 20 μl *chase buffer* containing 1.4 μM UBE3C. Reaction was incubated at 37 °C for the indicated time. Reaction was stopped by adding LDS sample buffer in the presence or absence of reducing agent.

### 2.8.3 Qualitative deubiquitinating assays

Prior to the assays, DUBs were incubated with *DUB buffer* for 10 min at room temperature. DUB assays were carried out in 20 μl *DUB buffer* containing 1.6 μM DUB and polyUb chains (2.2 μM K48-diUb, 2.2 μM tetraUb, 3.5 μM K48-pentaUb or 3.5 μg of K48-Ub5-n). Reaction was incubated at 30 °C for the indicated time. For DUB assays

in Figure 5.3B that compare FAM63A activity in cleaving different lengths of K48-polyUb chains, 1 µM of polyUb chains were used. For DUB assays of YPL191C in Figure 5.4, 160 nM of DUB was used. Reaction was stopped by adding reducing LDS sample buffer.

### 2.8.4   Quantitative deubiquitylating assays

In quantitative DUB assays, fluorescently labelled polyUb substrates (K48-polyUb$^{IR800}$) were used (Chapter 2.6). Prior to the assays, DUBs were incubated with *DUB buffer* for 10 min at room temperature. DUB assays were carried out in 20 µl *DUB buffer* containing 1 µM DUB, 500 nM K48-polyUb$^{IR800}$ and 0.25 mg/ml BSA. At the indicated time, 2.5 µl of the reaction was transferred to 7.5 µl LDS reducing sample buffer, which stops the reaction. Samples were separated on 4-12% SDS-gel and visualized using Odyssey imaging system (LI-COR) at 800 nm channel. Intensities of K48-chains were quantified using Image Studio Lite (LI-COR).

### 2.8.5   Steady-state deubiquitylation assay

Steady-state enzyme kinetics of FAM63A$^{cat}$ in hydrolysing K48-pentaUb were measured in *DUB buffer* containing 0.25 mg/ml BSA, 15 nM FAM63A$^{cat}$ and an increasing amount of fluorescently-labelled K48-pentaUb (K48-pentaUb$^{proximal-IR800}$) (75, 150, 300, 600, 1200, or 2400 nM). Reaction was incubated at 30 °C and was stopped at the indicated time (2.5, 5, 7.5, 10, 12.5 or 15 min). To stop the reaction, 2.5 µl was transferred to 7.5 µl reducing LDS sample buffer. Samples were separated and the formation of K48-tetraUb$^{proximal-IR800}$ was analysed and quantified as described in Chapter 2.8.4 (Figure 5.7B).

To convert the quantified intensity of the formed K48-tetraUb$^{proximal-IR800}$ to molar concentration, a standard curve of 1.17 to 75 nM K48-pentaUb$^{proximal-IR800}$ was made (Figure 5.7C). Since the fluorescent dye is only conjugated to the proximal end of the

polyUb chain, the intensity of K48-pentaUb$^{proximal-IR800}$ will translate to the same number of molecules of K48-tetraUb$^{proximal-IR800}$ or equal molar concentrations. The amount of K48-tetraUb$^{proximal-IR800}$ formed was plotted against time and the data was fitted to a linear regression curve, where slope is the initial velocity, $V_0$ (M.s$^{-1}$) (Figure 5.7D). The initial velocity values were then plotted against substrate concentration and the data was fitted to the Michaelis-Menten equation:

$$V_0 = \frac{V_{max}[S]}{K_m + [S]} = \frac{k_{cat}[E][S]}{K_m + [S]}$$

where $V_0$ (M.s$^{-1}$) is the initial velocity, $V_{max}$ (M.s$^{-1}$) is the maximum velocity, [S] (M) is substrate concentration, $K_m$ (M) is the Michaelis constant, and $k_{cat}$ (s$^{-1}$) is the turnover rate. Data fitting was carried out using GraphPad Prism 5 software.

### 2.8.6   Coupling Halo-tagged protein to HaloLink resins

Coupling reaction was carried out at 4 °C for 2 h in 500 µl *Halo coupling buffer* containing 21 µM Halo-tagged UBDs and pre-equilibrated 100 µl of HaloLink resin. Coupled resins were washed three times with *Halo coupling buffer*.

### 2.8.7   PolyUb linkage-selective binding assays

The selectivity of UBDs in binding polyUb chains was assayed by incubating 10 µl coupled Halo-UBD resins with 58.5 nM of tetraUb chains in 500 µl of *Halo pulldown buffer*. Reaction was incubated for 2 h at 4 °C. Resins were washed twice with *Halo wash buffer* and once with *Halo coupling buffer*. Captured tetraUb chains were eluted by adding LDS buffer, separated on 4-12% SDS-PAGE gel, and visualized by silver staining.

### 2.8.8   PolyUb enrichment from mammalian cells and DUB treatments

HEK293 cells transiently expressing Flag-tagged proteins were lysed as described in Chapter 2.7.5. To isolate Flag-tagged protein, 1 mg of cell lysate was incubated with 10

µl of pre-washed Flag-M2 resins (Sigma-Aldrich) for 2 h at 4 °C. To capture polyUb chains from HEK293 cells, 1 mg of cell lysate was incubated with 10 µl of Halo-UBD resins (Chapter 2.8.6) for 2 h at 4 °C. Resins were washed three times with *Halo wash buffer*.

To treat the captured material with DUBs, resins were washed two times with *DUB buffer*. Resins were then re-suspended in 20 µl of *DUB buffer* containing 2 µM vOTU and the reaction was incubated for 1 h at 30 °C. When second DUB assays were carried out, resins after first DUB treatment were washed twice with *DUB buffer*. Resins were then re-suspended in 20 µl *DUB buffer* containing 5 µM of the second DUBs (OTULIN, Cezanne, TRABID, OTUB1, AMSH, OTUB2, vOTU or USP2). Reaction was incubated for 1 h at 30 °C. Reaction was stopped by adding reducing LDS sample buffer. PolyUb chains were analysed by immunoblotting against anti-Ub (DAKO). Flag-tagged proteins were visualized by anti-Flag (SIGMA).

## 2.9 Protein analysis

### 2.9.1 Quantification of protein concentration

Protein concentration in whole cell lysate was determined using Bradford method (Bradford, 1976). In principle, when Coomassie dye binds to proteins in acidic medium, the maximum absorbance shifts from 465 nm to 595. This results a change in colour from brown to blue that can be measured using spectrophotometer. A standard curve was generated by plotting absorbance against a serial dilution of BSA standard (0.03 mg/ml – 2 mg/ml). Diluted cell lysate was mixed with Bradford reagent in a ratio of 1:50. After incubation for 5 min at room temperature, absorbance at 595 was measured. Concentration of protein was calculated from the BSA standard curve.

Alternatively, the concentration of purified recombinant proteins was determined using NanoDrop 2000 spectrometer. After calibrating NanoDrop with ddH$_2$O and blank

buffer, the absorbance of purified protein at 280 nm was measured. Using Beer-Lambert law, concentration of protein can be calculated:

$$Concentration\ (mg/ml) = \left(\frac{A_{280}}{\varepsilon \times path\ length}\right) \times MW \times dilution\ factor$$

$A_{280}$ is absorbance of protein at 280 nm. $\varepsilon$ is theoretical extinction coefficient, which was calculated using ExPASy ProtParam tool (http://web.expasy.org/protparam/). Path length of NanoDrop 2000 spectrophotometer is 1 mm. MW is molecular weight of protein in Da.

### 2.9.2 Resolution of protein samples by SDS-PAGE

Polyacrylamide gel electrophoresis (PAGE) is a commonly used technique to separate proteins according to their molecular weight and electrophoretic mobility. SDS-PAGE sample buffer commonly contains anionic detergents, such as sodium dodecyl sulphate (SDS) or lithium dodecyl sulphate (LDS). The hydrophobic tail of these detergent bind to proteins. In addition to this, the negative hydrophilic region of SDS or LDS gives proteins a net negative charge, which is proportional to the molecular weight of proteins. Sample buffer is supplemented with reducing agent, such as DTT or β-ME, to break disulphide bonds and any secondary structure and to ensure protein is linear.

Protein sample in reducing LDS buffer was loaded onto 4-12% Bis-Tris gel. The electrophoresis was carried out in MES buffer at 180 V for 45 min. Gel was then washed in ddH$_2$O.

### 2.9.3 Coomassie and Silver staining

For general protein analysis, washed 4-12% Bis-Tris gel was stained in Instant Blue solution for 1 hr to overnight at room temperature. Gel was de-stained in ddH$_2$O. Alternatively, proteins were visualised by Silver staining method (Chevallet *et al*, 2006).

The silver staining was carried out using a Silver Staining kit (ThermoScientific) according to manufacturer's instructions.

### 2.9.4 Immunoblotting

Initially, proteins were transferred from Bis-Tris gel onto a PVDF membrane. In a transfer cell, gels and PVDF membrane (pre-activated in 100% methanol) were sandwiched between Whatman 3-mm filter papers and nylon sponges, which were all soaked in *Tris-glycine transfer buffer*. The transfer cell was placed in Trans-Blot Cell filled with *Tris-glycine transfer buffer*. Transfer was carried out at 80V for 80 min.

After transfer, the PVDF membrane was soaked in *Denaturing buffer* and incubated for 30 min at 4 °C. This step is crucial to completely denature Ub, which ensures equal detection of Ub signal by anti-Ub antibody. Membrane was then washed three times in *TBST* and incubated with *TBST* containing 5% (w/v) skimmed milk for 30 min at room temperature. Afterwards, membrane was washed 3 × 5 min with *TBST*.

For immunoblotting, membrane was incubated with primary antibody diluted in TBST containing 5% (w/v) BSA overnight at 4 °C. Membrane was then washed 3 × 5 min with TBST. Membrane was incubated with HRP-conjugated secondary antibody, which has been diluted at 1:5000 in TBST containing 5% (w/v) skimmed milk. After 1 h incubation at room temperature, membrane was washed 3 × 5 min with TBST. Membrane was incubated with enhance chemiluminescence (ECL) substrate and exposed to X-ray film for various lengths of time. Film was developed using a Konica automatic developer.

## 2.10 Mass Spectrometry

### 2.10.1 In-gel tryptic digestion

For analysis of single species of polyUb, protein sample was fully resolved on 4-12% Bis-Tris gel and stained with Coomassie (Chapter 2.9.2 and 2.9.3). The band

corresponding to polyUb was excised into approximately 2×2×2 mm cubes and transferred to ddH$_2$O in 1.5-ml tube. Alternatively, to analyse whole polyUb chains, protein sample was resolved on 4-12% only until the whole sample had entered the gel. After visualising by Coomassie staining, gels region containing proteins were excised into approximately 2×2×2 mm cubes and transferred to ddH$_2$O in 1.5-ml tube. Gel pieces were washed with 0.5 ml of ddH$_2$O, 50% (v/v) ACN/H$_2$O, 0.1 M NH$_4$HCO$_3$ and 50% ACN/0.1 M NH$_4$HCO$_3$. These washes are important to destain proteins and equilibrate them for tryptic digestion. Ub does not contain any Cys residue and therefore, Ub does not form any disulphide bonds and hence, there is no need to alkylate proteins. Gel pieces were washed with 100% ACN and were dried under vacuum. Dried gels were rehydrated in 25 mM triethylammonium bicarbonate containing 5 µg/ml of mass-spec-grade trypsin. Gels were incubated at 30 °C overnight with constant agitation. One CV of ACN was added to gel pieces to extract the tryptic digested peptides. Supernatant was collected and dried. Gel pieces were washed with 50% ACN/2.5% formic acid and the supernatant was pooled with the first eluent and freeze dried. Lyophilised peptides were stored at -20 °C until further use.

### 2.10.2 Parallel reaction monitoring (PRM) (performed by David Campbell and Nicholas Morrice)

PolyUb chains that had been previously digested with trypsin were analysed on an LTQ-Velos mass spectrometer (Thermo) fitted with a Dionex RSLC HPLC system and an Easy-Spray Source (Thermo). Standard diUb chains were purchased from Boston Biochemicals and a synthetic peptide AK(GG)IQDK representing the tryptic Ub K29 linkage was purchased from Pepceuticals (Nottingham, UK). Tryptic-digested peptides were re-solubilised in 0.1%TFA/ddH$_2$O. Peptides were loaded onto 20 × 0.1 mm Nano-trap column (Thermo) equilibrated in 0.1% TFA/H$_2$O with flow rate of 10 µl/min. After

washing with 10 μl of the same buffer, peptides were separated on a 150 × 0.075 mm

PepMap C18, 3 μm Easy-Spray column (Thermo) equilibrated with 2% ACN/0.1% FA/

ddH$_2$O at 300 nl/min. It was critical that the samples were loaded and washed in TFA

buffers, as the trap column in the presence of FA did not retain the tryptic peptide

containing the K29 linkage. Peptides were separated at the same flow rate using a

discontinuous gradient of buffer B (80% ACN/0.1% FA/ddH$_2$O) as follows: 0-14 min =

1-30% B, 14-15 min = 30-80% B, 15-20 min = 80% B. LC-MS data was acquired in Data

Independent mode with 1 full scan (m/z 350-1800) followed by 8 product ion scans as

described below. The voltage applied to the Easy-Spray column was 1.9 kV, the isolation

width was set to 1 Da, normalised collision energy was 35 and the activation time was 10

ms.

Xcalibur software (Thermo) was used to process the data. The ion current for the

daughter ions was summed for each precursor mass analysed (Table 2.5). The resultant

summed intensities provide the y-axis values and the retention times on LC-MS provide

the x-axis values for Figure 3.6 and Figure 3.14. This method was more specific than

solely using the extracted ion current for the precursor mass for each Ub chain peptide.

*Table 2.5 Parameter used in the Parallel Reaction Monitoring (PRM) analysis*

| Linkage | Peptide Sequence | Charge | Retention Time (min) | Precursor (m/z) | Daughter masses used for quantification |
|---------|------------------|--------|----------------------|-----------------|------------------------------------------|
| M1 | M(gg)QIFVK | 2+ | 8.7 | 440.34 | y3, 393.25; y4, 506.33; y5, 634.39; b7, 733.37 |
| K6 | MQIFVK(gg)TLTGK | 2+ | 13.6 | 690.5 | y6, 761.45; y7, 860.50; y8, 1007.59; y9, 1120.67 |
| K11 | TLTGK(gg)TITLEVEPSDTIENVK | 3+ | 14.6 | 801.84 | y8, 905.46; y9 1002.51; y10, 1131.55 |
| K27 | TITLEVEPSDTIENVK(gg)AK | 2+ | 13.9 | 1051.56 | y8, 1016.57; y11, 1315.68; y12, 1444.73; y13, 1543.79 |
| K29 | AK(gg)IQDK | 2+ | 6.6 | 408.8 | b3, 427.26; y4, 503.30; b5, 670.35; y5, 745.40 |
| K33 | IQDK(gg)EGIPPDQQR | 3+ | 9.3 | 546.61 | y62+, 370.90; y6, 740.30; b7, 898.30 |
| K48 | LIFAGK(gg)QLEDGR | 2+ | 12.7 | 731.36 | y4, 476.40; y5, 589.45; y6, 717.20 |
| K63 | TLSDYNIQK(gg)ESTLHLVLR | 2+ | 14.5 | 1122.67 | y5, 637.41; y8,938.58; y9, 1067.62 |

## 2.11 Isothermal titration calorimetry

ITC is a technique that directly measures the thermodynamic parameters of interactions in solution: Gibbs energy ($\Delta$G), enthalpy ($\Delta$H), entropy ($\Delta$S), reaction stoichiometry and dissociation constant ($K_d$) (Velázquez-Campoy *et al*, 2004). ITC measurements were performed on MicroCal iTC$_{200}$ (GE Healthcare) and MicroCal PEAQ-ITC (Malvern). Prior to measurements, all proteins were dialysed into *ITC buffer* to avoid signal noise due to buffer mismatch. The syringe contained UBDs and the cell contained polyUb chains. For titration of MIU motifs (300 µM) to polyUb chains (30 µM), a total of 20 injections of 2 µl were dispensed in 5-sec duration with 120-sec spacing in between injections. For titration of NZF domains to polyUb chains, a total of 25 injections of 1.5 µl were dispensed in 5-sec duration with 120-sec spacing in between injections. Concentration of 300 µM and 20 µM was used for titrations of NZF1 and diUb, respectively. The concentrations of NZF domains and polyUb chains are listed in Table 2.6. All ITC measurements were carried out at constant temperature of 25 °C. Data was analysed and titration curves were fitted using MicroCal Origin software assuming a single binding site mode.

*Table 2.6 Concentration of proteins used in NZF titration into diUb*
*Higher protein concentration for NZF2, NZF3 and NZF1 mutant titrations were used to increase ITC signal.*

| Syringe | Cell |
|---|---|
| NZF1 (300 µM) | K29- and K33-diUb (20 µM) |
| NZF2 (550 µM) | K29- and K33-diUb (30 µM) |
| NZF3 (800 µM) | K33-diUb (40 µM) |
| NZF1 M26A (550 µM) | K29-diUb (30 µM) |

## 2.12 Protein crystallography

### 2.12.1 Crystallisation methods

All crystal structures described in this thesis were obtained using vapour diffusion techniques in the sitting drop and hanging drop format (Figure 2.1). In these methods, protein is mixed with mother liquor in a small droplet on the sample platform whereas a larger volume of mother liquor is placed on the reservoir (Figure 2.1). Sample platform and mother liquor reservoir are air-tight sealed, which allows vapour diffusion to occur between buffers in the sample droplet and mother liquor. As the two buffers equilibrate, the protein concentration on the droplets increases. When protein reaches supersaturation, nucleation occurs. Then protein molecules form a well-ordered interaction lattice on the nucleation site as the crystal begins to grow.
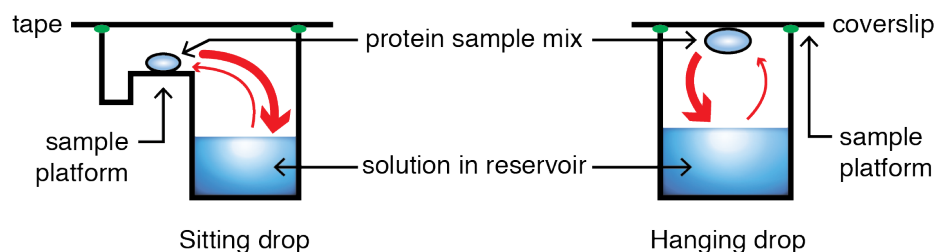


***Figure 2.1 Schematic diagrams illustrating two methods of vapour diffusion used in this thesis***
*Sitting drop (left) and hanging drop (right) methods contain a reservoir that holds mother liquor solution and a sample platform that holds protein sample mix. The sealed closed system (green dots) ensure vapour diffusion (red arrows) until equilibrium is reached. In an ideal situation, as protein concentration in the sample drop increases, supersaturation is reached. Then nucleation occurs and protein crystal begin to grow.*

### 2.12.2  Crystallisation screening and optimisation

Crystallisation screening was performed with sitting drop method using 96-well MRC Crystallisation Plates (Molecular Dimension). Each reservoir contained 60 µl of mother liquor from commercial crystallisation screens (Chapter 2.1.4). Sample drops were prepared by mixing 300 nl of protein sample and 300 nl of mother liquor using Mosquito liquid handling robot. Plates were sealed using Crystal Clear tape to allow easy visualisation of the drops. Crystallisation was carried out at 20 °C.

The initial hits of the protein obtained in certain conditions were further optimised using hanging drop method in 24-well VDX Plate with sealant (Hampton). On the y-axis and x-axis, the pH and the precipitant concentration of mother liquor were varied. Each well contained 500 µl of self-made mother liquor. On a glass cover slip, protein was mixed with mother liquor in 1:1 ratio with the drop size ranging between 1-3 µl each. The cover slip was placed up-side down with the drop facing the mother liquor. Crystallisation was carried out at 20 °C.

To further improve the diffraction quality of the protein crystals, micro-seeding technique was used. Clusters or needle-like crystals were harvested and transferred to the stabilising solution. Crystals were vortexed in Seed Bead (Hampton) and serial dilutions were made. Diluted crystal seeds were streaked across sample droplet that contain 1:1 ratio of protein and mother liquor (see above).

### 2.12.3 Crystal handling and diffraction experiments (performed by Syed Arif Abdul Rehman)

Protein crystals were harvested using CyroLoop of appropriate size (Hampton Research) and flash-frozen in liquid nitrogen in the presence of cryo-protectant. The cryo-protectant is a solution which is essential to prevent the formation of ice crystal during vitrification. Glycerol, low molecular weight (200-400 Da) PEGs and ethylene glycol are components of the commonly used cryo-protectants. The frozen protein crystals were stored in

suitable container or in dewar. Diffractions were collected at the European Synchrotron Radiation Facility (ESRF), Grenoble, France and at the Diamond Light Source (DLS), Oxfordshire, UK.

### 2.12.4 Crystallisation of K29-diUb (performed by Syed Arif Abdul Rehman)

K29-diUb was purified and concentrated to 12 mg/ml as described in Chapter 2.5.2. Diffraction quality crystals were obtained in 100 mM Bis-Tris propane pH 6.5, 200 mM sodium iodide, 20% PEG3350 and 5 mM sodium malonate at 20 °C. Micro-seeding technique was used to improve quality of crystals. The single crystals obtained were cryo-protected in solution containing 20% glycerol before freezing in liquid nitrogen. Diffraction data were collected at ESRF beamline ID23-1.

### 2.12.5 Crystallisation of K29-diUb in complex with TRABID NZF1 (performed by Syed Arif Abdul Rehman)

TRABID NZF1 and K29 diUb were purified as described (Chapter 2.4.5 and Chapter 2.5.2). They were mixed together in molar ratio of 1:1 and incubated for 3 h at 4 °C. Protein complex was concentrated to 18 mg/ml using 3 kDa MWCO concentrator (Millipore). The complex crystallized in 100 mM MES pH 6.5, 200 mM potassium iodide, and 25% PEG4000. Single crystals were cryo-protected in 100 mM MES (pH 6.5), 10% PEG20000 and 35% PEG400 before vitrification in liquid nitrogen. Diffraction data were collected at Diamond beamline I04.

### 2.12.6 Crystallisation of K33-diUb and K33-triUb

K33-diUb and K33-triUb were purified as described in Chapter 2.5.2. K33-diUb was crystallised at 9 mg/ml in 200 mM lithium sulphate, 100 mM sodium acetate pH 4.5 and 50% PEG400. Diffraction quality crystals were obtained using micro-seeding. Crystal

seeds were prepared in 200 mM potassium iodide and 20% PEG3350. Single crystals were cryo-protected in solution containing 20% ethylene glycol.

K33-triUb was crystallised at 8 mg/ml in 20 mM sodium/potassium phosphate, 100 mM Bis-Tris propane pH 7.5 and 20% PEG3350. Single crystals obtained were cryo-protected in solution containing 30% ethylene glycol. Diffraction data for both K33-diUb and K33-triUb were collected at ESRF beam line ID29.

### 2.12.7 Crystallisation of K48-diUb in complex with FAM63A tMIU

FAM63A tMIU and K48-diUb were purified and concentrated at 2 mg/ml and 12.9 mg/ml, respectively (Chapter 2.4.5 and Chapter 2.5.2). Both proteins were mixed in 1:1 molar ratio at 400 nmol each. After an overnight incubation, the protein complex was concentrated to 16.3 mg/ml. Protein crystals were obtained in 100 mM sodium acetate pH 5.4 and 18.5 % PEG3350. Crystals were cryo-protected in solution containing 30% PEG400 before vitrification in liquid nitrogen. Data were collected at ESRF beam line ID30A.

### 2.12.8 Structure determination (performed together with Syed Arif Abdul Rehman)

The initial data reductions was done using XDS (Kabsch, 2010). Further data processing was carried out using POINTLESS and SCALA (Evans, 2006). Alternatively, AIMLESS (Evans & Murshudov, 2013) was used. All the crystal structures were solved by molecular replacement using Phaser (McCoy *et al*, 2005). The structures of Ub chains were solved using Ub (1UBQ (Vijay-Kumar *et al*, 1987)) as a search model. The structure of NZF domain was solved using TAB2 NZF (2WWZ (Kulathu *et al*, 2009)) as a search model. The model refinements were done using Phenix (Adams *et al*, 2002) and REFMAC5 (Vagin *et al*, 2004). All the structures were manually inspected in Coot

(Emsley *et al*, 2010). In some cases, the structures were finally re-refined using PDB_REDO (Joosten *et al*, 2014).

## 2.13 Data analysis and figure preparations

Protein sequence analysis was carried out as follow: Protein sequences were retrieved from UniProt database (http://www.uniprot.org/), aligned using Clustal Omega (http://www.ebi.ac.uk/Tools/msa/clustalo/) and edited with the Jalview software (Waterhouse *et al*, 2009). Statistics and non-linear regression analysis were carried out using GraphPad Prism 5 software (https://www.graphpad.com/). Protein structures were analysed using PIC and PISA servers for protein inter- and intramolecular interactions (Tina *et al*, 2007; Krissinel & Henrick, 2007). Protein structure figures were made with the PyMOL Molecular Graphics System, Schrödinger, LLC (https://www.pymol.org/). All figures presented in this thesis were annotated using Adobe Illustrator (Adobe System Inc).

# 3 Assembly of K29- and K33-linked polyubiquitin chains and characterisation of their binding to NZF domains

## 3.1 Introduction

When this study was initiated, diUb of all eight linkage types could be generated using chemical synthesis approaches (Kumar *et al*, 2010; Virdee *et al*, 2010). These diUb chains have been invaluable to investigate linkage specificity of DUBs (Faesen *et al*, 2011; Mevissen *et al*, 2013). For example, an A20-like OTU DUB TRABID was widely known as K63-specific DUB until its activity was assayed against diUb of eight chain types. TRABID prefers to hydrolyse K29 and K33 over K63 diUb with catalytic efficiency ($k_{cat}/K_m$) ~40-fold higher (Virdee *et al*, 2010; Licchesi *et al*, 2011). However, generating large quantity of Ub chains chemically is costly and laborious. In addition, preparation of longer chains is challenging. Alternatively, polyUb chains can be generated through enzymatic assembly, which is more robust than chemical synthesis in term of quantity and lengths of polyUb chains produced. However, when this study was started, only limited linkage types could be enzymatically assembled, namely M1, K6, K11, K48 and K63 (Chapter 1.9). Therefore, there is a high demand in Ub research for methods to enzymatically assemble the remaining chain types, K27, K29 and K33.

In this Chapter, I report two methods to enzymatically assemble K29 and K33 polyUb chains, using HECT E3 UBE3C and AREL1 (Chapter 1.3.2.2), respectively in combination with linkage-specific DUBs (Chapter 1.6). These methods yield high quantity of pure chains of defined lengths that allow me to structurally characterise K29 and K33 diUb chains. Moreover, I also identified TRABID NZF1 domain as a K29- and K33-linkage selective UBD and structurally investigate how the linkage selectivity of the NZF domain is determined. Finally, using TRABID NZF1 as a K29-selective polyUb

binder, I demonstrate that K29-linked polyUb chains are present in heterotypic chains with other linkage types, including K48 linkage.

## 3.2 Results

### 3.2.1 Investigation into UBE3C mechanism in polyUb chains assembly

In early 2000, UBE3C (also known as KIAA10) was reported as a HECT E3 that can assemble K29 and K48 *in vitro* (You & Pickart, 2001). UBE3C is a 1083-residue protein in which N-terminal half of the protein mediates interaction with substrate and 26S proteasome. The C-terminal portion of UBE3C (656-1083), which contains a HECT domain, is both necessary and sufficient to assemble K29- and K48-linked polyUb chains (You & Pickart, 2001). It was reported that UBE3C assembles unanchored polyUb chains (Wang & Pickart, 2005). Taking advantage of these early studies, I wanted to characterised the enzymatic activity of UBE3C in detail to be able to exploit this system to make a large quantities of K29 chains.

As I wanted to establish an optimal method to assemble K29-linked polyUb chains using UBE3C, I first investigated the polyUb conjugation activity of three different construct boundaries of UBE3C. Sequence alignment of UBE3C and other HECT E3 ligases reveals a conserved region of HECT domain from 720 to 1083. Based on these analyses, three different construct boundaries of UBE3C were generated: 716-1083, 691-1083 and 636-1083, which all contain the HECT domain (Figure 3.1A). The polyUb conjugation activity of these constructs were monitored in autoubiquitylation assays in the presence of E1 and a panel of E2s, which has been shown to interact with HECT E3 ligases (Kar *et al*, 2012; Sheng *et al*, 2012). High molecular weight ubiquitylated products were formed by UBE3C together with UBE2D1, UBE2D2 and UBE2D3, but not with UBE2L3 (Figure 3.1B-C). This suggests that E2s of the UBE2D family (UbcH5) are the cognate E2 partner for UBE3C. In addition, these polyUb chains were assembled by the

longer UBE3C constructs 691-1083 and 636-1083, but not by the shorter construct 712-1083 (Figure 3.1B-C). Despite the similar activity of UBE3C 691-1083 and 636-1083, short unanchored chains of di-, tri- and tetraUb were formed only in UBE3C 691-1083. Autoubiquitylation assays monitoring polyUb conjugation at early time points reveal that UBE3C 636-1083 rapidly converts monoUb to polyUb of higher molecular weight whereas this process is delayed in UBE3C 691-1083 (Figure 3.1D-E). These observations suggest that UBE3C 636-1083 assembles polyUb chains more efficiently than the shorter UBE3C constructs tested.
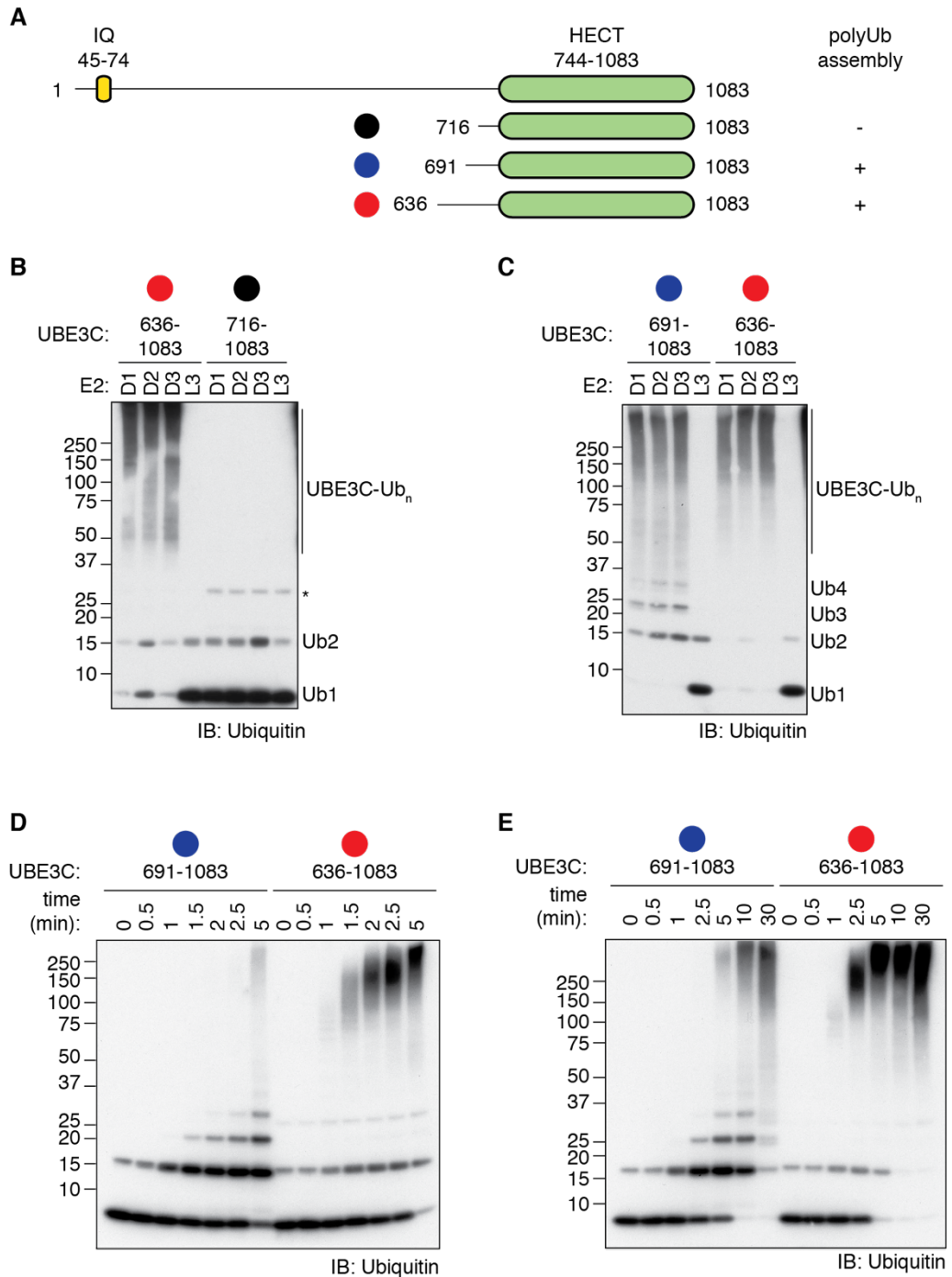
**Figure 3.1 Three constructs of UBE3C exhibit different polyUb conjugation activity**
*(A)* Schematic diagram of UBE3C constructs used in this study, which are colour coded: black, 716-1083; blue, 691-1083; red, 636-1083. The same colour codes are used throughout the Chapter. *(B-C)* Autoubiquitylation assays of UBE3C were carried out in the presence of Ub, UBE1 and the indicated E2 for 30 min at 37 °C. Ubiquitylated materials were visualised by anti-Ub immunoblotting. *(D-E)* Autoubiquitylation assays of UBE3C were carried out in the presence of Ub, UBE1 and UBE2D3 at 37 °C for the indicated periods of time.

It is fascinating how variations in ~80 residues upstream to the HECT domain affect UBE3C Ub-conjugating activity. HECT E3 Ub-conjugation cascade involves E3 binding to the Ub-loaded E2, followed by transfer of Ub from the E2 to the catalytic Cys of the HECT domain. Finally, HECT E3 catalyses Ub conjugation onto substrate lysines (Chapter 1.3.2.2). I then wondered whether the ~80 residues upstream to the HECT domain of UBE3C (referred as 80aa-upstream) affects one of the steps in the Ub-conjugation cascade. To investigate this, I carried out detailed pulse-chase assay using Ub-loaded UBE2D3 and UBE3C (Figure 3.2A). In this assay, E2 was first loaded with Ub in the presence of E1 and $Mg^{2+}$•ATP. After depleting ATP using apyrase, UBE3C was added into the reaction and the transfer of Ub from E2 to E3 was monitored. In the reaction containing UBE3C 636-1083, Ub was successfully unloaded from E2, but the UBE3C~Ub thioester intermediate was not observed (Figure 3.2C-E). Instead, the Ub was conjugated on UBE3C through isopeptide bonds, which is not cleaved in the presence of reducing-agent (Figure 3.2E). This suggest that UBE3C rapidly transfers Ub from its catalytic Cys to its own Lys residues. This explains the rapid formation of high molecular-weight ubiquitylated species in the autoubiquitylation assays (Figure 3.1D). In contrast, the Ub discharge from E2 was compromised in UBE3C 712-1083, which suggests defects in Ub transfer process from E2 to the catalytic Cys of UBE3C and thus, explains the incompetence of this minimal HECT domain to assemble polyUb chains (Figure 3.2C and Figure 3.1A). Interestingly, although Ub can be discharged from the E2 by UBE3C 691-1083, self-ubiquitylation of the E3 was not observed (Figure 3.2D-E). Instead, short polyUb chains of di- and triUb were observed. This suggests that the delay in polyUb assembly by UBE3C 691-1083 was caused by a defect in self-ubiquitylation. Collectively, these observations suggest that the 80aa-upstream modulates the Ub-conjugating cascade of UBE3C.

**A**

Ub
E1
E2 $\xrightarrow[37°C]{15'}$ + Apyrase $\xrightarrow[4°C]{15'}$ + UBE3C $\xrightarrow[37°C]{}$ + LDS ± reducing agent

|___ pulse ___|          |___ chase ___|

**B**

| | N-terminal stretch* | E2~Ub discharge | self-ubiquitylation |
|---|---|---|---|
| ● (black) | - | - | - |
| ● (blue) | 691-712 | + | - |
| ● (red) | 636-712 | + | + |

*HECT domain: 712-1083

**C**

UBE3C: 636-1083 (red) · 712-1083 (black)
time (min): 0, 0.5, 1, 2.5, 5, 10, 30 | 0, 0.5, 1, 2.5, 5, 10, 30

250, 150, 100, 75, 50, 37, 25, 20, 15, 10

UBE3C-Ubₙ
← UBE2D3~Ub
← Ub₂
← Ub₁

non-reducing    IB: Ubiquitin

25, 20
← UBE2D3~Ub
← UBE2D3

non-reducing    IB: His-tag

**D**

UBE3C: 691-1083 (blue) · 636-1083 (red)
time (min): 0, 0.5, 1, 1.5, 2.5, 5 | 0, 0.5, 1, 1.5, 2.5, 5

250, 150, 100, 75, 50, 37, 25, 20, 15, 10

UBE3C-Ubₙ
← UBE3C~Ub
← UBE2D3~Ub
← Ub2
← Ub1

non-reducing    IB: Ubiquitin

25, 20
← UBE2D3~Ub
← UBE2D3

non-reducing    IB: His-tag

**E**

UBE3C: 691-1083 (blue) · 636-1083 (red)
time (min): 0, 0.5, 1, 1.5, 2.5, 5 | 0, 0.5, 1, 1.5, 2.5, 5

250, 150, 100, 75, 50, 37, 25, 20, 15, 10

UBE3C-Ubₙ
← Ub4
← Ub3
← Ub2
← Ub1

reducing    IB: Ubiquitin

25, 20
← UBE2D3

reducing    IB: His-tag

***Figure 3.2 N-terminal stretch upstream of the HECT domain modulates Ub conjugation activity of UBE3C***

*(A) Schematic diagram of pulse-chase assays. In pulse reaction, Ub was loaded onto E2 in the presence of UBE1 and ATP. ATP was then depleted by the addition of Apyrase. Chase reaction was carried out by adding UBE3C into the pulse reaction (Chapter 2.8.2). (B) A summary of pulse-chase assays. (C-D) 1.4 µM of His-tagged UBE2D3~Ub was incubated with 1.4 µM of UBE3C at 37 °C for the indicated periods of time. UBE2D3~Ub and self-ubiquitylated UBE3C were visualised by anti-Ub immunoblotting, whereas UBE2D3 was visualised by anti-His immunoblotting. (E) Pulse-chase assays in (D) were stopped by adding reducing sample buffer. '~' denotes thioester bond whereas '-' denotes isopeptide bond. Asterisks indicate non-specific bands.*

Self-ubiquitylation of HECT E3s can occur *in cis* or *in trans* (Huibregtse *et al*, 1995; Pandya *et al*, 2010) (Figure 3.3A). I then was interested to investigate the nature of UBEC self-ubiquitylation and how it is modulated by the 80aa-upstream. In autoubiquitylation assays I monitored whether wild-type UBE3C (636-1083) can conjugate Ub onto

catalytically dead mutant, which is HA-tagged UBE3C (Figure 3.3B, lane 1-3). Indeed, the catalytic dead UBE3C is unable to assemble polyUb chains or self-ubiquitylate (Figure 3.3B, lane 2). Interestingly, in the presence of wild-type UBE3C, ubiquitylation of the catalytic dead UBE3C is now observed (Figure 3.3B, lane 3). This suggests that ubiquitylation occurs *in trans*. In the presence of wild-type UBE3C (636-1083), ubiquitylation of UBE3C lacking half (691-1083) or all (712-1083) of the 80aa-upstream is less compared to UBE3C containing full 80aa-upstream (Figure 3.3B, lane 5-6 and 8-9). Collectively, these observations suggest that self-ubiquitylation of UBE3C occurs *in trans*, which requires the 80aa-upstream of UBE3C.
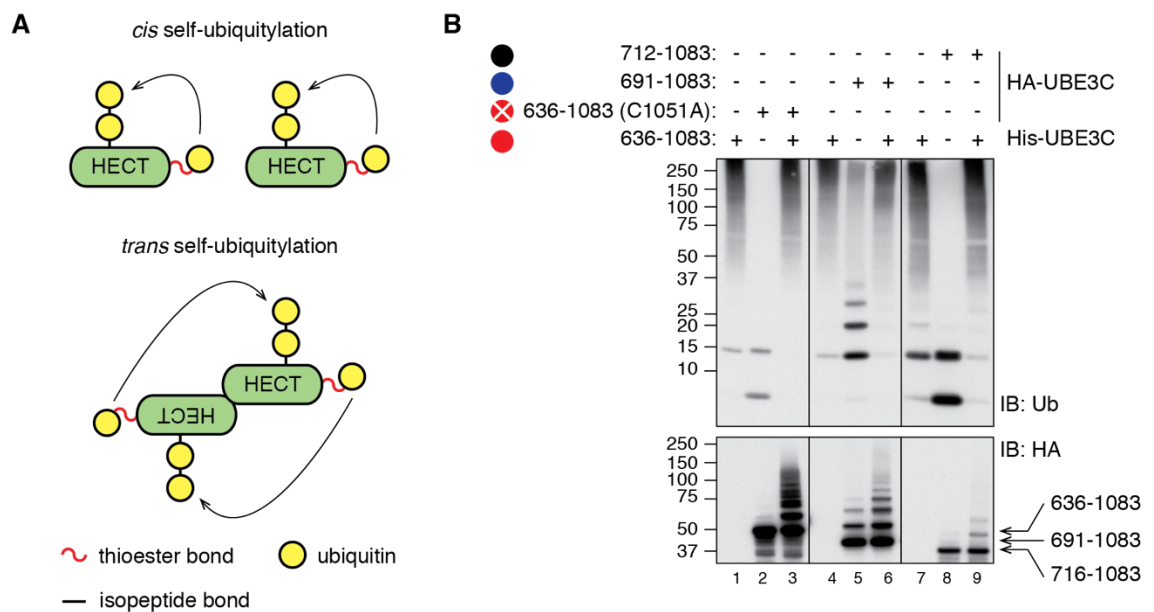


***Figure 3.3 Self-ubiquitylation of UBE3C occurs in trans and is modulated by the N-terminal stretch of the HECT domain***
*(A) A schematic diagram illustrates in cis and in trans self-ubiquitylation of HECT E3.*
*(B) Autoubiquitylation assays were carried out in the presence of Ub, UBE1, UBE2D3 and the indicated His-UBE3C and HA-UBEC at 37 °C for 1.5 h. The construct boundaries of UBE3C are indicated as in Figure 3.1A. C105A, catalytic dead UBE3C is represented as circle with white cross. Self-ubiquitylation of UBE3C was detected by anti-HA immunoblotting.*

### 3.2.2 Assembly and purification of K29-linked polyUb chains

Having established the optimal construct boundary of UBE3C and its cognate E2, I then focused on developing a strategy for isolating K29-linked polyUb chains generated. I have demonstrated that UBE3C prefers to conjugate polyUb chains on itself rather than generate unanchored polyUb chains (Figure 3.1, Figure 3.2 and Figure 3.3). According to the previous study, these polyUb chains on UBE3C contained mainly K29 and K48 linkage types (You & Pickart, 2001; Wang *et al*, 2006). Therefore, to release K29-linked polyUb chains from UBE3C and at the same time remove contaminating linkage types, I used a non-specific OTU DUB vOTU (Figure 3.4A). Although non-specific, this DUB, which is encoded by Crimean Congo Haemorrhagic fever virus (CCHV) does not hydrolyse M1, K27 and K29 linkage types (Akutsu *et al*, 2011; Ritorto *et al*, 2014).

To test whether incubation with vOTU can release K29-linked polyUb chains from UBE3C, I monitored the chain products released when vOTU was added to polyUb assembled by UBE3C from wild-type or Ub Lys-to-Arg mutants (Figure 3.4B-C). Incubation with vOTU releases polyUb chains from UBE3C into chains of defined lengths containing up to nine Ub moieties (Figure 3.4C). Higher molecular-weight polyUb chains were observed when chain products assembled from K48R Ub mutant were incubated with vOTU (Figure 3.4C, lane 7). In contrast, no polyUb chains were released by vOTU when Ub K29R mutant was used for UBE3C assembly (Figure 3.4C, lane 5). This is however, not due to a defect in UBE3C polyUb assembly when K29R was used (Figure 3.4B), strongly suggesting that the unanchored polyUb chains released by vOTU are K29-linked.
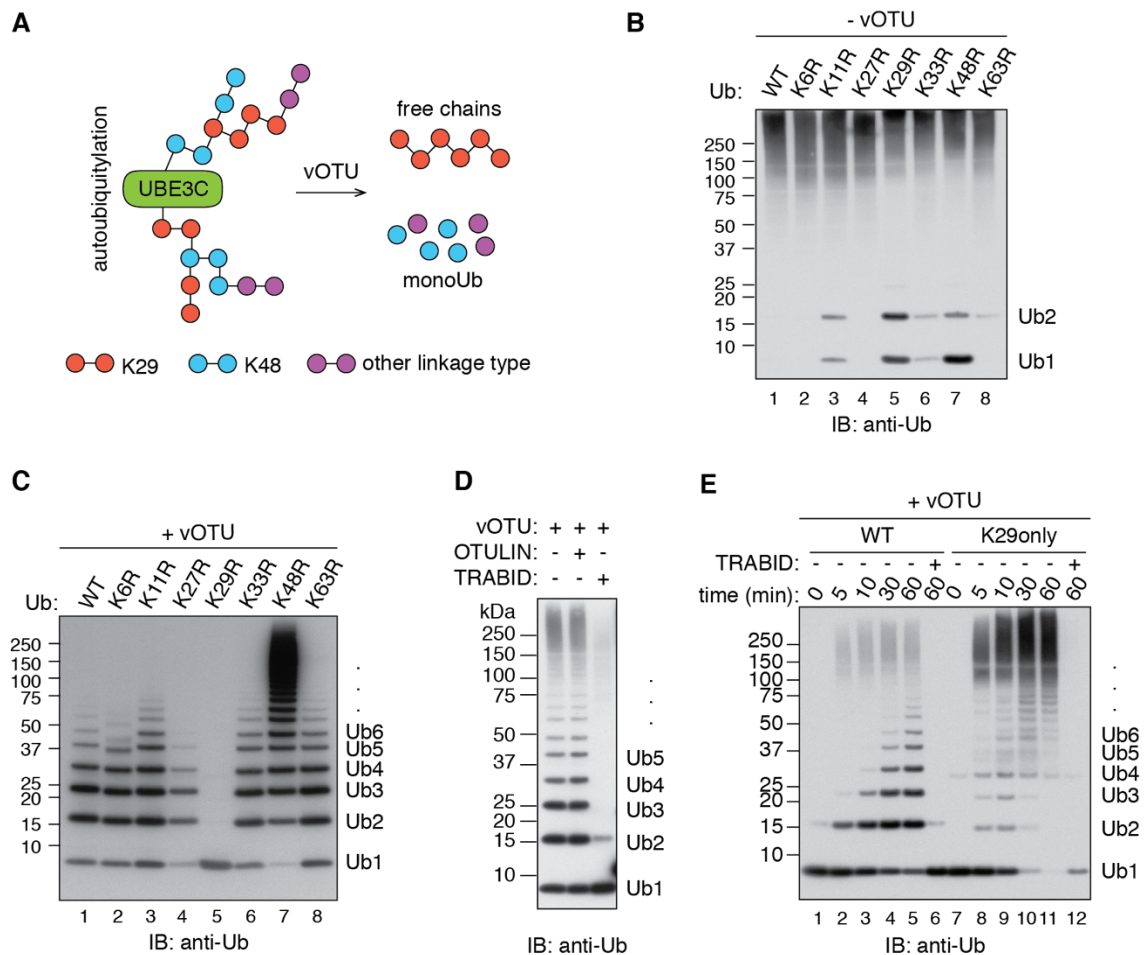
**Figure 3.4 vOTU releases unanchored K29-linked polyUb chains from UBE3C**
*(A) A schematic diagram illustrates how vOTU can be used to release K29-polyUb chains and remove contaminating linkage types from self-ubiquitylated UBE3C. (B-C) Autoubiquitylation assays of UBE3C were carried out in the presence of UBE1, UBE2D3 and wild-type Ub or K-to-R Ub mutants at 37 °C for 30 min. vOTU was added at the end of the ubiquitylation reaction (C). (D) Autoubiquitylation assays of UBE3C were carried in the presence of Ub, UBE1 and UBE2D3 at 37 °C for 30 min. DUBs were included in the reaction as indicated: vOTU, M1 linkages-specific OTULIN, and K29 linkages-specific TRABID. (E) Time course of autoubiquitylation of UBE3C in the presence of UBE1, UBE2D3, vOTU and wild-type Ub or K29only Ub mutant. For lane 6 and 12, reaction was stopped at 60 min by the addition of apyrase, which hydrolyse ATP, followed by DUB reaction using TRABID.*

In order to confirm the linkage type of the chains released by vOTU from the UBE3C ubiquitylation products, I added either the K29- and K33-selective DUB TRABID (Licchesi *et al*, 2011) or the M1-specific DUB OTULIN to the reaction (Keusekotten *et al*, 2013). Whereas polyUb chains released by vOTU were not affected by the addition of OTULIN, only monoUb was released upon the addition of TRABID,

which is similar to when K29R Ub mutant was used (Figure 3.4D). When Ub mutant that only has one Lys residue (K29only) was used in the polyUb conjugation by UBE3C, the chains produced were resistant to vOTU treatment but not to TRABID (Figure 3.4E). Collectively, these results confirm that the polyUb released by vOTU are K29-linked. Therefore, in conclusion, UBE3C together with vOTU can be used as a Ub-chain editing complex to assemble unanchored K29-linked polyUb of defined lengths.

By scaling up the ubiquitylation reaction using UBE3C and vOTU as described above, a large quantity of K29-linked polyUb chains was generated (Figure 3.5A). To purify chains of defined lengths, I used size-exclusion chromatography (SEC), which separates proteins based on their molecular weight (Figure 3.5B). Modest separation was achieved for shorter chains of mono and diUb, whereas longer chains were eluted in overlapping peaks. This may be due to the resolution limit of SEC. Therefore, SEC is not suitable to purify polyUb chains containing three or more Ub moieties.

An alternative purification technique is by using ion-exchange chromatography (IEC), which separate proteins based on their charge. The theoretical isoelectric point of Ub is 6.56 and therefore at pH 4.5, Ub is positively charged. This strength of the positive charge is directly proportional to the length of polyUb chains. In addition to this, lowering the pH of the assembly reaction to 4.5 destabilises the conjugating enzymes used. Therefore, they can be separated away from the ubiquitylation products either by centrifugation or filtration through 0.22-µm membrane. Taking advantage of these, I separated K29-polyUb chains using cation-exchange chromatography, which yields a better separation than SEC (Figure 3.5C). Well separated fractions of mono-, di-, tri-, tetra- and pentaUb were observed and the purity of these isolated chains was demonstrated on silver-stained SDS-PAGE gel (Figure 3.5D).
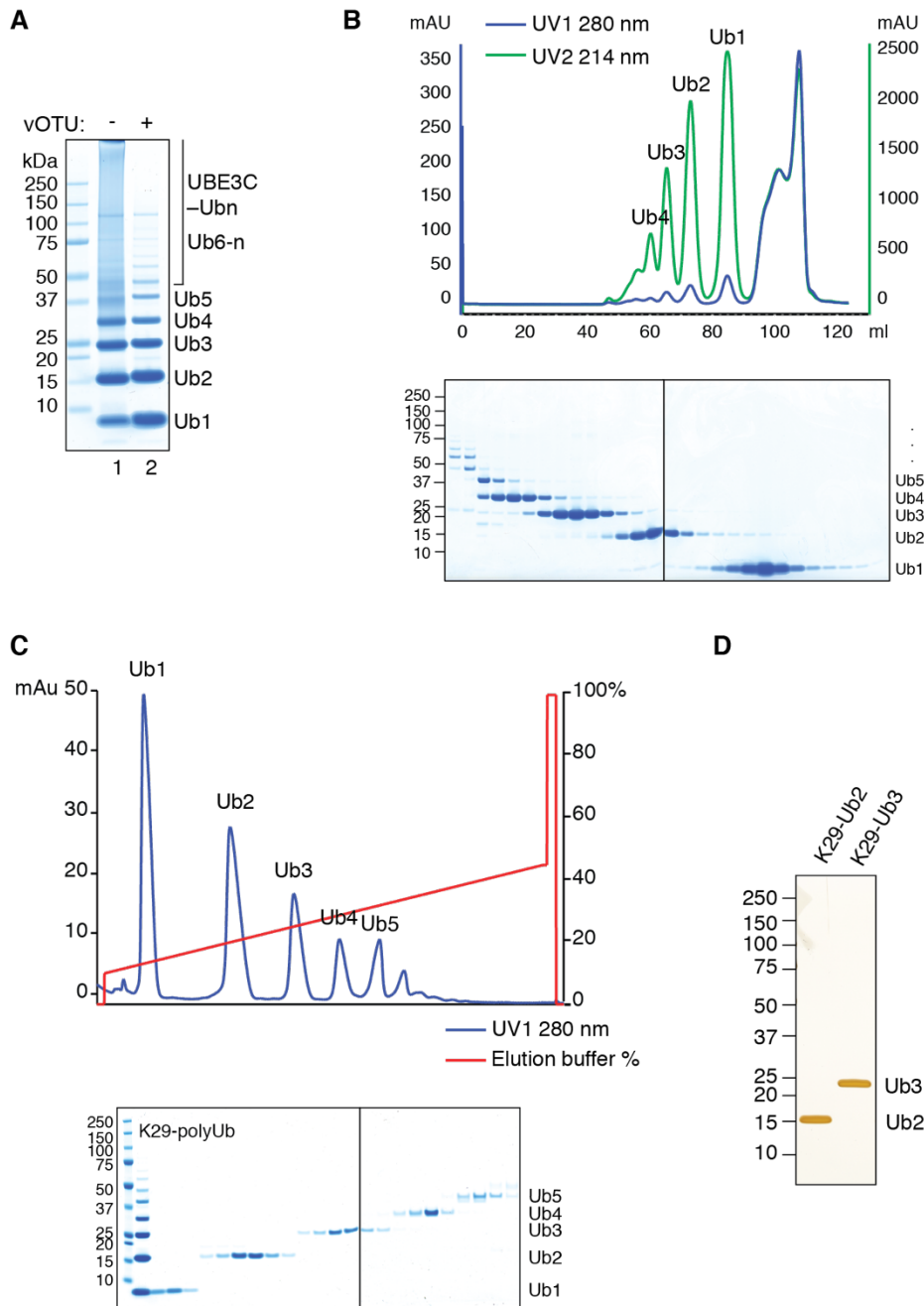
**Figure 3.5 Purification of K29-linked polyUb chains**
*(A)* *Large-scale assembly of polyUb chains by UBE3C in the presence of UBE1, UBE2D3 and Ub. The addition of vOTU releases unanchored polyUb chains.* *(B-C)* *Purification of K29-linked diUb, triUb, tetraUb and pentaUb using size-exclusion chromatography (B) and cation-exchange chromatography (C). Proteins from the corresponding peak fractions (top) were visualized on Coomassie-stained SDS-PAGE gel (bottom).* *(D)* *The K29-linked diUb and triUb purified in (C) were visualized in silver-stained SDS-PAGE gel and analysed by PRM-LC-MS/MS (Figure 3.6).*

Mass spectrometry has been widely used to analyse the linkage types within polyUb chains (Ordureau *et al*, 2015). The Lys within Ub that has been used as the conjugation site can be identified from the mass of the tryptic-digested peptides, as it has an additional of Gly-Gly adduct covalently linked to the modified Lys. Parallel reaction monitoring (PRM) is a LC-MS/MS-based technique that can be used to selectively monitor the GG-modified Ub peptides, since their abundance is far less compared to their unmodified counterparts. PRM LC-MS/MS only selects precursor ions (MS1) of the GG-modified peptides to be fragmented further to daughter ions (MS2) (Peterson *et al*, 2012) (Figure 3.6A) (Chapter 2.10.2). Finally, only the MS2 of the GG-modified peptides was used to determine the abundance of linkage types of polyUb chains. Using this approach, I further verified that the diUb and triUb purified are indeed K29-linked with no contamination from other linkage types (Figure 3.6B).
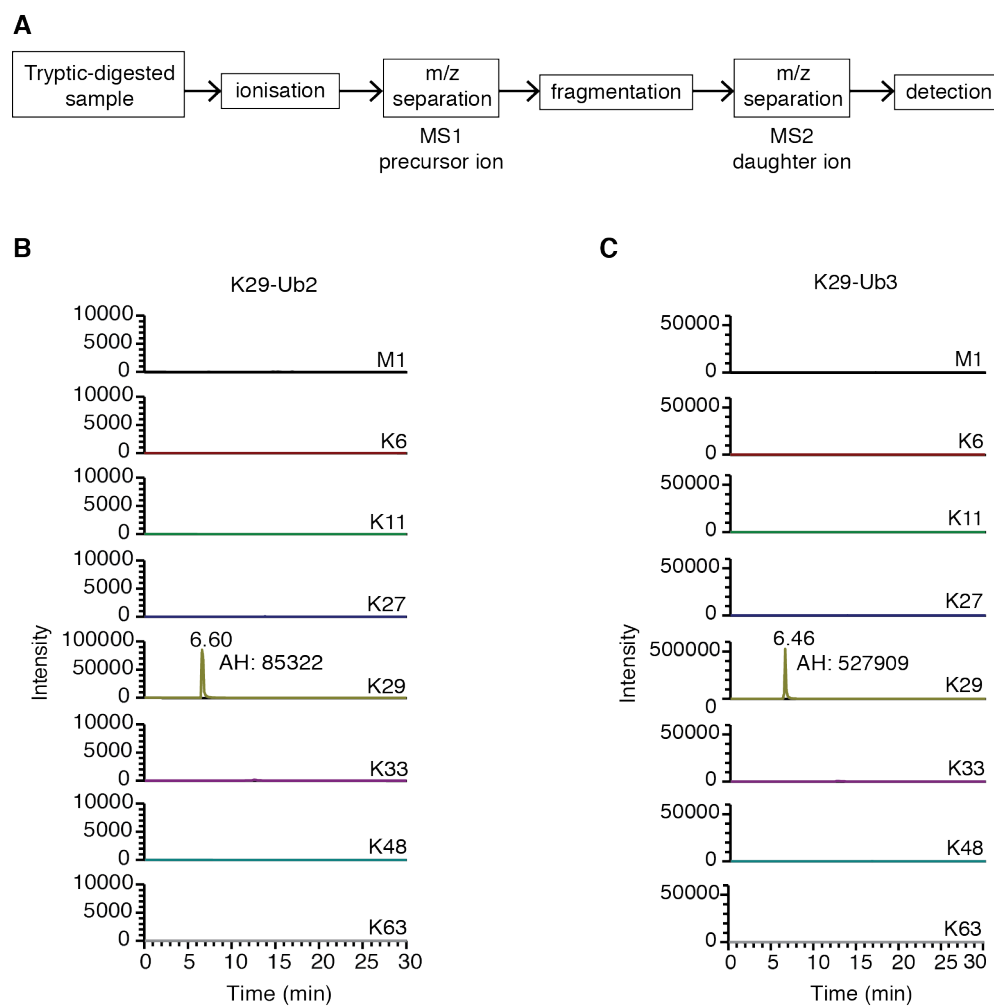
***Figure 3.6 PRM LC-MS/MS analysis confirms the purity of the assembled K29-linked diUb and triUb***

*(A) A schematic diagram illustrates pipeline of PRM LC-MS/MS analysis to monitor linkage types of polyUb chains. (B-C) PRM analyses of the abundance of polyUb linkages in the purified samples of K29-linked diUb (B) and triUb (C) (Figure 3.5D). The intensity scales for non-K29 linkages were set 10-fold lower. AH: automated height as determined by the XCalibur software (see Chapter 2.10.2).*

### 3.2.3   Crystal structure of K29-linked diUb

When this study was carried out, the structure of K29-linked diUb whether it adopts 'closed' or 'open' conformations was not known. This was due to the lack of a robust method to generate large quantity of pure K29 chains for biophysical and biochemical study. Having overcome this setback, I was determined to investigate the structure of

K29-diUb. Wide initial screens of crystal conditions were made possible by the large amount of K29-diUb produced enzymatically described above. However, these initial screens only produced either needle clusters or plate clusters-type crystals, which were not suitable for X-ray diffraction. Syed Arif Abdul Rehman, who is a Postdoctoral researcher in the lab helped me to optimise the crystallisation condition. Using micro-seeding technique we managed to get crystals of K29-diUb that diffracted to 2.3 Å (Chapter 2.12.4).

The structure was determined by molecular replacement using Ub (1UBQ (Vijay-Kumar *et al*, 1987)) as a search model and was refined to the final statistics as shown in Table 3.1. The asymmetric unit (ASU) contains two K29-linked diUb molecules (Figure 3.7A). The distal Ub is bound via its C terminus to K29 of the proximal Ub; and there is visible electron density for the isopeptide linkages (Figure 3.7A).

In this crystal structure, K29-diUb adopts an 'open' conformation, which resembles the structure of K63- and M1-diUb (Figure 3.7B, E-F). However, there is an interface formed between the two Ub moieties of K29-diUb, which is not observed in K63-diUb and M1-diUb structures (Figure 3.7C-F). Contacts between the two Ub moieties within K29-diUb are entirely polar and involve hydrogen bonds between distal Ub R42 and R72, and proximal Ub E16, E18 and D21 (Figure 3.7C). Therefore, K29-diUb observed here adopts a partially 'open' conformation, which has not been observed in other diUb chain types before.

***Table 3.1 Data collection and refinement statistics for K29-diUb***

|  | **K29-diUb** |
|---|---|
| Wavelength (Å) | 1.033 |
| Beamline | ID23-1 |
| Resolution range (Å) | 60.05 - 2.30  (2.38 - 2.30) |
| Space group | $P2_1$ |
| Unit cell dimensions | 33.45 69.25 60.06 |
|  | 90.00 90.22 90.00 |
| Total reflections | 22801 (2317) |
| Unique reflections | 11542 (1185) |
| Multiplicity | 1.9 (2.0) |
| Completeness (%) | 94.12 (92.88) |
| Mean I/sigma(I) | 8.71 (3.07) |
| R-merge | 0.0962 (0.4483) |
| CC1/2 | 0.977 (0.614) |
| R-work | 0.1981 (0.2581) |
| R-free | 0.2456 (0.3053) |
| Average B-factor ($Å^2$) | 29.2 |
| macromolecules | 2366 |
| water | 43 |
| RMS bonds (Å) | 0.018 |
| RMS angles (°) | 1.94 |
| Ramachandran favoured (%) | 100 |
| Ramachandran allowed (%) | 0 |
| Ramachandran outliers (%) | 0 |
| PDB accession code | 4S22 |
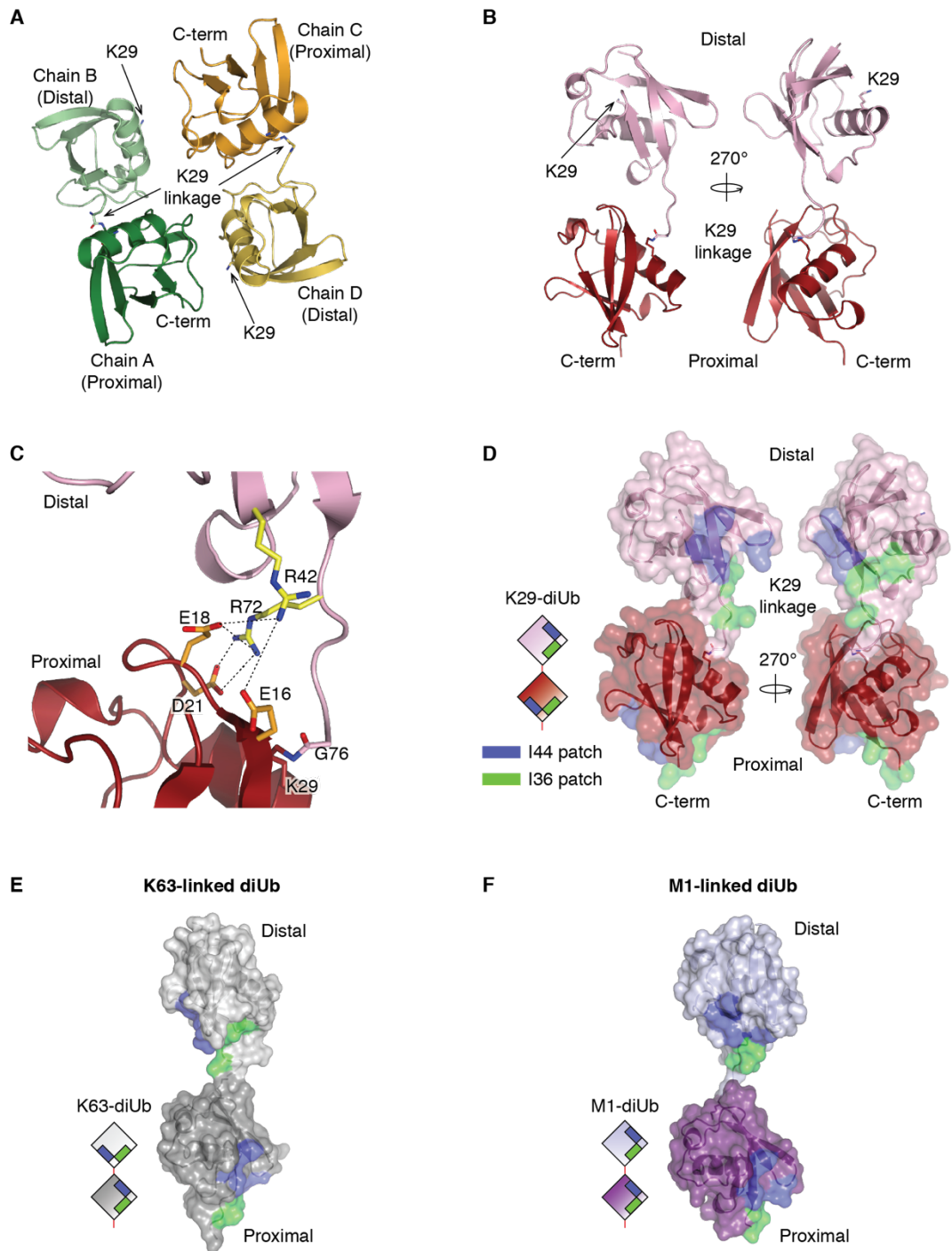
**Figure 3.7 Crystal structure of K29-linked diUb**

*(A) The asymmetric unit contains four Ub moieties and makes up two K29-linked diUb molecules coloured in shades of green and orange, respectively. (B) Crystal structure of K29-linked diUb is shown in two orientations. Distal and proximal Ub are coloured pink and red, respectively. (C) Residues at the interface between the two Ub moieties are shown in sticks. Hydrogen bonds between polar residues are shown as dotted lines. (D) K29-diUb in (B) is shown in surface representation. I44-patch and I36-patch of Ub are coloured blue and green, respectively. (E-F) 'Open' conformations of K63-diUb (E) and M1-diUb (F) are shown in surface representations. I44- and I36-patches of Ub are coloured as in (D) (PDB ID: 2JF5 and 2W9N (Komander et al, 2009b)).*

124

### 3.2.4    Screening HECT E3 ligase linkage specificity

Unlike K29 linked polyUb, the Ub-conjugation machinery to assemble K33 linkage type *in vitro* is poorly understood. HECT E3s display linkage selective polyUb conjugation despite of their E2s. This is in contrast to RING E3s, where linkage selectivity in polyUb conjugation is determined by their cognate E2s  (Chapter 1.3.2). Therefore, to find HECT E3s capable of assembling K33 linkages, I screened a number of HECT E3s, whose linkage selectivity is poorly characterised *in vitro,* for the types of polyUb they assemble.

Either full-length or the catalytic domain of 12 HECT E3 ligases were expressed as GST fusion proteins in *E. coli*  (Figure 3.8 and Table 2.2). Initially, to determine the optimal E2 pair for the given HECT E3, I monitored the polyUb conjugation activity of HECT E3s in combination with four different human E2s of UBE2D or UBE2L3 family. With the exception of UBE3B, KIAA1333, and EDD1, all the tested HECT E3 ligases assembled polyUb chains (Figure 3.9A). Further, all the HECT E3s work with all the E2s tested except UBE3C and HUWE1, which cannot work with UBE2L3 (Figure 3.9A). In this screen I found that AREL1 (also known as KIAA0137) assembled short polyUb chains at early time points and at later time points AREL1 assembles higher molecular weight ubiquitylated species (Figure 3.9B and Figure 3.10). This suggests that AREL1 has a slower enzyme kinetics compared to other HECT E3s tested. By contrast, UBE3B, KIAA1333 and EDD1 failed to assemble polyUb chains even after 6 h incubation, suggesting that they were inactive in the given ubiquitylation setting (Figure 3.9B). This may be caused by the non-optimal construct boundaries chosen for these HECT E3s, just as the minimal HECT domain of UBE3C was insufficient (Figure 3.1B). Other reasons for poor activity may be that to ubiquitylate substrates, these E3s prefer to work with other E2s, which were not studied in this screen.
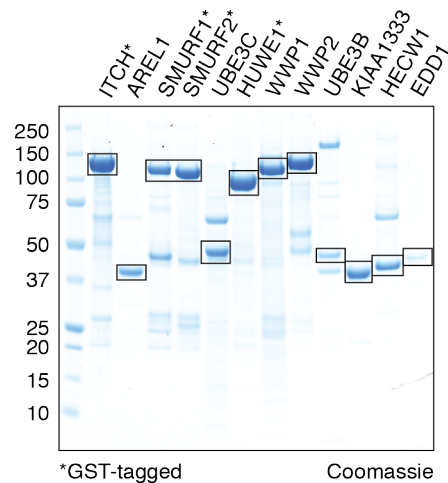
***Figure 3.8 HECT E3s used in the polyUb linkage assembly screen***
*HECT E3 ligases were separated on 4-12% SDS-PAGE gel and visualised by Coomassie-staining. Boxed are the purified HECT E3 ligases at the calculated molecular weight.*


The linkage types of polyUb chains assembled by the HECT E3 ligases tested were analysed using PRM LC-MS/MS technique as described previously (Chapter 2.10.2 and Chapter 3.2.2). In agreement with previous published studies and observations described above, UBE3C primarily assembles K29- and K48-linked polyUb chains (Figure 3.11 and Chapter 3.2.2) (You & Pickart, 2001). Most of the HECT E3s tested assembled K63 linkage types, similar to what had been observed previously for NEDD4-like type HECT E3s (Sheng *et al*, 2012; Maspero *et al*, 2013). K6 linkage type is assembled mostly by HUWE1, whereas K11 linkage type is assembled by AREL1, HECW1 and HUWE1 (Figure 3.11). Interestingly, AREL1 also assembles high amounts of K33 linkages (Figure 3.11). Therefore, AREL1 can be exploited to assemble large quantities of K33-linked polyUb chains *in vitro* (Figure 3.11).
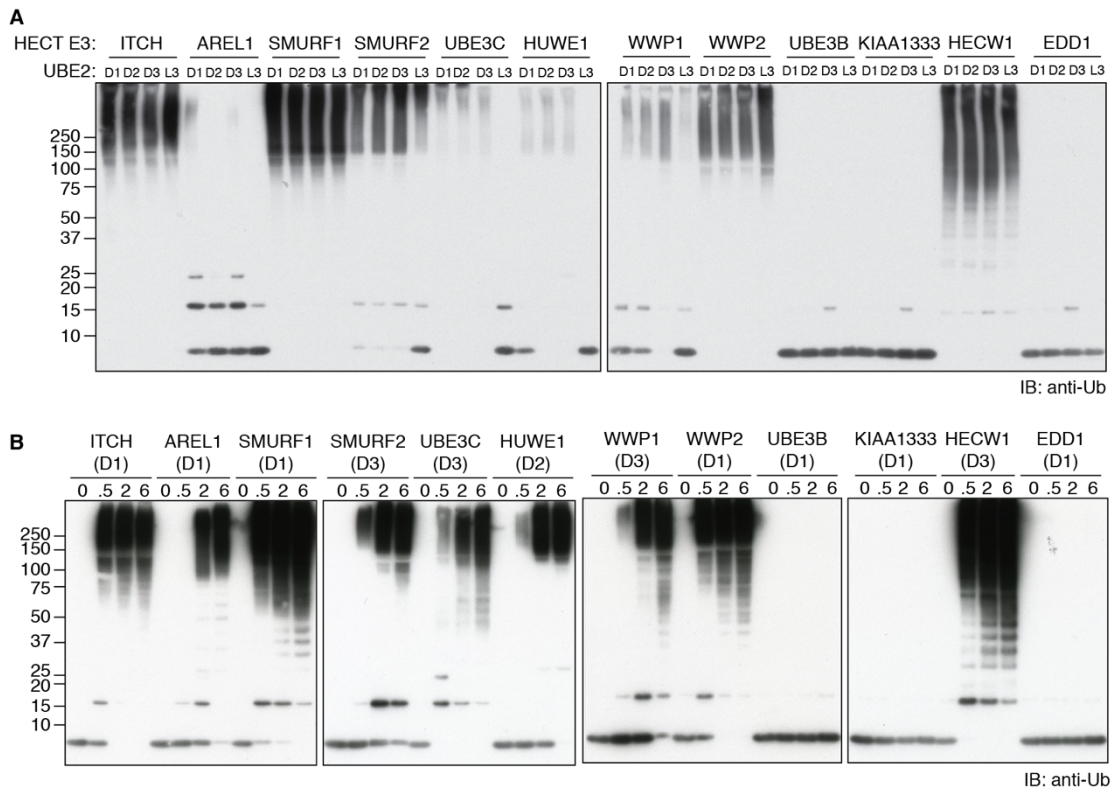
**Figure 3.9 Identification of optimal pair of HECT E3 and E2 in ubiquitylation reactions**
*(A) Autoubiquitylation assays of HECT E3 ligases were carried out in the presence of UBE1, Ub and the indicated E2 enzymes: UBE2D1, UBE2D2, UBE2D3 or UBE2L3 at 37 °C for 3 h. (B) Autoubiquitylation assays of HECT E3 ligases in the presence of UBE1, Ub and the indicated E2 for the indicated periods of time.*
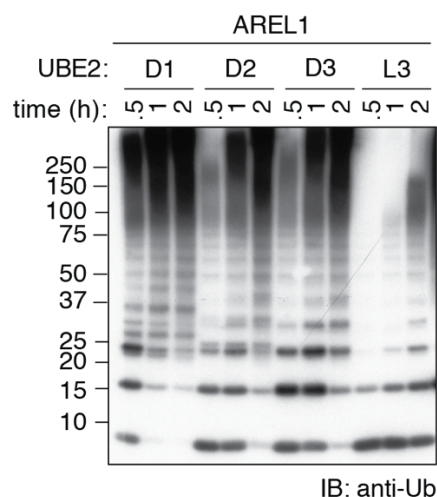


**Figure 3.10 AREL1 assembles polyUb chains most efficiently together with UBE2D1**
*Autoubiquitylation assays of AREL1 in the presence of UBE1, Ub and the indicated E2 enzymes: UBE2D1, UBE2D2, UBE2D3 or UBE2L3 at 37 °C for the indicated period of time.*

127
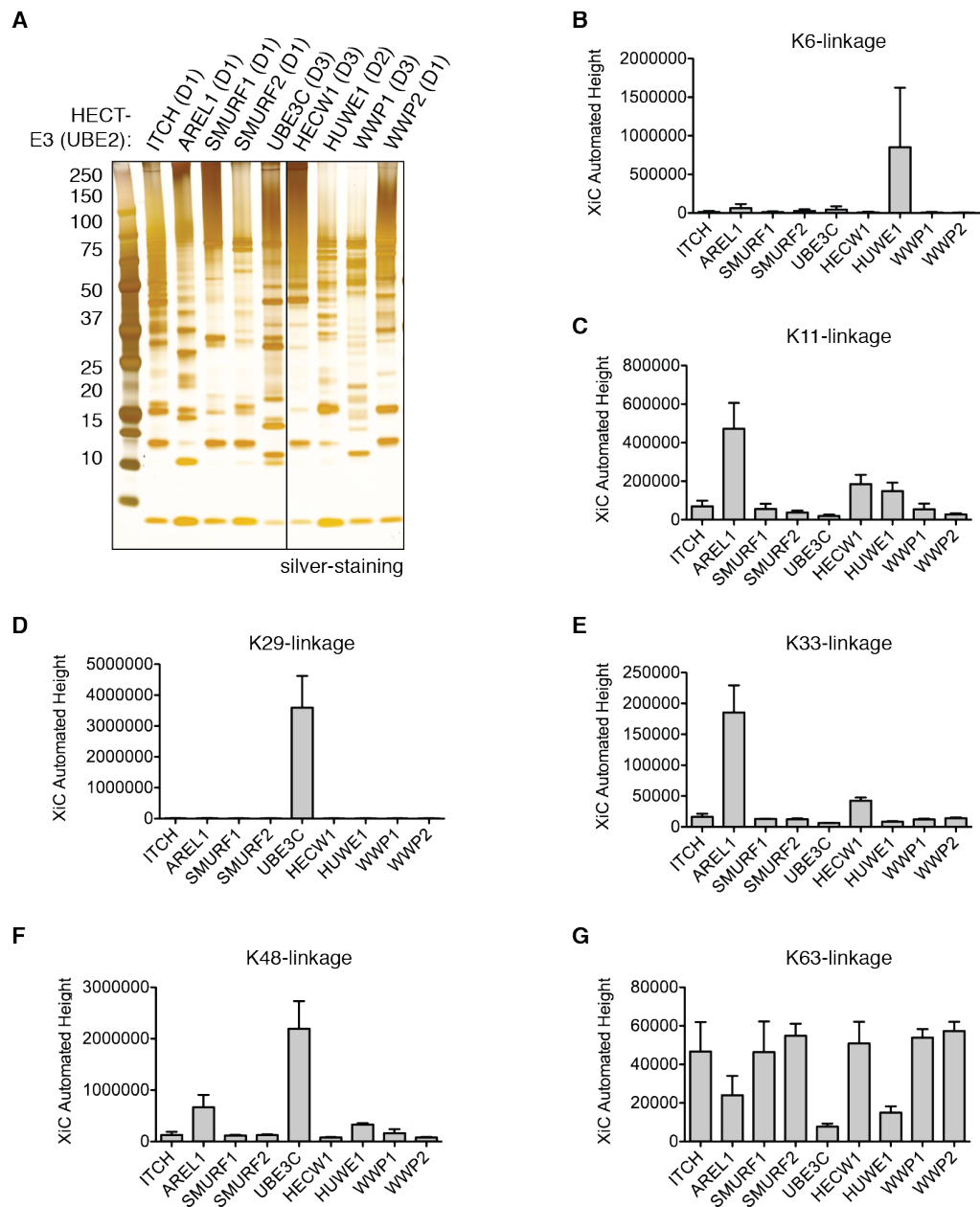
***Figure 3.11 Linkage analysis using parallel reaction monitoring (PRM) LC-MS/MS***
*(A) Autoubiquitylation assays of HECT E3 ligases as in Figure 3.9 for the optimal time*
*point. 10% of the reaction was visualised on silver-stained SDS-PAGE gel, whereas the*
*rest was processed for PRM LC-MS/MS (Chapter 2.10.2). (B-G) Abundance of linkage*
*types of polyUb chains generated in (A). Y-axes of bar graphs are the summed ion current*
*values for the relevant daughter ions of each precursor mass analysed (see Chapter*
*2.10.2). No signal was observed for M1 and K27 linkage types for any of the HECT E3*
*ligases tested.*

## 3.2.5 Assembly and purification of K33-linked polyUb chains

In addition to K33 linkages, AREL1 also assembles K11, K48 and K63 linkage types

(Figure 3.11). Similar to what has been observed in UBE3C, these polyUb chains might

be assembled on AREL1 as self-ubiquitylation products and thus, DUBs are required to cleave non-contaminating linkage types and release K33-chains from AREL1 (Figure 3.1 and Figure 3.4A). For this purpose, OTUB1 which selectively hydrolyses K48 linkage types and Cezanne which cleaves K11 were used (Bremm *et al*, 2010; Ritorto *et al*, 2014). Based on the crystal structure of Cezanne, mutating residues of the active loop may enhance activity (Mevissen *et al*, 2016). Indeed, time course DUB assays comparing wildtype and mutant reveal that Cezanne E287K/E288K (Cezanne EK) has higher DUB activity for cleaving K6, K11, K48 and K63 chains (Figure 3.12A-B).

To test whether incubation with Cezanne EK and OTUB1 can release K33-linked polyUb chains from AREL1, I monitored the chains released when Cezanne EK and OTUB1 were added to polyUb assembled by AREL1 (Figure 3.12C-D). PolyUb chains containing up to five Ub moieties were released when polyUb chains were assembled from wild-type Ub. Whereas polyUb assembly was not affected by most Ub K-to-R mutants, no polyUb products were formed with K33R Ub mutant (Figure 3.12D). Importantly, K33R Ub mutant did not significantly affect AREL1 polyUb conjugation in the absence of DUBs, which is consistent that AREL1 can use other Lys for polyUb assembly (Figure 3.12C). Collectively, these suggest that the unanchored polyUb chains released by Cezanne EK and OTUB1 are K33 linked, which is further confirmed as these chains were completely hydrolysed upon incubation with a K29- and K33-specific DUB TRABID (Figure 3.12E). In conclusion, AREL1 in combination with Cezanne EK and OTUB1 can be used as a Ub-chain editing complex to generate K33-linked polyUb chains of different lengths.
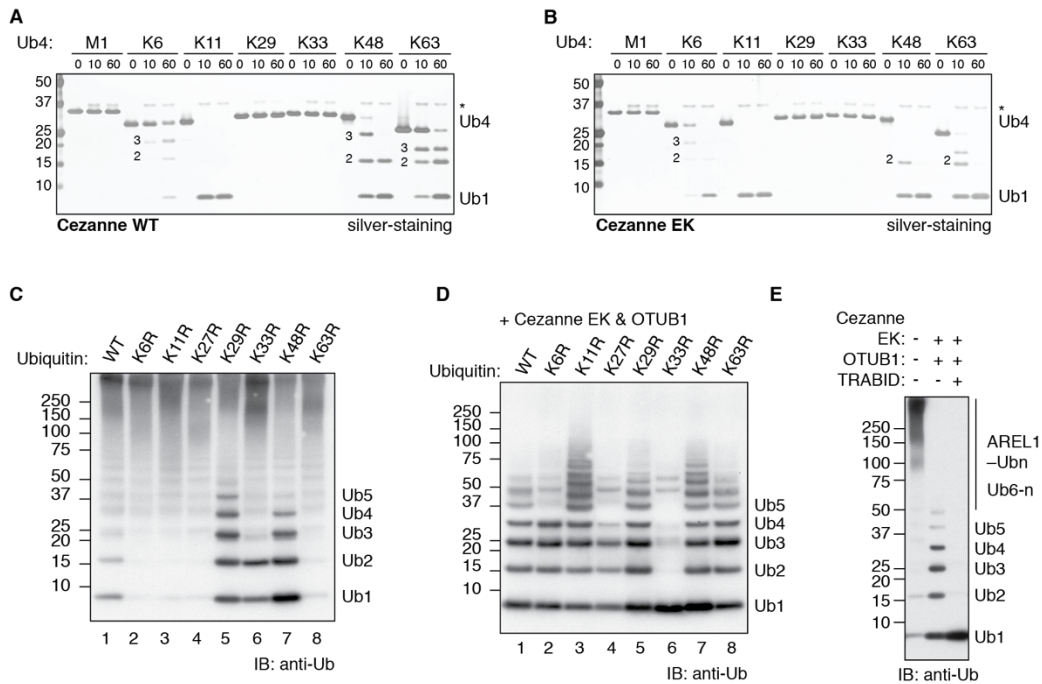
**Figure 3.12 Cezanne EK and OTUB1 release unanchored K33-linked polyUb chains from AREL1**

*(A-B) Deubiquitylating assays were carried out in the presence of 1.5 µM tetraUb chains of the indicated linkage types and 275 nM of Cezanne or Cezanne E287K/E288K (Cezanne EK) at 30 °C for the indicated periods of time. (C-D) Autoubiquitylation assays of AREL1 were carried out in the presence of UBE1, UBE2D1 and wild-type Ub or K-to-R Ub mutants at 37 °C for 3 h. Cezanne EK and OTUB1 was added at the end of the ubiquitylation reaction (D). (E) Autoubiquitylation assays of AREL1 were carried out in the presence of Ub, UBE1 and UBE2D1 at 37 °C for 3 h. DUBs were added at the end of the reaction, followed by incubation at 37 °C for 1 h.*

The reaction for assembling K33-linked polyUb chains was scaled up, from which milligram amounts of K33-linked polyUb chains of defined lengths were purified using procedure described in Chapter 3.2.2 and Chapter 2.5.2 (Figure 3.13). PRM LC-MS/MS analyses validated that the purified polyUb chains contained only K33 linkage type and none of the other linkages were detected (Figure 3.14). Taken together, this study describes a robust and reproducible method for generating high quantity of K33-linked polyUb enzymatically using AREL1 as the HECT E3.
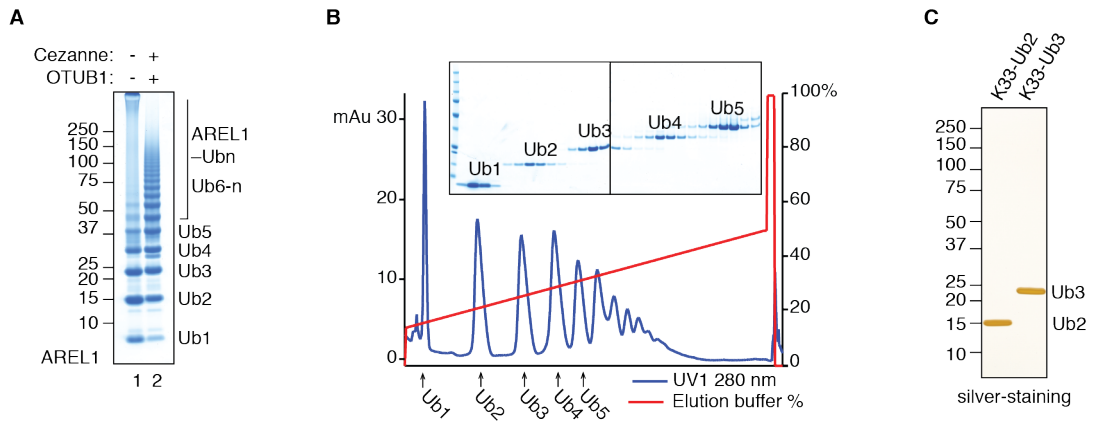
**Figure 3.13 Purification of K33-linked polyUb chains**
**(A)** *Large-scale assembly of polyUb chains by AREL1 in the presence of UBE1, UBE2D1 and Ub. The addition of DUBs, Cezanne EK and OTUB1, releases free polyUb chains.* **(B)** *Purification K33-linked polyUb chains of defined lengths by cation-exchange chromatography.* **(C)** *The K33-linked diUb and triUb purified in (B) were visualized in silver-stained SDS gel.*
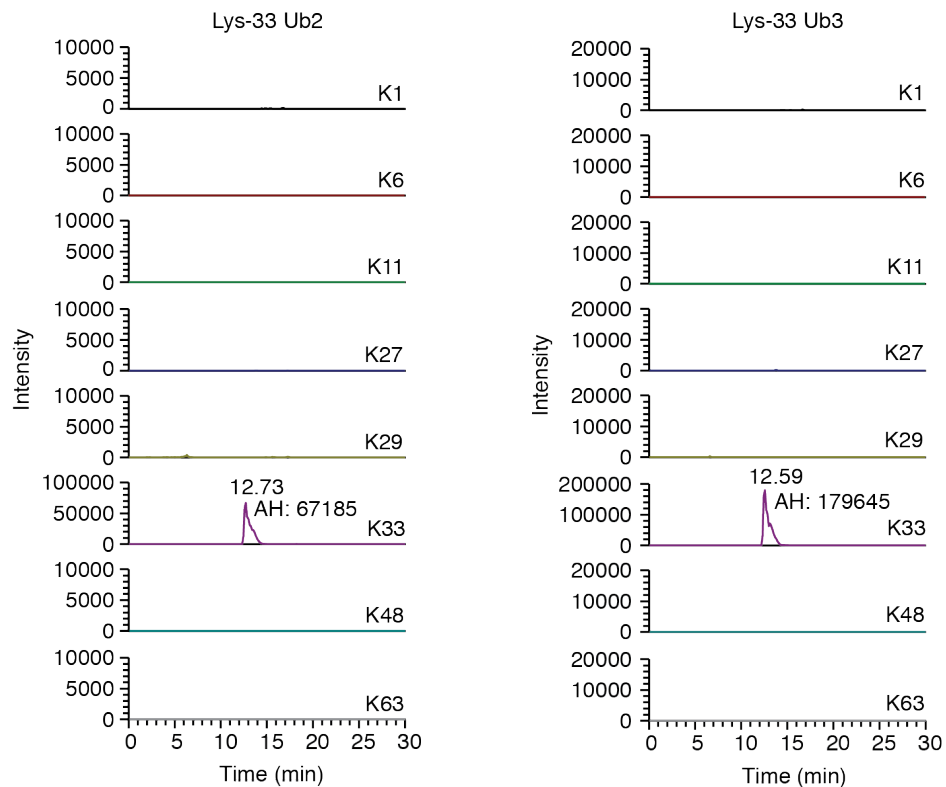


**Figure 3.14 PRM LC-MS/MS confirm the purity of the assembled K33-Ub2 and Ub3**
*PRM analysed the abundance of polyUb linkages in the purified samples of K33-linked diUb and triUb (Figure 3.13C). The intensity scales for non-K33 linkages were set 10-fold lower. AH: automated height as determined by the XCalibur software.*

131

### 3.2.6 Crystal structure of K33-diUb

For the lack of method to assemble large quantity of K33 diUb, structural characterisation of this chain type was challenging. Although, molecular modelling proposed that K33 diUb cannot adopt a 'closed' conformation (Fushman & Walker, 2010), there was no crystal structure to validate this model. Therefore, I was determined to investigate the crystal structure of K33 diUb. I then set crystallisation screens to obtain diffraction quality crystals of K33-diUb, which diffracted to 1.65 Å. Structure was solved by molecular replacement using Ub (1UBQ (Vijay-Kumar *et al*, 1987)) as a search model and was refined to the statistics shown in Table 3.2. The asymmetric unit (ASU) contains one K33-diUb molecule (Figure 3.15A). Although there is no electron density for the isopeptide linkage between two Ub moieties, the C-terminal tail of the distal Ub is pointing towards K33 of the proximal Ub.

K33-linked diUb adopts a 'closed' conformation with an interface made out of extensive hydrophobic contacts between the two Ub moieties. Residues forming the interface in both Ub moieties are identical, comprised of I36, L71 and L73 residues, which together form a hydrophobic patch also known as I36-patch (Figure 3.15B). This interface is reinforced by further hydrophobic interactions between L8, I13 and L69 and hydrogen bonding between E34 and Q40.

The 'closed' diUb conformations observed to date have unique combinations of hydrophobic I44- and I36-patches at the interface between the two Ub moieties (Figure 3.15C-F). (Virdee *et al*, 2010; Hospenthal *et al*, 2013; Cook *et al*, 1992). Interestingly, in K33-diUb, the interface is composed of I36-patches of the two Ub moieties. In contrast, in K6-diUb the interface is made up of the I36- and I44-patches of the distal and proximal Ub, respectively (Figure 3.15C-D). In K48-diUb, the interface is made up of I44-patches of both Ub moieties (Figure 3.15E). Intriguingly, the 'closed' conformation of K33-diUb is very similar to one the 'closed' K11-linked diUb (Figure 3.15F) (Matsumoto *et al*,

2010). Despite these similarities, DUBs like TRABID and Cezanne can distinguish between K33 and K11 chain types, suggesting that there are more conformations adopted by K33 and K11, which are the basis for the selectivity in the ubiquitin system.

***Table 3.2 Data collection and refinement statistics for K33-diUb and triUb***

|  | K33-diUb | K33-triUb |
|---|---|---|
| Wavelength (Å) | 0.999 | 0.976 |
| Beamline | ID29 | ID29 |
| Resolution range (Å) | 33.83 - 1.65 (1.71 - 1.65) | 31.42  - 1.40 (1.45 - 1.40) |
| Space group | $P2_1$ | $P2_1 2_1 2_1$ |
| Unit cell dimensions | 29.48 57.02 33.98 | 28.94 41.83 47.60 |
|  | 90.00 95.45 90.00 | 90.00 90.00 90.00 |
| Total reflections | 58324 (5866) | 74848 (7266) |
| Unique reflections | 13474 (1348) | 11652 (1127) |
| Multiplicity | 4.3 (4.4) | 6.4 (6.4) |
| Completeness (%) | 99.40 (99.04) | 98.06 (97.16) |
| Mean I/sigma(I) | 10.55 (4.20) | 18.51 (12.82) |
| R-merge | 0.1033 (0.2502) | 0.0948 (0.1303) |
| CC1/2 | 0.99 (0.936) | 0.99 (0.986) |
| R-work | 0.167 | 0.158 |
| R-free | 0.21 | 0.194 |
| Average B-factor ($Å^2$) | 12.8 | 18.6 |
| macromolecules | 1176 | 605 |
| water | 99 | 36 |
| RMS bonds (Å) | 0.014 | 0.027 |
| RMS angles (°) | 1.75 | 2.46 |
| Ramachandran favoured (%) | 100 | 100 |
| Ramachandran allowed (%) | 0 | 0 |
| Ramachandran outliers (%) | 0 | 0 |
| PDB accession code | 4XYZ | 4Y1H |
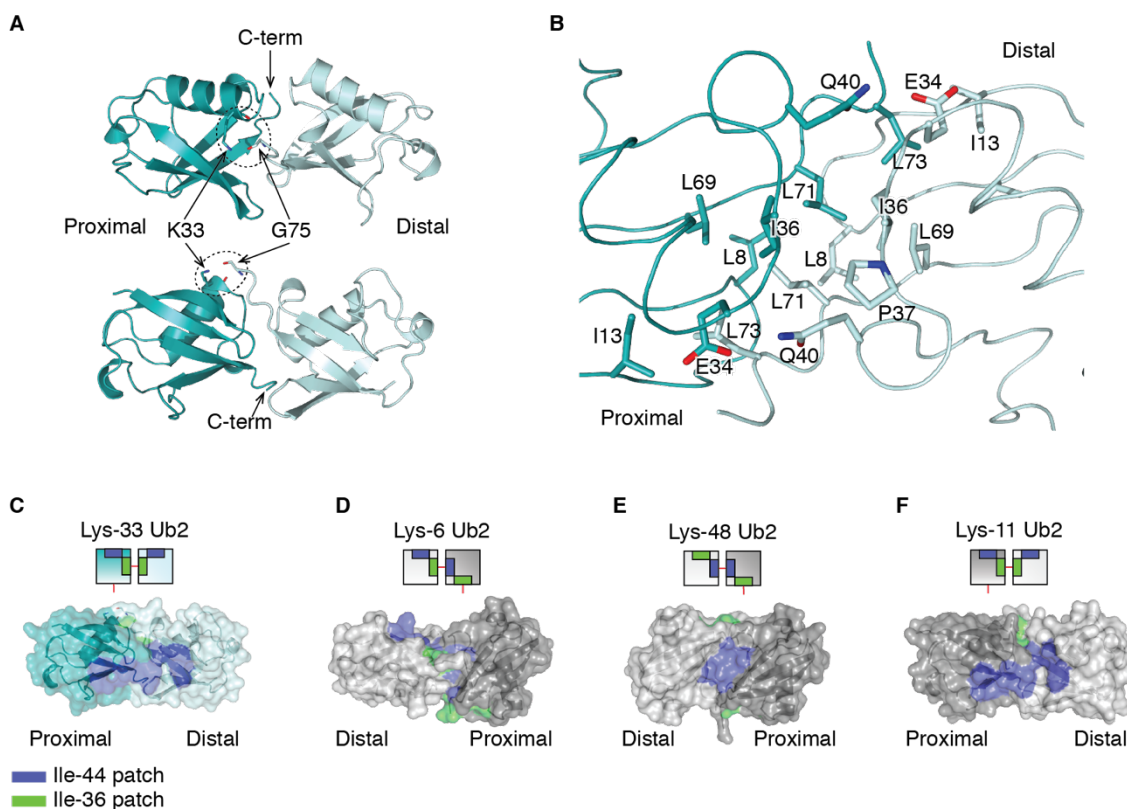
***Figure 3.15 Crystal structure of K33-linked diUb***
*(A) Crystal structure of K33-linked diUb in two orientations. (B) K33-linked diUb is shown in ribbon and the residues at the interface are shown in stick representation. (C-F) Surface representation of K33-, K6-, K48- and K11-linked diUb (PDB 2XK5, 3NOB, 1AAR (Virdee et al, 2010; Cook et al, 1992; Matsumoto et al, 2010)). Hydrophobic I44- and I36-patches of Ub are coloured blue and green, respectively.*

### 3.2.7  Crystal structure of K33-triUb

Different conformations have been observed between shorter and longer polyUb chains (Cook *et al*, 1992; 1994; Eddins *et al*, 2007). Thus, I was interested in knowing whether the conformation of K33-triUb is different from that observed of K33-diUb. So I purified and crystallised K33-triUb. The crystals of K33-linked triUb diffracted to a resolution of 1.4 Å and it has a space group and unit cell dimensions, which are different from those of K33-linked diUb crystal (Table 3.2). The structure was solved by molecular replacement using Ub (1UBQ (Vijay-Kumar *et al*, 1987)) as a search model and was refined to the final statistics shown in Table 3.2. Although triUb was crystallised, the

asymmetric unit (ASU) only contains one Ub molecule (Figure 3.16A-B, chain B). Two Ub molecules at the proximal and distal positions are derived from crystal contacts with symmetry-related molecules (Figure 3.16A-B, chain A & C). The C-terminal G76 of chain C and B are in a close proximity to K33 of chain B and A, respectively, which can be joined by isopeptide linkage to form a K33-linked triUb (Figure 3.16B). Electron density is observed for the isopeptide linkage connecting Ub moieties (Figure 3.16C).

In contrast to the closed conformation observed for K33-diUb, the crystal structure of K33-triUb reveals an 'open' conformation. The three Ub moieties within the triUb are arranged in the same orientation forming a linear array, where there are no interactions between the individual Ub moieties apart from the isopeptide linkage (Figure 3.16B). When compared to the compact diUb, the proximal Ub of K33-triUb is rotated by almost 65° suggesting lack of rotational constraints between individual Ub moieties (Figure 3.16D). Further, the hydrophobic patches are exposed to solvent, where symmetric arrangement positions the I44 hydrophobic patches on the same side of the triUb and the I36 patches on other side (Figure 3.16E). This extended conformation of K33-triUb differs from the fully extended conformations observed for K63- and M1-diUb (Komander *et al*, 2009b) (Figure 3.16F).
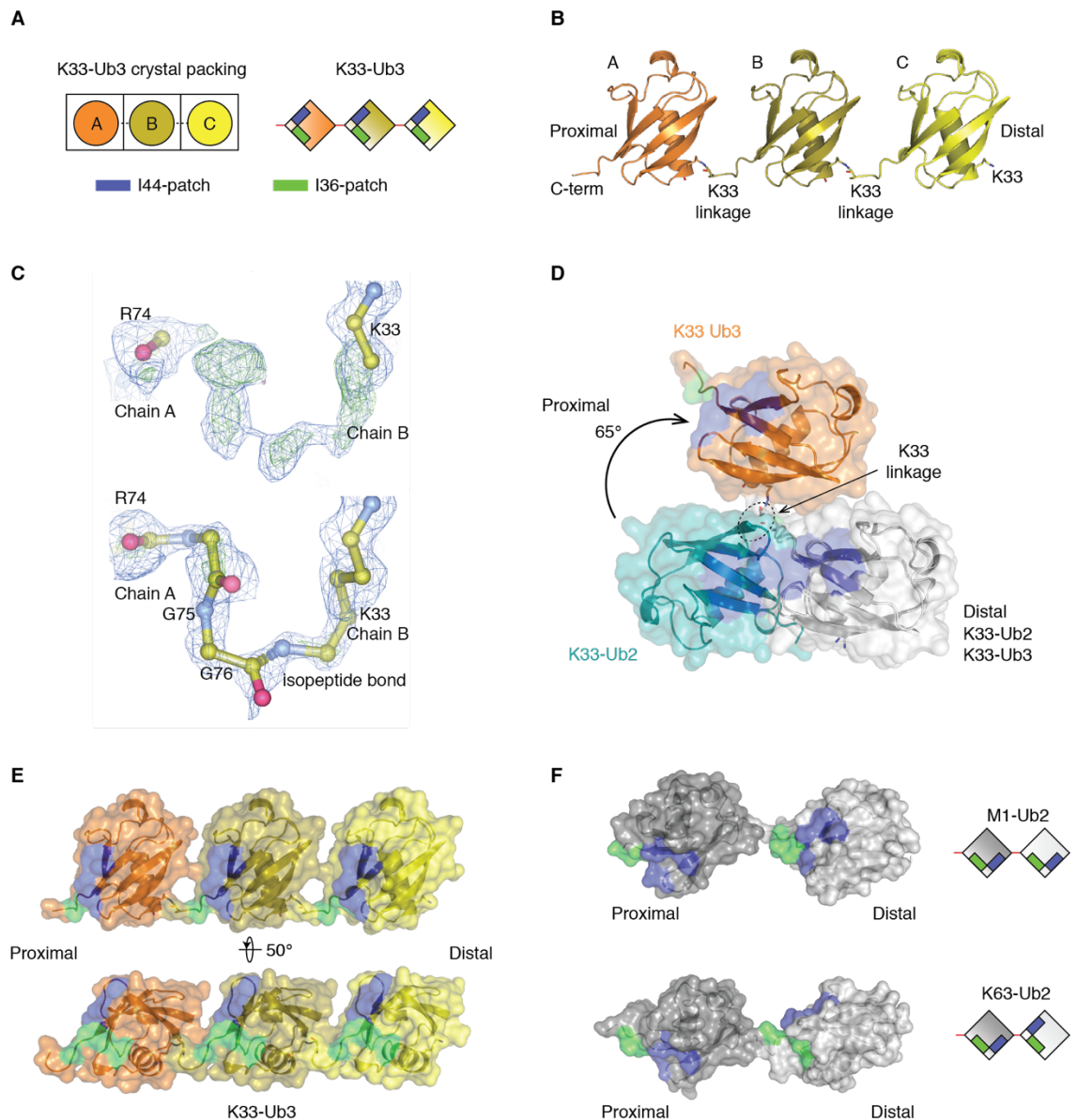
**Figure 3.16 Crystal structure of K33-linked triUb**

*(A) A schematic diagram illustrates how a Ub moiety in ASU contacts two Ub moieties from symmetry-related molecules to form K33-linked triUb. (B) Crystal structure of K33-linked triUb. (C) Electron densities between K33 residue of chain B Ub (ASU) and G76 residue of chain A Ub (symmetry-related molecule) when the residues are removed (top) or built (bottom) are shown. 2|Fo|-|Fc| (blue) and |Fo|-|Fc| (green) maps were contoured at 0.71σ and 3σ, respectively. (D) K33-diUb (dark teal) and K33-triUb (orange) were superposed on their distal Ub (white). Only two Ub moieties of K33-triUb are shown. The two proximal Ub moieties differ by ~65°. (E) A semi-transparent surface representation of K33-triUb, coloured as in (C). I44- and I36-patches are coloured blue and green, respectively. (F) K63-diUb (top) and M1-diUb (bottom) are shown in surface representation (PDB ID: 2JF5 and 2W9N (Komander* et al, *2009b)).*

136

### 3.2.8  Profiling polyubiquitin linkage specificity of ubiquitin binding domains

Crystal structures of unbound K29-diUb, K33-diUb and K33-triUb have increased the long list of conformations that polyUb chains that we have observed and further highlights the flexible nature of polyUb chains (Alfano *et al*, 2016). To deliver the Ub signal to specific cellular process, UBDs have to recognise and differentiate between types of polyUb chains (Chapter 1.7). Therefore, the biologically relevant conformations of polyUb chains have to be studied in complex with their UBDs or other binding partners.

At the time this study was carried out, there was no UBD known to selectively bind to K29- or K33-polyUb chains. To systematically test linkage-selective binding of UBDs, I expressed several UBDs as Halo-fusion proteins (Table 2.2). PolyUb binding assays were carried out by incubating resin-immobilised UBDs with a panel of tetraUb of seven linkage types. Captured chains were then analysed on SDS gel by silver-staining. Importantly, each tetraUb has a characteristic electrophoretic mobility, which allows distinction between linkage types (Figure 3.17A). In contrast to Coomassie and silver-staining, anti-Ub immunoblotting does not recognise chains of different linkage types equally, despite equal amount loaded on the gel. The UBDs to be profiled were expressed as Halo fusion proteins instead of GST-tagged because Halo-tag does not dimerise and therefore, circumvents any artefacts of tag-induced avidity (Sims & Cohen, 2009). Moreover, Halo-tag allows the fusion protein to be covalently conjugated to resin, which minimises background bands during analysis with silver-staining.

As proof of concept, I first analysed the linkage preference of the UBA domains of proteasome shuttling protein hHR23B that has been characterised as a K48-linked polyUb binding protein (Varadan *et al*, 2005). When compared across seven different linkage types, the UBA domains of hHR23B exhibit exquisite preference for K48 chains (Figure 3.17B). In contrast, the UBA domain of another protease shuttling factor Ubiquilin-1

(hPLIC1) is non-selective and binds to all linkage types. Although this hPLIC1 UBA has been characterised to bind to K48 and K63 chains without linkage selectivity, not all linkage types have been tested (Zhang *et al*, 2008). Thus, my observation confirmed that hPLIC1 binds to all Ub chains non-selectively (Figure 3.17B). In addition, these linkage profiling assays confirm the previous reports that the tandem UIMs (tUIM) of Rap80 and Epsin-15 selectively bind to K63-linked polyUb chains (Figure 3.17B) (Sims & Cohen, 2009; Sato *et al*, 2009a). All these observations demonstrate the robustness of the polyUb linkage-selective binding assay using tetraUb and Halo-tag fusion of UBDs.
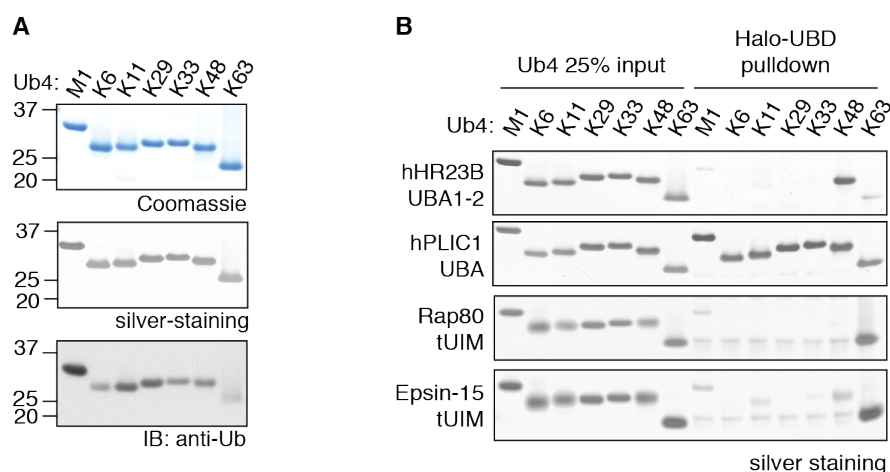


***Figure 3.17 PolyUb linkage-selective binding profile of UBDs***
*(A) Purified tetraUb of M1, K6, K11, K29, K33, K48 and K63 linkage types were separated on 4-12% SDS-PAGE gel and visualized by Coomassie- and silver-staining, and anti-Ub immunoblotting. (B) Immobilised Halo-tagged hHR23B UBA1-2, hPLIC1 UBA, Rap80 tUIM or Epsin-15 tUIM (1.05 nmol) was incubated with 58 nM of tetraUb chains of the indicated linkage types for 2 h at 4 °C. The captured materials were analysed on silver-stained 4-12% SDS-PAGE gel.*

138

### 3.2.9 TRABID NZF1 is a selective UBD in binding to K29- and K33-linked polyUb chains

TRABID is DUB that contains A20-like OTU domain at the C terminus and three NZF domains arranged in tandem (NZF1-3) at the N-terminus (Figure 3.18A). Due to the lack of polyUb of all chain types for biochemical characterisation, TRABID was reported to be a K63-selective DUB, whereas its NZF1-3 was thought to be M1- and K63-selective UBD (Tran *et al*, 2008; Komander *et al*, 2009b). Subsequent analysis against diUb of all linkage types reveals that TRABID is more efficient in hydrolysing K29 and K33 linkage types than K63 (Licchesi *et al*, 2011). Therefore, I hypothesised that TRABID NZF1-3 may also bind to K29 and K33 better than M1 and K63 linkage types, which could have been missed in the previous analysis. Indeed, when tested against a panel of tetraUb chains of seven linkage types, TRABID NZF1-3 domains bind to K29- and K33-linked polyUb chains in addition to M1 and K63 linkage types (Figure 3.18B).

PolyUb linkage-selective binding has been observed for NZF domains of TAB2 and HOIL-1L in which diUb is recognised by a single NZF (Kulathu *et al*, 2009; Sato *et al*, 2009b; 2011). Therefore, to investigate whether a single NZF of TRABID can selectively bind to K29 and K33 chain types, I tested the binding preference of Halo-fusions spanning permutations of NZF1-3 and individual NZF domains (Figure 3.18C). In comparison to NZF1-3, the two tandem NZF: NZF1-2 and NZF2-3 showed reduced binding to K63 and M1 chains while maintaining binding to K29 and K33 chains (Figure 3.18C lanes 1-4). The individual NZF1 and NZF2 domains showed selective binding towards K29 and K33 chains (Figure 3.18C, lanes 5-6). Interestingly, the binding properties of NZF3 was very different to NZF1 and NZF2. NZF3 mainly binds to K33 chains and showed weak binding to K6, K48 and K63 chains, but did not interact with K29 chains (Figure 3.18C, lane 7). In summary, the individual NZF1 and NZF2 domains

139

were selective in binding to K29 and K33 chains, whereas the tandem NZF1-3 domains

were able to bind to multiple linkages.
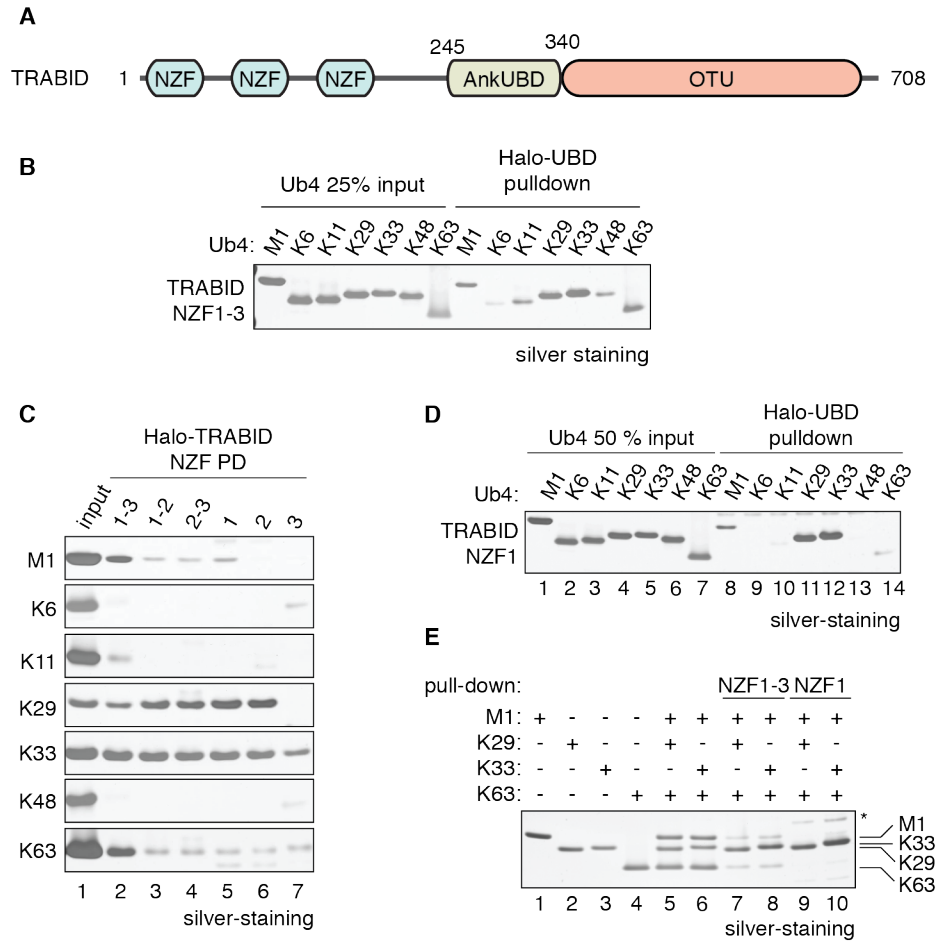


**Figure 3.18 The first NZF of TRABID selectively binds to K29 and K33 polyUb chains**
*(A) A schematic diagram illustrates the domains of TRABID. AnkUBD, ankyrin-repeat UBD. (B) PolyUb linkage-selective binding profile of TRABID NZF1-3 was assayed as in Figure 3.17B. (C) Immobilised Halo-tagged TRABID NZF domains were incubated with tetraUb of the indicated linkage types as in (B). (D) PolyUb linkage-selective binding profile of TRABID NZF1 was assayed as in (B). (E) Immobilised Halo-tagged NZF1-3 or NZF1 was incubated with M1, K29, K33 and K63 as indicated for 2 h at 4 °C. Captured materials were visualised as in (B).*

I focused on the NZF1 of TRABID, which binds mainly to K29 and K33 polyUb and captures small amounts of M1 and K63 chains (Figure 3.18D). I hypothesised that in a mixed environment, NZF1 will preferentially bind to K29 and K33 chains. I therefore performed a direct competition experiment where a mixture of chains was used in the pull-down assay and the differences in electrophoretic mobility were used to distinguish the different chain types. As predicted, NZF1 preferentially binds to K29 and K33 chains over K63 and M1 linkages (Figure 3.18E).

To compare the binding affinities of the individual NZF domains with diUb of different linkage types, I performed isothermal titration calorimetry (ITC) measurements in which NZF1 was titrated into diUb (Figure 3.19A). In agreement with the results observed with the pull down experiments, NZF1 binds to K29- and K33-linked diUb with higher affinities, 3.0 μM and 4.2 μM respectively, whereas no detectable binding was observed for monoUb, M1 or K63 diUb (Figure 3.19B-F). Whereas NZF2 has similar binding affinities for K29 and K33 chains as NZF1, the affinity of NZF3 for K33-linked diUb is too low to be determined by ITC (Figure 3.19G-I). In summary, these results reveal that the NZF1 of TRABID preferentially binds to K29 and K33 chains over K63 and M1.

ITC measures not only binding affinity, but also the stoichiometry, enthalpy and entropy of binding between two proteins. These can be used to predict the mechanism of binding (Table 3.3). Negative values for both enthalpy ($\Delta H$) and entropy ($\Delta S$) for NZF1 binding to K29- and K33-diUb suggest that the binding is driven by van der Waals interaction and hydrogen bonds (Ross & Subramanian, 1981). Unlike the other NZF to diUb interactions measured, the stoichiometry of NZF1:K33-diUb is close to 0.5, which suggests that one molecule of NZF1 can bind to two molecules of K33-diUb. However, this can also be caused by an overestimation in K33-diUb concentration. Alternatively, during the ITC measurement, half of NZF1 was defective to bind to K33-diUb. The

enthalpy value of NZF2 binding to diUb is more positive than for NZF1 binding to diUb,

suggesting the van der Waals and hydrogen interactions of NZF2 is weaker than NZF1.

Collectively, these observations posit that NZF1 is the major polyUb binding among the

three NZF domains of TRABID.

*Table 3.3 Thermodynamic parameters for the binding of NZF to K29- and K33-diUb measured by ITC*

*Stoichiometry (n), dissociation constant ($K_d$), enthalpy ($\Delta$H), entropy ($\Delta$S) and Gibbs energy ($\Delta$G) of binding titrations are shown.*

| Titration curve | Syringe | Cell | n | $K_d$ (μM) | $\Delta$H (kcal mol$^{-1}$) | $\Delta$S (cal mol$^{-1}$ K$^{-1}$) | $\Delta$G (kcal mol$^{-1}$) |
|---|---|---|---|---|---|---|---|
| Fig 3.19B | NZF1 | K29-Ub2 | 0.83 | 3.01 | -18.52 | -36.80 | -7.52 |
| Fig 3.19C | NZF1 | K33-Ub2 | 0.42 | 4.15 | -34.58 | -91.40 | -7.33 |
| Fig 3.19G | NZF2 | K29-Ub2 | 0.89 | 9.43 | -5.59 | 4.24 | -6.85 |
| Fig 3.19H | NZF2 | K33-Ub2 | 0.84 | 5.99 | -8.27 | -3.83 | -7.12 |
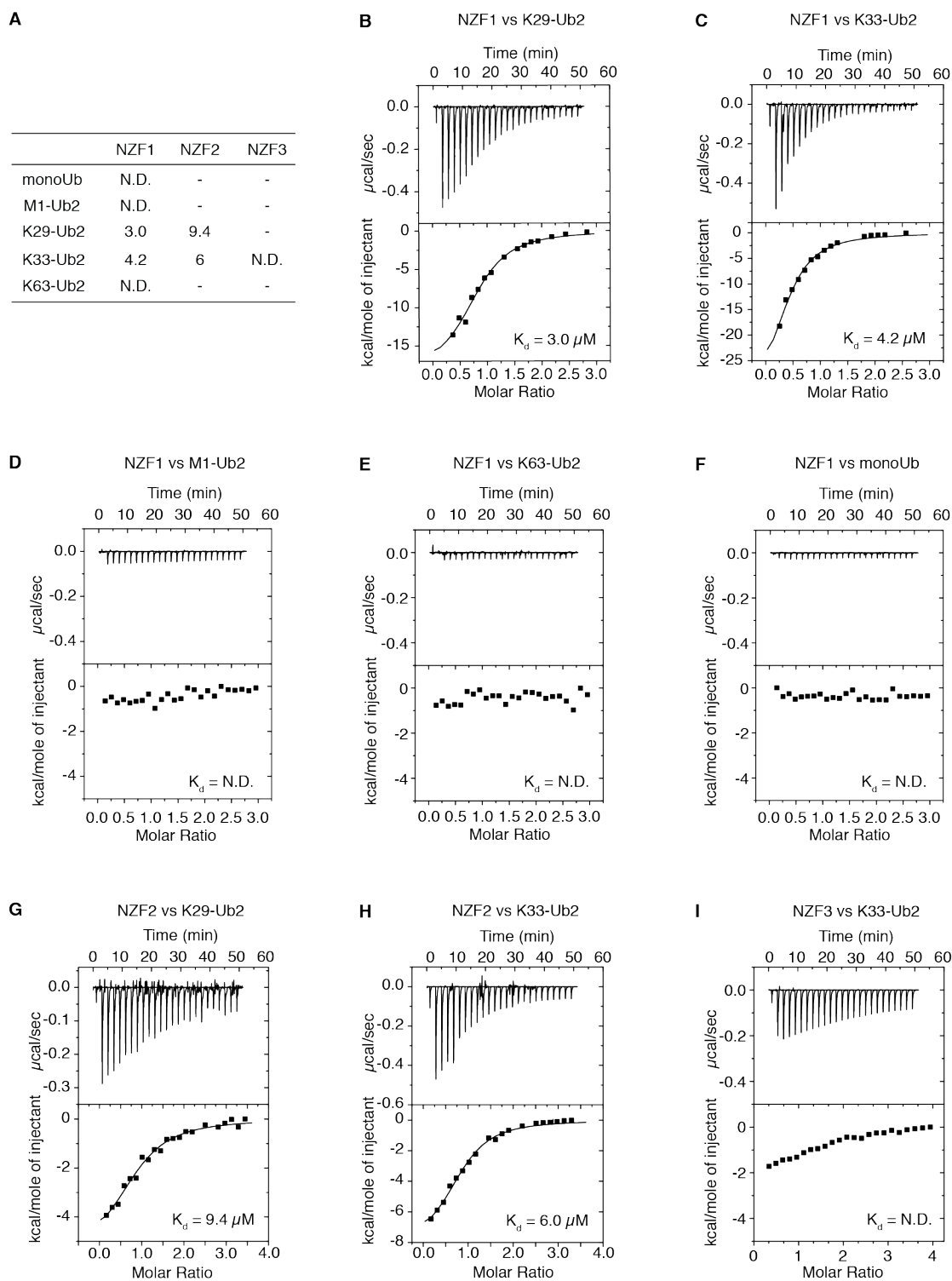
***Figure 3.19 ITC measurements highlight TRABID NZF1 selective binding to K29 and K33 chains***

*(A) Summary of binding affinity estimated from ITC measurements. (B-F) ITC measurements for TRABID NZF1 binding to K29-diUb (B), K33-diUb (C), M1-diUb (D), K63-diUb (E) and monoUb (F). (G-H) ITC measurements for TRABID NZF2 binding to K29-diUb (G) and K33-diUb (H). (I) ITC measurement for NZF3 binding to K33-diUb. The $K_d$ value for each measurement is indicated.*

### 3.2.10  Crystal structure of NZF1 in complex with K29-linked diUb

To understand the molecular mechanism underlying the selective recognition of K29-diUb by NZF1, I analysed the crystal structure of K29-diUb in complex with NZF1. Crystallisation and structure determination were carried out by Syed Arif Abdul Rehman. Diffraction data was obtained at 3.0-Å resolution and structure was solved by molecular replacement using Ub (1UBQ (Vijay-Kumar *et al*, 1987)) and TAB2 NZF (2WWZ (Kulathu *et al*, 2009)) as search models. The structure was refined to the final statistics as shown in Table 3.4. TRABID NZF1 crystallised as a stoichiometric complex with K29-linked diUb and the ASU contains five Ub and five NZF molecules (Figure 3.20A). The Ub moieties are arranged in such a way that the C terminus of one Ub points towards K29 of the next Ub moiety to form a continuous polyUb chain, and each NZF recognizes one diUb (Figure 3.20A-B and Figure 3.21A). In the crystal lattice, this arrangement allows the K29-linked polyUb chain to be extended infinitely and gives it the appearance of a helical filament (Figure 3.20A). The complexes found in the ASU superpose with root-mean-square deviation (RMSD) between 0.363 and 0.883 (Figure 3.20C).

The K29-linked diUb bound to TRABID NZF1 is in a different conformation compared to when it is unbound (Figure 3.21A and Figure 3.7C). When superposed on the distal Ub, the TRABID NZF1-bound proximal Ub is rotated by 45 °C and moved by approximately 20 Å, which results in a new interface formed between the distal and proximal Ub moieties (Figure 3.21B). This new interface in K29-diUb is entirely polar, which is formed by proximal Ub D32 and N49, and distal Ub R42, R72 and N31 (Figure 3.21C). Unlike the unbound diUb, there is no electron density for the C-terminal region of the distal Ub bound to TRABID1. However, it is evident that the C-terminal tail of the distal Ub is pointing towards the K29 of the proximal Ub and not the other Lys or N terminus Met (Figure 3.21D).

**Table 3.4 Data collection and refinement statistics for TRABID NZF1:K29-diUb complex**

| | TRABID NZF1: K29-diUb |
|---|---|
| Wavelength (Å) | 0.9795 |
| Beamline | I04 |
| Resolution range (Å) | 76.10 - 3.00 (3.14 - 3.00) |
| Space group | $C_2$ |
| Unit cell dimensions | 99.22 123.97 78.31 |
| | 90.00 103.68 90.00 |
| Total reflections | 61923 (5809) |
| Unique reflections | 17755 (1691) |
| Multiplicity | 3.5 (3.4) |
| Completeness (%) | 98.97 (95.32) |
| Mean I/sigma(I) | 15.64 (2.05) |
| R-merge | 0.0721 (0.4869) |
| CC1/2 | 0.998 (0.914) |
| R-work | 0.2222 (0.3777) |
| R-free | 0.2702 (0.4101) |
| Average B-factor (Å$^2$) | 85.71 |
| macromolecules | 3622 |
| water | 0 |
| RMS bonds (Å) | 0.005 |
| RMS angles (°) | 0.84 |
| Ramachandran favoured (%) | 97 |
| Ramachandran allowed (%) | 3 |
| Ramachandran outliers (%) | 0 |
| PDB accession code | 4S1Z |
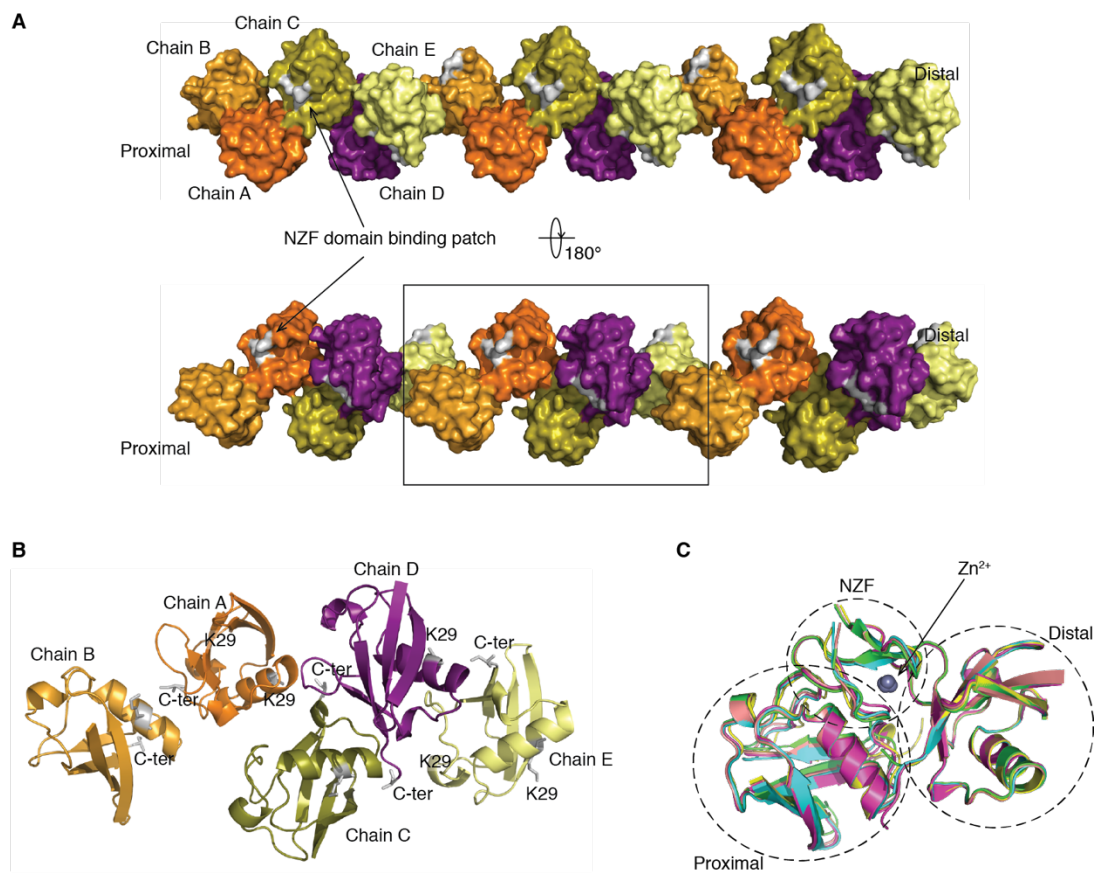
***Figure 3.20 K29-linked polyUb chains form a helical filament-like structure in the presence of NZF.***

*(A) Ub moieties in asymmetric unit (ASU) and symmetry-related molecules form a helical filament. (B) ASU contains five Ub moieties (chain A, B, C, D, E) and five NZF domains (chain F, G, H, I, J). K29 of each Ub moiety and the C-terminal of the adjacent Ub moiety are shown. (C) Superposition of all NZF1-K29-diUb complexes within the ASU. The RMSD values range between 0.363 and 0.883 Å.*
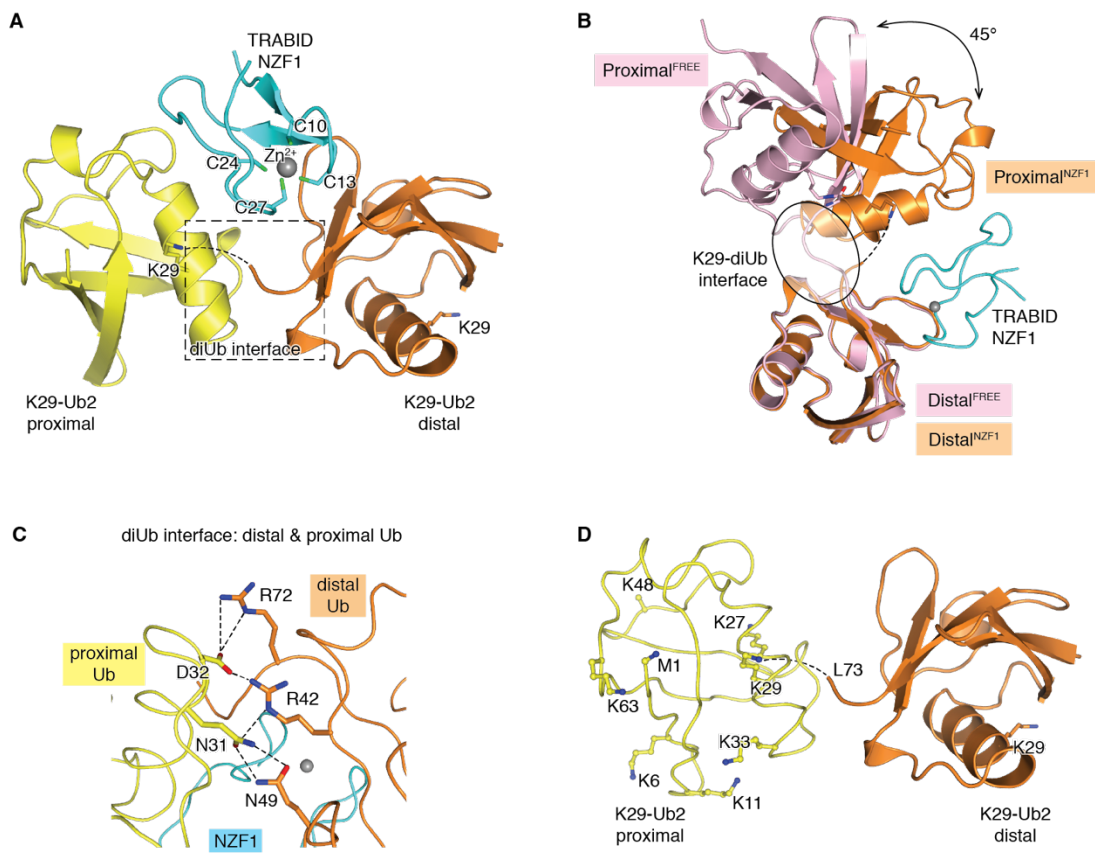
***Figure 3.21 Crystal structure of NZF1 in complex with K29-linked polyUb chains***
***(A)*** *Structure of TRABID NZF1 (cyan) bound to K29-diUb (yellow, proximal Ub; orange, distal Ub) in cartoon representation. K29 residue of Ub and Zinc (grey sphere)-coordinating Cys residues of NZF1 are shown in sticks.* ***(B)*** *Comparison of unbound (pink) and NZF1-bound K29-diUb (orange). Two diUb molecules are superposed on their distal Ub. TRABID NZF1 is shown in ribbon.* ***(C)*** *Interface between two Ub moieties of K29-diUb bound to TRABID NZF1. Hydrogen bonds between polar residues are shown as dotted lines.* ***(D)*** *Proximal and distal Ub of NZF1-bound K29-diUb are shown in ribbon and cartoon, respectively. Lys residues of the proximal Ub are shown in sticks. Dotted lines indicate isopeptide bond.*

The structure of the NZF1 of TRABID is almost identical to the NZF domains of Npl4, TAB2, TAB3 and HOIL-1L (RMSD ~<0.9 Å) (Figure 3.23A). At the centre of TRABID NZF1, four Cys residues (C10, C13, C24 and C27) coordinate a zinc ion (Figure 3.22B). TRABID NZF1 binds to distal and proximal Ub moieties with buried surface areas of 350 and 320 $Å^2$, respectively. Even though there is no electron density for the C-terminal tail of the distal Ub, it is evident that this region is not part of the binding interface between NZF1 and K29-linked diUb (Figure 3.22A-C).
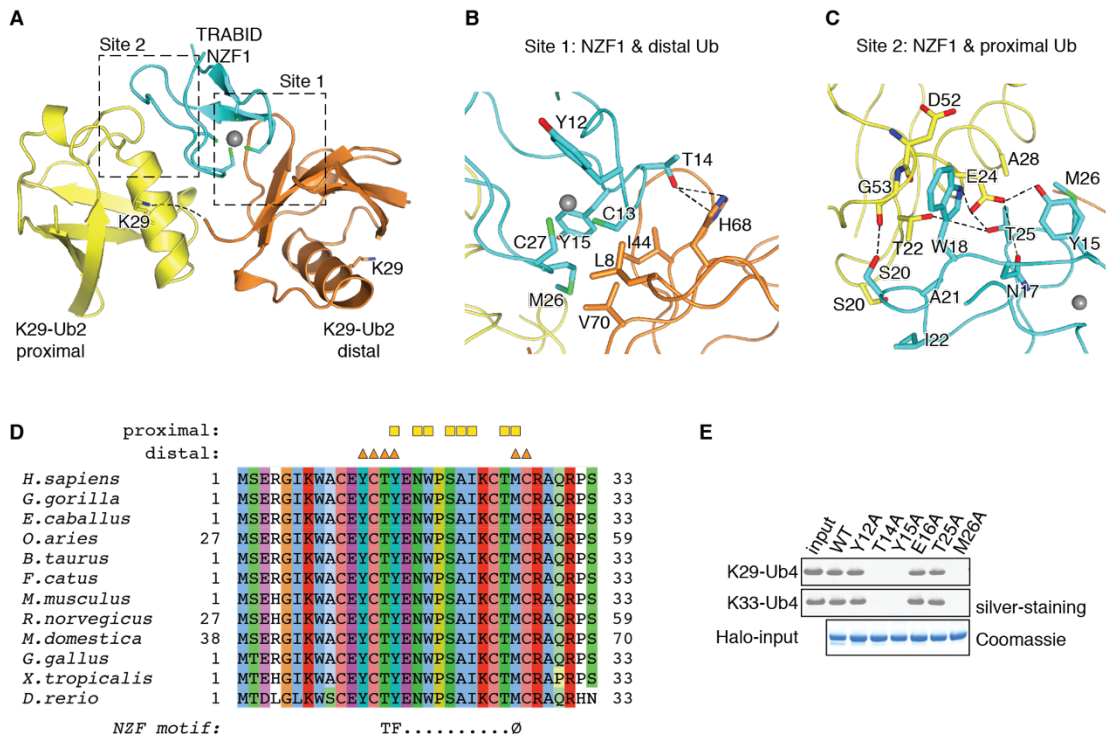
***Figure 3.22 Two Ub-binding sites on TRABID NZF1 facilitate binding to K29- diUb***
*(A) Structure of TRABID NZF1 bound to K29-diUb as in Figure 3.21A. Two Ub binding sites on TRABID NZF1 are highlighted in dashed box. (B-C) Residues at the interface of NZF1 and distal Ub (Site 1), and NZF1 and proximal Ub (Site 2) are shown in sticks. Hydrogen bonds are shown as dotted lines. (D) Sequence alignment of TRABID NZF1 from different organisms was carried out as in Figure 4.1. Residues of NZF1 at the interface with distal and proximal Ub are indicated. Conserved TF-Φ motif of NZF domain is shown. (E) The effect of mutating residues of NZF1 at the interface with Ub was assayed as in Figure 3.18C.*

At the binding interface between NZF1 and the distal Ub (Site 1), TRABID NZF1 Y12, C13, T14, Y15, M26 and C27 form a surface that interact with I44 hydrophobic patch of the distal Ub composed of L8, I44, H68 and V70 (Figure 3.22A-B). This binding mode at Site 1 interface is also observed for TAB2, TAB3, HOIL-1L and Npl4 NZF domains (Figure 3.23 and Figure 3.24A) (Kulathu *et al*, 2009; Sato *et al*, 2009b; 2011; Alam *et al*, 2004). T14, Y15 and M26 of TRABID NZF1 are part of the consensus TF-Φ motif, which is conserved in most NZF domains and facilitates NZF binding to Ub (Alam *et al*, 2004). Indeed, mutating T14, Y15 or M26 to Ala is sufficient to disrupt TRABID NZF1 binding to K29- and K33-linked tetraUb (Figure 3.22E).

148

At the second interface (Site 2), TRABID NZF1 binds to a region on the proximal Ub, formed by helix $\alpha1$, loop $\alpha1$-$\beta3$ and loop $\beta3$-$\alpha2$ (Figure 3.22A,C). TRABID NZF1 W18, I22, A21 and M26 interact with proximal Ub S20, T22, A28, D52 and G53 through van der Waals interaction. At the centre of the hydrogen bond network, proximal Ub E24 is surrounded by TRABID NZF1 Y15, N17, W18 and T25. These interactions form a unique binding interface for NZF1 to bind proximal Ub in a mode of binding that has not been observed before in any other NZF domains (Figure 3.23) (Kulathu *et al*, 2009; Sato *et al*, 2009b; 2011).

### 3.2.11 Linkage-selective binding by NZF domains is determined by the proximal Ub-binding site

Although TRABID NZF1, TAB2 NZF and HOIL-1L NZF are structurally similar, their polyUb binding properties vary and each has its own preference for binding to different types of polyUb chains (Figure 3.23). TRABID NZF1 selectively binds to K29-diUb, whereas TAB2 NZF and HOIL-1L NZF bind to K63-diUb and M1-diUb, respectively (Kulathu *et al*, 2009; Sato *et al*, 2009b; 2011). When bound to NZF domains, K29-, K63- and M1-diUb are bent that allow each Ub moiety to contact NZF domains (Figure 3.23B). When structures of the three NZFs in complex with diUb are superposed on the NZF, the distal Ub in all three complexes is in a similar orientation owing to the same distal Ub binding mode used by these NZFs (Figure 3.24B). In contrast, the orientation of the NZF-bound proximal Ub varies between the NZF domains. The proximal Ub of NZF-bound K29-diUb and K63-diUb are in the same position but in completely different orientations. These variations are due to the proximal Ub-binding sites of NZF domains which recognise different patches on Ub, and in turn determine the linkage-selective polyUb binding (Figure 3.23C).
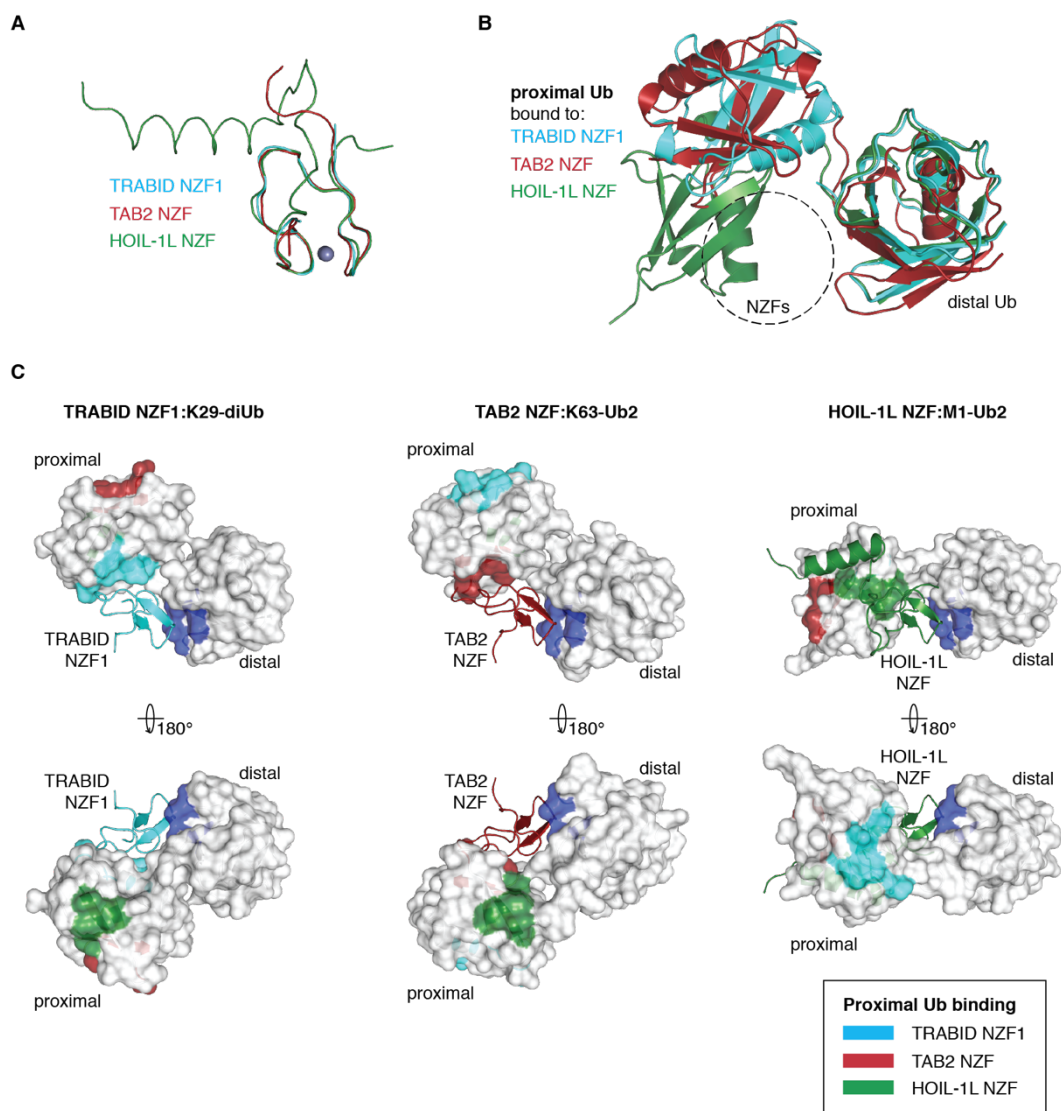
**Figure 3.23 The proximal Ub-binding sites of TRABID NZF1, TAB2 NZF and HOIL-1 NZF recognise different patches on Ub**

*(A) The NZF domains of TRABID (NZF1, cyan), TAB2 (red) and HOIL-1 (green) are superposed and shown in ribbon. Zinc coordinated by the NZF domains are shown in grey sphere. (B) The diUb chains bound to the superposed NZF domains in (A) are shown in cartoon and coloured as their NZF partners. Dashed circle indicate the position of the superposed NZFs, which are not shown. (C) Three NZF domains bound to their diUb partner in two orientations. NZF domains are shown in cartoon and coloured as in (A), whereas diUb chains are in white surface. All NZF domains recognise the same I44-patch on the distal Ub, coloured blue. On the contrary, the surfaces of the proximal Ub in contact with NZF domains differ, which are coloured as the NZF domains in (A). PDB ID: 2WWZ (Kulathu et al, 2009) for TAB2 NZF:K63-diUb and 3B08 (Sato et al, 2011) for HOIL-1L NZF:M1-diUb.*

Linkage-selective polyUb recognition requires a balance between the two Ub-binding sites on NZF domains. It is hypothesised that if the distal Ub-binding site is too strong, then polyUb binding will not depend on the contribution from the proximal Ub and therefore, polyUb binding will not be linkage selective (Sato *et al*, 2009b). A complete TF-Φ motif, in which Φ is any hydrophobic residue, is thought to constitute a stronger distal Ub binding site. For example, Npl4 NZF T590, F591 and M602 form a complete TF-Φ motif, which was proposed to enable the NZF to bind to monoUb with relatively higher affinity (Alam *et al*, 2004). Npl4 NZF binds to monoUb with $K_d$ of 120 μM whereas TAB2 NZF with an incomplete TF-Φ motif binds to monoUb with $K_d$ of >5000 μM. Therefore, Npl4 NZF binds polyUb chains non-selectively (Figure 3.24I). In TAB2, Φ is Q686 and it was posited to reduce TAB2 NZF binding affinity to distal Ub (Sato *et al*, 2009b) (Figure 3.24A). Indeed, TAB2 NZF Q686M is able to bind to monoUb and all different types of tetraUb tested (Sato *et al*, 2009b) (Figure 3.24B-C). Interestingly, HOIL-1L has a complete TF-Φ motif, but it does not bind to monoUb and it selectively binds to M1-linked diUb (Figure 3.24A) (Sato *et al*, 2011). Similarly, mutation of TRABID NZF1 Y15 to a Phe, which completes the TF-Φ motif does not affect its linkage selectivity (Figure 3.24D lane 4). In contrast, mutating TRABID NZF1 M26 (Φ) to Gln, the corresponding residue on TAB2 NZF, was sufficient to abolish binding to polyUb chains (Figure 3.24F). Similarly, mutating HOIL-1L M213 (Φ) to Ala also abolishes polyUb binding (Sato *et al*, 2011). Collectively these suggest that proximal Ub-binding site may compensate for the incomplete TF-Φ motif in NZF domains.

**Figure 3.24 Proximal Ub-binding site determines TRABID NZF1 linkage-selective binding to K29 and K33 chains**

*(A) Sequence alignment of NZF domains from TRABID, TAB2, TAB3 and Npl4 was carried out as in Figure 4.1. The distal and proximal Ub-binding sites on TRABID NZF1 (orange), TAB2 NZF (red) and HOIL-1L NZF (green) are indicated as triangles and squares, respectively. **(B-C)** The effect of TAB2 mutations on linkage selective binding was assayed as in Figure 3.18. **(D-H)** The effect of mutating TRABID NZF1 Y15 (D), W18 (E), M26 (F) and T25 (G-H) on linkage selective binding was assayed as in Figure 3.18. **(I)** Linkage-selective polyUb binding by Npl4 NZF was assayed as in Figure 3.18.*

152

To find residues on the proximal-Ub binding site that define linkage selectivity for TRABID NZF1 and TAB2 NZF, I made mutations on TRABID NZF1 to mimic the residues on TAB2 NZF and vice versa. Mutating TRABID NZF1 W18 to Ala or His does not affect its linkage-selective polyUb binding (Figure 3.24E). Although TRABID NZF1 W18 is at the centre of non-polar interactions with the proximal Ub, it is dispensable and its variation with His of TAB2 does not underlie the difference in linkage selectivity. Interestingly, mutating TRABID NZF1 T25 to Glu, the corresponding residue on TAB2 NZF, makes the mutant NZF bind to all types of polyUb chains (Figure 3.24G, lane 6). On the contrary, TAB2 NZF E685T binding to polyUb chains is abolished (Figure 3.24C). This suggests that E685 is key the residue that compensates for the weak binding of TAB2 to distal Ub. Therefore, introducing this residue to TRABID NZF1 makes its distal and proximal Ub to be stronger and therefore makes the NZF mutants to bind polyUb chains non-selectively.

The proximal Ub-binding sites of TRABID NZF1, TAB2 NZF and HOIL-1L NZF recognise different surfaces of Ub (Figure 3.23). TRABID NZF1 binds to N-terminal half of helix α1 and the surrounding loops of the proximal Ub (referred as α1+loops), whereas TAB2 NZF and HOIL-1L NZF bind to I44 patch and F4 patch of the proximal Ub, respectively (Figure 3.25D). These orient the proximal Ub so that only certain Lys residues are in close proximity with the C-terminal of distal Ub (Figure 3.33 and Discussion in Chapter 3.3.4). The residues that compose proximal-Ub binding site of the linkage-selective NZFs vary (Figure 3.25A). Therefore, the proximal Ub binding site on the NZF determines which types of polyUb chains the NZF can bind. Supporting this idea, mutating one of these residues on TRABID NZF1 T25E that mimics TAB2, makes TRABID NZF1 to bind all type of tetraUb chains (Figure 3.24H). Therefore, I wanted to investigate further how the variation in the residues forming the proximal-Ub binding site result in exclusive binding to a surface on Ub and not others.

To address this, I superposed NZF domains of TRABID (NZF1), TAB2 and HOIL-1L (Figure 3.26B). Then, I compared the interface between the superposed NZF domains and each one of the three surfaces of the proximal Ub: α1+loops (K29-diUb), I44-patch (K63-diUb) and F4-patch (M1-diUb) (Figure 3.26B). These comparisons reveal that residues forming the proximal-Ub binding sites are specific for binding to one surface on proximal Ub while preventing binding to other surfaces. There are two mechanisms by which variation in residues on this site prevent binding to other surfaces on Ub: 1) 'clashing with proximal Ub' or 2) 'insufficient for interaction' (Figure 3.26 and Table 3.5).

To illustrate the two mechanisms described above, I have taken as an example the interface between linkage-selective NZFs and the I44-patch of the proximal Ub. In TAB2 NZF, the residues forming the proximal binding site enable selective binding to I44-patch of the Ub (Figure 3.23C and Figure 3.25). These residues vary from the corresponding residues on TRABID NZF1 and HOIL-1 NZF (Figure 3.25A and C). TRABID NZF1 A21 (Leu in TAB2 NZF) may not be sufficiently hydrophobic to promote strong binding to the I44-patch (Figure 3.26B, middle). In addition to this, TRABID NZF1 T25 (Glu in TAB2 NZF) cannot form hydrogen bonds with the main chain A46 and G47 of proximal Ub (Figure 3.26B, right). On the contrary, HOIL-1L NZF R210 (L681 in TAB2 NZF) clashes with the I44-patch of the proximal Ub (Figure 3.26B, middle). In summary, residues of TRABID NZF1 and HOIL-1L NZF may not be able to interact with the I44-patch of the proximal Ub for two different reasons: 'insufficient for interaction' and 'clashing with proximal Ub', respectively. This may explain why TRABID NZF1 and HOIL-1 NZF are not able to bind to K63-diUb. To test the proposed explanation, I predict that mutants of TRABID NZF A21L or HOIL-1L R210L should increase the binding of the mutants to I44-patch and thereby allow interaction with K63-diUb and possibly other chain types.
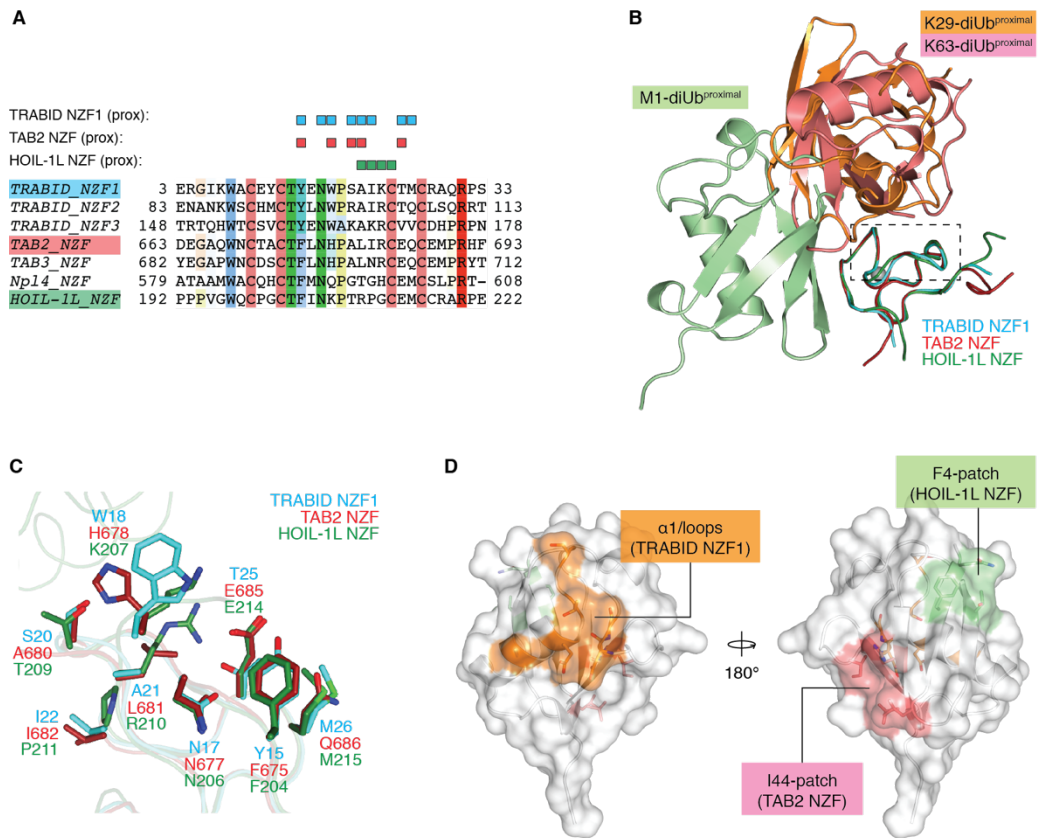
**Figure 3.25 Comparison between residues of TRABID NZF1, TAB2 NZF and HOIL-1L NZF in contact with proximal Ub of K29, K63 and M1 diUb**

*(A) Sequence alignment of NZF domains as in Figure 3.24A. (B) NZF domains of TRABID (NZF1, cyan), TAB2 (red) and HOIL-1L (green) are superposed and shown as ribbon. The interacting proximal Ub moieties from K29-diUb (orange), K63-diUb (pink) and M1-diUb (light green) are shown as cartoon. (C) Superposed NZFs within the dotted box in (B) are shown in transparent ribbon. Residues interacting with proximal Ub are shown in sticks and coloured as in (B). (D) Three different patches of the proximal Ub in contact with TRABID NZF1 (orange), TAB2 NZF (pink) and HOIL-1L NZF (light green). Related to Figure 3.25.*

155
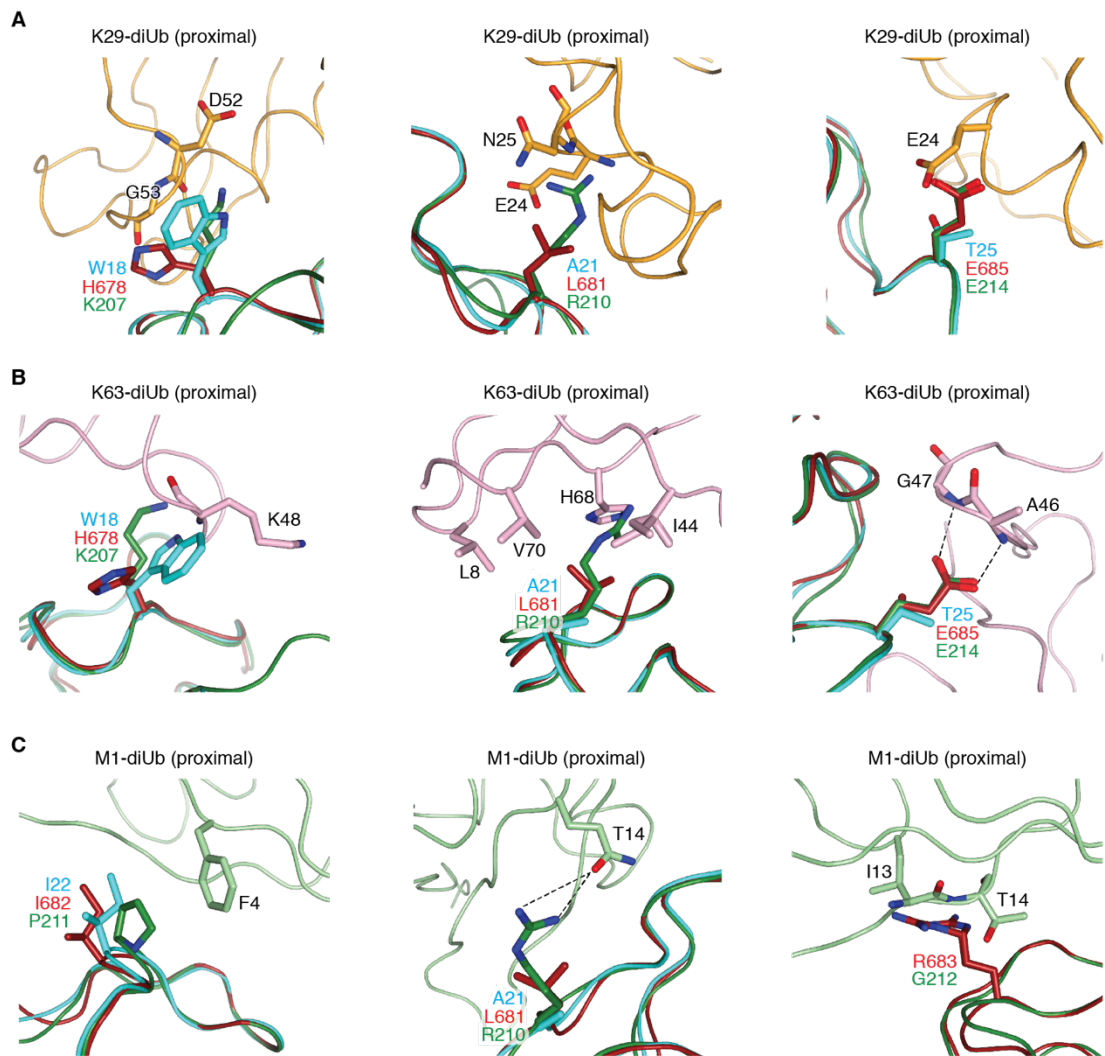
**Figure 3.26 Residues of the linkage-selective NZF allow binding to one surface of the proximal Ub while prevent binding to other surfaces**

*This figure is related to Figure 3.25. (A-C) Residues forming the the proximal Ub-binding sites of TRABID NZF1, TAB2 NZF and HOIL-1L NZF are shown along with the interacting residues on the proximal Ub of K29-diUb (A), K63 diUb (B) and M1-diUB (C). The comparison is summarised in Table 3.5.*

***Table 3.5 Comparison between residues of TRABID NZF1, TAB2 NZF and HOIL-1L***
***NZF in contact with proximal Ub of K29, K63 and M1-diUb***
*Three separate tables for proximal Ub of K29-diUb (top), K63-diUb (middle) and M1-diUb*
*(bottom). The first column is the residues of the NZF domain that in contact with the*
*indicated patch of the proximal Ub. The second and third columns are the corresponding*
*residues on the other linkage-selective NZFs. The highlighted residues on the second and*
*third columns prevent binding to the indicated patch of proximal Ub through 'clashing*
*with proximal Ub' (orange) or 'insufficient for interaction' (grey).*
*Related to Figure 3.25 and Figure 3.26.*

$\alpha$1+loops-patch (helix $\alpha$1, loop $\alpha$1-$\beta$3 and loop $\beta$3-$\alpha$2)
proximal Ub (K29-diUb)

| TRABID NZF1 | TAB2 NZF | HOIL-1L NZF |
|---|---|---|
| Y15 | F675 | F204 |
| N17 | N677 | N206 |
| W18 | H678 | K207 |
| S20 | A680 | T209 |
| A21 | L681 | R210 |
| I22 | I682 | P211 |
| T25 | E685 | E214 |
| M26 | Q686 | M215 |

I44-patch of proximal Ub (K63-diUb)

| TAB2 NZF | TRABID NZF1 | HOIL-1L NZF |
|---|---|---|
| F675 | Y15 | F204 |
| H678 | W18 | K207 |
| A680 | S20 | T209 |
| L681 | A21 | R210 |
| E685 | T25 | E214 |

F4 patch of proximal Ub (M1-diUb)

| HOIL-1L NZF | TRABID NZF1 | TAB2 NZF |
|---|---|---|
| R210 | A21 | L681 |
| P211 | I22 | I682 |
| G212 | K23 | R683 |
| C213 | C24 | C684 |

| Clashing with proximal Ub |
|---|
| Insufficient for interaction |

### 3.2.12  Investigating the linkage selectivity of unstudied NZF domains

It is fascinating how NZFs, small UBDs of ~30 residues, display such a wide range of linkage selective binding to polyUb. In order to find other unstudied NZFs that also have preference in certain types of polyUb chains, I carried out UBD linkage profiling of a number of NZF domains discovered through bioinformatics searches (Figure 3.27). The NZF domains tested can be classified into two main groups, those that bind to polyUb chains and those that do not. The TF-Φ motifs vary between these NZF domains. Whereas the variation of the residues at the position of F and Φ do not affect the binding to polyUb chains, the Thr of the TF-Φ motif is absolutely required for the binding as NZFs that do not bind to polyUb chains lack this residue (Figure 3.27A) (Alam *et al*, 2004).

The NZFs that bind to polyUb chains, can be classified further to two groups. Those that bind to three chain types or less are linkage selective whereas those that bind to four or more chain types are non-selective. Among the linkage selective NZFs, I found that HOIL-1L in the absence of its C-terminal tail binds to M1, K29 and K33 chain types (Figure 3.27C). RYBP1 NZF domain shows high selectivity in binding to K29-linked polyUb chains. However, when the linkage selectivity is tested in the context of full length protein, it no longer binds to K29 chains, but preferably binds to M1 chains (Figure 3.27D). This suggests that there are additional domains in RYBP1 that affect the protein binding to polyUb.

In this screen I also investigated the individual NZF domains from proteins that contain more than one NZF domains. Interestingly, like in TRABID, NZF domains within the same proteins display different binding preference for polyUb. SOLH has five NZF domains, but only three NZFs that bind to polyUb (NZF1, NZF3 and NZF5), flanking the NZF domains that do not bind polyUb (NZF2 and NZF4). Similarly, among two NZF domains in RNF31, only the first NZF binds to polyUb chains.

158
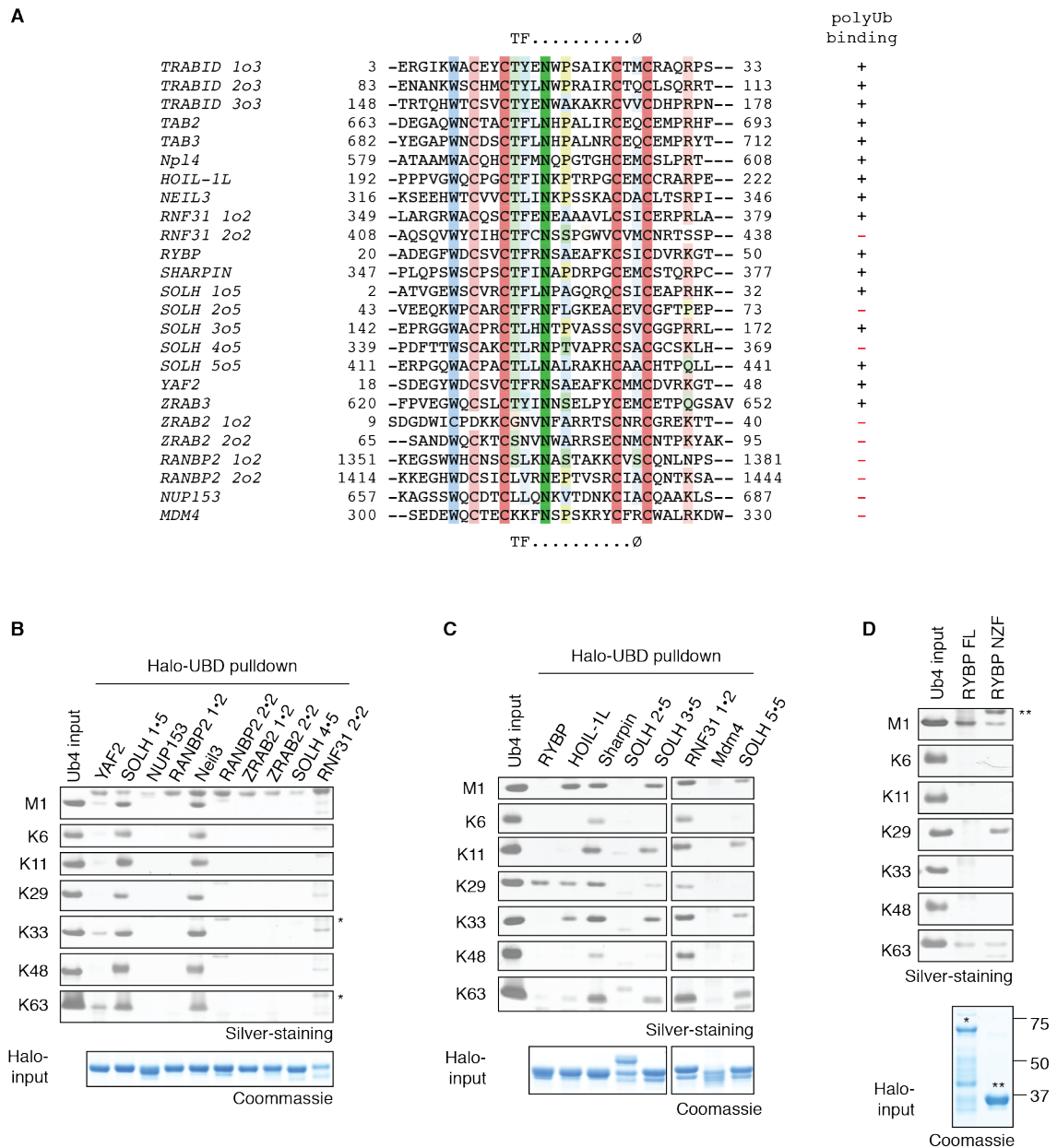
**Figure 3.27 Linkage-selective polyUb binding assays of unstudied NZF domains**
*(A-B) Isolated NZF domains were expressed as Halo-tagged fusion proteins (Table 2.2). Immobilised Halo-UBDs were incubated with tetraUb chains of the indicated linkage types. The captured materials were analysed as in Figure 3.17. (C) Sequence alignment of NZF domains analysed in (A-B) was carried out as in Figure 4.1.*

*Table 3.6 Qualitative analysis of the linkage-selective binding by the isolated NZFs*
*Qualitative assessment of linkage-selective polyUb binding profile of NZF domains tested in this study.*

| Halo-tagged NZF | Boundary | M1 | K6 | K11 | K29 | K33 | K48 | K63 |
|---|---|---|---|---|---|---|---|---|
| TRABID 1o3 | 1-33 | | | | ++ | ++ | | |
| TRABID 2o3 | 82-113 | | | | ++ | ++ | | |
| TRABID 3o3 | 139-187 | | | | | + | | |
| TAB2 | 663-693 | | ++ | | | | | ++ |
| Npl4 | 575-608 | + | | + | + | + | ++ | ++ |
| HOIL-1L | 192-222 | ++ | | + | + | | | |
| Neil3 | 316-346 | ++ | ++ | ++ | ++ | ++ | ++ | ++ |
| RNF31 1o2 | 349-379 | ++ | ++ | ++ | + | ++ | ++ | ++ |
| RYBP | 20-50 | | | | + | | | |
| SHARPIN | 347-377 | ++ | + | ++ | ++ | ++ | + | ++ |
| SOLH 1o5 | 2-32 | ++ | ++ | ++ | ++ | ++ | ++ | ++ |
| SOLH 3o5 | 142-172 | + | | + | + | + | | + |
| SOLH 5o5 | 411-441 | + | | + | | + | | + |
| YAF2 18-48 | 18-48 | | | | | + | | + |
| ZRANB3 | 620-652 | ++ | ++ | ++ | ++ | ++ | ++ | ++ |

## 3.2.13 Cellular K29-linked polyUb chains are present in mixed or branched heterotypic chains

Whilst K29 chains have been detected in proteomics studies (Dammer *et al*, 2011), we lacked antibodies and reagents to isolate them from cells and to study them. Linkage selective UBDs have been used as tools to capture and investigate certain types of polyUb chains in a cellular context (Emmerich *et al*, 2013). Having characterised TRABID NZF1 as a K29-selective polyUb binder, I tried to exploit this UBD to capture K29-linked polyUb chains from cells. I transiently expressed Flag-tagged versions of different TRABID constructs in HEK293 cells and analysed the polyUb chains captured from cell extracts by TRABID (Figure 3.28A). Full-length wild type TRABID should bind and hydrolyse K29-linked polyUb chains, whereas the catalytically inactive mutant C443A should bind to K29 chains but not hydrolyse them (Figure 3.28A). Both full length TRABID and the tandem NZFs capture high molecular mass polyUb from resting cells (Figure 3.28A, lanes 2, 4 and 6). To detect if K29 linkages are present in the captured polyUb material, I incubated the pull-down with the DUB vOTU that does not cleaves

M1, K27 and K29 linkages (Ritorto *et al*, 2014; Akutsu *et al*, 2011). In cell lysates expressing FLAG-tagged wild-type TRABID, the captured high molecular weight ubiquitylated species were all cleaved down to monoUb by vOTU (Figure 3.28A, lanes 2-3). In contrast, the ubiquitylated species captured by the catalytic dead TRABID were cleaved by vOTU to monoUb and unanchored polyUb chains of various lengths (Figure 3.28A, lanes 4-5). Despite their poor expression in HEK293 cells, the tandem NZF domains of TRABID also captured ubiquitylated proteins and unanchored polyUb chains of a similar pattern were released upon vOTU treatment (Figure 3.28A, lane 6-7).

To ensure that what I observed was not an artefact of overexpressing TRABID domains in cells, I used bacterially-expressed and purified Halo-fusions of TRABID NZFs to capture polyUb from cell extracts. Halo-NZF1-3, NZF1-2 and NZF2-3 all captured polyUb from cell extracts and released short chains when treated with vOTU (Figure 3.28B). Interestingly, the single NZF1 captured as much polyUb as the tandem fusion while isolated NZF2 only captured a limited amount of polyUb (Figure 3.28B, lanes 4-5 and 10-11). By contrast, NZF3 does not pull down any polyUb from cells. These are consistent with the ITC measurements that show that binding affinity to polyUb is higher for NZF1 as compared to NZF2 and NZF3 (Figure 3.19).

I observed that only short chains are released from the Halo-NZF capture after vOTU treatment, in contrast to the longer chains released when the capture was done using Flag-tagged tandem NZF domains expressed in cells (Figure 3.28A-B). This maybe because the Flag-tagged NZFs capture longer vOTU-resistant chains or alternatively, expression of the UBD in cells protected the chains from hydrolysis by cellular DUBs (Hjerpe *et al*, 2009; van Wijk *et al*, 2012; Sims *et al*, 2012). To test this idea, I compared the polyUb that was captured from untransfected cells or from cells expressing NZF1-3 of TRABID. Further, I tested if our findings could be recapitulated using a different UBD, for which I used the UBA domain of Ubiquilin-1 (hPLIC1) that is a non-selective polyUb

binder capable of binding to all linkage types (Figure 3.17B). Immobilized Halo-NZF1-3, NZF1 and hPLIC1 all captured polyUb from extracts of both untransfected and transfected cells (Figure 3.28C). When treated with vOTU, polyUb chains of defined lengths were released from the captured material and significantly longer vOTU-resistant chains were present in pull downs when cells expressed NZF1-3 (Figure 3.28C). These results support the idea that expressing NZF in cells protect K29 chains from being degraded.
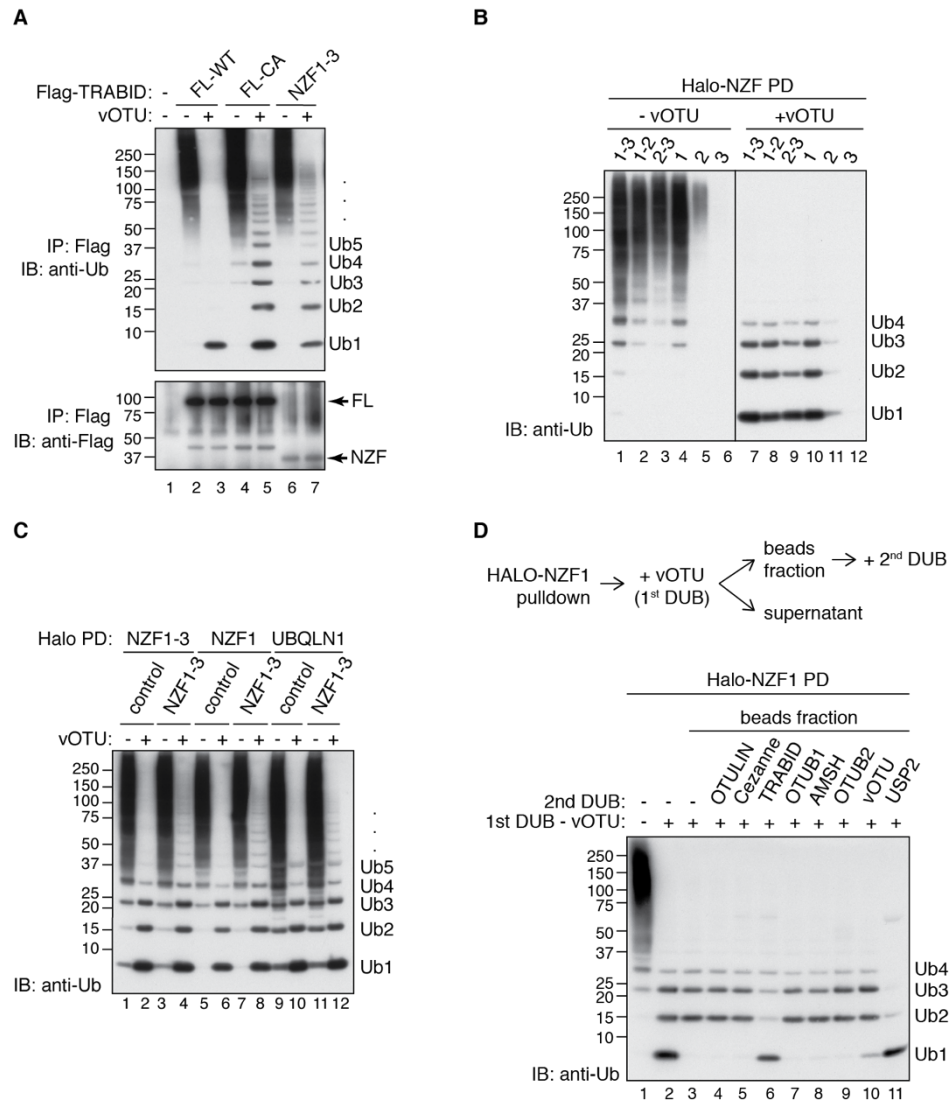
**Figure 3.28 Isolation and analysis of K29-linked polyUb chains isolated from mammalian cells**

*(A) Analysis of polyUb captured from HEK293 cells, which transiently express Flag-tagged full-length TRABID (FL-WT), full-length catalytically dead (FL-CA), or tandem NZF1-3 domains (NZF1-3). One half of the Flag-immunopurified sample was incubated with vOTU that hydrolyses all linkage types except M1, K27 and K29 linkages. (B) PolyUb chains from HEK293 extracts were captured using indicated bacterially-expressed Halo-tagged TRABID NZF domains, followed by DUB treatment as in (A). (C) PolyUb chains from untransfected (control) or Flag-TRABID NZF1-3 (NZF1-3)-expressing HEK293 cells were captured using Halo-TRABID NZF1-3, TRABID NZF1, or Ubiquilin-1 (UBQLN1) UBA domain. The isolated polyUb chains were either left untreated or treated with vOTU. (D) Immunoblotting analysis of polyUb chains captured from HEK293 extracts using immobilised Halo-tagged TRABID NZF1. Presence of K29 linkage type was assayed by the incubation with vOTU. The vOTU-resistant polyUb chains that bound to Halo-TRABID NZF1 were separated from monoUb, washed, and the linkage-types of these chains were assayed by incubation with a panel of DUBs that hydrolyse different linkage types. Schematic diagram on top illustrate experiment procedure.*

163

In summary, I have established a method to investigate K29 chains in cells that relies on TRABID NZF1 binding to K29 and K33 chains and subsequent cleavage with vOTU, a DUB that does not hydrolyse K29 linkages (Figure 3.29A). However, since vOTU does not hydrolyse M1 and K27 linkages in addition to K29 linkages, the short Ub chains released by vOTU from the high molecular weight ubiquitylated mixture could in addition contain these linkages. In order to determine the exact linkage type, I used linkage-selective DUBs. The polyUb species captured from HEK293 cell extracts using the immobilised Halo-TRABID NZF1 were first incubated with vOTU. Interestingly, these short vOTU-resistant chains stayed bound to Halo-TRABID NZF1 bead fraction while the supernatant only contained monoUb (Figure 3.28D). The bead fraction containing the short chains was first washed to remove vOTU along with any of the released monoUb, and then subsequently incubated with different linkage-selective DUBs. USP2, a linkage promiscuous DUB, hydrolysed these short chains to monoUb while DUBs that cleave M1 (OTULIN), K11 (Cezanne), K48 (OTUB1) and K63 (AMSH) did not disassemble these short chains (Figure 3.28D). Incubation with TRABID cleaved these chains down to monoUb, indicating that the vOTU-resistant chains are indeed primarily K29-linked. Using PRM LC-MS/MS analysis, I further confirmed that these short vOTU resistant chains isolated from cell extracts are indeed K29-linked (Figure 3.29B).

**A**

Ub4:  Met1   Lys6   Lys11  Lys29  Lys33  Lys48  Lys63

0 10 60  0 10 60  0 10 60  0 10 60  0 10 60  0 10 60  0 10 60  min

50
37
25
20
15
10

Ub4

3
2

Ub1

50 ng vOTU                                    silver-staining

**B**

NZF1 PD + vOTU

Automated Height

500000
400000
300000
200000
100000
0

Met1  Lys6  Lys11  Lys27  Lys29  Lys33  Lys48  Lys63
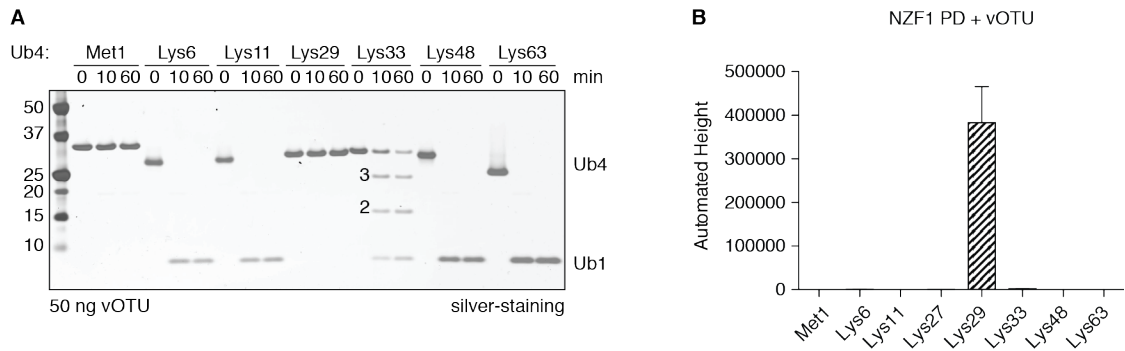
***Figure 3.29 Verification that the linkage type present in the vOTU-resistant polyUb chains is K29***

***(A)*** *Deubiquitylating assays were carried out in the presence of 1.5 µM tetraUb chains of the indicated linkage types and 235 nM of vOTU at 30 °C for the indicated periods of time. Reaction was quenched by adding LDS sample buffer and analysed on silver-stained 4-12% SDS-PAGE gel.* ***(B)*** *PolyUb chains captured from HEK293 cells using Immobilised Halo-TRABID NZF1 were treated with vOTU. The abundance of Ub linkages of the vOTU-resistant chains that were still captured on the resin was analysed by parallel reaction monitoring (PRM) as in Figure 3.6. The error bar represents the standard error of the mean of three measurements.*

Halo-NZF1 PD

-vOTU                          +vOTU

Brain Lung Heart Liver Kidney Testis    Brain Lung Heart Liver Kidney Testis

250
150
100
75
50
37
25
20
15
10

IB: anti-Ub

2% of input lysate
Coomassie staining
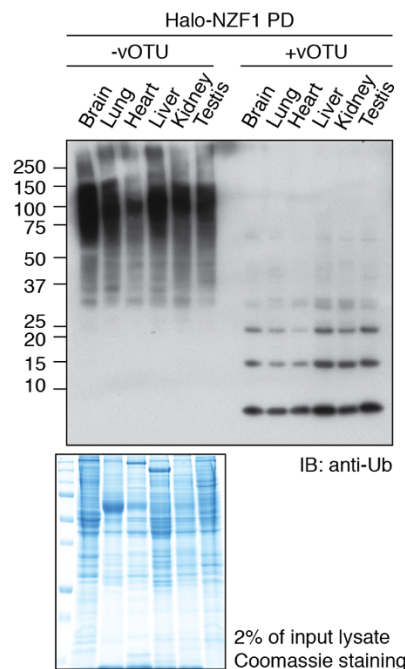
***Figure 3.30 K29-linked polyUb chains are isolated from mouse tissue lysates***

*PolyUb chains from the indicated mouse tissues were captured using Halo-TRABID NZF1 and the presence of K29 chains was assayed by treating one half of the samples with vOTU. For a loading control, 2% of input lysate for IP was separated and visualized on Coomassie-stained SDS-PAGE gel.*

The above experiments reveal that NZF1 captures K29-linked polyUb present in cells and suggest that these K29 linkages are present in heterotypic chains containing other linkages. I observed similar results when I performed pull-downs from extracts of different mouse tissues, suggesting that these heterotypic chains may be ubiquitous (Figure 3.30). K29 chains can be present together with other linkage types in three scenarios. They can be present as homogenous chains within the same modified proteins or two different proteins within the same complex (Figure 3.31A left and middle). Alternatively, K29 can be present with other linkage types within the same chains or heterotypic chains (Figure 3.31A right). With available methods, it is challenging to determine the topology of these chains. Nevertheless, I used a combination of linkage-selective UBDs and DUBs to investigate the different possibilities of how these chains may be present.
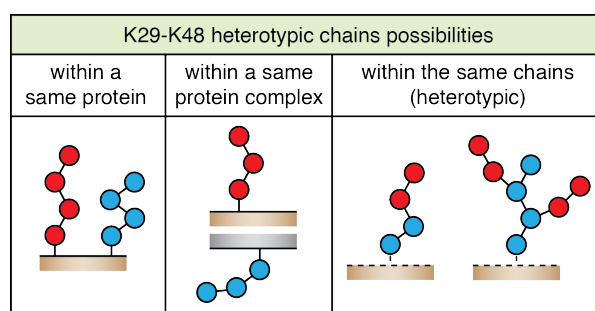


**Figure 3.31 Model of how K29 chains may be captured in heterotypic chains containing K48 linkages**
*Schematic diagrams illustrate different possibilities of how K29-linkages may be present in the heterotypic chains captured by TRABID NZF1.*

To test if these heterotypic chains are made up of K48 and K29 linkages, I captured polyUb chains from HEK293 cells using K48-specific hHR23B UBA1-2 and non-selective hPLIC1 UBA (Figure 3.31B) (Figure 3.17B). To detect the presence of K29 chains, the captured polyUb chains were treated with vOTU in the presence or absence of TRABID. Interestingly, hHR23B UBA1-2 captures polyUb chains that were cleaved

to monoUb and short polyUb chains (Figure 3.32A lane 4-6). These short chains were cleaved in the presence TRABID, suggesting that these chains are K29-polyUb. These demonstrate that K29 chains can be captured with K48-polyUb selective binder and therefore, suggest that K29 and K48 linkages may be present in heterotypic chains.

Although, hHR23B UBA1-2 is selective to bind K48-tetraUb *in vitro*, whether this preference is retained when it is used to capture polyUb chains from cells is more challenging to test. I have demonstrated that the vOTU-resistant short polyUb chains captured from cell lysates are K29 polyUb chains (Figure 3.28D and Figure 3.29B). To confirm that K29 chains were not captured by hHR23B UBA1-2 by direct interaction, I investigate whether hHR23B UBA1-2 binds to the vOTU-resistant short polyUb chains. To address this, I separated the Halo-UBDs from supernatant after treatment with vOTU and analyse the fractions separately (Figure 3.31B). The vOTU-resistant K29 chains were not bound to hHR23B UBA1-2, but were instead present in the supernatant (Figure 3.32B lane 3-4). In contrast, these K29 chains remained bound to the beads of TRABID NZF1 or hPLIC1 UBA, which all can bind to K29-tetraUb *in vitro* (Figure 3.32B lane 7-8 and 11-12). These observations suggest that hHR23B UBA1-2 capture K29 chains through its interaction with K48 chains and thus, indicates that K29 and K48 may be present in the same heterotypic chains.
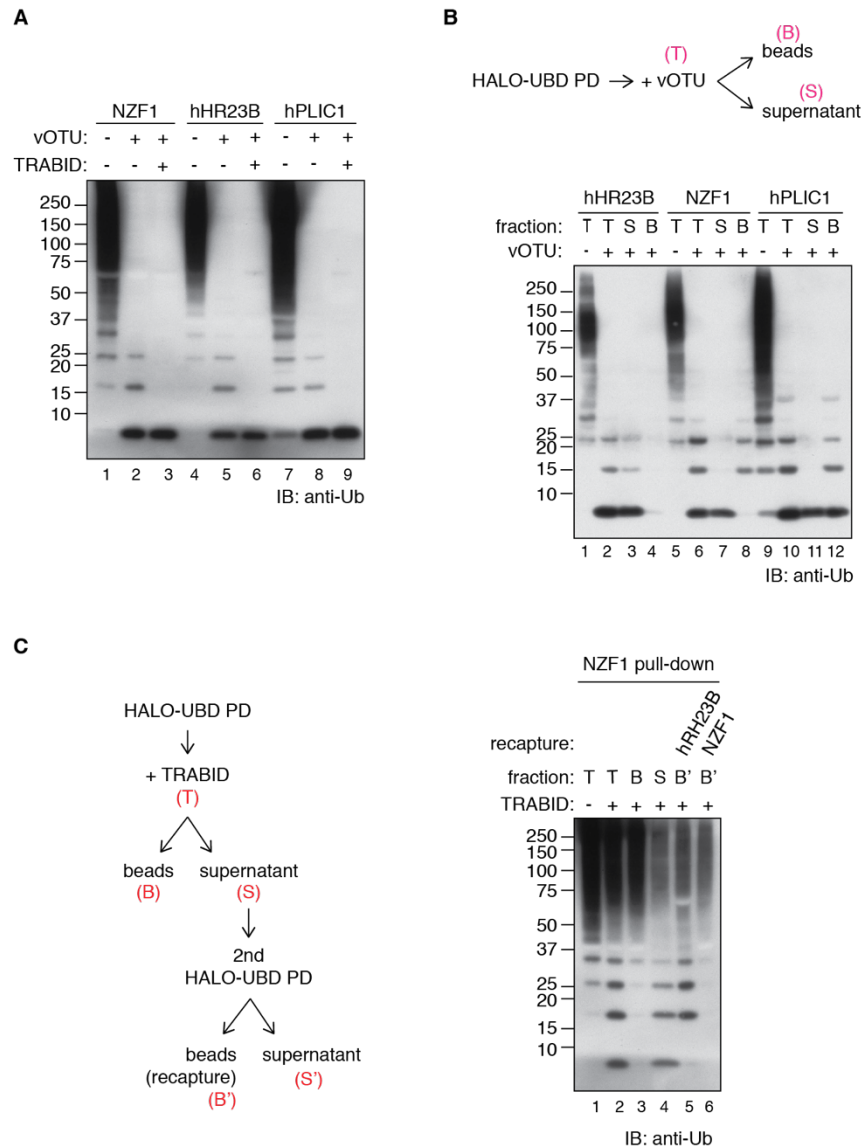
**Figure 3.32 K29-linked chains are present within mixed or branched heterotypic chains**

*(A) PolyUb materials from HEK293 cells captured by immobilised Halo-TRABID NZF1, Halo-hHR23B UBA1-2 and Halo-hPLIC1 UBA were treated with vOTU and TRABID as indicated. (B) Diagram on the top illustrates experiment procedures. PolyUb chains from the HEK293 were first captured using Halo-tagged hHR23B UBA1-2 (K48-selective binder), TRABID NZF1 (K29- and K33-selective binder), or hPLIC1 UBA (non-selective binder). Subsequently, samples in the indicated lanes were treated with vOTU. The total sample (T), supernatant (S) and beads (B) fractions after the DUB reaction were analysed separately. (C) Diagram on the left illustrate experiment procedures. PolyUb chains captured from HEK293 cell extracts using Halo-TRABID NZF1 were incubated with TRABID that cleaves K29 and K33 linkages. The unbound polyUb chains in the supernatant fraction after DUB treatment were recaptured using either the K48-selective Halo-hHR23B UBA1-2 or the K29/K33 selective Halo-TRABID NZF1.*

To further test whether K29 and K48 are present within same heterotypic chains, I captured polyUb chains from HEK293 cells using TRABID NZF1 (Figure 3.32). These chains were then treated with TRABID that cleaves K29 and K33 chains, which release short polyUb chains (Figure 3.32C lane 1-2). These chains were not bound to TRABID NZF1, but were instead present in the supernatant (Figure 3.32C lane 3-4). This suggest, that these TRABID-resistant short polyUb chains are not K29 chains. To investigate whether these chains are K48 chains, I incubated the supernatant fraction with Halo-hHR23B UBA1-2 (Figure 3.32C left). The short polyUb chains from the supernatant fraction were captured by hHR23B UBA1-2 and not by TRABID NZF1, suggesting that these short chains are K48-linked polyUb chains (Figure 3.32C lane 5-6). Thus, TRABID NZF1 might capture K48 chains when present in heterotypic chains with K29 chains. Collectively, these observations suggest that multiple blocks of K29-linked polyUb exist in cells as part of heterotypic chains that also contain K48 linkages.

## 3.3 Discussion

### 3.3.1 How does the N-terminal extension of HECT domain modulate UBE3C Ub-conjugating activity?

When investigating the optimal construct boundaries for UBE3C to assemble polyUb chains, I found that a stretch of 80-residue upstream the HECT domain of UBE3C (691-716; referred as 80aa-upstram) is crucial for polyUb conjugation (Figure 3.1). Early study proposed this 80aa-upstream to serve as a non-covalent acceptor Ub-binding site, which enables UBE3C to assemble unanchored polyUb chains (Wang & Pickart, 2005). However, I observed that the Ub transfer from E2 to E3 is disrupted in UBE3C lacking 80aa-upstream (Figure 3.2). This suggest that 80aa-upstream may regulate an early step in Ub conjugation.

Ub transfer from E2 to HECT E3 involves two successive steps. Initially, Ub-loaded E2 binds to the N-lobe of HECT E3 and then, the catalytic Cys of HECT E3 attacks the thioester bond of the E2~Ub intermediate (Chapter 1.3.2.2). Defect in any of these steps leads to a failure in the discharge of Ub from the E2~Ub intermediate (Kamadurai *et al*, 2009; Verdecia *et al*, 2003). UBE3C 80aa-upstream may modulate one of these two steps. 80aa-upstream may provide an additional binding surface for E2~Ub intermediate, which stabilises the E3:E2~Ub interaction. Alternatively, 80aa-upstream may help to orient thioester bond of E2~Ub in an optimal conformation for the nucleophilic attack by the catalytic Cys of UBE3C. Crystal structure of UBE3C HECT domain, which contains 80aa-upstream, in complex with E2~Ub will provide detailed molecular insight.

The C-terminal portion of 80aa-upstream (691-712) is conserved in some HECT E3s. It adopts an α-helical structure in WWP1 and HUWE1 that wraps around the N-lobe (Verdecia *et al*, 2003; Pandya *et al*, 2010). Although this α-helical extension increases the stability of recombinant HUWE1, it restricts HUWE1 Ub conjugation activity (Pandya *et al*, 2010). Although I have not investigated whether 80aa-upstream affects the stability of recombinant UBE3C, I observed that it is essential for polyUb conjugation activity of UBE3C. These suggest that the N-terminal stretch upstream of HECT domain may play different roles between HECT E3 ligases and requires further investigation.

Besides being involved in Ub transfer from E2 to E3, I observed that 80aa-upstream is also required for self-ubiquitylation of UBE3C (Figure 3.2). As UBE3C self-ubiquitylation occurs *in trans*, 80aa-upstream may induce dimerization of UBE3C. Supporting this hypothesis, when UBE3C 80aa-upstream is fused to the HECT domain of E6AP, the chimeric protein elutes as a dimer on gel-filtration chromatography (Wang & Pickart, 2005). Analogous to RING E3s dimerization, HECT E3s activity may be modulated by their dimerization, which require further studies. Based on my results and the published data, I propose that the 80-residue upstream of UBE3C HECT domain to

be crucial in two events HECT E3 Ub conjugation: Ub transfer from E2 to HECT E3 and self-ubiquitylation.

### 3.3.2 What is the most optimal method to assemble K29 and K33 polyUb chains?

In early 2015, two similar methods to assemble K29- and K33-linked polyUb chains were reported (Kristariyanto *et al*, 2015b; 2015a; Michel *et al*, 2015). One method was described in this thesis and the other was reported by Michel, et al. from Komander lab. Both methods use UBE3C and AREL1 as the HECT E3 ligases to conjugate K29 and K33 linkage types, respectively. Despite this similarity, there are some variations between the two methods, which include the selection of E2, construct boundaries for UBE3C and the DUB treatment step. These variations are key determinants in the amount of polyUb chains produced, which will be discussed below.

**Table 3.7 Variation in the compositions of K29 and K33 polyUb chains assembly reported by two different studies.**
Bold red font highlights key differences between two methods (Kristariyanto et al*, 2015a;*
*Michel* et al*, 2015).*

| K29-linked polyUb chains | | |
|---|---|---|
| | **Kristariyanto, et al.** | **Michel, et al.** |
| E1 | 0.65 µM UBE1 | 1 µM UBE1 |
| E2 | 9.5 µM **UBE2D3** | 10 µM **UBE2L3** |
| E3 | 3 µM **UBE3C (641-1083)** | 32 µM His-tagged SUMO **UBE3C (693-1083)** |
| DUBs | 2 µM vOTU | 1 µM OTUB1-UBE2D2 fusion 1 µM AMSH-STAM2 fusion 0.4 µM Cezanne |

| K33-linked polyUb chains | | |
|---|---|---|
| | **Kristariyanto, et al.** | **Michel, et al.** |
| E1 | 0.5 µM UBE1 | 1 µM UBE1 |
| E2 | 9.0 µM **UBE2D1** | 10 µM **UBE2L3** |
| E3 | 6.3 µM AREL1 | 36 µM AREL1 |
| DUBs | 20 µM Cezanne EK 5 µM OTUB1 | 1 µM OTUB1-UBE2D2 fusion 1 µM AMSH-STAM2 fusion 0.4 µM Cezanne |

The major difference between the two methods is the selection of E2 to pair with UBE3C and AREL1 (Table 3.7). The methods reported by Michel, et al. use UbcH7/UBE2L3, which according to my observation is not the optimal E2 for UBE3C and AREL1 to assemble polyUb chains (Figure 3.1B-C and Figure 3.10) (Michel *et al*, 2015). Other studies also observed that UBE3C assembles polyUb chains with UBE2D and not UBE2L3 as the E2 (Okada *et al*, 2015). It is likely that the N-lobe of UBE3C and AREL1 accommodate binding to UbcH5 E2s, but not to other members of E2 families (Kumar *et al*, 1997). The suboptimal E3-E2 pair may explain the relatively higher concentration of UBE3C and AREL1 used to assemble polyUb chains in Michel, et al. method (Table 3.7).

The other variation is within the selection of construct boundaries for UBE3C (Table 3.7). The UBE3C used by Michel, et al. lacks 80aa-upstream (UBE3C 693-1083), which I have observed to be inefficient to assemble polyUb chains (Figure 3.1). Therefore, the combination of sub-optimal UBE3C construct and UBE2L3 may lead to relatively low amount of K29-linked polyUb chains produced.

What also varies is the procedures of DUB treatments to remove contaminating linkage types from the assembled polyUb chains. Before treating polyUb chains with DUBs, Michel, et al. initially depleted polyUb-conjugating enzymes using acid precipitation. The depleted enzymes include UBE3C and AREL1, which I observed to conjugate polyUb chains on themselves through self-ubiquitylation (Figure 3.1 and Figure 3.10). Therefore, removing HECT E3s prior to DUB treatments may lead to major loss of polyUb chains. Based on the variations that I have discussed above, it is evident that the method to assemble K29- and K33-linked polyUb chains described in this study to be more optimal than the one proposed by Michel, et al. The optimised methods that I have established were instrumental to obtain milligram amounts of pure phospho-Ub chains of different types (Huguenin-Dezot *et al*, 2016).

### 3.3.3 Structures of K29-diUb and K33-linked diUb: beyond open and closed conformations

PolyUb chains adopt multiple conformations owing to the flexible C-terminal tail (Chapter 1.5.3). In this study, I observed multiple conformations of K29-diUb and K33-diUb chains. K29-diUb adopts two different 'open' conformations in the presence or absence of TRABID NZF1 (Figure 3.20B). K33-diUb are in 'closed' and 'open' conformations depending on the length of the polyUb chains (Figure 3.15D). A recent study also observed different K33-diUb conformations when it is bound to TRABID NZF1 (Michel *et al*, 2015). In addition to these, solution studies suggest that both K29-diUb and K33-diUb can adopt open conformations (Michel *et al*, 2015). In the absence of a binding partner, crystal structures may capture few out of many conformations that polyUb chains can adopt in solution. These conformations captured through crystal contacts may or may not lead to a physiological relevant information. In cells, specific Ub signalling occurs when polyUb chains are bound and differentiated by binding partners, for example UBDs or DUBs. Therefore, to study physiological relevant of polyUb chains, structural characterisation of polyUb should be carried out in the presence of a binding partner. In the following section I will discuss the relevance of unbound structures of K29-diUb and K33-diUb observed in my study.

### 3.3.3.1 Residues of the proximal Ub at the interface of the unbound K29-diUb have been observed to regulate linkage selective conjugation by UBE3C

The two Ub moieties of K29-diUb are in contact with each other in which E16, E18 and D21 of the proximal Ub are at the interface (Figure 3.7C). Interestingly, the same residues have been proposed to be essential for K29-polyUb conjugation by UBE3C (Wang *et al*, 2006). Mutating any one of these residues on the acceptor Ub to Ala severely disrupted UBE3C polyUb conjugation of K29, but not K48 linkage type. It was posited that E16, E18 and D21 form a patch on the acceptor Ub that interact with the residues near the

active site of UBE3C. This may orient K29 at the optimal position to attack thioester bond between the catalytic Cys of UBE3C and the donor Ub.

A recent study reported that phosphorylation of Ub S20 disrupts K29 chains conjugation and completely shifts UBE3C polyUb conjugation to K48 linkage type (Huguenin-Dezot *et al*, 2016). In the 'open' K29-diUb structure observed in this study, the S20 of the proximal Ub is at the interface between two Ub moieties. Phosphorylation of S20 may prevent K29-diUb to adopt this conformation since phospho-S20 of the proximal Ub may clash with D39 of the distal Ub. However, this does not explain why phosphorylation of S20 shift UBE3C specificity to complete conjugation via K48 chain type. The explanation may be given by the model proposed by Pickart and co-worked described above (Wang *et al*, 2006). Phosphorylation of S20 may disrupt the interaction between the acceptor Ub and the C-lobe of UBE3. Consequently, K29 of the acceptor Ub may be misaligned and thus, may not be able to attack the thioester bond of E3~Ub.

### 3.3.3.2 Conflict in molecular dynamic prediction of K33-diUb conformation

Molecular modelling predicted that K33-linked diUb chains are unable to form 'closed' conformations (Fushman & Walker, 2010). This report seems in conflict with my observation in which K33-diUb can adopt both 'open' and 'closed' conformations. In the molecular modelling study, Fushman, et al. assumed that 'closed' diUb conformations are when I44 patches of two Ub moieties form the interface (Fushman & Walker, 2010). This is an exclusive definition since I36-patch can also form the interface of 'closed' conformations of diUb chains (Virdee *et al*, 2010; Matsumoto *et al*, 2010). Indeed, the 'closed' conformation of K33-diUb observed in this study has I36-patches at the interface.

One interesting observation made in this study is that the 'closed' conformation of K33-diUb is highly similar to the one of K11-diUb (Figure 3.15C, F) (Matsumoto *et al*, 2010). The interfaces are formed by I36 patches of the two Ub moieties. As discussed

previously, these structures may capture only one of many conformations of K33-diUb and K11-diUb (Figure 3.16D) (Michel *et al*, 2015; Bremm *et al*, 2010; Castañeda *et al*, 2016a). Thus, K33-diUb and K11-diUb may be recognised by TRABID and Cezanne, respectively in two different conformations, which explain selective hydrolysis of these linkage-selective DUBs (Licchesi *et al*, 2011; Bremm *et al*, 2010). Indeed, recent crystal structure of Cezanne in complex with K11-diUb reveals that K33-diUb cannot adopt the same conformation as K11-diUb to interact with Cezanne, which explain Cezanne exclusive activity for K11-diUb (Mevissen *et al*, 2016). This is because K33 of the proximal Ub is in contact with S1' binding site of Cezanne. Interestingly, OTUD2 may bind to K33-diUb and K11-diUb in the same conformation, which explain cross reactivity of this DUB in cleaving K33-diUb and K11-diUb (Mevissen *et al*, 2013; Flierman *et al*, 2016). In summary, Ub systems may recognise K33-diUb and K11-diUb in various conformations, which is the basis for selectivity.

### 3.3.4 Mechanism underlying diverse linkage-specific polyUb binding by NZF domains

Due to limitations in assembling large quantity of atypical chains in the past, linkage-specific polyUb binding preferences of UBDs were commonly screened against M1, K48 or K63 linkage types (Komander *et al*, 2009b; Sato *et al*, 2009b; 2011; 2009a). In this study, I used a panel of tetraUb of seven linkage types, which provide a wider analysis of linkage-selective polyUb binding profile of UBDs (Figure 3.17). I observed that TRABID NZF1-3, which was earlier described as M1 and K63 selective polyUb binder also binds to K29 and K33 linkage types (Figure 3.18B) (Komander *et al*, 2009b). Further investigation revealed that single domain of TRABID NZF1 is highly selective in binding K29 and K33 linkage types (Figure 3.18 and Figure 3.19). These polyUb binding assays against tetraUb of seven chain types also reveal new insights into TAB2 NZF and HOIL-1L NZF that were previously missed. The K63-selective TAB2 NZF also binds to K6

linkage type whereas the M1-selective HOIL-1L NZF also binds to K29 and K33 linkage types (Figure 3.24 and Figure 3.27C). The crystal structures of TAB2 NZF and HOIL-1L NZF in complex with K63- and M1-diUb, respectively have observed these possibilities in other polyUb chain types binding (Sato *et al*, 2009b; 2011). However, these have never been validated in pulldown assays before, mainly because of the lack of method to assemble atypical polyUb chains.

Linkage-selective NZF domains are all characterised by two Ub-binding sites that contact distal and proximal Ub moieties in linkage-dependent manner (Kulathu *et al*, 2009; Sato *et al*, 2009b; 2011; Kristariyanto *et al*, 2015a; Michel *et al*, 2015). These linkage-selective NZF domains all contact I44-patch of the distal Ub using their conserved TF-Φ motif. In contrast, these linkage-selective NZF domains recognise different patches on the proximal Ub, which are available in certain linkage-specific polyUb chains conformations. For example, TRABID NZF1 binds to proximal Ub in an orientation in which only K29 and K33 of the proximal Ub are within the contact range with the C-terminal tail of the distal Ub (Figure 3.21D and Figure 3.33B). This explains the dual specificity of TRABID NZF1 for K29- and K33-linked polyUb chains. The recent crystal structure of TRABID NZF1 in complex with K33-diUb confirm that both K29- and K33-diUb are bound to TRABID NZF1 in the same conformation (Figure 3.33B) (Michel *et al*, 2015). The same explanation applies to dual specificities of TAB2 NZF and HOIL-1L NZF. K6- and K63-diUb may adopt a similar conformation when bound to TAB2 NZF since K6 is situated near the C-terminal of the distal Ub. Similarly, M1-, K29- and K33-diUb may adopt similar conformations when bound to HOIL-1L NZF (Figure 3.33C-D). Although TRABID NZF1 and HOIL-1L NZF capture K29- and K33-diUb, the diUb captured by the two NZF domains may not be in the same conformations (Figure 3.33B, D). In summary, linkage selective binding of NZF domains is determined by their proximal-Ub binding sites (Chapter 3.2.11).
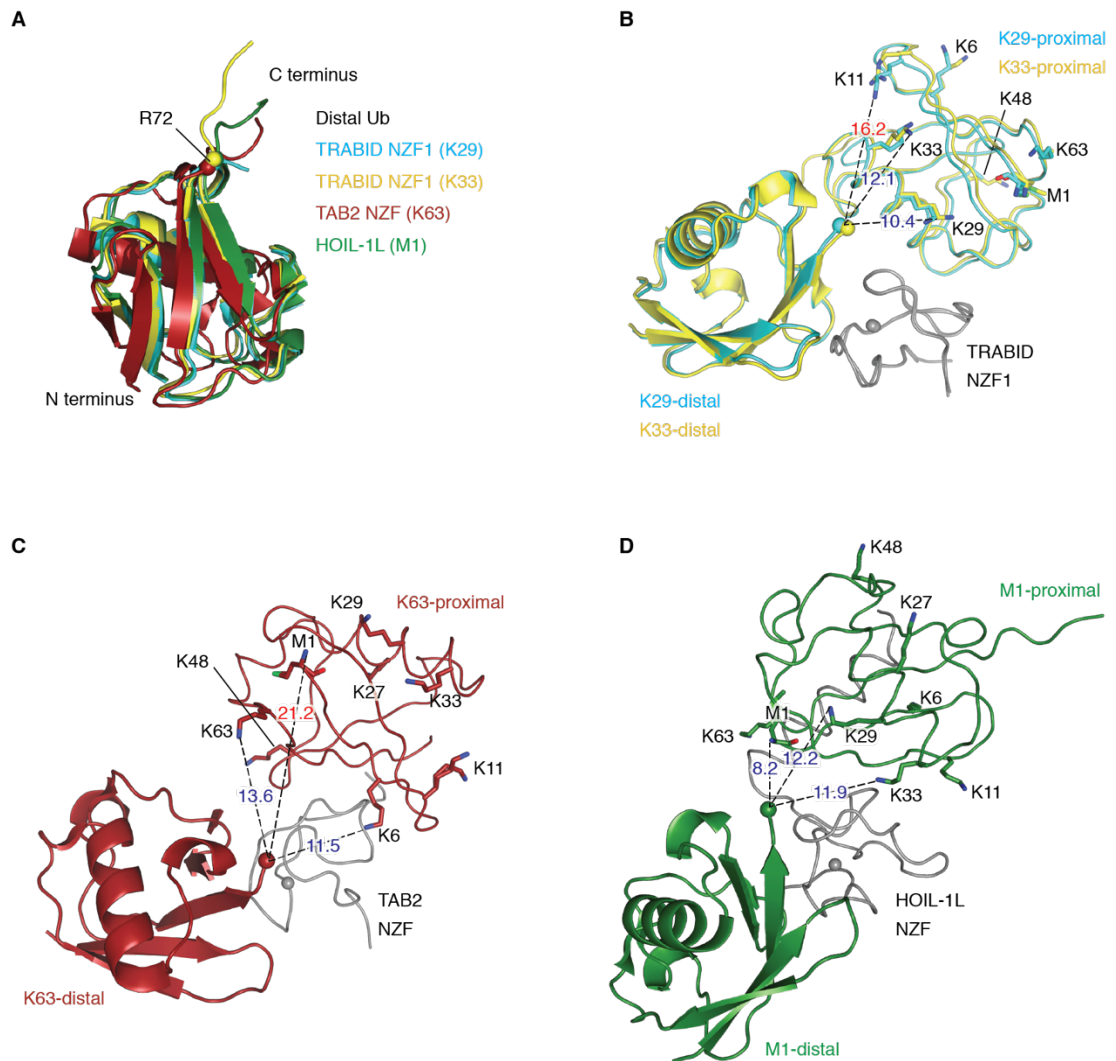
***Figure 3.33 The orientation of the NZF-bound proximal Ub explains linkage
selectivity of NZF domain***

*(A) NZF domains were superposed and their interacting distal Ub moieties are shown
in cartoon. The conformations of Ub moieties are highly similar, except the flexible C-
terminal region (L73-G76). (B) TRABID NZF1 (grey ribbon) were superposed and the
interacting K29- (cyan) and K33-diUb (yellow) are shown in cartoon (distal) and ribbon
(proximal). The flexible C-terminal regions of the distal Ub were not shown. The
distances between distal Ub R72 Cα and the nearest Lys on the proximal Ub are shown.
(C-D) K63-diUb (red) in complex with TAB2 NZF (C) and M1-diUb (green) in complex
with HOIL-1L (D) are shown as in (B). PDB ID: 4S1Z (Kristariyanto* et al*, 2015a), 5AF6
(Michel* et al*, 2015), 2WWZ (Kulathu* et al*, 2009), 3B08 (Sato* et al*, 2011).*

One application of linkage-selective UBDs is to be used as molecular sensors to

detect abundance and location of certain types of polyUb chains in vivo following certain

stimuli (van Wijk *et al*, 2012; Sims *et al*, 2012). GFP-tagged TAB2 NZF translocate to

mitochondria upon mitochondria depolarisation (van Wijk *et al*, 2012). As TAB2 NZF

was widely characterised as K63 selective polyUb binder (Sato *et al*, 2009b; Kulathu *et*

*al*, 2009), it was concluded that K63 chains were involved in mitochondria biogenesis. I demonstrated that TAB2 NZF also bind to K6 tetraUb *in vitro* (Figure 3.24C). Therefore, K6 chains level may also increase upon mitochondria depolarisation, which recruit GFP-tagged TAB2 NZF. Indeed, recent study using Ub proteomics revealed that PARKIN assembled K6 chains on mitochondria when mitochondria is damaged (Ordureau *et al*, 2014). This suggests that the specificity of UBDs used as molecular sensor has to be thoroughly investigated to be able to decipher the observation to Ub signalling.

It remains to be investigated how Ub moieties come in contact with NZF domains. There are two models proposed: induced-fit and conformational selection (Liu *et al*, 2015). The first one involves two-step binding event whereas the second involves single-step binding event. In the induced-fit model, NZF binds to distal or proximal Ub, which allow the other Ub moiety to sample several conformations until it binds the optimal binding surface to achieve higher avidity-binding. As TRABID NZF1 and HOIL-1L NZF have a complete TF-Φ motif and thus, a relatively stronger distal binding site, they would bind distal Ub first (model I-a). On the contrary, although TAB2 NZF has an incomplete TF-Φ motif, it has an extended proximal Ub binding and thus, it would bind proximal Ub first (model I-b). However, there is a caveat in this induced-fit model proposed here, which is the affinity of linkage-selective NZF domains for a single Ub molecule may be too small for binding (Sato *et al*, 2011) (Figure 3.19F). Therefore, NZF won't be able to bind a Ub moiety whilst the other Ub moiety sample the other binding site on NZF.

In conformational-selection-binding model, NZF binds to diUb in a conformation where the two Ub moieties can be simultaneously engaged. The open and compact conformations of Ub chains exist in equilibrium in solution (Castañeda *et al*, 2016a; Liu *et al*, 2015) and TAB2 NZF and Rap80 tUIM bind K63-diUb in two different conformations: partially 'closed' and 'open', respectively (Sato *et al*, 2009b; 2009a). Recent study reported that mutating the interface of the partially 'closed' K63-diUb

178

dramatically reduces the mutant K63-diUb binding to TAB2 NZF, but not to Rap80 tUIM (Liu *et al*, 2015). This thesis supports the second model, which is the conformational selection.
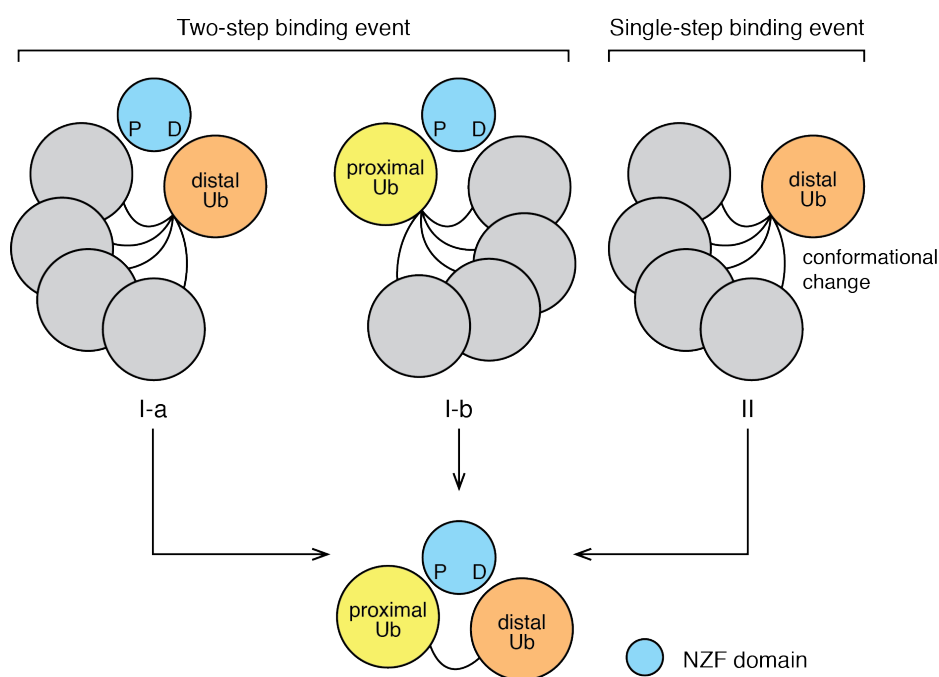


***Figure 3.34 Two models of how NZF domains capture diUb: Induced-fit and conformational selection.***
*Induce-fit model (I) involves two-step binding event. The distal Ub (I-a) or the proximal Ub (I-b) is initially bound to NZF. This allows the other Ub moieties to sample different orientation to contact the second binding patch on NZF. Alternatively, in the conformational selection model, NZF binds to two Ub moieties in single-step binding event to have higher binding avidity.*

### 3.3.5 Biological relevance of linkage-specific NZF domains

NZF domains (NZF1-3) are dispensable for the activity and specificity of TRABID DUB in hydrolysing K29, K33 and to lesser extent K63 linkage types (Licchesi *et al*, 2011). They are crucial however, to mediate TRABID co-localisation with K29/K33/K63 polyUb-rich puncta in cells and this function is centred on NZF1, which is the major polyUb binder (Licchesi *et al*, 2011; Michel *et al*, 2015). Because the physiological role of TRABID is not well understood, our understanding of role of NZF domains in the

biology of TRABID is limited. TRABID was associated with Wnt signalling although this remains controversial. Early studies reported siRNA-mediated TRABID knock-down repressed Wnt reporter gene expression (Tran *et al*, 2008). However, when TRABID was inhibited using small molecules, there was no effect on Wnt signalling and therefore, earlier report of TRABID function in Wnt signalling might be caused by off target effect of the siRNA used (Shi *et al*, 2012).

Recently, TRABID function in epigenetic regulation was observed. Upon TLR stimulation, TRABID deubiquitylates K29-linked polyUb chains on a histone demethylase Jmjd2d (Jin *et al*, 2016). This stabilises and thus, allows Jmjd2d to release the repression on IL12 and IL23 gene promoters. Co-immunoprecipitation reveals that TRABID interacts with Jmjd2d. However, whether this interaction is direct or mediated by polyUb chains has not been investigated. Moreover, although the catalytic Cys of TRABID is essential for stabilisation of Jmjd2d, the role of NZF domains has not been investigated. Therefore, the role of NZFs can be investigated in TRABID function in regulating epigenetic expression of IL12 and IL23 upon TLR activation in dendritic cells.

Similarly, the cellular role of HOIL-1L NZF is not fully understood. HOIL-1L is part of a large multi-subunit complex, which conjugates M1-linked polyUb chains essential for NF-κB activation (Chapter 1.5.2). Mutations on NZF domain that abolish polyUb binding disrupt NF-κB activation although the conjugation of M1-linked polyUb chains by LUBAC were not affected (Sato *et al*, 2011). Therefore, the role of NZF domain of HOIL-1L and its M1/K29/K63 chain types specific binding remains to be investigated.

Unlike TRABID and HOIL-1L NZF domains, the role of TAB2 NZF domain is relatively well established. TAB2 is responsible to recruit TAK1 to K63-linked polyUb chains, which are rapidly generated upon NF-κB pathway activation. This leads to TAK1 oligomerisation and autophosphorylation, leading to downstream activation of NF-κB and AP-1 transcription factors. NZF domain of TAB2 is crucial in this event as mutations

or deletion of NZF attenuates TAK1 activation and NF-κB signalling (Kanayama *et al*, 2004). Similarly, methylation of a zinc-coordinating Cys of NZF by bacteria effector *E. coli* NleE compromises the Ub-chains binding of TAB2 and thus, abrogates NF-κB signalling (Zhang *et al*, 2011). Interestingly, although polyUb binding of NZF domain is necessary, its linkage selective binding may not be essential. TAB2 mutants in which the NZF domain is replaced by UBD from Npl4 (NZF), S5a (UIM) and p62 (UBA) can restore TAK1 activation *in vitro* (Kanayama *et al*, 2004). However, Npl4 NZF, S5a UIM and p62 UBA can all bind to K63-linked polyUb chains and therefore, has not rule out the requirement for K63-selective binding in NF-κB activation (Figure 3.24I) (Tan *et al*, 2008).

The points discussed above suggest that cellular relevance of linkage-selective NZF domains of TRABID, HOIL-1L and TAB2 have not been completely understood. As cellular roles of TRABID, HOIL-1L and TAB2 have been reported, it is interesting to investigate the consequences of swapping their NZF domains. This may address the requirement of linkage-selective NZF domains for their cellular role.

### 3.3.6   What is the physiological significance of heterotypic chains containing K29 linkage types?

K29-linked polyUb chain type is a relatively abundant atypical chain in resting cells (Dammer *et al*, 2011), although its cellular roles are not completely understood. This is partly caused by the lack of tools, such as antibodies to probe this linkage type in cells. In this study, I have characterised TRABID NZF1 as linkage-selective UBD that bind to K29 and K33 linkage types (Figure 3.18 and Figure 3.19). Using TRABID NZF1 as a bait, I managed to isolate heterotypic chains containing K29 linkage type from resting HEK293 cells and different mouse tissues. Although K29-linked polyUb chains within the heterotypic chains are relatively short containing no more than four moieties, longer

K29 chains were detected only when the tandem NZFs of TRABID was expressed in cells (Figure 3.28). Transient expression of TRABID NZFs in cells may act as dominant negative inhibitor that sequester, protect and prevent downstream K29 chains signalling (Hjerpe *et al*, 2009; van Wijk *et al*, 2012; Sims *et al*, 2012). This suggests that in resting cells K29-linked polyUb chains do not grow very long, which may be caused by the activity of cellular DUBs.

In the follow up study using K48-linkage selective binder hHR23B UBA1-2, I observed that K48 chain type is present in the heterotypic chains containing K29 linkages (Figure 3.31). Several studies have reported unique role of heterotypic chains containing K48 linkage type. APC/C modifies its substrate with K11/K48 heterotypic chains, which are more efficient proteasomal degradation signal for the modified substrates (Meyer & Rape, 2014; Grice *et al*, 2015). In addition to this, recently HUWE1 conjugates branched K48/K63 polyUb chains, which was proposed to protects K63 chains from CYLD-mediated deubiquitylation (Ohtake *et al*, 2016). Similarly, short K29 chains that I observed in this study may be added to other chain types, such as K48 chains, as capping modifications. As cellular level of K29 linkage type increases upon proteasomal inhibition, it is tempting to speculate that K29/K48 heterotypic chains may be involved in proteasomal degradation, which has been observed in Ub-fusion degradation (UFD) pathway. Whether these heterotypic K29/K48 chains are better degradation substrates or not remains to be determined.

### 3.3.6.1 K29/K48 heterotypic chains in Ub-fusion degradation pathway

Short-lived proteins, such as β-gal or DHFRHa, contains N-terminal recognition elements (N-recognins), which target them for proteolysis through N-end rule degradation pathway (Tasaki *et al*, 2012). However, if these N-recognins are masked by N-terminal Ub conjugation, which cannot be removed by DUBs, the Ub-fusion short-lived proteins are degraded through an alternative pathway called Ub-fusion degradation (UFD) pathway.

This involves polyubiquitylation on the non-removable Ub conjugate, which target for proteasomal degradation (Johnson *et al*, 1992). Studies into the UFD pathway in yeast observed that when the non-removable Ub lacks K29 or K48 residue, the UFD substrates cannot be efficiently polyubiquitylated and thus, are more stable (Johnson *et al*, 1995; Koegl *et al*, 1999). Similarly, a Ub mutant which has a 20-residue extension at the C-terminus (UBB[+1]) is targeted to proteasome through UFD pathway in mammalian cells (Lindsten *et al*, 2002). This process requires Ub conjugation on K29 and K48 residue of UBB[+1] by the HECT E3 TRIP12 (Park *et al*, 2009). Therefore, these studies propose the role of K29 and K48 chain types, which may be present in branched chains, to be essential in the UFD pathway.

### 3.3.7   TRABID NZF1 as a tool to study K29 and K33 polyUb chains signalling

Our understanding of the cellular roles of K29 as well as K33 polyUb chain types is still in its infancy. Lack of tools such as linkage-selective antibodies and UBDs makes isolation and detection of these chains challenging. In this chapter I identified and characterised TRABID NZF1 as UBD that is highly selective in binding to K29 and K33 chains. I used TRABID NZF1 to isolate K29 chains from mammalian cell and mouse tissue lysates and discovered that K29 chains are present in heterotypic chains containing other linkage types, such as K48. This demonstrates that this linkage-selective TRABID NZF1 is a promising tool to dissect the biology of K29 and K33 chains. This following section will discuss the potential applications of TRABID NZF1 to investigate the cellular roles of K29 and K33 chains

The dual specificity of TRABID NZF1 for K29 and K33 chains means that the captured polyUb chains from cell lysates may contain both chain types. To selectively monitor K29 chains, I relied on a DUB that cleaves all linkage types but not K29. So I incubated the captured ubiquitylated materials with vOTU that cleaves K33 but not K29 chains. This reveals that in resting cells K29 chains are present as short chains. However,

it is more challenging to evaluate K33 chains from these captured ubiquitylated materials. This is because there is no DUB reported to cleave K29 but not K33 chains. Identification of such a linkage-selective DUB may aid the differentiation of K33 from K29 chains within the TRABID NZF1 pulldown materials. Nevertheless, being aware of K29 and K33 binding, TRABID NZF1 can be exploited to dissect pathways where both K29 and K33 linkages are used.

Other potential applications of TRABID NZF1 is to use it as a molecular sensor to monitor the formation and localisation of K29 or K33 chains upon certain stimuli (van Wijk *et al*, 2012; Sims *et al*, 2012). When transiently expressed in cells, TRABID NZF1 may sequester, protect and thus compromise cellular signalling regulated through K29 and K33 chains. Therefore, it can also be used as a dominant negative inhibitor for signalling pathways that use K29 and K33 linkages. Compromising downstream signalling means preventing K29 and K33 chains from being recognised by their natural binding partners, such as DUBs or UBDs. Thus, as a negative inhibitor, ectopic expression of TRABID NZF1 could be used to preserve K29 and K33 modification on protein substrates, which can later be isolated and detected by mass-spectrometry analysis.

K29 chains have been linked to lysosomal degradation. In the absence of Notch signalling, Deltex is modified with K29 chains leading to its lysosomal degradation (Chastagner *et al*, 2006). Similarly, TRAF7 promotes K29 chains modification on NEMO and p65/RelA that result in their lysosomal degradation and thus, alter the NF-κB signalling (Zotti *et al*, 2011). TRABID NZF1 can be used to further investigate the role of K29 in lysosomal degradation pathway. Transient expression of TRABID NZF1 may protect and stabilise the K29-modified proteins from lysosomal degradation. This can be coupled with quantitative global proteomics to identify increases in protein abundance or stability. Thus, this approach may identify K29-modified substrates that are targeted for

lysosomal degradation. It is also interesting to investigate whether TRABID NZF1 sensors localize to a distinct sub-cellular localisation when the lysosomal degradation pathway is inhibited.

In the section above I described the potential role of K29 and K48 chains in UFD pathway (Chapter 3.3.6.1). It was observed that both K29 and K48 residues on Ub-fused to UFD substrates are required for efficient ubiquitylation and proteasomal targeting of UFD substrates (Johnson *et al*, 1995; Koegl *et al*, 1999; Park *et al*, 2009; Segref *et al*, 2011). This suggest that branched K29/K48 chains are cellular signal for protein degradation in UFD pathway. However, the precise chain topology has not been fully investigated. To address this, one can use a model UFD substrate in which a non-cleavable Ub is fused to the N terminus of GFP (Ub$^{G76V}$-GFP). First, I am interested to see whether I can isolate Ub$^{G76V}$-GFP using TRABID NZF1 to confirm K29 modification on UFD substrate. Furthermore, I want to see whether transient expression of TRABID NZF1 would affect Ub$^{G76V}$-GFP degradation and localisation. Collectively, this will address the cellular role of K29 chains in the UFD pathway.

Cellular roles of K29 chains in protein aggregation have recently been observed (Nucifora *et al*, 2016; Zucchelli *et al*, 2011; 2010). Mutation on LRRK2 is a common cause of Parkinson's Disease. WSB1 (WD repeat and SOCS box-containing protein 1) is an E3 Ub ligase that was identified in yeast two-hybrid screen as interacting protein of LRRK2. WSB1 conjugates K29 and K27-linked polyubiquitylation on LRRK2, which promotes its aggregation (Nucifora *et al*, 2016). In Drosophila, K29/K27 chains-mediated LRRK2 aggregation alleviates toxicity of LRRK2 mutation. This role of K29 chains is also observed in other neurodegenerative disorders. Expansion of polyQ repeats in huntingtin (HTT) protein is the main cause of Huntington disease (HD). One hallmark of HD is the aggregations or inclusions containing polyQ-HTT. It was reported that ubiquitylation of polyQ-HTT with K29 and K27 polyUb chains increases polyQ-HTT

aggregation (Zucchelli *et al*, 2011). Therefore, K29 chains may function as a protein aggregation signal to protect cells from toxic proteins or difficult-to-degrade proteins. Using TRABID NZF1 sensors I would like to confirm whether K29 chains are indeed within the inclusion bodies of proteins involved neurodegenerative disorders. Using this screen, I can also investigate whether this function of K29 chains is universal for proteins involved neurodegenerative disorders and proteins that are difficult to degrade.

Recent proteomics studies discovered that the abundance of K33 chains increases in response to DNA damage upon UV irradiation (Elia *et al*, 2015). Much is known about roles of K63 chains in DNA damage response (Ulrich & Walden, 2010). However, the role of K33 chains in DNA damage response is less understood. The molecular sensor TRABID NZF1 can be used to confirm this increase in the level of K33 chains upon UV irradiation. In addition to this, TRABID NZF1 can also be used to isolate K33-modified proteins to further study how K33 regulates DNA damage response.

In summary, there are multiple pathways where K29 and K33 chains are observed to be involved. I characterised TRABID NZF as K29 and K33 specific UBDs and I foresee this UBD to be a very useful tool to study the cellular roles of K29 and K33 chains.

# 4 Characterisation of K48-linked polyubiquitin selective recognition by a single MIU motif of FAM63A

## 4.1 Introduction

To understand linkage-selective polyUb binding in Ub signalling, I assembled tetraUb chains of seven linkage types that allow me to profile linkage selective binding of UBDs (Chapter 3.2.8). In the previous Chapter I have discussed how a ~30-residue NZF domain can achieve such wide variety of linkage-selective polyUb binding. This made me wonder whether this selectivity is present in other small UBDs. Our lab was then interested in motif interacting with Ub (MIU), a small UBD consisting of ~20-residue α-helical structure that binds to monoUb (Chapter 1.7.1.1) (Lee *et al*, 2006; Penengo *et al*, 2006). When investigating this class of UBDs, our lab identified conserved tandem MIU motifs (tMIU) at the C terminus of an uncharacterised protein FAM63A to selectively bind to K48-linked tetraUb.

Although, MIU binding to monoUb has been characterised, the molecular mechanism underlying linkage-selective binding of MIU to polyUb is not well understood. In this Chapter, I describe structural, biochemical and biophysical characterisation of FAM63A tMIU binding to polyUb, which unravel the molecular determinants underlying its high-selective binding to K48-linked polyUb chains.

## 4.2 Results

### 4.2.1 FAM63A contains a tandem MIU repeat, highly selective in binding to K48-linked polyUb chains

Sequence analysis of FAM63A and its closely related protein FAM63B reveals several highly conserved regions: 1) DUF544 (domain of unknown function 544)-containing region; 2) two MIU motifs arranged in tandem (tMIU); and 3) C-terminal CaaX-box (Figure 4.1 and Figure 4.2). Whilst, the sequence of the MIU motifs are highly conserved between FAM63A and FAM63B, the linker region connecting the two motif is not (Figure 4.3A-B). Despite this similarity, the tMIU of FAM63A is highly specific for binding to K48 chains whereas the tMIU of FAM63B is non-specific and binds to all type of polyUb chains (Figure 4.3B). I therefore wanted to understand how the tMIU of FAM63A achieves linkage specificity for binding to K48 chains.

### 4.2.2 Single MIU2 is sufficient for selective binding to K48-linked polyUb chains

I first evaluated the contribution of each individual MIU motif of FAM63A towards polyUb binding. Mutating the key central alanine of the MIU motif to glycine has been reported to disrupt the motif from binding to monoUb (Penengo *et al*, 2006). I therefore mutated the central alanine or deleted the whole motif of MIU1 or MIU2 and tested the effect of such mutations on K48-linked tetraUb binding. Mutating or deleting MIU1 did not disrupt binding to K48-tetraUb (Figure 4.4A, lane 4&6). In contrast, mutating or deleting MIU2 completely abolished binding to K48-tetraUb (Figure 4.4A lane 3&5&7). These observations were further confirmed in pull-down assays of ubiquitylated materials from HEK293 cells (Figure 4.4B). Together, my data suggest that MIU2 is the dominant polyUb chain binder in FAM63A.
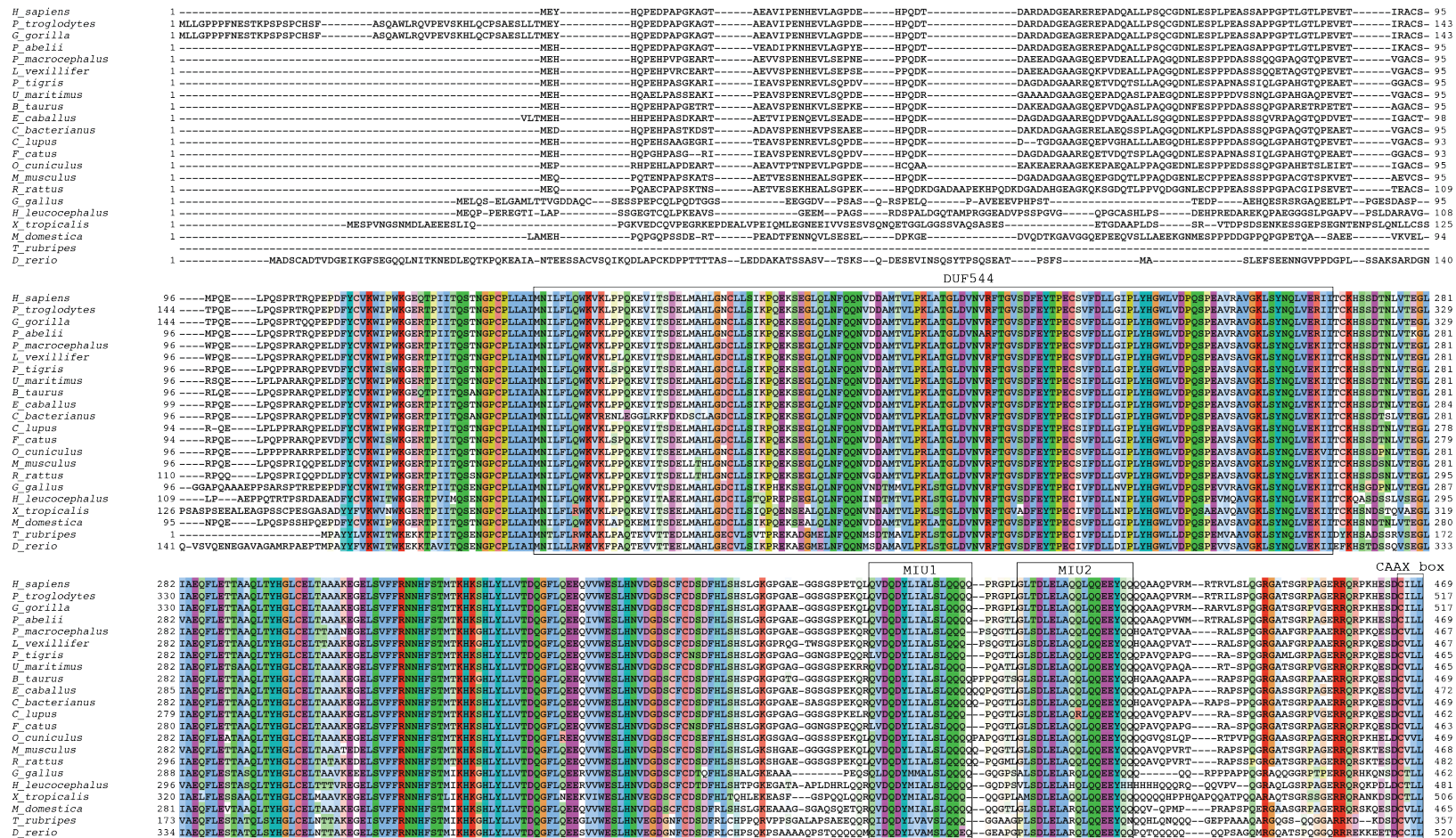
**Figure 4.1 Sequence alignment of FAM63A orthologues from different organisms.**
*Protein sequences were retrieved from UniProt database, aligned using the Clustal Omega program and edited with the Jalview software (Waterhouse* et al, *2009). ClustalX colours reflect the chemical properties of the amino acids and are applied whenever group conservation exceeds 20%.*

**Figure 4.2 Sequence alignment of FAM63B orthologues from different organisms.**

Sequence alignment was carried out as described in Figure 4.1.

A

| | | MIU1 | | linker | | MIU2 | | |
|---|---|---|---|---|---|---|---|---|

```
Hs_FAM63A   385  TQLQVDQDYLIALSLQQQQ-P------RGPLGLTDLELAQQLQQEEYQQQQ   428
Pa_FAM63A   385  KQLQVDQDYLIALSLQQQQ-P------RGTLGLTDLELAQQLQQEEYQQQQ   428
Bt_FAM63A   385  KQRQVDQDYLIALSLQQQQPP-----PQGTSGLSDLELAQQLQQEEYQQHQ   430
Mm_FAM63A   385  KQLQVDQDYLIALSLQQQQQP------QGTLGLSDLELAQQLQQEEYQQQQ   429
Rn_FAM63A   399  KQLQVDQDYLIALSLQQQQQP------QGMLGLSDLELAQQLQQEEYQQQQ   443

Hs_FAM63B   508  QQDQIDQDYLMALSLQQEQQSQEINWEQIPEGISDLELAKKLQEEEDRRAS   558
Pa_FAM63B   508  QQDQIDQDYLMALSLQQEQQSQEINWEQIPEGISDLELAKKLQEEEDRRAS   558
Bt_FAM63B   509  QQDQIDQDYLMALSLQQEQQSQEINWEQIPEGISDLELAKKLQEEEDRRAS   559
Mm_FAM63B   486  QQDQIDQDYLMALSLQQEQQSQDINWEQIPEGISDLELAKKLQEEEDRRAS   536
Rn_FAM63B   484  QQDQIDQDYLMALSLQQEQQSQDINWEQIPEGISDLELAKKLQEEEDRRAS   534
```

xxDϕxLAxxLxx###x                    xxDϕxLAxxLxx###x

**Figure 4.3 Uncharacterised FAM63A contains tandem MIU repeat that is selective in binding K48-linked polyUb chains**
(A) Sequence alignment of FAM63A and FAM63B tMIUs from different species. MIU1, MIU2 and the tMIU linker are indicated. The conserved motif of MIU is shown: ϕ, large hydrophobic; #, acidic; x, any residues. Hs, Homo sapiens; Pa, Pongo Abelii; Bt, Bos taurus; Mm, Mus musculus; Rn, Rattus norvegicus. Protein sequences were retrieved from UniProt database, aligned using the ClustalO program and edited with the Jalview software (Waterhouse et al, 2009). (B) Schematic diagram illustrates conserved domains of FAM63A and FAM63B based on sequence alignments on Figure 4.1 and Figure 4.2. The MIU motifs of FAM63A and FAM63B are coloured red and blue, respectively. (C) PolyUb linkage selectivity profiling for FAM63A and FAM63B tMIU. TetraUb chains of the indicated linkage types (29 pmol) were incubated with 1.05 nmol Halo-tagged tMIU of FAM63A or FAM63B immobilized on HaloLink resin for 2 h at 4 °C. The captured materials were analysed on silver-stained 4-12% SDS-PAGE gel.

Tandem UIMs and MIUs have been reported to prefer binding to longer polyUb chains (Young *et al*, 1998; Swanson *et al*, 2003; Raasi *et al*, 2004; Burnett *et al*, 2003; Chai *et al*, 2004; Penengo *et al*, 2006; Rahighi *et al*, 2016; Pinato *et al*, 2009). Pulldowns from HEK293 cell extracts using FAM63A tMIU did not capture lower molecular weight polyUb chains, suggesting a preference of this tMIU also for binding to longer polyUb chains (Figure 4.4B). To investigate this further, I incubated Halo-tagged tMIU with K48-linked polyUb chains of different lengths that varied from monoUb to pentaUb (Figure 4.5A). I found that the tMIU binds to tri-, tetra- and pentaUb, but does not bind to monoUb and diUb, supporting a preference of tMIU to bind longer polyUb chains. To measure the

affinity of the tMIU for polyUb chains of the varying lengths, I performed ITC measurements where FAM63A tMIU was titrated into either K48-diUb, triUb or tetraUb (Figure 4.5B-D). I observed affinities of 23 μM, 1.2 μM and 185 nM for diUb, triUb and tetraUb, respectively, suggesting that the affinity of FAM63A tMIU for polyUb chains increases with chain length. Interestingly, although tMIU binds to K48-triUb and tetraUb with binding affinities varies by ~7-fold, their binding enthalpy and entropy are similar (Table 4.1). This suggests that tMIU binds to triUb and tetraUb using similar binding mechanism. Collectively, my results demonstrate that FAM63A tMIU preferably binds to longer K48-linked polyUb chains.
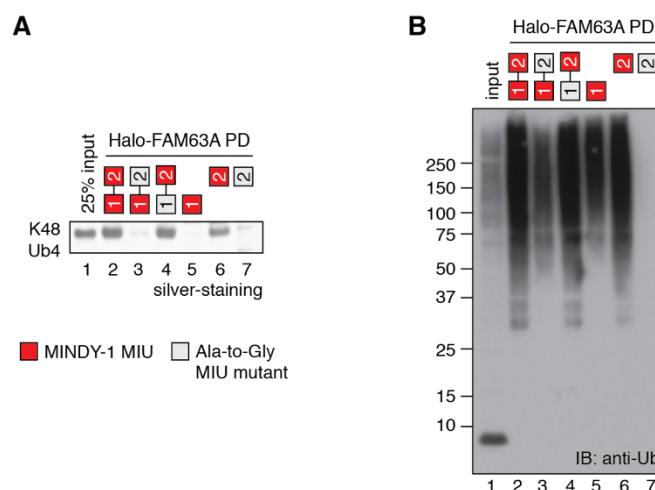


***Figure 4.4 MIU2 is the dominant polyUb binder in FAM63A***
*(A) K48-linked tetraUb chains were captured by Halo-tagged tMIU wild-type or mutants of FAM63A as in Figure 4.3. Red and grey squares indicate wild-type and mutant MIU (Ala-to-Gly), respectively. (B) HEK293 cell lysates (1 mg) were incubated with 1.05 nmol Halo-tagged tMIU wild-type or mutants. The captured Ub was visualized by anti-Ub immunoblotting.*

To explore the role of MIU1 in the binding of FAM63A tMIU to polyUb chains, I compared the binding of MIU1 and MIU2 on their own to K48-triUb by ITC. If MIU1 has no role in overall binding, I predict the affinity of MIU2 for K48-triUb to be the same

as that observed with tMIU. Consistent with my previous finding, MIU1 on its own has no measurable affinity towards polyUb chains (Figure 4.5E). Surprisingly, I found that the affinity of the tMIU containing both MIU1 and MIU2 for K48-triUb is ~10-fold higher than that of MIU2 on its own (Figure 4.5F). This suggests that even though the affinity of the isolated MIU1 for K48-triUb is negligible, it contributes to tMIU binding through avidity.
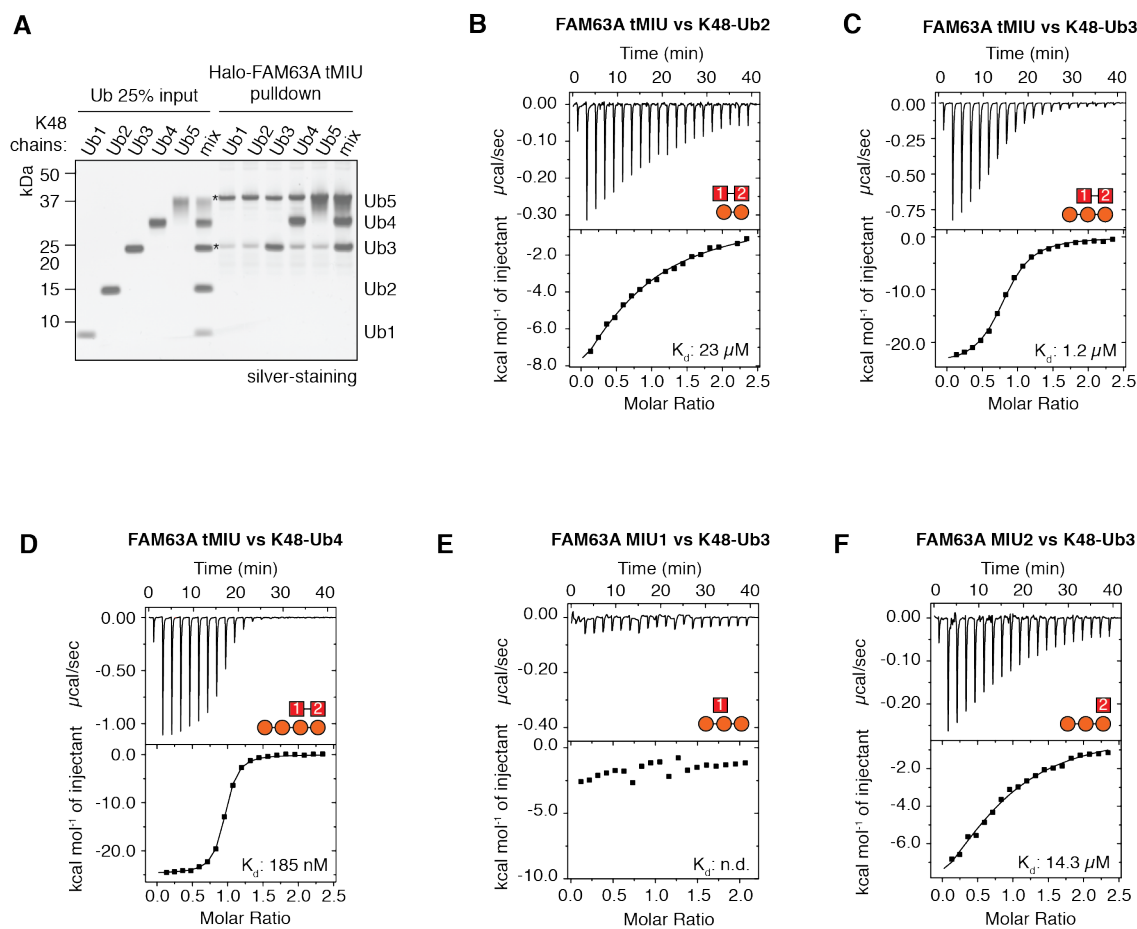


**Figure 4.5 FAM63A tMIU binds to longer polyUb chains with higher binding affinity**

*(A) MonoUb and K48-linked polyUb chains of different lengths (29 pmol each) were incubated with 1.05 nmol of Halo-tagged tMIU. The captured materials were visualized as in Figure 4.3. (B-D) ITC measurements for FAM63A tMIU binding to K48-linked diUb (B), triUb (C), and tetraUb (D). The $K_d$ value of each measurement is indicated. (E-F) ITC measurements for FAM63A MIU1 (E) and MIU2 (F) binding to K48-linked triUb. The $K_d$ value of each measurement is indicated.*

*Table 4.1 Thermodynamic parameters for the binding of FAM63A MIU motifs to K48-linked polyUb chains measured by ITC*
*Stoichiometry (n), dissociation constant ($K_d$), enthalpy (ΔH), entropy (ΔS) and Gibbs energy (ΔG) of binding titrations are shown.*

| Titration curve | Syringe | Cell | n | $K_d$ (μM) | ΔH (kcal mol⁻¹) | ΔS (cal mol⁻¹ K⁻¹) | ΔG (kcal mol⁻¹) |
|---|---|---|---|---|---|---|---|
| Fig 4.4D | FAM63A tMIU | K48-Ub2 | 0.66 | 23 | -19.3 | -43.5 | -6.3 |
| Fig 4.4E | FAM63A tMIU | K48-Ub3 | 0.8 | 1.2 | -24.5 | -55.1 | -8.1 |
| Fig 4.4F | FAM63A tMIU | K48-Ub4 | 0.9 | 0.185 | -24.7 | -52.1 | -9.2 |
| Fig 4.4G | FAM63A MIU1 | K48-Ub3 | N.D. | N.D. | N.D. | N.D. | N.D. |
| Fig 4.4H | FAM63A MIU2 | K48-Ub3 | 0.8 | 14.3 | -13.1 | -21.7 | -6.6 |

Since MIU1 only provides weak binding to polyUb chains, I hypothesise that MIU2 is the main determinant of K48-linkage selectivity. Indeed, when Halo-tagged MIU2 was incubated with a panel of seven types of polyUb chains it only captured K48-tetraUb (Figure 4.6). This implies that on its own MIU2 is still selective towards K48 linkages and therefore is the linkage specificity determinant in FAM63A tMIU.
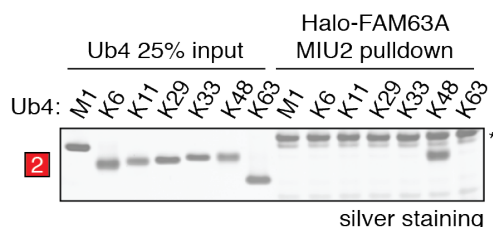


***Figure 4.6 FAM63A MIU2 on its own binds to K48 chains***
*TetraUb chains of the indicated linkage types were incubated with Halo-tagged FAM63A MIU2 and captured materials were analysed as in Figure 4.3.*

### 4.2.3 Cooperativity between MIU1 and MIU2 results in high selective polyUb interaction

Even though MIU2 is sufficient to capture K48-linked polyUb chains, MIU1 is still required for the tMIU to bind polyUb chains with higher affinity. However, it remains

unclear whether MIU1 also contributes to the overall linkage selectivity of the tMIU. To address this, I first explored the contribution of the linker separating the two motifs. One major difference between the K48-linkage-specific FAM63A tMIU and the linkage-unspecific FAM63B tMIU is their linker length and composition (Figure 4.3A). In Rap80, the linker length separating the two UIM motifs defines the specificity for K63-linked polyUb (Sims & Cohen, 2009; Sato *et al*, 2009a). Therefore, to test whether the linker length and composition of FAM63A tMIU regulate polyUb binding, I replaced the 5-residue linker of FAM63A tMIU with the one of FAM63B tMIU. Swapping the linker made no difference to linkage specificity of the tMIU (Figure 4.7A, lane 6). The presence of two proline residues results in a rigid linker (Figure 4.3A). To make the linker relatively flexible, I mutated the two proline residues to alanine or replaced the whole linker with poly-Ser-Gly or poly-Ala linker (Figure 4.7A, lane 7-9). Again, I found that altering the composition of the linker does not convert the K48-linkage specificity of the tMIU. In summary, the length and composition of the linker does not affect the specificity of FAM63A tMIU for K48-linked polyUb chains.

Despite being very similar to the tMIU of FAM63A, it is intriguing that the tMIU of FAM63B binds to polyUb chains of all linkage types (Figure 4.3C). I therefore characterised the binding properties of the individual MIU motifs of FAM63B and found that the first MIU (MIU1) motif of FAM63B is the dominant Ub-binder whereas the second motif (MIU2) shows no detectable binding (Figure 4.7B). Further, FAM63B MIU1 has no linkage selectivity as it captures polyUb chains of all linkage types (Figure 4.7C). The affinity of FAM63B MIU1 on its own to polyUb chains is weaker compared to the tMIU (Figure 4.7C and Figure 4.3C). This suggests that the weak polyUb-binder MIU2 in FAM63B also contributes to overall polyUb binding of the tMIU through avidity, which is similar to FAM63A MIU1.
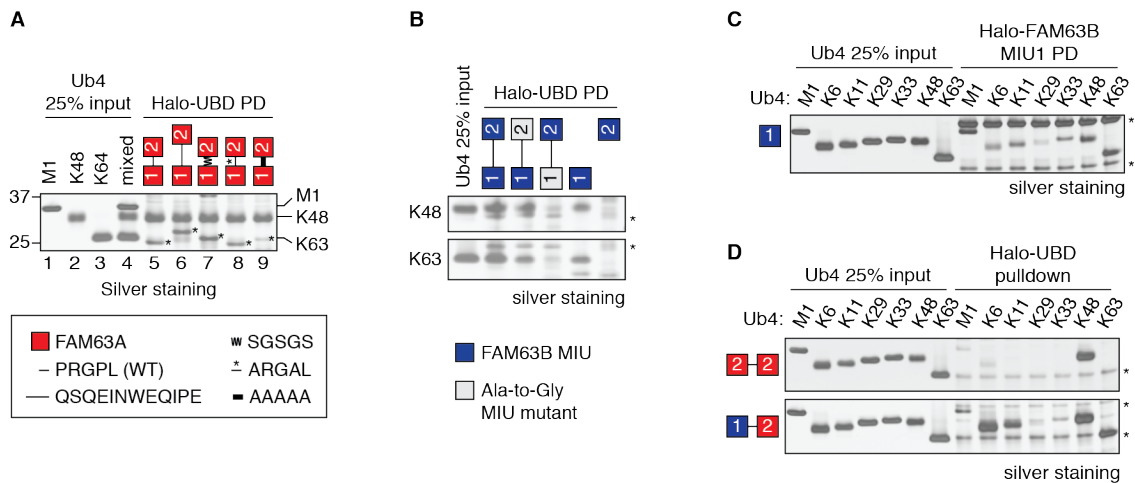
**Figure 4.7 Synergy between MIU1 and MIU2 in polyUb binding**
*(A) M1-, K48- and K63-tetraUb chains were mixed in equal amount of 29 pmol each and incubated with 1.05 nmol Halo-FAM63A tMIU with wild-type or mutant linkers. The captured materials were analysed as in Figure 4.3. Asterisks indicate non-specific bands from Halo-UBD, which run at the similar electrophoretic mobility as K63-tetraUb. (B) K48- or K63-linked tetraUb chains were captured by Halo-tagged tMIU wild-type or mutants of FAM63B as in Figure 4.4A. Blue and grey squares indicate wild-type and mutant MIU (Ala-to-Gly), respectively. Asterisks indicate non-specific bands from Halo-UBD. (C) PolyUb linkage selectivity assay of FAM63B MIU1 was carried out as in Figure 4.3C. Asterisks indicate non-specific bands from Halo-UBD. (D) PolyUb linkage selectivity assays of hybrid tMIUs were carried out as in Figure 4.3C. The first MIU motif of FAM63A tMIU was replaced by FAM63A MIU2 (top) or FAM63B MIU1 (bottom). Asterisks indicate non-specific bands from Halo-UBD, which have a similar electrophoretic mobility as M1- and K63-tetraUb chains.*

I then wondered whether replacing MIU1 of FAM63A with a motif that binds non-selectively to polyUb chains could alter the linkage preference of FAM63A tMIU. First I tested if introducing a K48-selective MIU at the position of MIU1, alters the specificity of the tandem MIU. When analysed, a tandem repeat of the K48-selective FAM63A MIU2 is still K48-linkage selective and in fact appears to bind to K48 chains with higher binding affinity (Figure 4.7D, top).   Next, I performed a domain swap, where I replaced FAM63A MIU1 with the non-selective polyUb binder of FAM63B MIU1. The hybrid tMIU is no longer K48-selective and binds to K6, K11, K48 and K63 chains, which is similar to the profile of FAM63B tMIU (Figure 4.7, bottom and Figure 4.3C). Thus, within the tMIU of FAM63A, having a non-selective polyUb binder at the position of

MIU1 converts the K48-specific binder to a non-specific one. In summary, the weak polyUb-binding property of MIU1 allows MIU1 to work in synergy with MIU2 to increase the affinity of FAM63A tMIU for polyUb without altering its selectivity towards K48-linked polyUb chains.

### 4.2.4 MIU2 binds to open conformations of K48-linked polyUb chains

To understand how FAM63A MIU2 specifically recognizes K48-linked polyUb and how this interaction is enhanced by MIU1, I attempted to crystallize the tMIU in complex with K48-triUb. Unfortunately, I was unable to obtain any crystals. I therefore crystallized the tMIU in complex with K48-diUb and these crystals diffracted to 2.0 Å. The structure was solved by molecular replacement using Ub as a search model. There are two Ub moieties present in the asymmetric unit (ASU) (Figure 4.8). Although there is no discernible electron density for the linkage between the two Ub moieties, L73 of the distal Ub is pointing towards K48 of the proximal Ub, suggesting a K48-G76 isopeptide bond. Clear electron density for a helix was visible upon refinement of the Ub. The helix was manually built in to the density and the structure was refined to the final statistics shown in Table 4.2. To my surprise, only one 4-turn-helix corresponding to MIU2 (residues 408 to 426) could be modelled into the electron density. The weak affinity of MIU1 for polyUb chains (Figure 4.4G) and the unstructured linker connecting the two MIU motifs might explain the absence of electron density for MIU1.

*Table 4.2 Data collection and refinement statistics for FAM63A tMIU:K48-diUb complex*

| | FAM63A tMIU:K48-diUb |
|---|---|
| Wavelength (Å) | 0.96769 |
| Beamline | ID30A |
| Resolution range (Å) | 48.87-2.05 (2.05-2.11) |
| Space group | $I4_1$ |
| Unit cell dimensions | 55.14 55.14 105.51 |
| | 90.00 90.00 90.00 |
| Total reflections | 65512 (5060) |
| Unique reflections | 9899 (765) |
| Multiplicity | 6.6 (6.6) |
| Completeness (%) | 100 (100) |
| Mean I/sigma(I) | 19.4 (2.9) |
| R-merge | 0.043 (0.544) |
| CC1/2 | 0.999 (0.818) |
| R-work | 0.1826 |
| R-free | 0.2234 |
| Average B-factor | 37 |
| macromolecules | 1335 |
| water | 3 |
| RMS(bonds) | 0.01 |
| RMS(angles) | 1.441 |
| Ramachandran favored (%) | 100 |
| Ramachandran allowed (%) | 0 |
| Ramachandran outliers (%) | 0 |
| PDB accession code | 5MN9 |

Interestingly, when I analysed the crystal packing I found that the diUb from the ASU makes contact with the diUb from the symmetry-related molecule, forming a cyclic K48-linked tetraUb chain (Figure 4.8B). This cyclic chain adopts a doughnut-like shape with two grooves at its centre where the two MIU2 molecules bind (Figure 4.8C). All the I44-patches are no longer at the interface between Ub moieties and therefore, this cyclic K48-tetraUb chain is in an 'open' conformation.
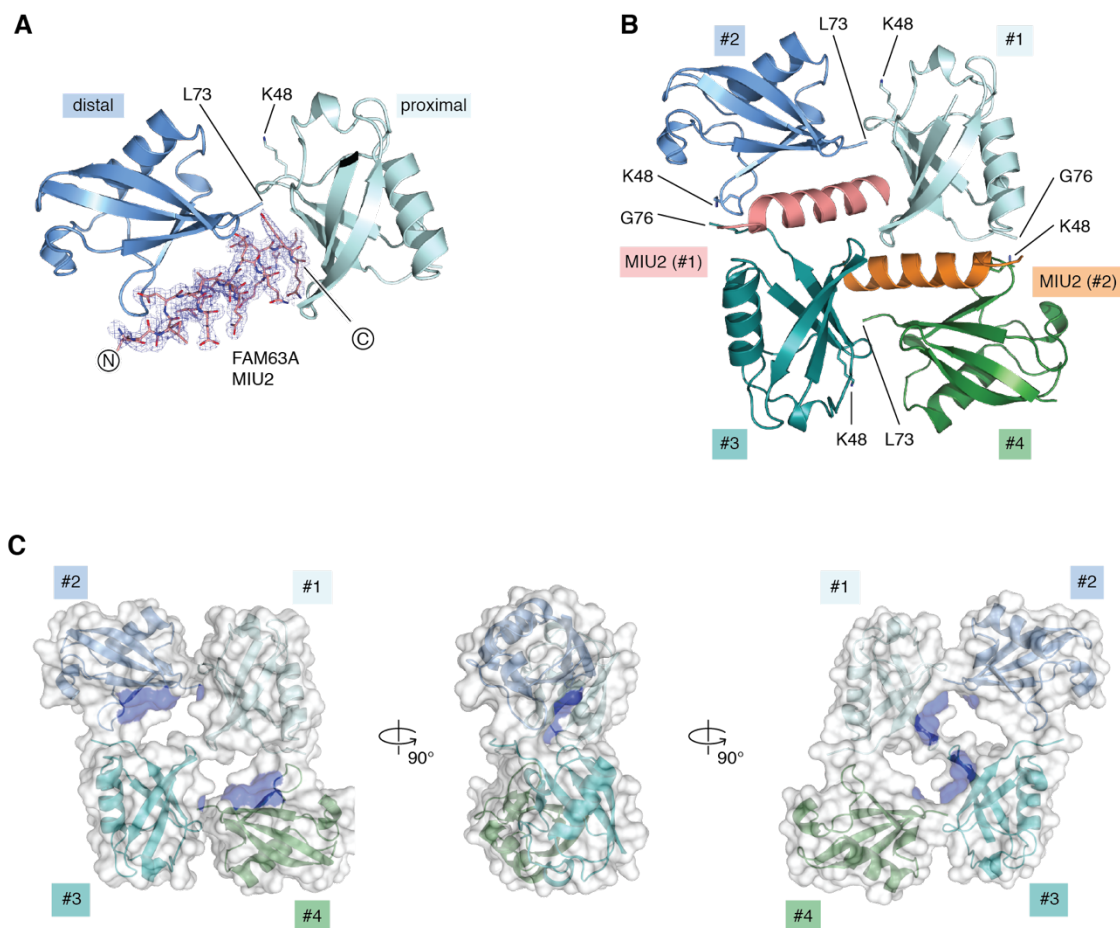
**Figure 4.8 Crystal structure of K48-diUb in complex with FAM63A MIU2**
*(A) Structure of FAM63A MIU2 and K48-diUb complex within an asymmetric unit (ASU) with 2|Fo|-|Fc| (blue) electron density maps for MIU2 contoured at 1σ. Proximal (light cyan) and distal (blue) are in cartoon representation and MIU2 (salmon) is in sticks. (B) 'Open' cyclic K48-linked tetraUb chains. Ub moiety #1 (light cyan), #2 (blue) and MIU2 moiety #1 (salmon) are from ASU. Ub moiety #3 (teal), #4 (green) and MIU2 moiety #2 (salmon) are from symmetry-related molecules. K48 and the C-terminal tail of Ub moieties are indicated. (C) The cyclic open K48-linked tetraUb forms a doughnut-like shape with two grooves at centre where two MIU2 helices bind. Four Ub moieties in (B) are shown in white surface representation. The structure is rotated on the y-axis to show three different orientations. I44-patch (L8, I44, H68 and V70) is coloured blue.*
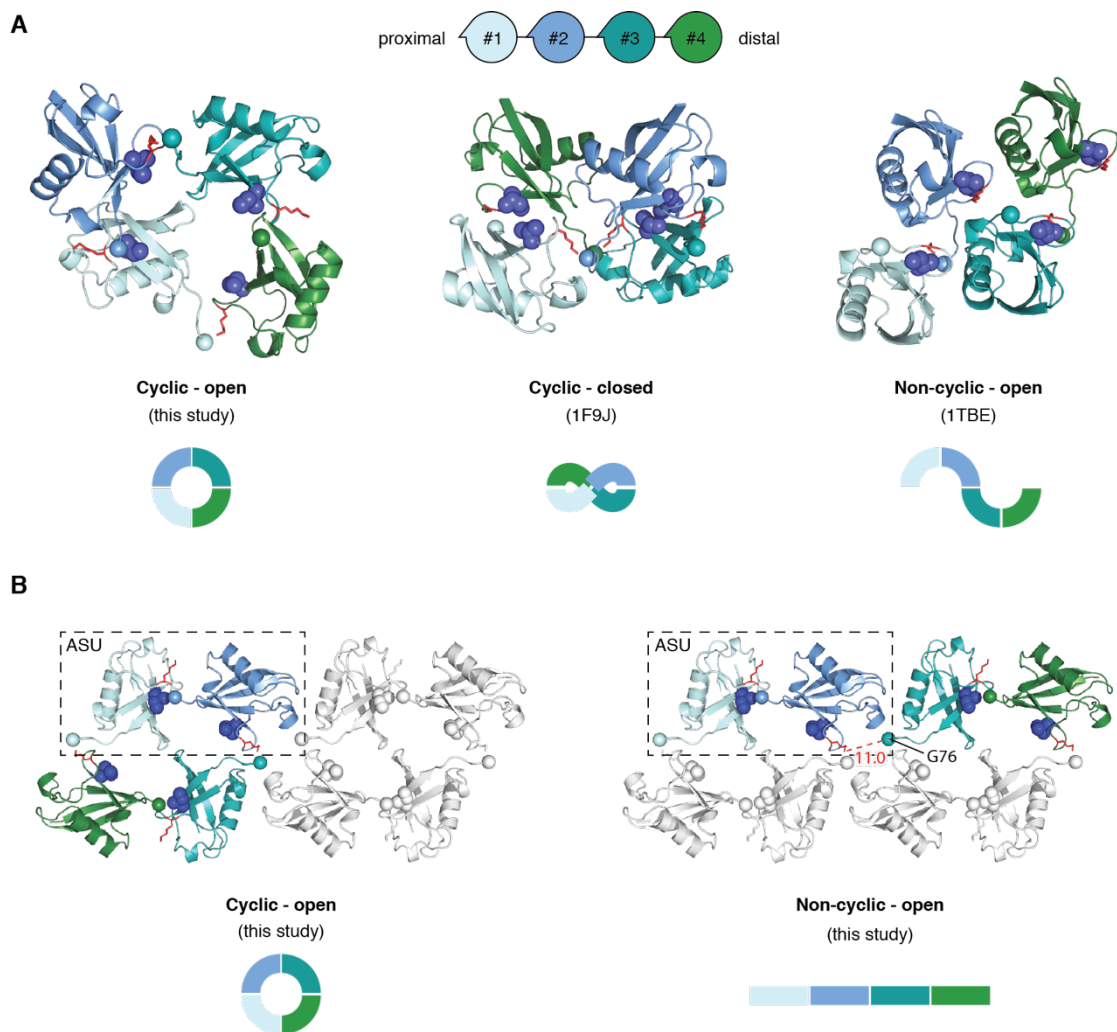
***Figure 4.9 New structure of 'open' K48-linked tetraUb chains***

*(A) Comparison of the conformations of K48-linked tetraUb. Schematic diagram illustrates the colouring and numbering of Ub moieties, which are the same as for Figure 4.8B. K48 and C-terminal tail are shown in red-sticks and spheres, respectively. For simplicity, only I44 is shown in blue spheres to represent the hydrophobic I44-patch (L8, I44, H68 and V70). PDB ID: 1TBE (Cook et al, 1994) and 1F9J (Phillips et al, 2001). (B) A non-cyclic open conformation of K48-lined tetraUb can also be modelled from symmetry-related molecules of the structure of K48-diUb in complex with FAM63A MIU2. Structures are presented as in Figure 4.8B. Ub moieties within the asymmetric unit are indicated with dotted boxes. Red dotted line indicates the distance between Ub #2 K48 and Ub #3 G76.*

To date, four structures of K48-tetraUb chains have been observed (Phillips *et al*, 2001; Eddins *et al*, 2007; Satoh *et al*, 2010; Cook *et al*, 1994). In three of these structures (1F9J, 2O6V and 3ALB), K48-linked tetraUb forms cyclic chains. However, these are all in closed conformations where the I44-patches of all Ub moieties are buried in the

interface (Figure 4.9A, middle). Even though the other crystal structure of K48-tetraUb is in an open conformation (1TBE), the fourth and the first Ub moieties are not linked and therefore, is a non-cyclic chain and different from the K48-tetraUb chain observed in this study (Figure 4.9A, right). Interestingly, looking further into the symmetry-related molecules, I can also model an open non-cyclic K48-tetraUb (Figure 4.9B, right). However, the distance between K48 and G76 of the second and third Ub moieties (~11 Å) is too far-apart for an isopeptide bond to form. Therefore, this conformation is less likely to exist in nature. In summary, I here report a novel structure of open cyclic K48-linked tetraUb chains when in complex with two FAM63A MIU2 motifs.

### 4.2.5   Mechanism of polyUb chain recognition by MIU2

The four Ub moieties of the cyclic K48-tetraUb chain are wrapped around the two MIU2 helices (Figure 4.8B). In such an arrangement, a single MIU2 interacts simultaneously with three Ub moieties using three different binding-sites on the MIU2 helix (Figure 4.10). Only K48-linked polyUb chains can adopt this conformation, as K48 is the only lysine residue within close proximity to the C terminus of the distal Ub (Figure 4.10B). This structure of MIU2 with K48-linked triUb explains the preference of FAM63A to bind to longer polyUb chains (Figure 4.7).

The first binding interface (Site 1) is formed through hydrophobic interactions and hydrogen bonds between MIU2 and the middle Ub (Figure 4.11A-C). This mode of binding is similar to the one reported for Rabex-5 MIU and monoUb (Lee *et al*, 2006; Penengo *et al*, 2006). The conserved A416 of MIU2 is buried deep within the I44 patch of the middle Ub. As with other MIUs and UIMs, mutation of A416 completely abolishes polyUb binding (Figure 4.12A). L413, L415 and L419 that surround A416 also contribute in binding to I44 patch. Hydrogen bonds are formed between the side chains of D412 and Q420 and the main chains of Ub A46, G47 and L71. In addition to this, the side chains of MIU2 Q420 and Ub R42 and R72 also interact. Indeed, mutating residues D412, Q420

or E423 on MIU2 significantly reduces the tMIU binding to K48-tetraUb, highlighting the importance of these Site 1 interactions (Figure 4.12B). Collectively, these networks of hydrophobic interactions and hydrogen bonds suggest a tight binding of the middle Ub to MIU2.
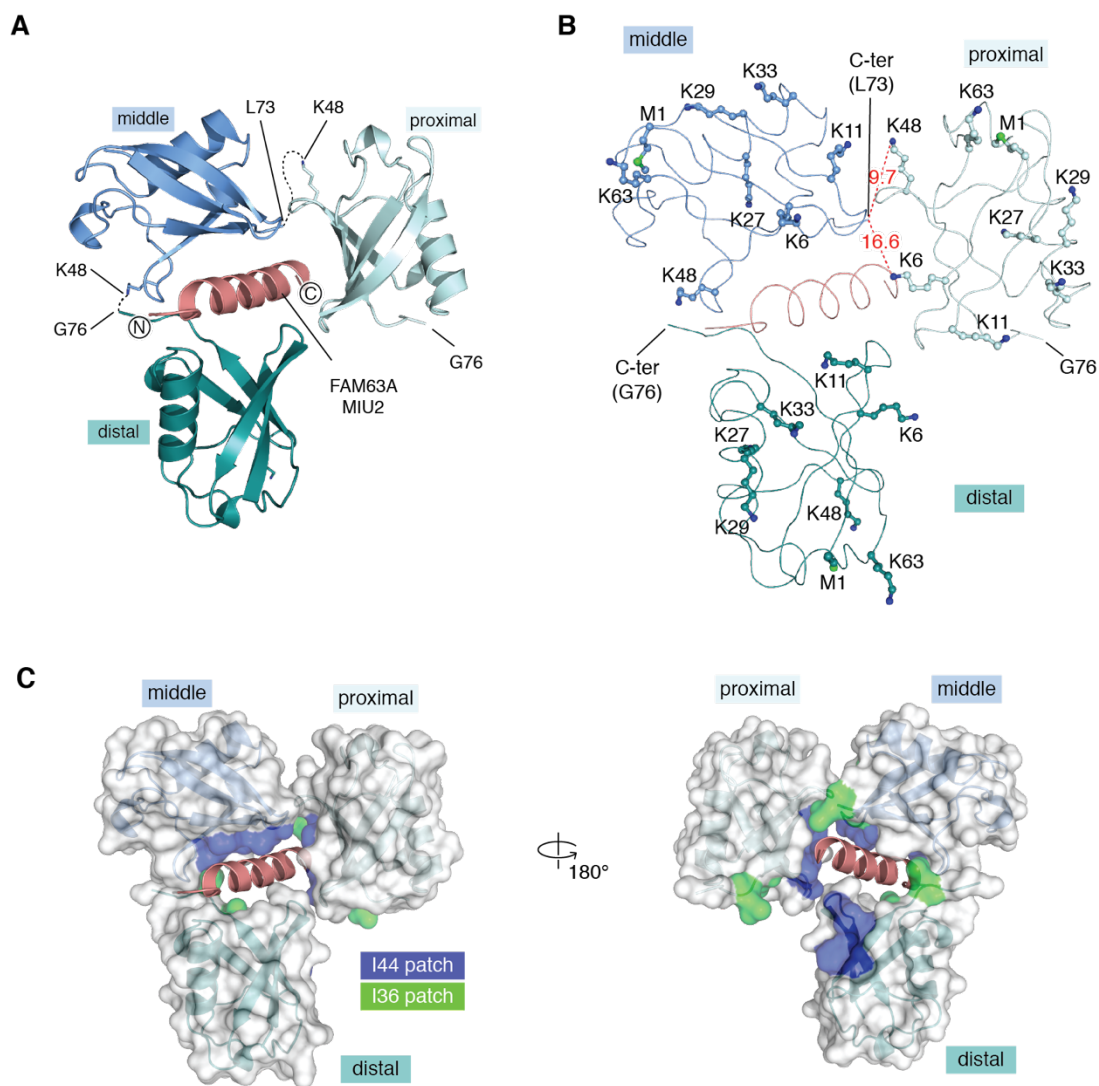


**Figure 4.10 Crystal structure of FAM63A MIU2 in complex with K48-linked triUb**
*(A) Structure of MIU2 in complex with K48-linked triUb is shown in cartoon. K48-triUb proximal (light cyan) and middle (blue) Ub are from asymmetric unit, whereas the distal Ub (teal) is from symmetry-related molecule (Figure 4.8B). K48 and the C-terminal tail of Ub are indicated. (B) Crystal structure in (A) is represented in ribbon. Lysine residues of Ub moieties are shown in sticks and spheres. The distances between C-terminal tail of the middle Ub and the K48 or K6 of the proximal Ub are shown. (C) Crystal structure of MIU2 in complex with K48-triUb is shown in two orientations, rotated on the y-axis. Ub moieties are shown in white surface. The two hydrophobic patches of Ub: I44-patch and I36-patch are coloured blue and green, respectively.*
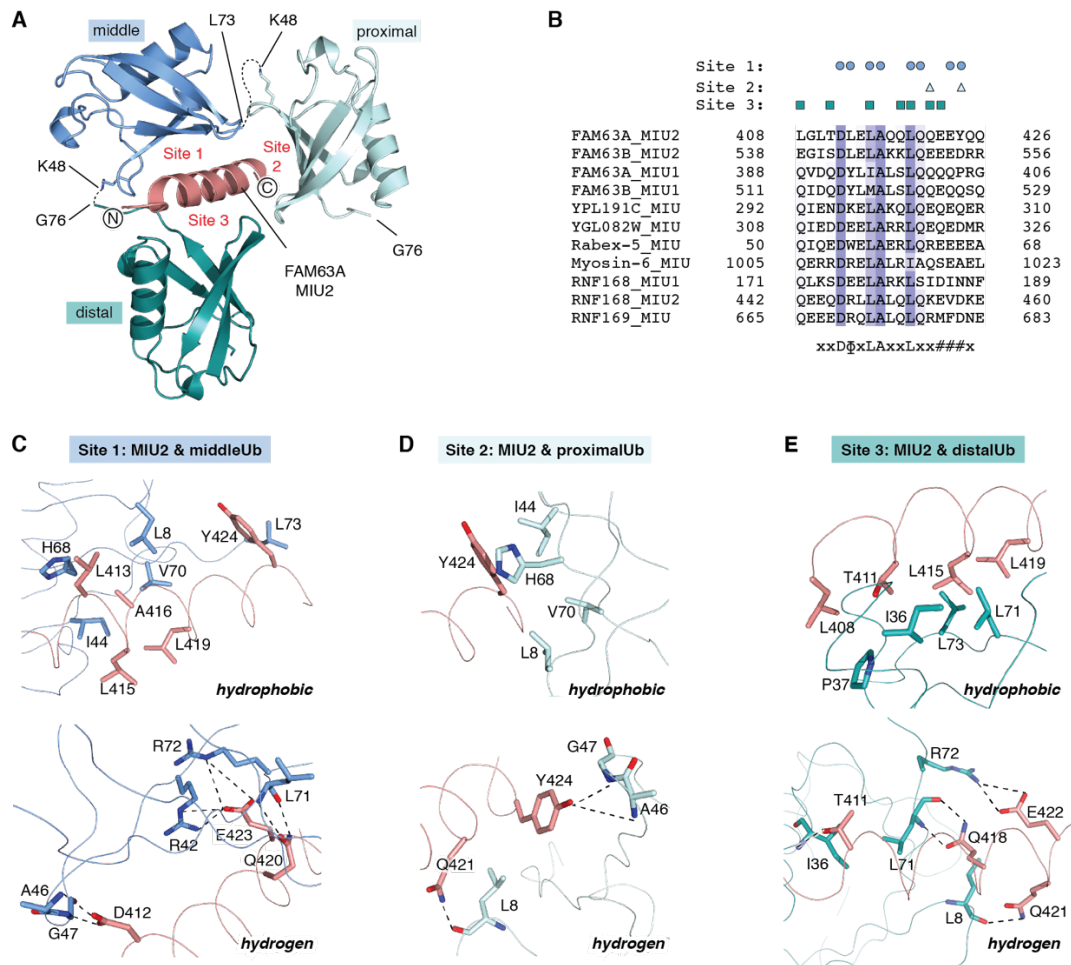
***Figure 4.11 Mechanism of polyUb chain recognition by MIU2***
*(A) Structure of FAM63A MIU2 in complex with K48-triUb as in Figure 4.10A. Three Ub-binding sites on MIU2 are indicated. (B) Sequence alignment of MIU motifs from various proteins. All sequences are from H. sapiens, except for YPL191C and YGL082W, which are from S. cerevisiae. Residues of FAM63A MIU2 that form the three Ub-binding sites are indicated. The conserved motif of MIU is shown: ϕ, large hydrophobic; #, acidic; x, any residues. (C-E) Close-up views of interactions between FAM63A MIU2 and the middle Ub (Site 1), proximal Ub (Site 2), distal Ub (Site 3). Hydrophobic interactions and hydrogen bonds are shown on the top and bottom panels, respectively. Residues at the interface are shown in sticks and coloured as in Figure 4.10A. Dotted lines indicate hydrogen bonds.*

The second binding interface (Site 2) is formed between MIU2 and the proximal Ub, which occupies a smaller buried surface area of ~240 Å$^2$ in comparison to Site 1 (~500 Å$^2$) and Site 3 (~480 Å$^2$) (Figure 4.11A). The proximal Ub is bound by MIU2 in an unusual way, where a bulky hydrophobic residue on Site 2, Y424, mediates key interactions: the hydrophobic aromatic ring of Y424 interacts with the I44 patch of the

proximal Ub, and the hydroxyl group of Y424 interacts with the main chain amide group of A46 and G47 (Figure 4.11D). These interactions are analogous to MIU2 A416 and D412 on Site 1, respectively (Figure 4.11C). Mutating Y424 to Ala or acidic residues but not Phe or Trp abolishes tMIU binding to K48-tetraUb, confirming the crucial role of the hydrophobic aromatic ring for Ub binding (Figure 4.12C). Y424 also interacts with L73 of the middle Ub and therefore highlights the key role of Y424 in stabilizing MIU2 interaction with polyUb. In other MIU motifs, the position corresponding to Y424 is commonly occupied by acidic residues and therefore, the mode of binding by Y424 is a unique feature of FAM63A MIU2 (Figure 4.11B).

The third binding interface (Site 3) is formed between MIU2 and the distal Ub, which was determined from crystal contacts with the symmetry-related molecule (Figure 4.8A-B). MIU2 L408, T411, L415 and L419 interact with the hydrophobic patch on the distal Ub formed by I36, P37, L71 and L73 (Figure 4.11E). In addition, the side chains of MIU2 T411, Q418 and Q421 form hydrogen bonds with the main chains of Ub I36, L71 and L8. Further interactions between the side chains of MIU2 E422 and Ub R72 reinforce the binding. To determine the contribution of Site 3 to polyUb binding, I individually mutated residues forming Site 3. With the exception of L415 and L419, mutation of L408, T411, Q418, Q421 or E422 did not disrupt polyUb binding of the tMIU (Figure 4.12A-B). L415 and L419 also bind to the middle Ub (Site 1) and therefore, the loss of binding observed upon mutating these residues could be a result of simultaneously disrupting Site 1 interaction with the middle Ub (Figure 4.11B).

FAM63A tMIU requires MIU1 to bind to K48 polyUb chains with higher binding affinity (Figure 4.5). Therefore, I postulated that MIU1 may provide additional interactions with the distal Ub, which may compensate for the mutations on Site 3 (Figure 4.13). To test this hypothesis, I mutated residues on Site 3 in MIU2 and found that in the absence of MIU1, mutating L415, Q418 and L419 abolishes binding to polyUb (Figure

4.12D). This suggests that the residual binding of L415, Q418 and L419 mutants observed in tMIU was due to MIU1 binding to Ub. In addition to highlighting the contribution of Site 3 of MIU2 to Ub binding, these observations suggest that MIU2 binding to the distal Ub is enhanced by MIU1 through mechanisms yet to be elucidated (Figure 4.13).
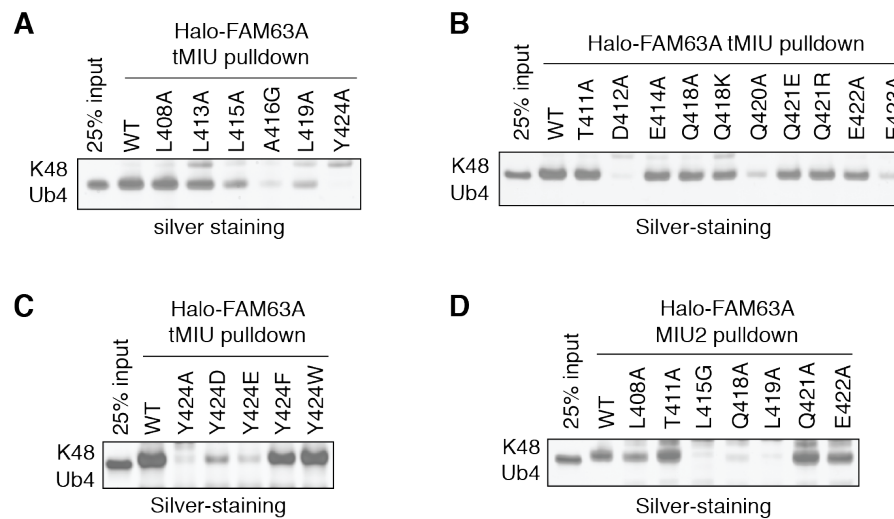


**Figure 4.12 Three Ub-binding sites on FAM63A MIU2 are essential for binding to polyUb chains**
*(A-B) Residues of MIU2 involved in hydrophobic interactions (A) and hydrogen bonds (B) were mutated and the effect on tMIU binding to K48-tetraUb was investigated as in Figure 4.4A. (C) Role of Y424 in tMIU binding to K48-tetraUb was investigated by mutating MIU2 Y424 to the indicated residues and pulldown assays were performed as in Fig 2A. (D) Residues of MIU2 forming Site 3 binding site were mutated and the effect on MIU2 binding to K48-tetraUb was investigated as in Figure 4.4A.*
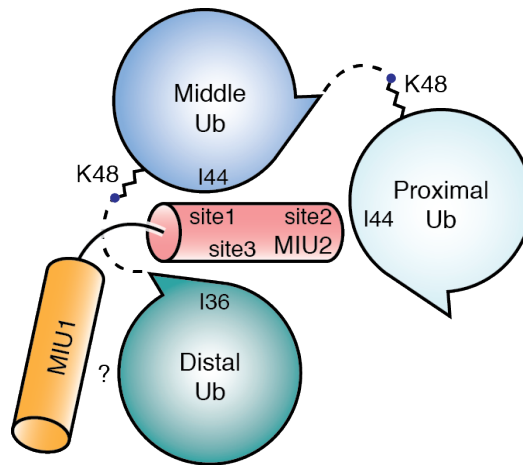
***Figure 4.13 A model of how FAM63A tMIU achieves its K48-linkage selectivity.***
*Three Ub-binding sites on MIU2 engage the I44 patches of the middle and proximal Ub,
and the I36 patch of the distal Ub. It is speculated that Ub binding to the third site of
MIU2 is enhanced by MIU1.*

MIU2 A416 and Y424 bind the middle Ub and proximal Ub, respectively, in an
orientation that can only be accommodated by K48-linked diUb, which explains the
linkage selectivity of MIU2 (Figure 4.14A and Figure 4.10A-B). This mode of binding is
analogous to Rap80 tUIM, where the linker connecting the two UIMs of Rap80 stretches
and positions the interacting surfaces of the two UIMs in an orientation that only K63-
linked diUb can accommodate (Figure 4.14B) (Sims & Cohen, 2009; Sato *et al*, 2009a).
Altering the distance between the key alanine residues of the two UIMs abrogates Rap80
tUIM binding to K63 chains (Sato *et al*, 2009a). To test if FAM63A MIU2 also employs
the same mode of binding, I altered the distance between the two binding sites within
MIU2 by deleting E423 or introducing Ala residues in-between A416 and Y424 (Figure
4.14C). Indeed, altering the distance between these two key residues completely disrupts
tMIU binding to polyUb chains (Figure 4.14D-E). These results highlight the importance
of the spatial arrangements between two Ub-binding sites within FAM63A MIU2 to bind
and orient Ub moieties within K48-linked polyUb chains.
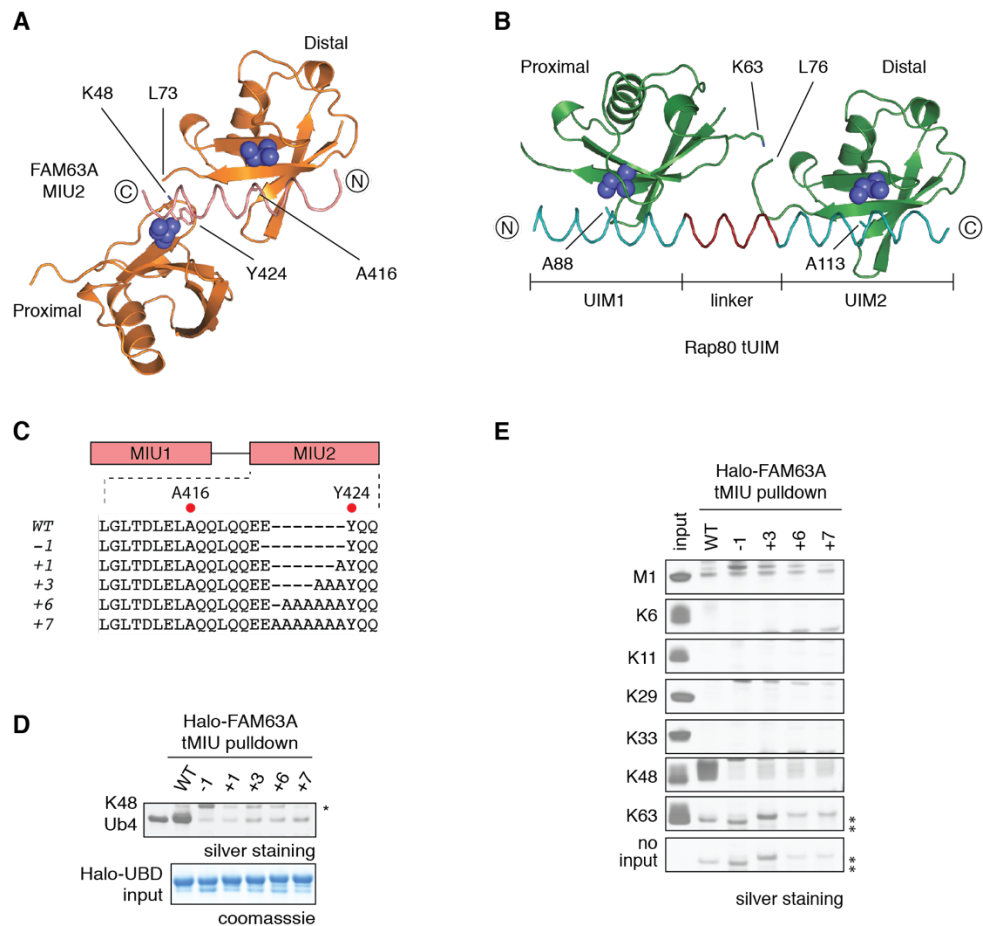
**Figure 4.14 The distance between Ub-binding Site 1 and Site 2 on FAM63A is essential for binding to polyUb**

*(A-B) K48-diUb (orange) (A) and K63-diUb (green) (B) in complex with FAM63A MIU2 and Rap80 tUIM, respectively are shown in cartoon. The distal moieties of the two diUb chains were superposed. The N- and C-terminal ends of MIU2 and tUIM are indicated. The key residues of MIU/UIM that engage with I44 (blue spheres) are shown in sticks. The linker of Rap80 tUIM is coloured red. PDB ID: 3A1Q (Sato* et al, *2009a). (C-D) The distance between two Ub-binding sites on MIU2 was altered by deleting E423 or inserting Ala residues N terminus to Y424 (C). The effect of mutations on FAM63A tMIU binding to K48-tetraUb was investigated as in Figure 4.4A (D). (E) As in (D), but the effect of the mutations on FAM63A tMIU binding to tetraUb of seven linkage types were investigated. Asterisks indicate non-specific bands from Halo-UBD, which has a similar electrophoretic mobility as K63-tetraUb.*

## 4.3 Discussion

### 4.3.1 FAM63A tMIU preferentially binds to longer polyUb chains

In this study I observed that the tMIU of FAM63A selectively senses both the length and type of polyUb chains. The preference to bind to longer polyUb chains observed in FAM63A tMIU has also been reported in other UBDs as well, including hHR23A UBA1-2, S5a UIM1-2, AIRAPL UIM1-2 (Raasi *et al*, 2004; Young *et al*, 1998; Rahighi *et al*, 2016; Burnett *et al*, 2003; Chai *et al*, 2004). Although the mechanism underlying this preference remains elusive, it is generally speculated that longer polyUb chains increase the binding avidity, which compensates for the relatively weak binding affinity of UBDs for Ub (Rahighi & Dikic, 2012). There are three Ub-binding sites on FAM63A MIU2 and based on my results, I proposed that Ub binding to the third site (Site 3) is enhanced by MIU1 (Figure 4.13). Collectively, these interactions contribute to higher binding affinity and thus, explain the preference of FAM63A tMIU to bind to K48-linked polyUb chains consisting minimum of three or more Ub moieties (Figure 4.4C).

The speculation that longer polyUb chains increase avidity does not explain how FAM63A tMIU has ~10-fold higher binding affinity to tetraUb as compared to triUb chains (Figure 4.4E-F). This difference in binding affinity is not accompanied by change in binding enthalpy when tMIU was titrated into K48-triUb and tetraUb, which suggests a same mode of interaction (Table 4.1). This is in contrast to the enthalpy of tMIU binding to diUb, which is much lower due to decreased avidity. Therefore, the increase of FAM63A tMIU binding affinity to tetraUb chains as compared to triUb may not be caused solely by increased avidity.

Alternatively, longer polyUb chains may affect kinetics of UBDs interaction with polyUb chains, which involve binding on-rate ($k_{on}$) and off-rate ($k_{off}$). Assuming that FAM63A tMIU binds to three Ub moieties at a time regardless of the length of polyUb

chains, the $k_{off}$ may be constant. In longer polyUb chains, there are more sets of three Ub moieties available for binding (Figure 4.15A). Therefore, once FAM63A tMIU dissociates from the first set of Ub moieties, it may readily bind to the next set of three Ub moieties (Figure 4.15B). This hypothesis proposes that longer chains may increase the $k_{on}$ of UBDs to polyUb without much affecting the $k_{off}$, which overall results in increased binding affinity. To test this, Surface Plasmon Resonance (SPR) can be used to study the kinetics of binding by measuring the on- and the off-rates of UBD and polyUb chains.
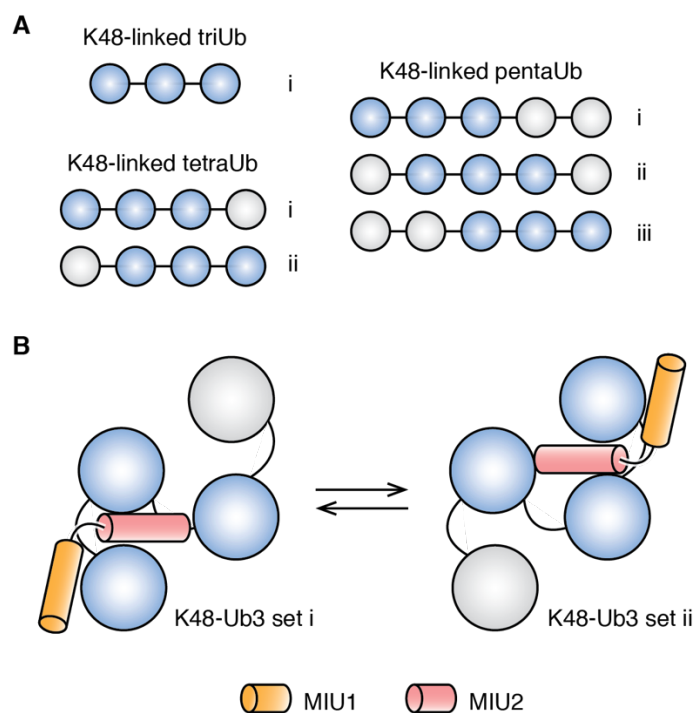


***Figure 4.15 Model how longer polyUb chains may affect kinetics of FAM63A tMIU binding to longer polyUb chains***
*(A) Longer polyUb chains contain more set of three Ub moieties, which can bind to FAM63A tMIU at a time. (B) Longer polyUb chains may increase the binding on-rate of FAM63A tMIU. When tMIU dissociates from the first set of Ub moieties, it can readily bind to the next set of three Ub.*

### 4.3.2 Multiple Ub-binding sites on FAM63A MIU2 determines its linkage-selective binding to K48-linked polyUb chains

In the previous chapter I described that the linkage-selective binding of NZF domains arise from two distinct binding sites on the NZF domain that orient Ub moieties in

conformations that can only be accommodated by specific linkage types. Similarly, FAM63A MIU2 contacts K48-linked polyUb chain via three different binding sites on the MIU and thus, imparting the linkage-selective binding of FAM63A tMIU. Site 1 on FAM63A MIU2 binds to I44-patch of Ub using its DΦxLAxxL motif that is conserved in other MIUs (Figure 4.11B) (Penengo *et al*, 2006). Thus, Ub binding to Site 1 of FAM63A MIU2 is similar to Ub binding to Rabex-5 MIU and possibly other MIUs. This site is analogous to the distal binding site on NZF domains, which uses conserved TF-Φ motif (Chapter 3.3.4). Analogous to the proximal Ub-binding site on NZF domains, the other two binding sites on FAM63A MIU2 (Site 2 and 3) are unique, which position only K48 residue of the proximal Ub in contact range with the C terminus of the distal Ub (Figure 4.11B). Consequently, only K48-linked polyUb chains can adopt this conformation in which three Ub moieties can bind at a time to FAM63A MIU2. Thus, this explains the linkage selective binding.

It is fascinating how a short α-helix of 20 residues bears multiple Ub-binding sites. Like FAM63A MIU2, individual UIM motifs in Hrs and AIRAPL have been reported to contain multiple Ub-binding sites (Hirano *et al*, 2006a; Rahighi *et al*, 2016). Hrs UIM has two hydrophobic strips on either side of its helix, which each binds to the I44-patch of independent Ub molecules (Hirano *et al*, 2006a). The two Ub molecules bound to Hrs are not linked by any isopeptide bond and therefore, the double-sided Ub-binding on Hrs UIM does not provide linkage specificity but a higher efficiency in binding to multiple monoubiquitylated cargoes in the endocytic pathway (Urbé *et* al, 2003; Hirano *et al*, 2006a). On the other hand, the tUIM of AIRAPL recognizes K48-linked triUb where the two Ub-binding sites on UIM2 bind to two moieties of Ub simultaneously, whereas UIM1 binds to the proximal Ub (Rahighi *et al*, 2016). Even though AIRAPL UIM2 was described as the K48 linkage determinant for the tUIM, in the absence of UIM1, UIM2 of AIRAPL failed to bind K48-triUb. In contrast, FAM63A MIU2 uses distinct

mechanisms in which the three Ub-binding sites simultaneously bind to all three Ub moieties (Figure 4.13).

### 4.3.3   Why does FAM63B tMIU bind to all types of polyUb chain?

FAM63A and FAM63B are two uncharacterised proteins that contain tandem of two MIU motifs at the C terminus. The sequence of these tMIU motifs are highly similar apart from the linker region and yet their polyUb binding properties vary. FAM63A tMIU binds selectively to K48 chains whereas FAM63B tMIU binds to all chain types. Further, I observed that the two MIU motifs arranged in tandem have different role in polyUb binding. In FAM63A, MIU2 is the dominant polyUb binder whereas in FAM63B, MIU1 is the major polyUb binder (Figure 4.4A and Figure 4.7B). Interestingly, the isolated FAM63A MIU2 and FAM63B MIU1 both display the same binding preferences as FAM63A tMIU and FAM63B tMIU respectively, although with reduced binding affinity. Thus, the tMIU in both FAM63A and FAM63B employ similar mechanisms wherein one MIU is the dominant binder whereas the other enhances binding affinity to polyUb through weak auxiliary interactions.

This study addresses how FAM63A selectively binds to K48 chains, which has been thoroughly discussed above. However, how FAM63B MIU1 binds to all type of polyUb chains has not been fully investigated. Sequence comparisons suggest that FAM63B MIU1 may not have binding sites similar to FAM63A Site 2 and Site 3. This is because FAM63A Y424 and Q418, two residues that are essential in Site 2 and Site 3, respectively are not conserved in FAM63B. Thus, FAM63B MIU1 may depend more on its DΦxLAxxL motif, a signature motif of MIU, which also forms the binding Site 1 on FAM63A MIU2 (Figure 4.11B) (Penengo *et al*, 2006). Interestingly, in FAM63B MIU1, the MIU motif is DΦxMAxxL, where the canonical Leu residue is replaced by Met. The presence of Met may increase the binding affinity of FAM63B MIU1 for monoUb and

thus, result in binding to polyUb chains regardless of the linkage type. It would be interesting to investigate whether introducing L415M mutation on FAM63A tMIU would alter its linkage-selective binding. This will address the concept of linkage-selective binding of multi-sided UBDs that each Ub-binding site has to be weak to bind to monoUb and consequently depends on avidity to bind to polyUb (Sims *et al*, 2009).

### 4.3.4 FAM63A tMIU as tools to study K48 chain signalling: Should I go with TUBEs?

I have characterised and described in this chapter that FAM63A tMIU is a highly selective K48-linked polyUb binder. One potential application of FAM63A tMIU is to be used as affinity reagents to selectively capture K48 chains from cells. TUBEs (tandem Ub-binding entities) were designed to increase binding affinity of UBDs towards polyUb chains by having multiple repeats of UBD arranged in tandem (Hjerpe *et al*, 2009). One advantage of using TUBEs is that its higher binding affinity ensure that it can compete with natural binding partners of polyUb chains within cells. Therefore, TUBEs are more efficient tools to purify polyUb chains from cells or to be used as dominant negative inhibitors of polyUb signalling. However, an important consideration in designing such TUBEs is that linkage specificity must be maintained while increasing binding affinity.

A K48-selective binder with high binding affinity would be an instrumental tool to dissect K48 Ub signalling. There are increasing reports of K48 chains present in branched chains with other linkage types, including work described in this thesis (Chapter 3.2.13) (Meyer & Rape, 2014; Grice *et al*, 2015; Ohtake *et al*, 2016; Kristariyanto *et al*, 2015a). APC/C assembles branched K11/K48 chains on its substrates that signal more efficient proteasomal degradation (Meyer & Rape, 2014; Grice *et al*, 2015). The K48-linkage selective FAM63 tMIU can be used as tool to dissect the individual role of K48 chains within the K11/K48 branched chains. Transiently expressing FAM63A tMIU in cells would bind to K48 chains but not K11 chains and thus, may inhibit K11/K48 branched

chains only through the K48 linkages. Thus, linkage-selective UBDs can be used to individually dissect individual linkage type within branched chains. This is not possible employing the widely used hPLIC1-UBA TUBE since it binds to all type of polyUb chains.

To further exploit the K48-specific UBD described in this chapter, I tried to engineer a TUBE based on FAM63A MIU2 that can bind to K48 chains with higher binding affinity. As tandem of MIU2-MIU2 still retains specificity of binding to K48 tetraUb chains (Figure 4.7D), I designed a tandem of four FAM63A MIU2 repeats (4×MIU2-TUBE). Surprisingly, this 4×MIU2-TUBE is no longer selective, and binds to K6, K11, K48 and K63 tetraUb chains (Figure 4.16). This binding profile is similar to FAM63B tMIU and the hybrid of FAM63B MIU1-FAM63A MIU2 (Figure 4.3C and Figure 4.7D). From these qualitative assays, it does not seem that 4×MIU2-TUBE has any stronger binding affinity for tetraUb chains, although 4×MIU2-TUBE may bind with higher affinity to longer polyUb chains. Collectively, placing four repeats of FAM63A MIU2 in tandem alters linkage selectivity of the individual FAM63A MIU2 motif.
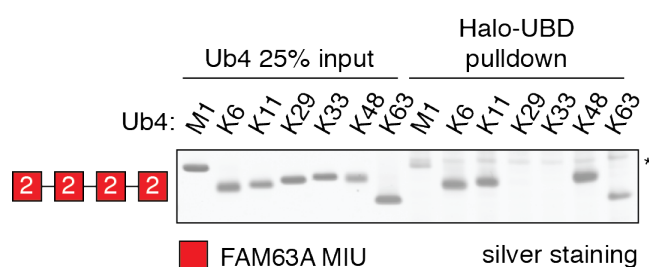


***Figure 4.16 TUBE containing four repeats of FAM63A MIU2 motifs loses linkage-selectivity to bind to K48 chains***
*TetraUb chains of the indicated linkage types were incubated with Halo-tagged FAM63A 4X(MIU2) and the captured materials were analysed as in Figure 4.3.*

The loss of specificity in 4×MIU2-TUBE may have been caused by avidity effects that allow various conformations of polyUb chains to bind to the TUBE. Through structural study, I reported that FAM63A MIU2 has three Ub-binding sites. Thus, the

twelve Ub-binding sites on 4×MIU2-TUBE may accommodate multiple conformations of tetraUb chains, which no longer specific for K48 types. These avidity effects have been observed in previous studies by Robert Cohen and colleagues (Sims *et al*, 2009). Introducing a GST-tag that homo-dimerizes onto isolated UBA domains lead to avidity effects akin to having multiple copies of UBA domains in tandem. These avidity effects explain why UBA domains that do not bind to K63 chains in solution can bind to K63 chains when they are used in pulldown assays as GST-tagged proteins (Sims *et al*, 2009; Raasi *et al*, 2005). In summary, the same avidity effect may explain why 4×MIU2-TUBE containing copies of K48 linkage-selective MIU2 to lose linkage-selective binding.

Although a tandem MIU2-MIU2 (2×MIU2-TUBE) may not have significant difference in its K48 linkage selectivity, the artificial tandem MIU motifs may have six Ub-binding sites that can bind to other types of chains as well. This may be missed in my assays with using tetraUb chains, but may be evident when longer polyUb chains are used in the pulldown assays. To support this, I observed faint bands corresponding to M1 and K6 chains captured by 2×MIU2-TUBE (Figure 4.5D). The nanomolar affinity of FAM63A tMIU for K48-tetraUb, lead me to conclude that the naturally occurring FAM63A tMIU and not its artificial TUBEs may be used as tools to study K48 signalling. My results also provide an important caution to other researchers who create TUBEs from linkage-selective UBDs and assume that the new synthetic TUBE maintains the same binding specificity. In support of this, I observed that a TUBE containing two TRABID NZF1 domains no longer binds exclusively to K29 and K33, but to all chain types (data not shown).

# 5 Characterisation of deubiquitylating activity of FAM63A

## 5.1 Introduction

FAM63A is an uncharacterised protein, which is highly conserved in mammalians. Its C-terminal region contains a tandem repeat of MIU motifs that exclusively binds K48-linked polyUb chain (Chapter 4). In addition to this, FAM63A contains two conserved regions at the N- and C-terminus of the tMIU. The first has been annotated as domain of unknown function 544 (DUF544) and the latter is a CaaX motif (Figure 5.1A). Given the presence of a functional UBD, our lab posited a Ub-related function for DUF544 (Marcotte *et al*, 1999). Sequence analysis suggests conserved residues typical of a cysteine protease in the DUF544 of FAM63A. Therefore, we hypothesised that FAM63A is a cysteine DUB that cleaves (iso)peptide bonds between Ub moieties.

Our lab confirmed this hypothesis by testing FAM63A activity in cleaving tetraUb chains of seven different linkage types in DUB assays (Figure 5.1B). Remarkably, both full length and the catalytic domain alone of FAM63A cleave only K48-linked tetraUb (Figure 5.2). Sequence analysis of the catalytic domain of FAM63A reveals that it does not share any sequence homology with any of the other known DUBs. In addition to this, structural characterisation of the catalytic domain reveals a distinct architecture that has not been observed for DUBs of other family (Abdul Rehman *et al*, 2016). Based on these, our lab posited that FAM63A belongs to a novel DUB family. Given FAM63A is the only DUB identified to date that contains MIU motif, we named the novel DUB family MINDY or "MIU-containing novel DUB family", with FAM63A as MINDY-1 (Abdul Rehman *et al*, 2016).

Human genome sequence analysis found several other members of MINDY DUBs including the closely related protein FAM63B and the more distant proteins FAM188A and FAM188B (Abdul Rehman *et al*, 2016). In addition to these, orthologs have been

found in other organisms, including budding yeast, *C. elegans*, *Drosophila*, *Dictyostelium* and plants. When tested in DUB assays, FAM63B and yeast ortholog YPL191C cleaved only K48-linked polyUb chains (Figure 5.1C-D). This K48 selective cleavage is a remarkable feature of the first three-to-be-discovered members of MINDY DUBs. Whether this is retained in other members has to be further investigated. As little was known about the catalytic property and the biological function of FAM63A, I wanted to characterise the deubiquitylating activity of FAM63A.
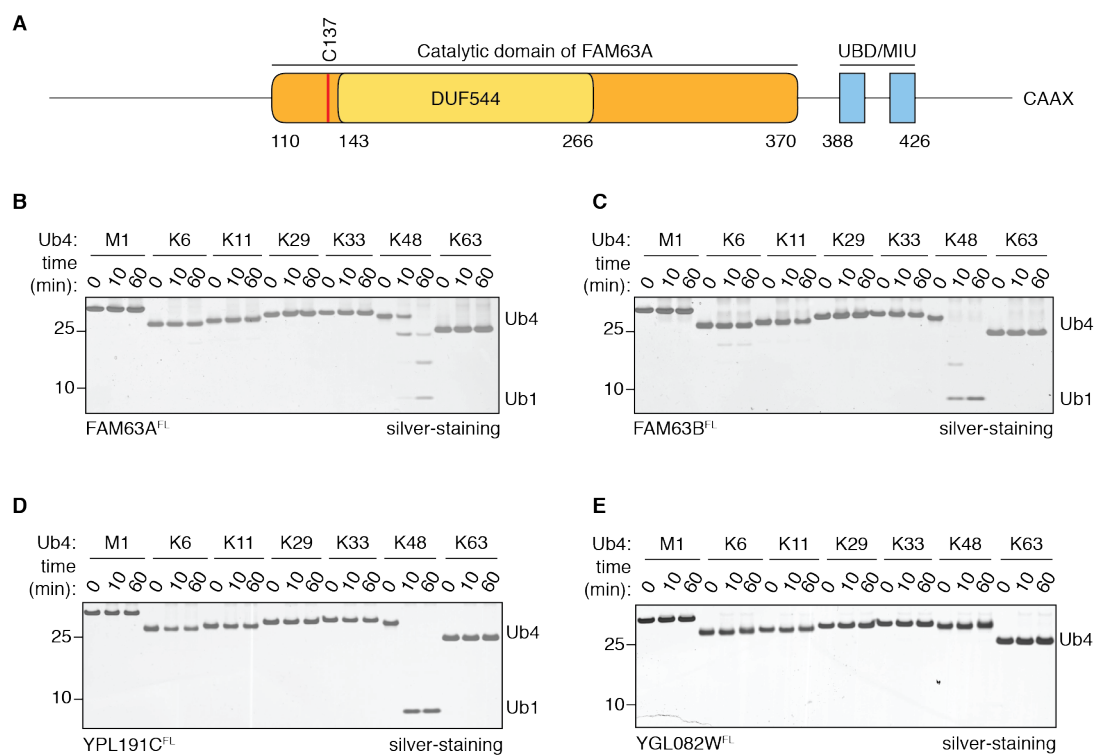


***Figure 5.1 FAM63A is a DUB specific for cleaving K48 chains***
*(A) Schematic diagram illustrates domain structure of human FAM63A. (B-E) DUB assays testing activity and specificity of polyUb cleavage by FAM63A (B), FAM63B (C), YPL191C (D) and YGL082W (E). DUB assays were carried out by incubating 1.6 μM of DUB with 2.2 μM of tetraUb chains of the indicate linkage types at 30 °C for the indicated periods of time. Reactions were stopped by adding LDS sample buffer and analysed on silver-stained 4-12% SDS-PAGE gel.*
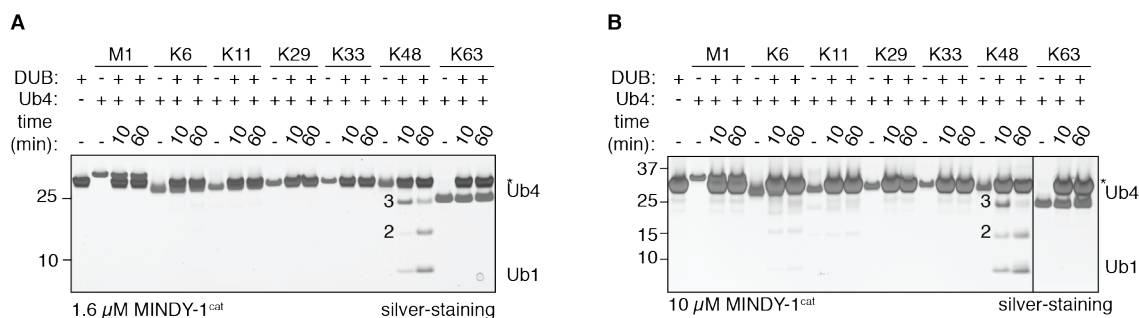
***Figure 5.2 The catalytic domain of FAM63A selectively hydrolyses K48-linked polyUb chains***
**(A-B)** *DUB assays were carried out by incubating 1.6 µM (A) or 10 µM (B) of FAM63A catalytic domain (110-384) with tetraUb chains of the indicate linkage types at 30 °C for the indicated periods of time. Asterisks indicates FAM63A, which migrates at a similar electrophoretic mobility as tetraUb chains.*

## 5.2 Results

### 5.2.1 FAM63A cleaves longer polyUb chains through an exo-DUB activity

One approach to monitor the catalytic activity of a DUB is through investigating its ability to cleave a fluorogenic Ub substrate, such as Ub-Rho110-G substrate. This substrate contains a fluorogenic dye rhodamine (Rho110-G), which is non-fluorescent when it is conjugated to the C-terminal tail of Ub. When cleaved off from Ub by a DUB, rhodamine is released and it exhibits intense fluorescence when excited at 485 nm (Hassiepen *et al*, 2007). Such fluorogenic Ub substrates have been used extensively to study USP and UCH family of DUBs (Faesen *et al*, 2011; Sahtoe *et al*, 2015; Lee *et al*, 2010).

Initially, to investigate the activity of the catalytic domain of FAM63A (FAM63A$^{cat}$), I monitored the cleavage of fluorogenic Ub-Rho110-G substrate. As a positive control, I used UCH-L3, a UCH family DUB that removes small adducts from the C-terminal of Ub (Hassiepen *et al*, 2007). FAM63A$^{cat}$ does not hydrolyse Ub-Rho110-G even when 1.6 µM of DUB was used (Figure 5.3A). In contrast, UCH-L3 readily cleaves Ub-Rho110-G substrate at a concentration as low as 5 pM. This suggests that FAM63A has a poor C-terminal hydrolytic activity.
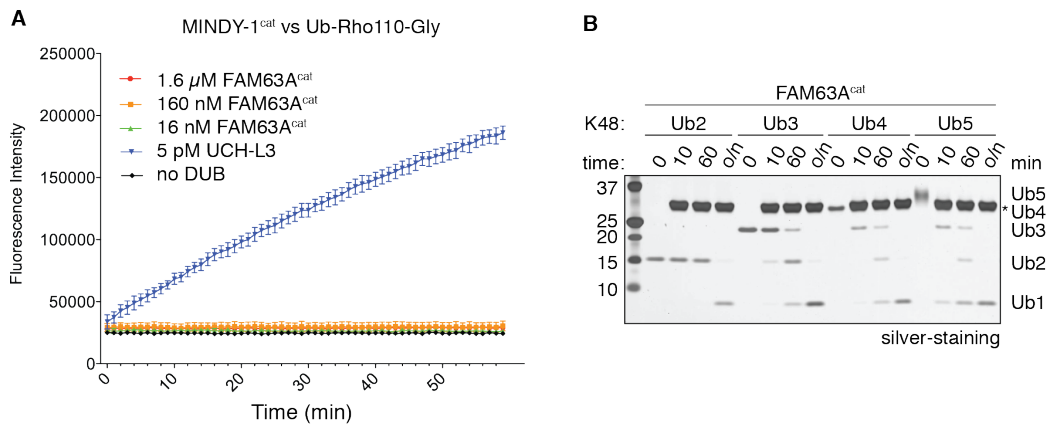
***Figure 5.3 FAM63A prefers to hydrolyse long polyUb chains***
*(A) FAM63Acat does not hydrolyse the fluourogenic DUB substrate Ub-Rho110-G. DUB assays containing 50 nM of Ub-Rho110-G and increasing concentration of FAM63Acat or 5 pM UCH-L3 were carried out at 30 °C for the indicated period of time. Cleaved Rho110-G was detected by excitation and emission of 485 and 520, respectively. n = 3; means ± s.d. **(B)** DUB assays containing 1.6 µM of FAM63Acat and 750 nM of polyUb chains were carried out at 30 °C for the indicated periods of time.*

Several DUBs have been reported to have a poor activity towards fluorogenic Ub substrate and preferably cleave polyUb (Keusekotten *et al*, 2013; Békés *et al*, 2015; Winborn *et al*, 2008). We have observed that FAM63A cleaves K48-linked tetraUb chains (Figure 5.2) and hence, it is likely that FAM63A also exhibits substrate preference for longer polyUb chains. To investigate this, I monitored FAM63A activity in cleaving K48-linked di-, tri-, tetra- and pentaUb over time. I observed that longer polyUb chains are hydrolysed faster, suggesting that FAM63A preferably hydrolyses longer polyUb chains (Figure 5.3B).

DUBs can either cleave within chains (endo-DUB) or remove Ub from one end of the chain (exo-DUB), and the mode of cleavage employed by a DUB provides insights into its function (Komander *et al*, 2009a). For instance, POH1/RPN11, a JAMM DUB that is part of 19S proteasome complex cleaves within chains to release Ub chains *en bloc* from substrates (Yao & Cohen, 2002). In contrast, DUBs such as USP14 trim Ub chains and can edit the degradation signal on substrates to rescue them from the proteasome (Lee

*et al*, 2010). To determine the mode of chain cleavage employed by FAM63A, I carefully monitored the time-dependent cleavage of K48-linked pentaUb chains (Figure 5.4). Upon cleavage by FAM63A$^{FL}$ and FAM63A$^{cat}$, the products at the earliest time points are tetraUb and monoUb, followed by the appearance of triUb (Figure 5.4A, lane 3-4 and 10-11). DiUb is only detected at later time points, while there is a steady increase in the intensity of monoUb from the start (Figure 5.4A, lane 3-7 and 10-14). This suggests that FAM63A cleaves Ub chains in a step-wise manner releasing one Ub at a time (exo-DUB). This exo-DUB activity is a property of the catalytic domain and cleavage is not influenced by the MIU.

To investigate whether this mode of cleavage is conserved in other members of MINDY DUBs, I monitored the product of pentaUb cleavage by YPL191C, which is the yeast ortholog of FAM63A. Interestingly, at the early time points YPL191C cleaves pentaUb and releases equal amount of mono-, di-, tri- and tetraUb (Figure 5.4A, lane 17-21 and Figure 5.4B). This suggests that YPL191C is an endo-DUB. These observations reveal that MINDY DUBs may have distinct modes of cleaving K48-linked polyUb chains.
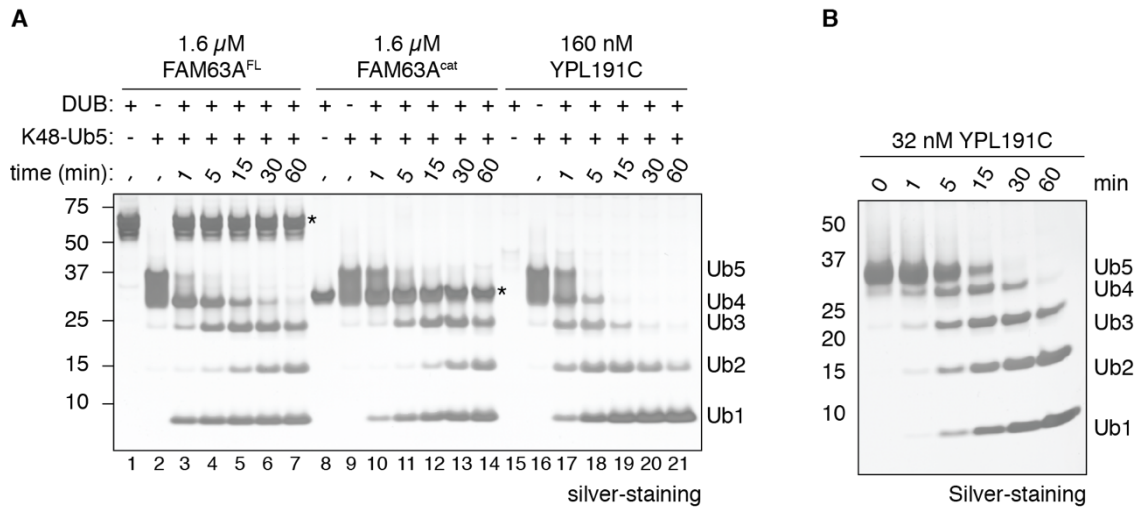
**Figure 5.4 FAM63A is an exo-DUB**

*(A) DUB assays were carried out containing 3.5 μM K48-pentaUb and 1.6 μM of FAM63A or 160 nM YPL191C at 30 °C for the indicated periods of time. FL, full-length; cat, catalytic domain. Asterisks indicate FAM63A, which catalytic domain has similar electrophoretic mobility as tetraUb. (B) As in (A), but 32 nM of YPL191C was used.*

## 5.2.2  Determining the efficiency of FAM63A DUB activity

To explore the efficiency of FAM63A in cleaving K48-polyUb chains, I set out to determine the kinetics of FAM63A and to compare its activity to OTUB1, a well-studied DUB, which is also highly selective at cleaving K48-linked chains (Wang *et al*, 2009). To do so, I developed fluorescently-labelled K48-linked diUb and triUb chains. These chains contain an infrared fluorogenic dye conjugated at the distal Ub (Chapter 2.6). Using in-gel DUB assays, the formation of cleaved chain products can be monitored quantitatively (Chapter 2.8.4). I found that FAM63A$^{cat}$ cleaves diUb poorly whereas YPL191C and OTUB1 efficiently cleave diUb substrates (Figure 5.5A-B). Similarly, FAM63A cleaves triUb weakly, suggesting that diUb and triUb are poor substrates for FAM63A (Figure 5.5C-D). Therefore, these short chains are not suitable to study the kinetics of FAM63A$^{cat}$.
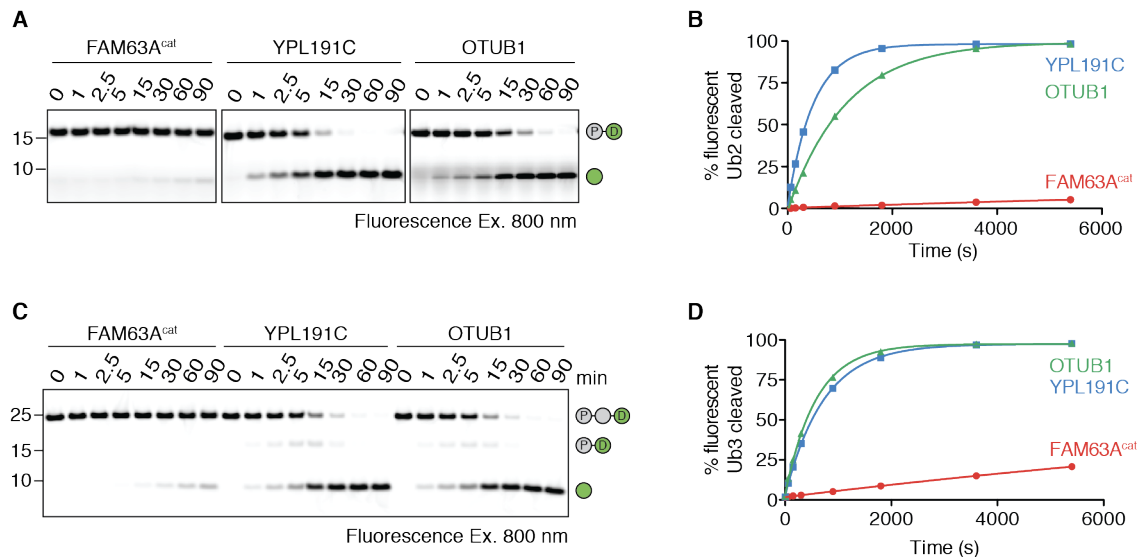
***Figure 5.5 Fluorescently-labelled K48-linked diUb and triUb are poor substrates for FAM63A^cat***

*(A) Kinetics of cleavage of fluorescently labelled K48-diUb by FAM63A^cat, YPL191C, and OTUB1. DUBs (1 μM) were incubated with 500 nM of K48-diUb that has been labelled with an infrared fluorescent dye at its distal Ub (green circle) for the indicated times. Fluorescent Ub was visualized using Odyssey LI-COR system at 800 nm channel. P, proximal Ub; D, distal Ub. **(B)** Quantification of K48-diUb hydrolysis in (B). Percentage of the formed monoUb intensity is shown on the y-axis (n = 3; means ± s.d.). **(C)** Kinetics of cleavage of fluorescently labelled K48-triUb by FAM63A^cat, YPL191C, and OTUB1 were carried out as in (A). **(D)** Quantification of K48-triUb hydrolysis in (C). The percentage of the total intensities of Ub4, Ub3, Ub2, and Ub1 formed is shown on the y-axis. (n = 3; means ± s.d.).*

Several DUBs have been reported to preferably cleave long polyUb chains (Békés *et al*, 2015; Winborn *et al*, 2008). Qualitative DUB assays suggest that FAM63A also hydrolyses longer polyUb chains more efficiently (Figure 5.3B). Therefore, I prepared K48-linked pentaUb that carries an infrared fluorescent label at the proximal Ub end. When pentaUb was used as the substrate, FAM63A^cat cleaves the chain as efficiently as YPL191C and OTUB1 (Figure 5.6A-B). Interestingly, although the rates of K48-pentaUb cleavage of FAM63A^cat, YPL191C and OTUB1 are comparable, the generated products vary. For YPL191C and OTUB1, the cleavage products range from monoUb to tetraUb at the early time point. This is consistent as these two DUBs are endo-DUB (Figure 5.4 and Figure 5.6). In contrast, the products of FAM63A^cat cleavage are exclusively tetraUb chains at the early time points. After pentaUb has been converted to tetraUb, the tetraUb

is then cleaved to produce triUb (Figure 5.6A,C). The fluorescent dye is at the proximal end of the chains. Thus, the tetraUb and triUb chains are the pentaUb chains that progressively loose one distal Ub, cleaved by FAM63A (Figure 5.6A). This suggests a marked directionality in chain cleavage in which FAM63A acts as a chain trimming enzyme and cleaves polyUb chains from the distal end.
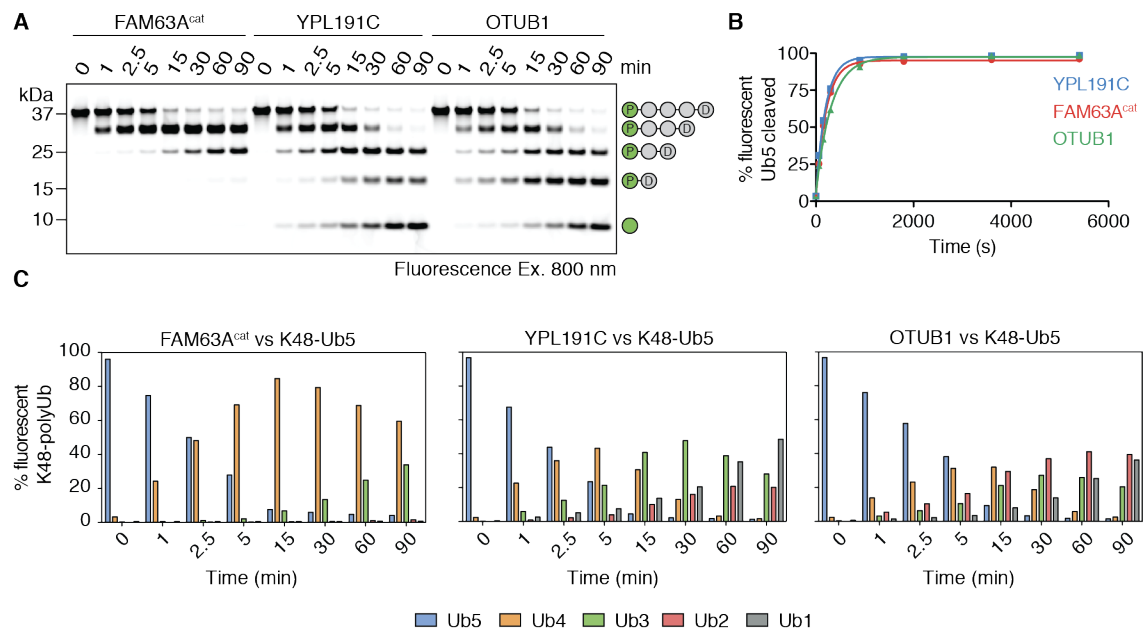


**Figure 5.6 FAM63A is a chain trimming enzymes preferably cleaving longer polyUb chains from distal end**

*(A) DUB assays monitoring time-dependent cleavage of fluorescently labelled pentaUb by FAM63A[cat], YPL191C, and OTUB1 as in (Figure 5.5A). The proximal Ub of the chain (indicated by green circle) was labelled with an infrared fluorescent dye. (B) Quantification of cleavage of K48-linked pentaUb by FAM63A[cat], YPL191C, and OTUB1 in (D). The percentage of the total intensities of Ub4, Ub3, Ub2, and Ub1 formed is shown on the y-axis. (n = 3; means ± s.d.). (C) Percentages of polyUb chains at each time points of DUB assays in (A) were shown as bar graphs.*

Enzymes kinetics are commonly presented quantitatively through $k_{cat}$, the number of substrate molecules converted per unit of time, and $K_m$, the substrate concentration at which the reaction rate is half of the maximum rate ($V_{max}$) (Cornish-Bowden, 2013). While it is challenging to determine the $k_{cat}$ and $K_m$ of FAM63A against K48-diUb and K48-triUb due to slow reaction rate, it is possible to do so using K48-pentaUb as a substrate. However, it has to be noted that the kinetics of FAM63A measured here is

limited to its activity in hydrolysing pentaUb to produce tetraUb chains. I determined the $k_{cat}$ and $K_m$ of FAM63A for hydrolysing K48-Ub5 to be ~5.71 x $10^{-3}$ $s^{-1}$ and ~872 nM. The low Km values suggest a strong interaction of FAM63A with pentaUb chains.
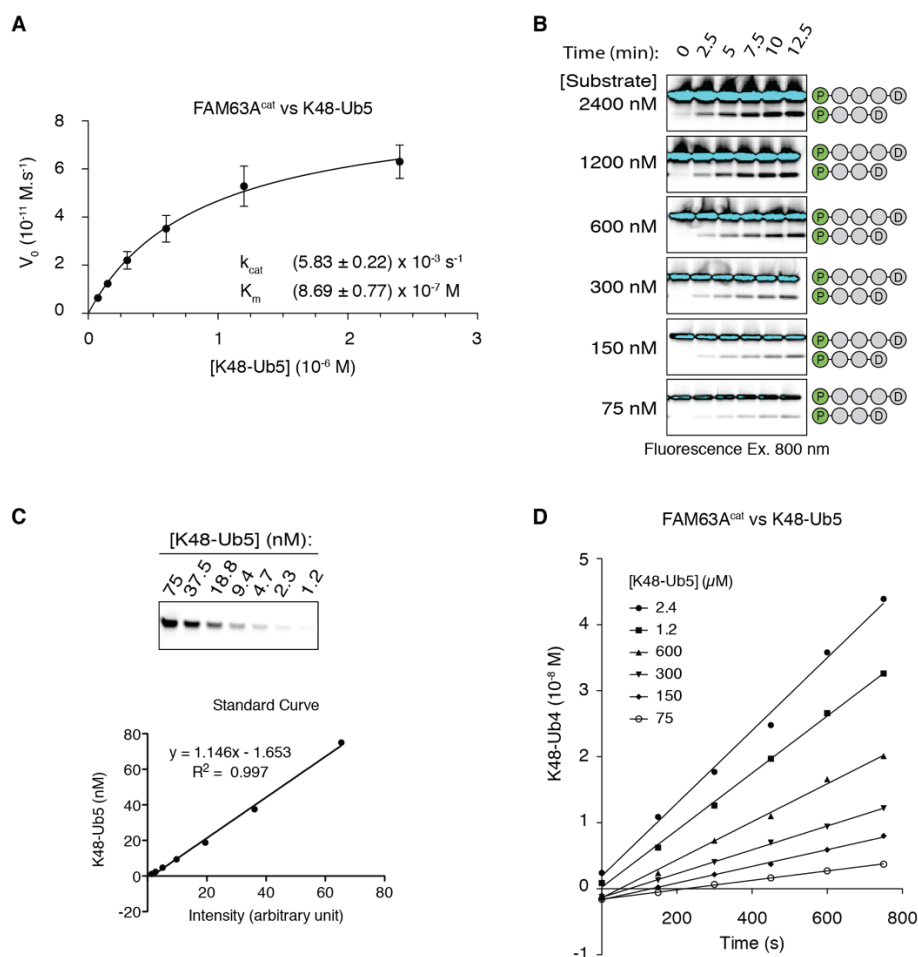


**Figure 5.7 Characterisation of FAM63A$^{cat}$ kinetics in hydrolysing K48-linked pentaUb chains**
*(A) Steady state kinetics of K48-linked pentaUb cleavage by FAM63A$^{cat}$. FAM63A$^{cat}$ (15 nM) was incubated with 0.075-2.4 μM fluorescently-labelled pentaUb. The K48-Ub4 formed at the early time point (less than 10% of the substrate) was quantified to obtain initial velocities (V$_0$). The V$_0$ was plotted against pentaUb concentration and the data was fitted to the Michaelis-Menten equation to derive k$_{cat}$ and K$_m$. (n = 3; means ± s.d.). (B) Steady state kinetics of FAM63A$^{cat}$ for K48-pentaUb. K48-pentaUb chains that have been labelled with an infrared fluorescent dye at the proximal Ub (green circle) at different concentrations were hydrolysed by 15 nM of FAM63Acat over the indicated times. (C) Since the fluorescence label is only on one Ub molecule (proximal), the intensity on K48-pentaUb will be the same number of molecules of K48-tetraUb, where distal Ub has been cleaved by FAM63A$^{cat}$. Therefore, the standard curve of K48-pentaUb can be used to convert the intensity of K48-tetraUb in (A) to a molar concentration. (D) The K48-tetraUb produced is plotted against time. Data was fitted to linear regression curve in which the slope is the initial velocity, V$_0$. Figure 5.7B-D are representative data from one of three replicates that were used to derive Michaelis-Menten kinetics in Figure 5.7A.*

The same kinetics of K48-pentaUb hydrolysis cannot be determined for YPL191C and OTUB1. The first cleavage event of pentaUb by YPL191C or OTUB1 may result in tetraUB, triUb or diUb (Figure 5.6A). These different chain products may all be substrates for the next round of cleavage. Therefore, measuring the kinetics of pentaUb hydrolysis by YPL191C and OTUB1 is challenging and complex process.

### 5.2.3 Tandem MIU is crucial for efficient hydrolysis of long K48-linked polyUb chains by FAM63A

One remarkable feature of FAM63A is its high specificity in cleaving K48-linked polyUb chains. This selectivity is contained within the catalytic domain of FAM63A and is independent of the C-terminal tMIU. The lingering question is what role the tMIU has for FAM63A DUB activity. UBDs in DUBs may provide additional binding sites that help to bind to polyUb chains and thus, enhance efficiency in cleaving chains. This is observed in UCH37/Iso-T and TRABID (Reyes-Turcu *et al*, 2008; Licchesi *et al*, 2011). To investigate whether tMIU affect catalytic efficiency of FAM63A, I compared the hydrolysis of fluorogenic K48 pentaUb (K48 pentaUb[proximal-IR800]) by full-length and catalytic domain of FAM63A. There was no difference in the kinetics of pentaUb hydrolysis by FAM63A whether tMIU is present or absent (Figure 5.8B). This suggest that tMIU does not affect FAM63A activity in cleaving K48-pentaUb chains.

Next, I wondered whether tandem MIU is required for FAM63A to cleave chains longer than pentaUb. To address this, I used polyUb chains that contain five or more Ub moieties as substrates. Interestingly, FAM63A lacking tMIU cleaves these long chains poorly compared to the full-length FAM63A (Figure 5.9). This suggests that the tMIU is required for FAM63A to efficiently cleave long K48-linked polyUb chains.
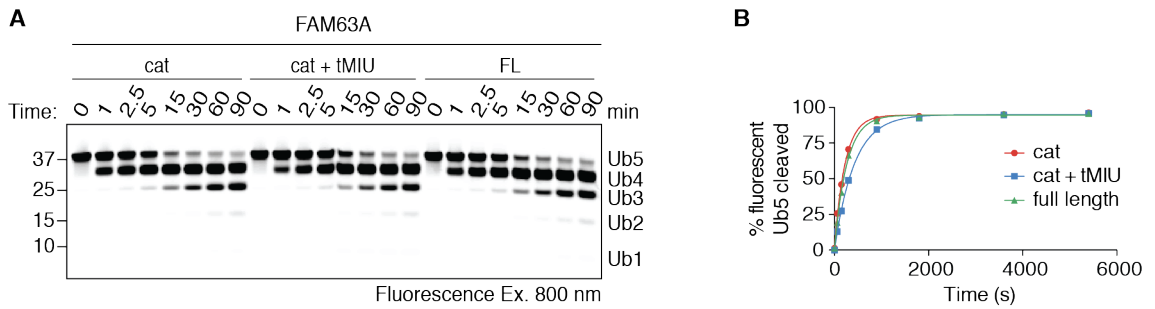
**Figure 5.8 tMIU is does not affect FAM63A activity in hydrolysing K48-pentaUb**
*(A) DUB assays monitoring time-dependent cleavage of fluorescently labelled pentaUb by FAM63A$^{cat}$, FAM63A$^{cat+tMIU}$, and FAM63A$^{FL}$ as in (Figure 5.6A). Cat, catalytic domain; FL, full length. **(B)** Quantification of cleavage of K48-linked pentaUb in (D). The percentage of the total intensities of Ub4, Ub3, Ub2, and Ub1 formed is shown on the y-axis.*
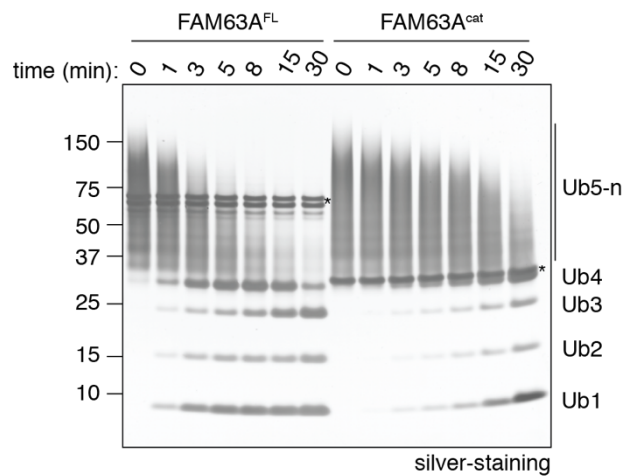


**Figure 5.9 FAM63A needs tMIU to efficiently cleave long K48-linked polyUb**
*DUB assays containing 1.6 μM FAM63A and polyUb chains containing at least five Ub moieties were carried out at 30 °C for the indicated times. FL, full-length; cat, catalytic domain.*

225

## 5.3 Discussion

### 5.3.1 How does FAM63A sense length of polyUb chains?

Our lab recently discovered the sixth family of DUBs which we named MINDY. The characterised members of MINDY DUBs all selectively cleave only K48 chains and not any other linkage type (Figure 5.1). In this study I characterised FAM63A DUB activity beyond its K48 selective hydrolysis. I found that FAM63A preferably cleaves longer polyUb from the distal end of the chain in a step-wise manner (Figure 5.6). This suggests a chain trimming activity. In contrast, YPL191C, the yeast homolog of FAM63B does not differentiate between chain length and acts as an endo-DUB. These distinct features of two different MINDY DUBs suggest a specialised role in cellular signalling, which is yet to be discovered.

In this study I found that FAM63A does not cleave Ub-Rho110-G (Figure 5.3A). Fluorogenic Ub substrates, such as Ub-Rho110-G and Ub-AMC, are commonly used to study enzyme kinetics of DUBs (Faesen *et al*, 2011; Sahtoe *et al*, 2015; Lee *et al*, 2010). The ability of a DUB to cleave a fluorogenic Ub substrate depends on the DUB S1 site that binds Ub and positions the Ub C-terminal tail at the catalytic centre for hydrolysis of the isopeptide bond. FAM63A S1 active site may have a weak binding affinity for Ub, which explains why FAM63A does not cleave fluorogenic Ub substrate. Alternatively, there may be additional binding sites on FAM63A catalytic domain that increase binding affinity to polyUb chains. This is analogous to linkage selective UBDs, like TRABID NZF1 or FAM63A MIU2 (Chapter 3.2.11 and Chapter 4.2.5). I observed that FAM63A is an exo-DUB that cleaves polyUb chains from distal end. Therefore, I predict the additional Ub binding sites on the catalytic domain of FAM63A should be present at the proximal of the S1' binding pocket (Chapter 1.6.2).

The requirement for Ub moieties to occupy both S1 and S1' sites on DUB for polyUb chain cleavage has been observed in several DUBs. In OTULIN, proximal Ub binding to S1' induce conformational change on the catalytic triad, which activates the DUB to cleave M1-linked polyUb chains via substrate-assisted catalysis. Structural analysis of FAM63A catalytic domain reveals that the catalytic triad is in an unproductive state (Abdul Rehman *et al*, 2016). Binding to Ub on S1 site may not be sufficient to relieve this inhibition. Therefore, like OTULIN, FAM63A may need to bind proximal Ub on S1' site to induce a productive catalytic triad through conformational change.

If Ub binding to S1 and S1' is sufficient to induce a productive catalytic site, FAM63A should efficiently cleave diUb. However, diUb is a poor substrate for FAM63A. I have demonstrated that FAM63A preferably cleaves longer polyUb chains, which suggests that FAM63A may have additional binding sites for Ub other than S1 and S1' pockets. This has been observed in DUBs that cleave long polyUb chains, including SARS PLpro, OTUD2 and Ataxin-3 (Békés *et al*, 2015; 2016; Mevissen *et al*, 2013; Winborn *et al*, 2008). As discussed above, the additional binding sites on FAM63A should be on the proximal side of the S1' binding pocket. Therefore, there is a high possibility for FAM63A to have S2', S3' and even S4' sites that provide high binding avidity to polyUb chains (Figure 5.10).

This hypothesis is supported by FAM63A that acts as a chain trimming enzyme. I observed that FAM63A initially processes pentaUb to produce tetraUb chains. Remarkably, tetraUb chains are not processed immediately to triUb. Only when pentaUb level has been depleted, FAM63A begins to process tetraUb. This suggest that the catalytic domain of FAM63A may bind pentaUb better than tetraUb and bind to tetraUb better than triUb. This may explain the chain processivity mechanism of FAM63A. To test this hypothesis, the binding affinity of FAM63A catalytic domain to pentaUb, tetraUb, triUb and diUb needs to be determined. In summary, I proposed that FAM63A

may have additional binding sites that accommodate more efficient binding to longer

polyUb chains (Figure 5.10).
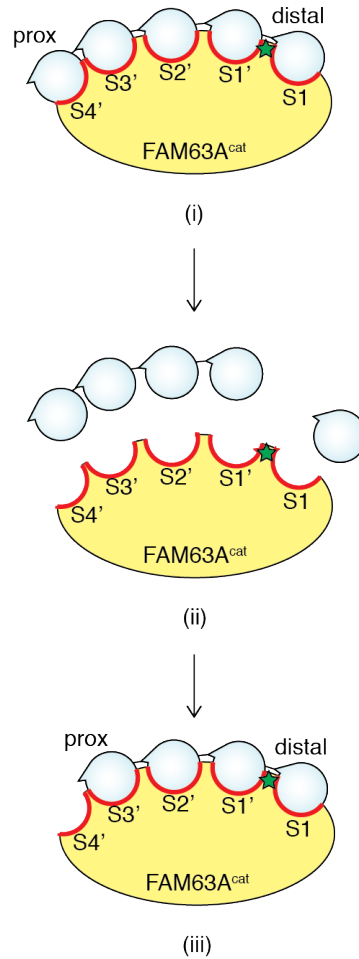


**Figure 5.10 Model of how FAM63A acts as chain-trimming enzyme that preferably cleaves longer polyUb from distal end**

In this model, the catalytic domain of FAM63A (FAM63A$^{cat}$) is depicted with five Ub-binding sites. Green star illustrates the active site located between S1 and S1' sites that allow exclusive cleavage from distal end. FAM63A$^{cat}$ may have higher affinity to bind to K48-pentaUb than to tetraUb (i). This ensure that tetraUb is cleaved once pentaUb has been depleted (ii) and (iii).

### 5.3.2 Methods to determine affinities of FAM63A for binding to K48 chains of various lengths

To test the model proposed above, I need to determine binding affinities of FAM63A to K48-diUb, triUb, tetraUb and pentaUb. One most widely used technique to determine affinity of DUB binding to polyUb chains is by using isothermal titration calorimetry (ITC). The binding affinity can be determined by titrating polyUb chains into the catalytic dead mutant of DUB. Using this approach Keith Wilkinson and colleagues observed that IsoT/USP5 contains four Ub-binding sites, formed by its four UBDs (Reyes-Turcu *et al*, 2008). The limitation of this approach is that it is laborious, time consuming and large quantities of pure materials are required. This is more challenging when longer polyUb chains are to be used for titration experiment.

Alternatively, the preference of FAM63A to bind to longer polyUb chains can be addressed through comparing $k_{cat}$ and $K_m$ of FAM63A kinetics in cleaving different lengths of polyUb chains. I observed that FAM63A poorly cleaves fluorogenic K48-triUb chain (Figure 5.5C). However, FAM63A may cleave K48-tetraUb chains more efficiently and thus, can be used to determine $k_{cat}$ and $K_m$ of FAM63A in cleaving tetraUb. I have determined the $k_{cat}$ and $K_m$ of FAM63A kinetics in cleaving pentaUb hydrolysis to be ~5.71 x $10^{-3}$ $s^{-1}$ and ~872 nM, respectively. If the chain trimming activity of FAM63A is based on its higher affinity for longer chains, the kinetics of FAM63A to cleave polyUb of different lengths should vary only on the $K_m$ while the $k_{cat}$ remains constant.

Another approach to investigate FAM63A binding affinity for different length of polyUb chains is to measure the inhibitory effect or inhibition constant ($K_i$) of polyUb chains towards FAM63A activity in cleaving K48-pentaUb chains. In this study, I used fluorogenic pentaUb substrate to monitor the cleavage efficiency of FAM63A. To determine the $K_i$ of different lengths of K48 chains, I can titrate increasing amounts of unlabelled K48-polyUb chains to the reaction of FAM63A and the fluorogenic pentaUb

chains. These $K_i$ values will reflect the binding affinity of polyUb chains to FAM63A. Such inhibition DUB assays have been used to characterised binding affinity of BRCC36 for monoUb and diUb of K48 and K63 chains (Cooper *et al*, 2010). From such assays it was found that S1 binding site has sufficient affinity to bind monoUb and therefore, monoUb and diUb of K48 and K63 types can bind to BRCC36. The specificity of BRCC36 comes from the positioning of the K63 isopeptide scissile bond on the active site. In early 2000, Pickart and colleagues proposed that the minimal length of polyUb to be recognised by the 26S proteasome is tetraUb (Thrower *et al*, 2000). In this study, they measured the $K_i$ of various lengths of K48 chains and discovered that tetraUb and longer chains do not result in significant decrease in $K_i$. Therefore, it was proposed that tetraUb chains are the minimal recognition length of proteasome. In summary, using inhibition DUB assays to monitor inhibition constants, we can estimate FAM63A binding affinity to K48-chains of different lengths.

### 5.3.3    Designing tools to study exo-DUB activity

In this study I observed that human FAM63A and yeast YPL191C have two different mechanisms in cleaving polyUb chains despite their identical preference to cleave K48 chain type (Figure 5.1). Time course DUB assays monitoring cleaved polyUb products are commonly used to investigate whether a DUB is an exo- or an endo-DUB (Figure 5.4) (Hospenthal *et al*, 2013; Hu *et al*, 2005). An exo-DUB cleaves polyUb chains in a step-wise manner from either end of the chain, releasing monoUb and various amount of shorter chains. On the contrary, an endo-DUB cleaves within chains and releases equal amounts of all possible cleavage products. Based on these assays, I concluded that FAM63A is an exo-DUB whereas YPL191C is an endo-DUB. These are confirmed in quantitative DUB assays using fluorogenic pentaUb substrates (Figure 5.6).

A more careful examination on YPL191C activity in cleaving fluorogenic pentaUb chains may provide an alternative explanation of its DUB mechanism. In YPL191C DUB

assays, there was a delay in the production of diUb in comparison to monoUb and triUb, which resembles the pattern of pentaUb cleavage by the exo-DUB FAM63A (Figure 5.6 vs Figure 5.4). This pattern was not observed in OTUB1 cleavage products of flurogenic pentaUb. A step-wise cleavage or chain-trimming activity of exo-DUB is observed only when the DUB progressively cleaves longer polyUb, followed by shorter chains at later time points. However, a chain-trimming DUB may also have equal efficiency to cleave all lengths of polyUb chains. In the first cycle of catalysis, this type of exo-DUB cleaves pentaUb to tetraUb and monoUb. In the next cycle of catalysis, this exo-DUB is equally efficient at cleaving pentaUb and tetraUb. Consequently, we can already observe triUb and possibly diUb produced at early time points of DUB assays. Therefore, this kind of exo-DUB may not be easily characterised solely from the product of polyUb hydrolysis over periods of time. This highlights the necessity for tools to dissect the activity of DUB at the first cycle of catalysis.

Activity-based probes (ABPs) have been widely used to study catalytic activity of DUBs (Gopinath *et al*, 2016). These probes are based on Ub substrates that contain reactive moiety near the scissile bond, which can react with the catalytic Cys of DUB and form a covalent adduct. Consequently, once this occurs, the ABP-modified DUB is inactive. At present, there are three types or three generations of Ub-based ABPs available. These probes have the reactive moiety at the C-terminus of monoUb (1st gen), in between two Ub moieties (2nd gen) or at the C-terminus of diUb (3rd gen) (Figure 5.11A) (Flierman *et al*, 2016). These probes target DUBs depending on the binding surfaces present on the catalytic domain of the DUBs (Figure 5.11A). However, there is no ABPs available to specifically study exo-DUB. Therefore, I proposed here designs of ABPs to study exo-DUB activity.

I call these ABPs to study exo-DUB as the fourth generation probes (4th gen-ABPs). These probes are based on polyUb chains containing three or more Ub moieties. The

active site reactive moiety is placed in between the S1 and S1' Ub (Figure 5.11B). Exo-DUBs that cleaves polyUb chains from the distal end will immediately be covalently conjugated with the 4th gen-ABPs, which can be monitored from the shift in their electrophoretic mobility (Figure 5.11C). Because the 4th gen-ABPs use native isopeptide bonds, endo-DUBs can still cleave within chains and produce multiple products of shorter Ub chains. When these DUBs cleave the distal end will be covalently conjugated to the various length of polyUb cleavage products, forming multiple bands of covalently conjugated DUB+polyUb bands (Figure 5.11D).

As described above, classification of a DUB as an exopeptidase or endopeptidase can be challenging. For example, USP14 has been proposed as proteasomal-associated DUB that cleaves polyUb chains from distal end (Hu *et al*, 2005). However, a recent study found that USP14 acts as an endo-DUB, cleaving polyUb chains *en bloc* from the modified substrates (Lee *et al*, 2016). Therefore, the 4th gen-ABPs that I proposed can be used to reconcile this dispute over DUB catalytic mechanism of USP14. In addition to this, I can use the 4th gen-ABPs to screen various DUBs to identify exo-DUB activity that may have not been identified or missed.

The application of these 4th gen-ABPs is wider than to be used to characterise endo- and exo-cleaving activity of DUBs. PentaUb, tetraUb and triUb of the 4th gen-ABPs can be used as substrates in steady-state kinetic assays to determine $k_{cat}$ and $K_m$ of a DUB in cleaving particular chain lengths. Therefore, using these tools I can also address whether FAM63A has a lower $K_m$ or higher affinity for longer polyUb chain substrates. In addition to this, DUBs that have been covalently bound to the 4th gen-APBs can be purified and crystallised. This will stabilise polyUb chains in post cleavage conformation, capturing polyUb at the S1-S1'-S2'-etc. Collectively, these 4th gen ABPs may provide valuable tools to study chain trimming activity of DUBs. Therefore, I would like to invest time to generate these probes.
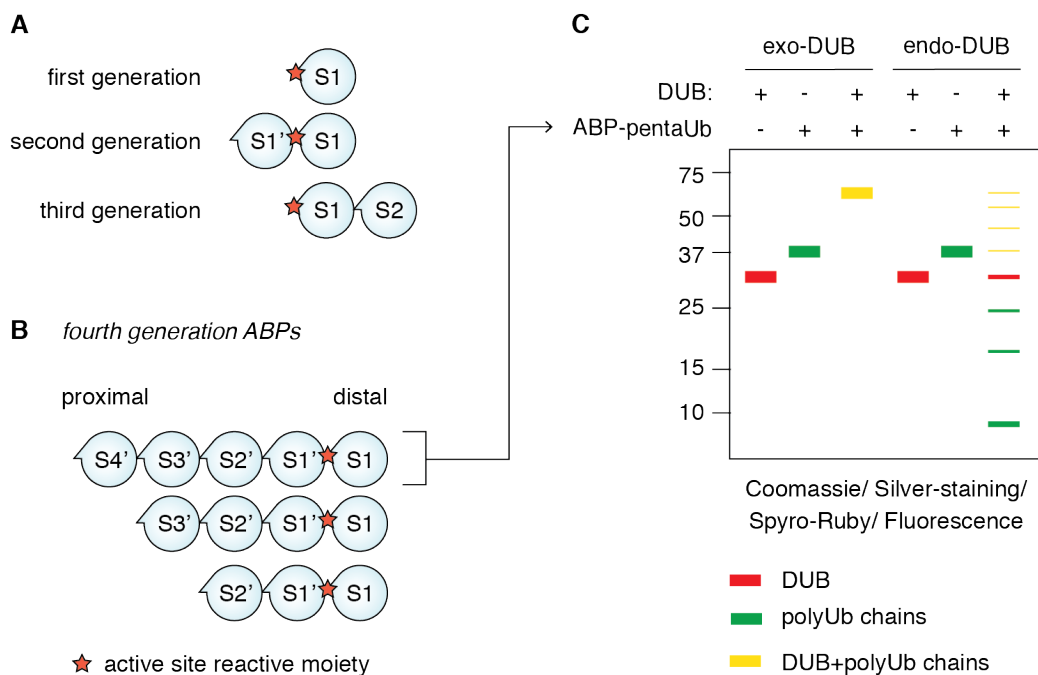
**Figure 5.11 Designing the fourth generation of activity based probes to study exo-DUB activity**

*(A) Three generations of activity-based probes (ABPs) that have been used to study different mechanisms of action of DUBs (Flierman* et al, *2016). (B) Design of the fourth generation of ABPs. These ABPs are based on polyUb chains composed of three or more Ub moieties. Active site reactive moiety is placed in between of S1 and S1' Ub. (C) Hypothetical scenario of reaction between pentaUb-ABP and exo-DUB (first three) or endo-DUB (last three).*

### 5.3.4    How does FAM63A sense distal/proximal end of Ub chains

Another puzzling question is how FAM63A senses the polarity of polyUb chains and cleaves only from distal end of Ub chains (Figure 5.6). IsoT/USP5 is an exo-DUB that cleaves polyUb from the proximal end of the chain through a mechanism that is well established (Wilkinson *et al*, 1995; Reyes-Turcu *et al*, 2006). A UBD called ZnF_UBP forms the S1' site on the catalytic domain of IsoT. ZnF_UBP recognises the C-terminal end of the proximal Ub and therefore, ensure that the cleavage occurs at the proximal end of the chain (Reyes-Turcu *et al*, 2006). Analogous to this, it is possible that FAM63A senses the distal end of Ub chains when the Ub binds to the S1 site. FAM63A S1 site may interact with residues surrounding K48, which are available only on distal end Ub moiety.

This mechanism of distal Ub sensing has been observed in USP21 that cleaves K6 chains from distal end (Hospenthal *et al*, 2013). USP21 S1 site interact with K6 and its surrounding residues on distal Ub (Ye *et al*, 2011). Similar mechanism is also observed in USP14 which cleaves K48 chains from distal end (Hu *et al*, 2005). Whether this mode of sensing is used in FAM63A can be addressed by determining the crystal structure of FAM63A in complex with K48-linked polyUb chains.

### 5.3.5   What are the potential roles of tMIU for FAM63A?

FAM63A (MINDY-1) and FAM63B (MINDY-2) are the first two members of MINDY DUBs to be identified, which selectively cleave K48 chain type (Abdul Rehman *et al*, 2016). These two proteins contain C-terminal tandem MIU motifs (tMIU) that bind to polyUb chains. The tMIU of FAM63A is not required for K48 linkage selective hydrolysis by the catalytic domain (Figure 5.2). In this Chapter, I demonstrated that FAM63A needs its C-terminal tMIU to cleave long polyUb chains (Figure 5.9). Similarly, NZF domains of TRABID is essential for the DUB to cleave long polyUb chains (Licchesi *et al*, 2011). In addition to this, the UBDs recruit TRABID to cellular puncta rich with K29 and K33 polyUb chains, which are the preferred substrate of TRABID. The chain trimming activity of FAM63A suggests that its substrate may be polyUb chains, which can be unanchored or conjugated to protein substrates. Therefore, the C-terminal tMIU may facilitate FAM63A binding to polyUb substrates.

How long polyUb chains have to be to elicit Ub response remains a lingering question in the field. However, varying lengths of polyUb chains have been observed to have various effects on DUB activity. For example, Ubp15 (USP7 in human) efficiently cleaves fluorogenic monoUb substrate and K48-diUb (Schaefer & Morgan, 2011). However, it poorly cleaves longer polyUb chains and this is alleviated when I44 of Ub was mutated to Ala or when Lys48-polyUb was fused to K63-chains. It was proposed that structure of long polyUb chains affect DUB activity. In this chapter I found that the catalytic domain

of FAM63A is inefficient to cleave long K48-linked polyUb in the absence of tMIU (Figure 5.9). Only in the presence of tMIU, FAM63A can cleaves long K48 chains more efficiently. In Chapter 4, I observed that FAM63A tMIU binds to K48-linked polyUb chains in open conformations (Figure 4.8 and Figure 4.13). Therefore, I hypothesise that tMIU may help FAM63A to bind long K48 polyUb chains and facilitate DUB to bind to its substrate (Figure 5.12).
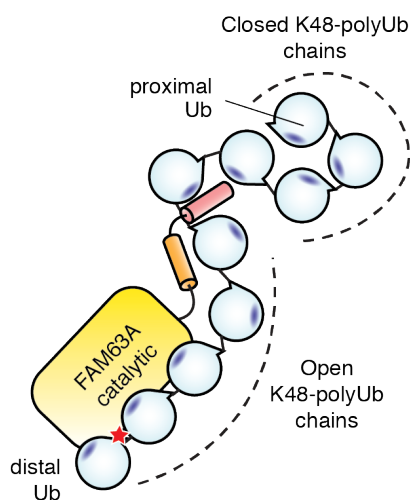


**Figure 5.12 Model: tMIU may help FAM63A to bind to long polyUb chains**

*A model of how tMIU contributes in FAM63A DUB activity to efficiently cleave long K48-linked polyUb chains. tMIU may help FAM63A to bind to the regions where long K48 chains are in open conformations. Ub moieties are in sky-blue spheres; FAM63A catalytic domain is in yellow square; tMIU is in orange-pink tubes. The hydrophobic I44 patches are coloured in blue and illustrate the open and closed conformations of the polyUb chains.*

Many proteins that contain UBDs are ubiquitylated and this process requires intact UBDs (Hicke *et al*, 2005). This is also observed in Rabex-5 that contains MIU (Penengo *et al*, 2006). It is tempting to speculate that the tMIU induces ubiquitylation of FAM63A, and ubiquitylation may modulate FAM63A catalytic activity or its stability.

### 5.3.6 What are the consequences of chain-trimming activity of FAM63A for its biological functions?

The work described in this chapter focused in the characterisation of FAM63A catalytic mechanism in cleaving K48-linked polyUb chains. This reveals that FAM63A is a chain-trimming enzyme that preferably cleaves longer K48-linked polyUb chains. Cellular roles of K48 chains have been widely linked to proteasomal degradation. Therefore, the high selectivity toward K48 chains suggests protein homeostasis-related roles of FAM63A. It is tempting to speculate that FAM63A may regulate ubiquitylation status of proteasomal substrates.

There are three DUBs associated with proteasome, RPN11/POH1, UCH37 and USP14, which use two different mechanisms of polyUb cleavage on proteasomal substrates (Lee *et al*, 2011). RPN11/POH1 acts as an endo-DUB that cleaves polyUb chains *en bloc* from substrates that have been committed for degradation by the core proteasome (Yao & Cohen, 2002). This accelerates protein substrate degradation. On the contrary, UCH37 and USP14 antagonise protein degradation by trimming polyUb chains from distal end (Lam *et al*, 1997; Hu *et al*, 2005; Lee *et al*, 2010). Long polyUb chains on proteins are thought to increase their retention time at the proteasome. Trimming chains would therefore, reduce the substrates affinity for proteasome and consequently, rescue substrate from degradation. This mechanism is crucial to liberate proteasome from difficult to degrade substrates that stall proteasome. Alternatively, chain trimming activity of proteasomal DUBs is crucial to cleave unanchored polyUb chains released by RPN11/POH1 and thus, recycle Ub for further use. Similarly, FAM63A chain trimming

activity may regulate the fate of proteins marked for degradation. This hypothesis remains to be studied thoroughly in the future.

Our understanding of FAM63A biology is still at infancy and there are many questions need to be addressed: What are its substrates? Where does it localise? How is it regulated? Cancer genomic database cBioPortal (http://www.cbioportal.org/) reveals that FAM63A is highly amplified in many cancers, in particularly breast cancer. FAM63A is also highly expressed in the brain, suggesting its role in Ub signalling in neurons (Soo-Youn Choi, unpublished data). In cells, FAM63A may be tethered onto specific organelles or subcellular membranes, due to farnesylation on its CaaX motif (Liu *et al*, 2009; Akhavantabasi *et al*, 2010). This may regulate the localisation of FAM63A and the nature of its signalling. Collectively, FAM63A may function in wide array of signalling which remains to be addressed in the future.

### 5.3.7 FAM63A chain trimming activity as tools to study heterotypic polyUb containing K48 chains

Linkage-specific DUBs are widely used to decipher complex topology of heterotypic polyUb chains on proteins (Hospenthal *et al*, 2015). This method, also known as UbiCRest (ubiquitin chain restriction), involves treating isolated proteins with a panel of linkage-selective DUBs. The content of polyUb chains can be interpreted from the cleavage products. To date, only OTUB1 is commonly used to cleave K48 chains. Members of the recently discovered MINDY DUB family are selective to cleave K48 chains, which therefore can be used as alternative DUBs to investigate K48 chain in UbiCRest experiments (Abdul Rehman *et al*, 2016).

The chain trimming activity of FAM63A provides a powerful approach to investigate the topology of K48 chains within heterotypic polyUb. The conventional way to detect K48 chains is by treating polyUb materials with OTUB1. Although, cleavage by OTUB1 can confirm the presence of K48 chains, their topology is hard to interpret.

Hence, the unique chain trimming activity of FAM63A can be very useful. When FAM63A is used to treat heterotypic chains containing K48 linkages, FAM63A will only cleave K48 chains that are located at the distal end of heterotypic chains. Therefore, any residual K48 signal left after FAM63A treatment may be interpreted as K48 chains that are capped or sandwiched by other types of polyUb chains. For example, this approach can be used to study the topology of APC/C substrates, such as CyclinB, that are modified by branched K48/K11 chains (Meyer & Rape, 2014; Grice *et al*, 2015). In addition to this, FAM63A can be used to investigate the topology of heterotypic chains containing K29 and K48 chains observed in Chapter 4 of this thesis. In summary, the exo-DUB FAM63A can be used along with OTUB1 or other K48-specific endo-DUB to decipher the topology of K48 chains within heterotypic polyUb.

# 6 Future perspective

In the past, only limited types of polyUb chain could be used to investigate linkage-selective polyUb binding by UBDs or hydrolysis by DUBs. Consequently, conclusions drawn may be incomplete. In this study, I developed methods to assemble K29 and K33 chains enzymatically, from which milligrams of polyUb chains of defined lengths can be obtained. With these, I have assembled a complete arsenal of tetraUb chains of seven different linkage types. This wide array of tetraUb formed the basis for characterizing UBDs that led to the discoveries of TRABID NZF1 as a K29 and K33-selective UBD (Chapter 3) and FAM63A tMIU as a K48-selective UBD (Chapter 4). In addition, these tetraUb chains were instrumental in the detailed biochemical characterisation of FAM63A, the founding member of a novel DUB family, that selectively cleaves long K48-linked ubiquitin chains (Chapter 5). Collectively, these results highlight the necessity of having all types of polyUb chains for analyses of linkage selectivity in UBDs and DUBs.

In my mass spectrometry-based approach to screen linkage types assembled by HECT ligases, the only setback was a failure to identify a ligase that assembles K27 chains. One promising approach is through enzymatic assembly, which can employ one of the several RING E3 enzymes recently reported to conjugate K27 *in vitro*. RNF168 was observed to modify histone H2A/H2A.X with K27-linked polyUb chains upon DNA damage and this activity of RNF168 was also observed *in vitro* (Gatti *et al*, 2015). In addition, a recent study demonstrated that the recombinant RING E3 LRSAM1 (leucine-rich repeat and sterile alpha motif containing 1) assembles K6, K27, K29 and K48 chains *in vitro* (Guo *et al*, 2017). Thus, I proposed to harness the potential of these E3 ligases in combination with linkage selective DUBs to produce pure K27 chains.

Linkage-selective UBDs have huge potential to be exploited as affinity purification reagents or molecular sensors to study Ub signalling in cells (Scott *et al*, 2014). In this

study, I demonstrated that TRABID NZF1 can be used to isolate K29 chains from cells. I discovered that K29 may be present in heterotypic chains containing other linkage type, such as K48 (Chapter 3). Due to time constraints, I have not had the opportunity to explore the full potential of the linkage-selective UBDs that I have characterised in this study, which also includes the K48-selective FAM63A tMIU (Chapter 4). I strongly believe that applying these linkage-specific UBDs will reveal cellular signalling pathways that use K29, K33 and K48 chains (also see Chapter 3.3.7 and 4.3.4).

Although linkage-selective UBDs can be assayed in a controlled environment in vitro, their behaviour when they are used to isolate polyUb chains from cells are harder to monitor. One solution for such a challenge is to spike in *in vitro*-assembled polyUb chains into the cell lysates, which will serve as an internal control for the linkage selectivity of UBDs during polyUb enrichment from cell lysates. If these control polyUb chains are labelled with heavy isotope, they can be differentiated from the native polyUb chains enriched by UBDs when analysed through mass-spectrometry (Kaiser *et al*, 2011). If for example a UBD enriches K48-linked polyUb chain from the cell lysate, but does not bind to the spiked in K48 chains, it can be inferred with confidence that the K48 chains captured from cells by the UBD are heterotypic chains or Ub chains present within protein complexes. I have assembled $^{15}$N-labelled tetraUb of seven different linkage types (data not presented in this thesis) that I plan to use to establish this method.

Another interesting question raised in this study is "What is the most optimal approach to screen for novel linkage-selective UBDs?" In Chapter 3, I tried to screen several isolated UBDs from various proteins to find uncharacterised linkage-selective NZF domains. These NZFs were selected through bioinformatics searches against consensus motif of NZFs. To test their linkage-selective binding, the isolated NZFs were screened against the purified tetraUb chains and the captured tetraUb chains were analysed on silver-stained SDS PAGE gels. I found that this approach to screen for novel

linkage-selective UBDs is laborious, time consuming and not effective. First, although UBDs can be identified through sequence motif conservation, their linkage-selective binding property may not easily be predicted. Second, isolating the minimal UBDs may lead to loss of some additional elements situated outside the domain that regulates binding properties of the UBDs. For example, HOIL-1L NZF requires an additional helix at the C terminus of the NZF domain to bind to M1 chains with higher affinity (Sato *et al*, 2011). Isolating the NZF domain alone leads to the loss of binding affinity to M1 chains by ~10-fold. Hence, this is an important caveat to consider when studying specificity of UBDs. An unbiased approach would be to immobilize chains of different linkage types on a resin and use this to capture full length UBD-containing proteins from cells.

To study ubiquitin signalling, it would be beneficial to have high affinity linkage-specific UBDs. The structural and mechanistic insights gained from this study could be exploited to design UBDs with desired binding properties. However, this approach will involve generating and testing several point mutants. An alternative approach would be to use phage display methods. I believe that the single MIU of FAM63A that harbours three distinct ubiquitin binding sites may be a good template to start with as it is a simple scaffold that in contrast to domains should express well on the cell surface.

Lastly, my results clearly point to K29 chains existing in heterotypic chains. Accumulating evidence points to wider roles for mixed and branched chains than envisaged before. This not only increases the complexity of the Ub system but also makes it a more information rich system with added layers of specificity. It also raises the question of how prevalent heterotypic chains really are and whether homotypic chains are even used in a cellular setting. While homotypic chains are a more simplistic model, whenever we see western blots depicting smears of K48 or K63 chains, we must question what other linkages lie within. Studying heterotypic chains isn't trivial and requires novel approaches and some of the methods outlined in this thesis will be useful. Further, it also

raises the question of whether specialized UBDs exist that can selectively recognize particular branched or mixed chain topologies. An attractive model is that heterotypic chains may provide a better platform to nucleate different signalling complexes with UBDs that recognize the different linkage types within the heterotypic chain. This has been exemplified in the NF-κB signalling pathway with K63 and M1 linkage containing heterotypic chains. Exploring heterotypic chains – how they are assembled by the combined actions of different E3 ligases, ubiquitin chain editing complexes, what the topology of the heterotypic chains assembled in cells is and how these heterotypic chains are produced and decoded in decoded in different cellular settings - are some questions to be addressed in the future. Answering these questions will not be trivial but will reveal how the same protein Ub can regulate so many diverse cellular processes.

# 7 References

Abdul Rehman SA, Kristariyanto YA, Choi SY, Nkosi PJ, Weidlich S, Labib K, Hofmann K & Kulathu Y (2016) MINDY-1 Is a Member of an Evolutionarily Conserved and Structurally Distinct New Family of Deubiquitinating Enzymes. *Mol Cell* **63:** 146–155

Adams PD, Grosse-Kunstleve RW, Hung LW, Ioerger TR, McCoy AJ, Moriarty NW, Read RJ, Sacchettini JC, Sauter NK & Terwilliger TC (2002) PHENIX: building new software for automated crystallographic structure determination. *Acta Crystallogr D Biol Crystallogr* **58:** 1948–1954

Akhavantabasi S, Akman HB, Sapmaz A, Keller J, Petty EM & Erson AE (2010) USP32 is an active, membrane-bound ubiquitin protease overexpressed in breast cancers. *Mamm Genome* **21:** 388–397

Akutsu M, Ye Y, Virdee S, Chin JW & Komander D (2011) Molecular basis for ubiquitin and ISG15 cross-reactivity in viral ovarian tumor domains. *Proc. Natl. Acad. Sci.* **108:** 2228–2233

Al-Hakim A, Escribano-Diaz C, Landry M-C, O'Donnell L, Panier S, Szilard RK & Durocher D (2010) The ubiquitous role of ubiquitin in the DNA damage response. *DNA Repair* **9:** 1229–1240

Al-Hakim AK, Zagorska A, Chapman L, Deak M, Peggie M & Alessi DR (2008) Control of AMPK-related kinases by USP9X and atypical Lys29/Lys33-linked polyubiquitin chains. *Biochem. J.* **411:** 249

Alam SL, Langelier C, Whitby FG, Koirala S, Robinson H, Hill CP & Sundquist WI (2006) Structural basis for ubiquitin recognition by the human ESCRT-II EAP45 GLUE domain. *Nat Struct Mol Biol* **13:** 1029–1030

Alam SL, Sun J, Payne M, Welch BD, Blake BK, Davis DR, Meyer HH, Emr SD & Sundquist WI (2004) Ubiquitin interactions of NZF zinc fingers. *EMBO J* **23:** 1411–1421

Alfano C, Faggiano S & Pastore A (2016) The Ball and Chain of Polyubiquitin Structures. *Trends Biochem. Sci.* **41:** 371–385

Alpi AF, Pace PE, Babu MM & Patel KJ (2008) Mechanistic insight into site-restricted monoubiquitination of FANCD2 by Ube2t, FANCL, and FANCI. *Mol Cell* **32:** 767–777

Asao H, Sasaki Y, Arita T, Tanaka N, Endo K, Kasai H, Takeshita T, Endo Y, Fujita T & Sugamura K (1997) Hrs is associated with STAM, a signal-transducing adaptor molecule. Its suppressive effect on cytokine-induced cell growth. *J. Biol. Chem.* **272:** 32785–32791

Baboshina OV & Haas AL (1996) Novel multiubiquitin chain linkages catalyzed by the conjugating enzymes E2EPF and RAD6 are recognized by 26 S proteasome subunit 5. *J. Biol. Chem.* **271:** 2823–2831

Bache KG, Raiborg C, Mehlum A & Stenmark H (2003) STAM and Hrs are subunits of a multivalent ubiquitin-binding complex on early endosomes. *J. Biol. Chem.* **278:** 12513–12521

Bellare P, Kutach AK, Rines AK, Guthrie C & Sontheimer EJ (2006) Ubiquitin binding by a variant Jab1/MPN domain in the essential pre-mRNA splicing factor Prp8p. *RNA* **12:** 292–302

Ben-Saadon R, Zaaroor D, Ziv T & Ciechanover A (2006) The polycomb protein Ring1B generates self atypical mixed ubiquitin chains required for its in vitro histone H2A ligase activity. *Mol Cell* **24:** 701–711

Bennett EJ, Shaler TA, Woodman B, Ryu K-Y, Zaitseva TS, Becker CH, Bates GP, Schulman H & Kopito RR (2007) Global changes to the ubiquitin system in Huntington's disease. *Nature* **448:** 704–708

Berndsen CE & Wolberger C (2014) New insights into ubiquitin E3 ligase mechanism. *Nat Struct Mol Biol* **21:** 301–307

Bertolaet BL, Clarke DJ, Wolff M, Watson MH, Henze M, Divita G & Reed SI (2001) UBA domains of DNA damage-inducible proteins interact with ubiquitin. *Nat. Struct. Biol.* **8:** 417–422

Bett JS, Ritorto MS, Ewan R, Jaffray EG, Virdee S, Chin JW, Knebel A, Kurz T, Trost M, Tatham MH & Hay RT (2015) Ubiquitin C-terminal hydrolases cleave isopeptide- and peptide-linked ubiquitin from structured proteins but do not edit ubiquitin homopolymers. *Biochem. J.* **466:** 489–498

Békés M, Rut W, Kasperkiewicz P, Mulder MPC, Ovaa H, Drag M, Lima CD & Huang TT (2015) SARS hCoV papain-like protease is a unique Lys48 linkage-specific di-distributive deubiquitinating enzyme. *Biochem. J.* **468:** 215–226

Békés M, van der Heden van Noort GJ, Ekkebus R, Ovaa H, Huang TT & Lima CD (2016) Recognition of Lys48-Linked Di-ubiquitin and Deubiquitinating Activities of the SARS Coronavirus Papain-like Protease. *Mol Cell* **62:** 572–585

Bienko M, Green CM, Crosetto N, Rudolf F, Zapart G, Coull B, Kannouche P, Wider G, Peter M, Lehmann AR, Hoffman K & Dikic I (2005) Ubiquitin-binding domains in Y-family polymerases regulate translesion synthesis. *Science* **310:**

Bomar MG, Pai M-T, Tzeng S-R, Li SS-C & Zhou P (2007) Structure of the ubiquitin-binding zinc finger domain of human DNA Y-polymerase η. *EMBO Rep.* **8:** 247–251

Bomar MG, Souza SD, Bienko M, Dikic I, Walker GC & Zhou P (2010) Unconventional Ubiquitin Recognition by the Ubiquitin-Binding Motif within the Y Family DNA Polymerases i and Rev1. *Mol Cell* **37:** 408–417

Boname JM, Thomas M, Stagg HR, Xu P, Peng J & Lehner PJ (2010) Efficient Internalization of MHC I Requires Lysine-11 and Lysine-63 Mixed Linkage Polyubiquitin Chains. *Traffic* **11:** 210–220

Bosanac I, Wertz IE, Pan B, Yu C, Kusam S, Lam C, Phu L, Phung Q, Maurer B, Arnott D, Kirkpatrick DS, Dixit VM & Hymowitz SG (2010) Ubiquitin binding to A20 ZnF4 is required for modulation of NF-κB signaling. *Mol Cell* **40:** 548–557

Bradford MM (1976) A rapid and sensitive method for the quantitation of microgram quantities of protein utilizing the principle of protein-dye binding. *Anal Biochem* **72:** 248–254

Branigan E, Plechanovová A, Jaffray EG, Naismith JH & Hay RT (2015) Structural basis for the RING-catalyzed synthesis of K63-linked ubiquitin chains. *Nat Struct Mol Biol* **22:** 597–602

Bremm A, Freund SMV & Komander D (2010) Lys11-linked ubiquitin chains adopt compact conformations and are preferentially hydrolyzed by the deubiquitinase Cezanne. *Nat Struct Mol Biol* **17:** 939–947

Bremm A, Moniz S, Mader J, Rocha S & Komander D (2014) Cezanne (OTUD7B) regulates HIF-1α homeostasis in a proteasome-independent manner. *EMBO Rep.* **15:** 1268–1277

Brzovic PS, Lissounov A, Christensen DE, Hoyt DW & Klevit RE (2006) A UbcH5/ubiquitin noncovalent complex is required for processive BRCA1-directed ubiquitination. *Mol Cell* **21:** 873–880

Buetow L & Huang DT (2016) Structural insights into the catalysis and regulation of E3 ubiquitin ligases. *Nat Rev Mol Cell Biol*

Burnett B, Li F & Pittman RN (2003) The polyglutamine neurodegenerative protein ataxin-3 binds polyubiquitylated proteins and has ubiquitin protease activity. *Hum Mol Genet* **12:** 3195–3205

Castañeda CA, Chaturvedi A, Camara CM, Curtis JE, Krueger S & Fushman D (2016a) Linkage-specific conformational ensembles of non-canonical polyubiquitin chains. *Phys Chem Chem Phys* **18:** 5771–5788

Castañeda CA, Dixon EK, Walker O, Chaturvedi A, Nakasone MA, Curtis JE, Reed MR, Krueger S, Cropp TA & Fushman D (2016b) Linkage via K27 Bestows Ubiquitin Chains with Unique Properties among Polyubiquitins. *Structure* **24:** 423–436

Castañeda CA, Kashyap TR, Nakasone MA, Krueger S & Fushman D (2013) Unique structural, dynamical, and functional properties of k11-linked polyubiquitin chains. *Structure* **21:** 1168–1181

Chai Y, Berke SS, Cohen RE & Paulson HL (2004) Poly-ubiquitin binding by the polyglutamine disease protein ataxin-3 links its normal function to protein surveillance pathways. *J. Biol. Chem.* **279:** 3605–3611

Chang L & Barford D (2014) Insights into the anaphase-promoting complex: a molecular machine that regulates mitosis. *Current Opinion in Structural Biology* **29:** 1–9

Chastagner P, Israël A & Brou C (2006) Itch/AIP4 mediates Deltex degradation through the formation of K29-linked polyubiquitin chains. *EMBO Rep.* **7:** 1147–1153

Chau V, Tobias JW, Bachmair A, Marriott D, Ecker DJ, Gonda DK & Varshavsky A (1989) A multiubiquitin chain is confined to specific lysine in a targeted short-lived protein. *Science* **243:** 1576–1583

Chaugule VK, Burchell L, Barber KR, Sidhu A, Leslie SJ, Shaw GS & Walden H (2011) Autoregulation of Parkin activity through its ubiquitin-like domain. *EMBO J* **30:** 2853–2867

Chen H, Fre S, Slepnev VI, Capua MR, Takei K, Butler MH, Di Fiore PP & De Camilli P (1998) Epsin is an EH-domain-binding protein implicated in clathrin-mediated endocytosis. *Nature* **394:** 793–797

Chevallet M, Luche S & Rabilloud T (2006) Silver staining of proteins in polyacrylamide gels. *Nat Protoc* **1:** 1852–1858

Chiu Y-H, Sun Q & Chen ZJ (2007) E1-L2 activates both ubiquitin and FAT10. *Mol Cell* **27:** 1014–1023

Chong RA, Wu K, Spratt DE, Yang Y, Lee C, Nayak J, Xu M, Elkholi R, Tappin I, Li J, Hurwitz J, Brown BD, Chipuk JE, Chen ZJ, Sanchez R, Shaw GS, Huang L & Pan ZQ (2014) Pivotal role for the ubiquitin Y59-E51 loop in lysine 48 polyubiquitination. *Proc. Natl. Acad. Sci.* **111:** 8434–8439

Ciechanover A, Heller H, Elias S, Haas AL & Hershko A (1980) ATP-dependent conjugation of reticulocyte proteins with the polypeptide required for protein degradation. *Proc. Natl. Acad. Sci.* **77:** 1365–1368

Ciechanover A, Heller H, Katz-Etzion R & Hershko A (1981) Activation of the heat-stable polypeptide of the ATP-dependent proteolytic system. *Proc. Natl. Acad. Sci.* **78:** 761–765

Ciehanover A, Hod Y & Hershko A (1978) A heat-stable polypeptide component of an ATP-dependent proteolytic system from reticulocytes. *Biochem Biophys Res Commun* **81:** 1100–1105

Clague MJ, Barsukov I, Coulson JM, Liu H, Rigden DJ & Urbé S (2013) Deubiquitylases from genes to organism. *Physiol. Rev.* **93:** 1289–1315

Cook WJ, Jeffrey LC, Carson M, Chen Z & Pickart CM (1992) Structure of a diubiquitin conjugate and a model for interaction with ubiquitin conjugating enzyme (E2). *J. Biol. Chem.* **267:** 16467–16471

Cook WJ, Jeffrey LC, Kasperek E & Pickart CM (1994) Structure of tetraubiquitin shows how multiubiquitin chains can be formed. *J Mol Biol* **236:** 601–609

Cooper EM, Boeke JD & Cohen RE (2010) Specificity of the BRISC deubiquitinating enzyme is not due to selective binding to Lys63-linked polyubiquitin. *J. Biol. Chem.*

Cooper EM, Cutcliffe C, Kristiansen TZ, Pandey A, Pickart CM & Cohen RE (2009) K63-specific deubiquitination by two JAMM/MPN+ complexes: BRISC-associated Brcc36 and proteasomal Poh1. *EMBO J* **28:** 621–631

Cope GA, Suh GSB, Aravind L, Schwarz SE, Zipursky SL, Koonin EV & Deshaies RJ (2002) Role of predicted metalloprotease motif of Jab1/Csn5 in cleavage of Nedd8 from Cul1. *Science* **298:** 608–611

Cornish-Bowden A (2013) Fundamentals of Enzyme Kinetics. John Wiley & Sons

Cripps D, Thomas SN, Jeng Y, Yang F, Davies P & Yang AJ (2006) Alzheimer disease-specific conformation of hyperphosphorylated paired helical filament-Tau is polyubiquitinated through Lys-48, Lys-11, and Lys-6 ubiquitin conjugation. *J. Biol. Chem.* **281:** 10825–10838

Cunningham CN, Baughman JM, Phu L, Tea JS, Yu C, Coons M, Kirkpatrick DS, Bingol B & Corn JE (2015) USP30 and parkin homeostatically regulate atypical ubiquitin chains on mitochondria. *Nature Cell Biology* **17:** 160–169

Dammer EB, Na CH, Xu P, Seyfried NT, Duong DM, Cheng D, Gearing M, Rees H, Lah JJ, Levey AI, Rush J & Peng J (2011) Polyubiquitin Linkage Profiles in Three Models of Proteolytic Stress Suggest the Etiology of Alzheimer Disease. *J. Biol. Chem.* **286:** 10457–10465

Datta AB, Hura GL & Wolberger C (2009) The structure and conformation of Lys63-linked tetraubiquitin. *J Mol Biol* **392:** 1117–1124

Deng L, Wang C, Spencer E, Yang L, Braun A, You J, Slaughter C, Pickart C & Chen ZJ (2000) Activation of the IkappaB kinase complex by TRAF6 requires a dimeric ubiquitin-conjugating enzyme complex and a unique polyubiquitin chain. *Cell* **103:** 351–361

Deveraux Q, Ustrell V, Pickart C & Rechsteiner M (1994) A 26 S protease subunit that binds ubiquitin conjugates. *J Biol Chem* **269:** 7059–7061

Dong KC, Helgason E, Yu C, Phu L, Arnott DP, Bosanac I, Compaan DM, Huang OW, Fedorova AV, Kirkpatrick DS, Hymowitz SG & Dueber EC (2011) Preparation of distinct ubiquitin chain reagents of high purity and yield. *Structure* **19:** 1053–1063

Dou H, Buetow L, Sibbet GJ, Cameron K & Huang DT (2012) BIRC7–E2 ubiquitin conjugate structure reveals the mechanism of ubiquitin transfer by a RING dimer. *Nat Struct Mol Biol* **19:** 876–883

Duda DM, Olszewski JL, Schuermann JP, Kurinov I, Miller DJ, Nourse A, Alpi AF & Schulman BA (2013) Structure of HHARI, a RING-IBR-RING Ubiquitin Ligase: Autoinhibition of an Ariadne-Family E3 and Insights into Ligation Mechanism. *Structure/Folding and Design* **21:** 1030–1041

Durcan TM, Tang MY, Pérusse JR, Dashti EA, Aguileta MA, McLelland G-L, Gros P, Shaler TA, Faubert D, Coulombe B & Fon EA (2014) USP8 regulates mitophagy by removing K6-linked ubiquitin conjugates from parkin. *EMBO J* **33:** 2473–2491

Eddins MJ, Carlile CM, Gomez KM, Pickart CM & Wolberger C (2006) Mms2-Ubc13 covalently bound to ubiquitin reveals the structural basis of linkage-specific polyubiquitin chain formation. *Nat Struct Mol Biol* **13:** 915–920

Eddins MJ, Varadan R, Fushman D, Pickart CM & Wolberger C (2007) Crystal structure and solution NMR studies of Lys48-linked tetraubiquitin at neutral pH. *J Mol Biol* **367:** 204–211

Edelmann MJ, Iphöfer A, Akutsu M, Altun M, di Gleria K, Kramer HB, Fiebiger E, Dhe-Paganon S & Kessler BM (2009) Structural basis and specificity of human otubain 1-mediated deubiquitination. *Biochem. J.* **418:** 379–390

Eletr ZM & Wilkinson KD (2014) Regulation of proteolysis by human deubiquitinating enzymes. *Biochim. Biophys. Acta* **1843:** 114–128

Elia AEH, Boardman AP, Wang DC, Huttlin EL, Everley RA, Dephoure N, Zhou C, Koren I, Gygi SP & Elledge SJ (2015) Quantitative Proteomic Atlas of Ubiquitination and Acetylation in the DNA Damage Response. *Mol Cell* **59:** 867–881

Emmerich CH, Bakshi S, Kelsall IR, Ortiz-Guerrero J, Shpiro N & Cohen P (2016) Lys63/Met1-hybrid ubiquitin chains are commonly formed during the activation of innate immune signalling. *Biochem Biophys Res Commun* **474:** 452–461

Emmerich CH, Ordureau A, Strickson S, Arthur JSC, Pedrioli PGA, Komander D & Cohen P (2013) Activation of the canonical IKK complex by K63/M1-linked hybrid ubiquitin chains. *Proc. Natl. Acad. Sci.* **110:** 15247–15252

Emsley P, Lohkamp B, Scott WG & Cowtan K (2010) Features and development of Coot. *Acta Crystallogr D Biol Crystallogr* **66:** 486–501

Erpapazoglou Z, Walker O & Haguenauer-Tsapis R (2014) Versatile Roles of K63-Linked Ubiquitin Chains in Trafficking. *Cells* **3:** 1027–1088

Evans P (2006) Scaling and assessment of data quality. *Acta Crystallogr D Biol Crystallogr* **62:** 72–82

Evans PR & Murshudov GN (2013) How good are my data and what is the resolution? *Acta Crystallogr D Biol Crystallogr* **69:** 1204–1214

Faesen AC, Luna-Vargas MPA, Geurink PP, Clerici M, Merkx R, van Dijk WJ, Hameed DS, Oualid El F, Ovaa H & Sixma TK (2011) The differential modulation of USP activity by internal regulatory domains, interactors and eight ubiquitin chain types. *Chem. Biol.* **18:** 1550–1561

Finley D (2009) Recognition and processing of ubiquitin-protein conjugates by the proteasome. *Annu. Rev. Biochem.* **78:** 477–513

Finley D, Bartel B & Varshavsky A (1989) The tails of ubiquitin precursors are ribosomal proteins whose fusion to ubiquitin facilitates ribosome biogenesis. *Nature* **338:** 394–401

Fletcher AJ, Christensen DE, Nelson C, Tan CP, Schaller T, Lehner PJ, Sundquist WI & Towers GJ (2015) TRIM5α requires Ube2W to anchor Lys63-linked ubiquitin chains and restrict reverse transcription. *EMBO J* **34:** 2078–2095

Flierman D, van der Heden van Noort GJ, Ekkebus R, Geurink PP, Mevissen TET, Hospenthal MK, Komander D & Ovaa H (2016) Non-hydrolyzable Diubiquitin Probes Reveal Linkage-Specific Reactivity of Deubiquitylating Enzymes Mediated by S2 Pockets. *Cell Chem Biol* **23:** 472–482

Fu Q-S, Zhou C-J, Gao H-C, Jiang Y-J, Zhou Z-R, Hong J, Yao W-M, Song A-X, Lin D-H & Hu H-Y (2009) Structural basis for ubiquitin recognition by a novel domain from human phospholipase A2-activating protein. *J. Biol. Chem.* **284:** 19043–19052

Fushman D & Walker O (2010) Exploring the Linkage Dependence of Polyubiquitin Conformations Using Molecular Modeling. *J Mol Biol* **395:** 803–814

Gatti M, Pinato S, Maiolica A, Rocchio F, Prato MG, Aebersold R & Penengo L (2015) RNF168 promotes noncanonical K27 ubiquitination to signal DNA damage. *Cell Rep* **10:** 226–238

Gerlach B, Cordier SM, Schmukle AC, Emmerich CH, Rieser E, Haas TL, Webb AI, Rickard JA, Anderton H, Wong WWL, Nachbur U, Gangoda L, Warnken U, Purcell AW, Silke J & Walczak H (2011) Linear ubiquitination prevents inflammation and regulates immune signalling. *Nature* **471:** 591–596

Goldstein G, Scheid M, Hammerling U, Schlesinger DH, Niall HD & Boyse EA (1975) Isolation of a polypeptide that has lymphocyte-differentiating properties and is probably represented universally in living cells. *Proc. Natl. Acad. Sci.* **72:** 11–15

Gopinath P, Ohayon S, Nawatha M & Brik A (2016) Chemical and semisynthetic approaches to study and target deubiquitinases. *Chemical Society Reviews* **45:** 4171–4198

Grabbe C, Husnjak K & Dikic I (2011) The spatial and temporal organization of ubiquitin networks. *Nat Rev Mol Cell Biol* **12:** 295–307

Grice GL & Nathan JA (2016) The recognition of ubiquitinated proteins by the proteasome. *CMLS, Cell. Mol. Life Sci.* **73:** 3497–3506

Grice GL, Lobb IT, Weekes MP, Gygi SP, Antrobus R & Nathan JA (2015) The Proteasome Distinguishes between Heterotypic and Homotypic Lysine-11-Linked Polyubiquitin Chains. *Cell Rep* **12:** 545–553

Guo Y, Bian W, Zhang Y & Li H (2017) Expression in Escherichia coli, purification and characterization of LRSAM1, a LRR and RING domain E3 ubiquitin ligase. *Protein Expr. Purif.* **129:** 158–161

Haas AL, Bright PM & Jackson VE (1988) Functional diversity among putative E2 isozymes in the mechanism of ubiquitin-histone ligation. *J. Biol. Chem.* **263:** 13268–13275

Haas AL, Warms JV, Hershko A & Rose IA (1982) Ubiquitin-activating enzyme. Mechanism and role in protein-ubiquitin conjugation. *J. Biol. Chem.* **257:** 2543–2548

Haas TL, Emmerich CH, Gerlach B, Schmukle AC, Cordier SM, Rieser E, Feltham R, Vince J, Warnken U, Wenger T, Koschny R, Komander D, Silke J & Walczak H (2009) Recruitment of the linear ubiquitin chain assembly complex stabilizes the TNF-R1 signaling complex and is required for TNF-mediated gene induction. *Mol Cell* **36:** 831–844

Haglund K, Di Fiore PP & Dikic I (2003) Distinct monoubiquitin signals in receptor endocytosis. *Trends Biochem. Sci.* **28:** 598–603

Hassiepen U, Eidhoff U, Meder G, Bulber J-F, Hein A, Bodendorf U, Lorthiois E & Martoglio B (2007) A sensitive fluorescence intensity assay for deubiquitinating proteases using ubiquitin-rhodamine110-glycine as substrate. *Anal Biochem* **371:** 201–207

Hay-Koren A, Caspi M, Zilberberg A & Rosin-Arbesfeld R (2011) The EDD E3 ubiquitin ligase ubiquitinates and up-regulates beta-catenin. *Molecular Biology of the Cell* **22:** 399–411

He Y, Hicke L & Radhakrishnan I (2007) Structural basis for ubiquitin recognition by SH3 domains. *J Mol Biol* **373:** 190–196

Hemantha HP & Brik A (2013) Bioorganic & Medicinal Chemistry. *Bioorg. Med. Chem.* **21:** 3411–3420

Hershko A, Ciechanover A, Heller H, Haas AL & Rose IA (1980) Proposed role of ATP in protein breakdown: conjugation of protein with multiple chains of the polypeptide of ATP-dependent proteolysis. *Proc. Natl. Acad. Sci.* **77:** 1783–1786

Hicke L, Schubert HL & Hill CP (2005) Ubiquitin-binding domains. *Nat Rev Mol Cell Biol* **6:** 610–621

Hirano S, Kawasaki M, Ura H, Kato R, Raiborg C, Stenmark H & Wakatsuki S (2006a) Double-sided ubiquitin binding of Hrs-UIM in endosomal protein sorting. *Nat Struct Mol Biol* **13:** 272–277

Hirano S, Suzuki N, Slagsvold T, Kawasaki M, Trambaiolo D, Kato R, Stenmark H & Wakatsuki S (2006b) Structural basis of ubiquitin recognition by mammalian Eap45 GLUE domain. *Nat Struct Mol Biol* **13:** 1031–1032

Hirano T, Serve O, Yagi-Utsumi M, Takemoto E, Hiromoto T, Satoh T, Mizushima T & Kato K (2011) Conformational Dynamics of Wild-type Lys-48-linked Diubiquitin in Solution. *J. Biol. Chem.* **286:** 37496–37502

Hjerpe R, Aillet F, Lopitz-Otsoa F, Lang V, England P & Rodriguez MS (2009) scientific report. *EMBO Rep.* **10:** 1250–1258

Hofmann K & Bucher P (1996) The UBA domain: a sequence motif present in multiple enzyme classes of the ubiquitination pathway. *Trends Biochem. Sci.* **21:** 172–173

Hofmann K & Falquet L (2001) A ubiquitin-interacting motif conserved in components of the proteasomal and lysosomal protein degradation systems. *Trends Biochem. Sci.* **26:** 347–350

Hofmann RM & Pickart CM (2001) In vitro assembly and recognition of Lys-63 polyubiquitin chains. *J. Biol. Chem.* **276:** 27936–27943

Hook SS, Orian A, Cowley SM & Eisenman RN (2002) Histone deacetylase 6 binds polyubiquitin through its zinc finger (PAZ domain) and copurifies with deubiquitinating enzymes. *Proc. Natl. Acad. Sci.* **99:** 13425–13430

Hospenthal MK, Freund SMV & Komander D (2013) Assembly, analysis and architecture of atypical ubiquitin chains. *Nat Struct Mol Biol* **20:** 555–565

Hospenthal MK, Mevissen TET & Komander D (2015) Deubiquitinase-based analysis of ubiquitin chain architecture using Ubiquitin Chain Restriction (UbiCRest). *Nat Protoc* **10:** 349–361

Hu M, Li P, Li M, Li W, Yao T, Wu J-W, Gu W, Cohen RE & Shi Y (2002) Crystal structure of a UBP-family deubiquitinating enzyme in isolation and in complex with ubiquitin aldehyde. *Cell* **111:** 1041–1054

Hu M, Li P, Song L, Jeffrey PD, Chenova TA, Wilkinson KD, Cohen RE & Shi Y (2005) Structure and mechanisms of the proteasome-associated deubiquitinating enzyme USP14. *EMBO J* **24:** 3747–3756

Huang DT, Hunt HW, Zhuang M, Ohi MD, Holton JM & Schulman BA (2007) Basis for a ubiquitin-like protein thioester switch toggling E1-E2 affinity. *Nature* **445:** 394–398

Huang H, Jeon M-S, Liao L, Yang C, Elly C, Yates JR & Liu Y-C (2010) K33-linked polyubiquitination of T cell receptor-zeta regulates proteolysis-independent T cell signaling. *Immunity* **33:** 60–70

Huang L, Kinnucan E, Wang G, Beaudenon S, Howley PM, Huibregtse JM & Palvetich NP (1999) Structure of an E6AP-UbcH7 complex: insights into ubiquitination by the E2-E3 enzyme cascade. *Science* **286:** 1321–1326

Huguenin-Dezot N, De Cesare V, Peltier J, Knebel A, Kristariyanto YA, Rogerson DT, Kulathu Y, Trost M & Chin JW (2016) Synthesis of Isomeric Phosphoubiquitin Chains Reveals that Phosphorylation Controls Deubiquitinase Activity and Specificity. *Cell Rep* **16:** 1180–1193

Huibregtse JM, Scheffner M, Beaudenon S & Howley PM (1995) A family of proteins structurally and functionally related to the E6-AP ubiquitin-protein ligase. *Proc. Natl. Acad. Sci.* **92:** 2563–2567.

Hurley JH, Lee S & Prag G (2006) Ubiquitin-binding domains. *Biochem. J.* **399:** 361–372

Husnjak K & Dikic I (2012) Ubiquitin-binding proteins: decoders of ubiquitin-mediated cellular functions. *Annu. Rev. Biochem.* **81:** 291–322

Husnjak K, Elsasser S, Zhang N, Chen X, Randles L, Shi Y, Hofmann K, Walters KJ, Finley D & Dikic I (2008) Proteasome subunit Rpn13 is a novel ubiquitin receptor. *Nature* **453:** 481–488

Ikeda F, Deribe YL, Skånland SS, Stieglitz B, Grabbe C, Franz-Wachtel M, van Wijk SJL, Goswami P, Nagy V, Terzic J, Tokunaga F, Androulidaki A, Nakagawa T, Pasparakis M, Iwai K, Sundberg JP, Schaefer L, Rittinger K, Macek B & Dikic I (2011) SHARPIN forms a linear ubiquitin ligase complex regulating NF-κB activity and apoptosis. *Nature* **471:** 637–641

Ikeda H & Kerppola TK (2008) Lysosomal localization of ubiquitinated Jun requires multiple determinants in a lysine-27-linked polyubiquitin conjugate. *Molecular Biology of the Cell* **19:** 4588–4601

Inn K-S, Gack MU, Tokunaga F, Shi M, Wong L-Y, Iwai K & Jung JU (2011) Linear ubiquitin assembly complex negatively regulates RIG-I- and TRIM25-mediated type I interferon induction. *Mol Cell* **41:** 354–365

Jin J, Li X, Gygi SP & Harper JW (2007) Dual E1 activation systems for ubiquitin differentially regulate E2 enzyme charging. *Nature* **447:** 1135–1138

Jin J, Xie X, Xiao Y, Hu H, Zou Q, Cheng X & Sun S-C (2016) Epigenetic regulation of the expression of Il12 and Il23 and autoimmune inflammation by the deubiquitinase Trabid. *Nat Immunol* **17:** 259–268

Jin L, Williamson A, Banerjee S, Philipp I & Rape M (2008) Mechanism of ubiquitin-chain formation by the human anaphase-promoting complex. *Cell* **133:** 653–665

Johnson ES, Bartel B, Seufert W & Varshavsky A (1992) Ubiquitin as a degradation signal. *EMBO J* **11:** 497–505

Johnson ES, Ma PC, Ota IM & Varshavsky A (1995) A proteolytic pathway that recognizes ubiquitin as a degradation signal. *J. Biol. Chem.* **270:** 17442–17456

Johnston SC, Larsen CN, Cook WJ, Wilkinson KD & Hill CP (1997) Crystal structure of a deubiquitinating enzyme (human UCH-L3) at 1.8 A resolution. *EMBO J* **16:** 3787–3796

Johnston SC, Riddle SM, Cohen RE & Hill CP (1999) Structural basis for the specificity of ubiquitin C-terminal hydrolases. *EMBO J* **18:** 3877–3887

Joosten RP, Long F, Murshudov GN & Perrakis A (2014) The PDB_REDO server for macromolecular structure model optimization. *IUCrJ* **1:** 213–220

Juang Y-C, Landry M-C, Sanches M, Vittal V, Leung CCY, Ceccarelli DF, Mateo A-RF, Pruneda JN, Mao DYL, Szilard RK, Orlicky S, Munro M, Brzovic PS, Klevit RE, Sicheri F & Durocher D (2012) OTUB1 co-opts Lys48-linked ubiquitin recognition to suppress E2 enzyme function. *Mol Cell* **45:** 384–397

Kabsch W (2010) XDS. *Acta Crystallogr D Biol Crystallogr* **66:** 125–132

Kaiser SE, Riley BE, Shaler TA, Trevino RS, Becker CH, Schulman H & Kopito RR (2011) Protein standard absolute quantification (PSAQ) method for the measurement of cellular ubiquitin pools. *Nat Meth* **8:** 691–696

Kamadurai HB, Qiu Y, Deng A, Harrison JS, MacDonald C, Actis M, Rodrigues P, Miller DJ, Souphron J, Lewis SM, Kurinov I, Fujii N, Hammel M, Piper R, Kuhlman B & Schulman BA (2013) Mechanism of ubiquitin ligation and lysine prioritization by a HECT E3. *eLife* **2:** e00828

Kamadurai HB, Souphron J, Scott DC, Duda DM, Miller DJ, Stringer D, Piper RC & Schulman BA (2009) Insights into ubiquitin transfer cascades from a structure of a UbcH5B approximately ubiquitin-HECT(NEDD4L) complex. *Mol Cell* **36:** 1095–1102

Kanayama A, Seth RB, Sun L, Ea C-K, Hong M, Shaito A, Chiu Y-H, Deng L & Chen ZJ (2004) TAB2 and TAB3 activate the NF-kappaB pathway through binding to polyubiquitin chains. *Mol Cell* **15:** 535–548

Kang RS, Daniels CM, Francis SA, Shih SC, Salerno WJ, Hicke L & Radhakrishnan I (2003) Solution structure of a CUE-ubiquitin complex reveals a conserved mode of ubiquitin binding. *Cell* **113:**

Kar G, Keskin O, Nussinov R & Gursoy A (2012) Human proteome-scale structural modeling of E2-E3 interactions exploiting interface motifs. *J. Proteome Res.* **11:** 1196–1207

Kee Y & Huibregtse JM (2007) Regulation of catalytic activities of HECT ubiquitin ligases. *Biochem Biophys Res Commun* **354:** 329–333

Keusekotten K, Elliott PR, Glockner L, Fiil BK, Damgaard RB, Kulathu Y, Wauer T, Hospenthal MK, Gyrd-Hansen M, Krappmann D, Hofmann K & Komander D (2013) OTULIN Antagonizes LUBAC Signaling by Specifically Hydrolyzing Met1-Linked Polyubiquitin. *Cell* **153:** 1312–1326

Kimura Y & Tanaka K (2010) Regulatory mechanisms involved in the control of ubiquitin homeostasis. *J. Biochem.* **147:** 793–798

Kirisako T, Kamei K, Murata S, Kato M, Fukumoto H, Kanie M, Sano S, Tokunaga F, Tanaka K & Iwai K (2006) A ubiquitin ligase complex assembles linear polyubiquitin chains. *EMBO J* **25:** 4877–4887

Kleijnen MF, Shih AH, Zhou P, Kumar S, Soccio RE, Kedersha NL, Gill G & Howley PM (2000) The hPLIC proteins may provide a link between the ubiquitination machinery and the proteasome. *Mol Cell* **6:** 409–419

Koegl M, Hoppe T, Schlenker S, Ulrich HD, Mayer TU & Jentsch S (1999) A novel ubiquitination factor, E4, is involved in multiubiquitin chain assembly. *Cell* **96:** 635–644

Komander D & Barford D (2008) Structure of the A20 OTU domain and mechanistic insights into deubiquitination. *Biochem. J.* **409:** 77–85

Komander D, Clague MJ & Urbé S (2009a) Breaking the chains: structure and function of the deubiquitinases. *Nat Rev Mol Cell Biol* **10:** 550–563

Komander D, Lord CJ, Scheel H, Swift S, Hofmann K, Ashworth A & Barford D (2008) The Structure of the CYLD USP Domain Explains Its Specificity for Lys63-Linked Polyubiquitin and Reveals a B Box Module. *Mol Cell* **29:** 451–464

Komander D, Reyes-Turcu F, Licchesi JDF, Odenwaelder P, Wilkinson KD & Barford D (2009b) Molecular discrimination of structurally equivalent Lys 63-linked and linear polyubiquitin chains. *EMBO Rep.* **10:** 466–473

Krissinel E & Henrick K (2007) Inference of macromolecular assemblies from crystalline state. *J Mol Biol* **372:** 774–797

Kristariyanto YA, Abdul Rehman SA, Campbell DG, Morrice NA, Johnson C, Toth R & Kulathu Y (2015a) K29-selective ubiquitin binding domain reveals structural basis of specificity and heterotypic nature of K29 polyubiquitin. *Mol Cell* **58:** 83–94

Kristariyanto YA, Choi SY, Abdul Rehman SA, Ritorto MS, Campbell DG, Morrice NA, Toth R & Kulathu Y (2015b) Assembly and structure of Lys33-linked polyubiquitin reveals distinct conformations. *Biochem. J.* **467:** 345–352

Kulathu Y & Komander D (2012) Atypical ubiquitylation - the unexplored world of polyubiquitin beyond Lys48 and Lys63 linkages. *Nat Rev Mol Cell Biol* **13:** 508–523

Kulathu Y, Akutsu M, Bremm A, Hofmann K & Komander D (2009) Two-sided ubiquitin binding explains specificity of the TAB2 NZF domain. *Nat Struct Mol Biol* **16:** 1328–1330

Kumar KSA, Spasser L, Erlich LA, Bavikar SN & Brik A (2010) Total chemical synthesis of di-ubiquitin chains. *Angew. Chem. Int. Ed.* **49:** 9126–9131

Kumar S, Kao WH & Howley PM (1997) Physical interaction between specific E2 and Hect E3 enzymes determines functional cooperativity. *J. Biol. Chem.* **272:** 13548–13554

Lai M-Y, Zhang D, LaRonde-LeBlanc N & Fushman D (2012) Structural and biochemical studies of the open state of Lys48-linked diubiquitin. *Biochim. Biophys. Acta* **1823:** 2046–2056

Lam YA, Xu W, DeMartino GN & Cohen RE (1997) Editing of ubiquitin conjugates by an isopeptidase in the 26S proteasome. *Nature* **385:** 737–740

Lange OF, Lakomek N-A, Farès C, Schröder GF, Walter KFA, Becker S, Meiler J, Grubmüller H, Griesinger C & de Groot BL (2008) Recognition dynamics up to microseconds revealed from an RDC-derived ubiquitin ensemble in solution. *Science* **320:** 1471–1475

Larsen CN, Krantz BA & Wilkinson KD (1998) Substrate specificity of deubiquitinating enzymes: ubiquitin C-terminal hydrolases. *Biochemistry* **37:** 3358–3368

Lauwers E, Jacob C & André B (2009) K63-linked ubiquitin chains as a specific signal for protein sorting into the multivesicular body pathway. *J Cell Biol* **185:** 493–502

Lee B-H, Lee MJ, Park S, Oh D-C, Elsasser S, Chen P-C, Gartner C, Dimova N, Hanna J, Gygi SP, Wilson SM, King RW & Finley D (2010) Enhancement of proteasome activity by a small-molecule inhibitor of USP14. *Nature* **467:** 179–184

Lee B-H, Lu Y, Prado MA, Shi Y, Tian G, Sun S, Elsasser S, Gygi SP, King RW & Finley D (2016) USP14 deubiquitinates proteasome-bound substrates that are ubiquitinated at multiple sites. *Nature* **532:** 398–401

Lee I & Schindelin H (2008) Structural Insights into E1-Catalyzed Ubiquitin Activation and Transfer to Conjugating Enzymes. *Cell* **134:** 268–278

Lee MJ, Lee B-H, Hanna J, King RW & Finley D (2011) Trimming of ubiquitin chains by proteasome-associated deubiquitinating enzymes. *Molecular & Cellular Proteomics* **10:** R110.003871

Lee S, Tsai YC, Mattera R, Smith WJ, Kostelansky MS, Weissman AM, Bonifacino JS & Hurley JH (2006) Structural basis for ubiquitin recognition and autoubiquitination by Rabex-5. *Nat Struct Mol Biol* **13:** 264–271

Lenkinski RE, Chen DM, Glickson JD & Goldstein G (1977) Nuclear magnetic resonance studies of the denaturation of ubiquitin. *Biochim. Biophys. Acta* **494:** 126–130

Licchesi JDF, Mieszczanek J, Mevissen TET, Rutherford TJ, Akutsu M, (null), Oualid FE, (null), (null), Bienz M & Komander D (2011) An ankyrin-repeat ubiquitin-binding domain determines TRABID's specificity for atypical ubiquitin chains. *Nat Struct Mol Biol* **19:** 62–71

Lin DYW, Diao J, Zhou D & Chen J (2010) Biochemical and Structural Studies of a HECT-like Ubiquitin Ligase from Escherichia coli O157:H7. J. Biol. Chem. **286:** 441–449

Lin M, Zhao Z, Yang Z, Meng Q, Tan P, Xie W, Qin Y, Wang R-F & Cui J (2016) USP38 Inhibits Type I Interferon Signaling by Editing TBK1 Ubiquitination through NLRP4 Signalosome. *Mol Cell* **64:** 267–281

Lindsten K, de Vrij FMS, Verhoef LGGC, Fischer DF, van Leeuwen FW, Hol EM, Masucci MG & Dantuma NP (2002) Mutant ubiquitin found in neurodegenerative disorders is a ubiquitin fusion degradation substrate that blocks proteasomal degradation. *J Cell Biol* **157:** 417–427

Liu J, Han C, Xie B, Wu Y, Liu S, Chen K, Xia M, Zhang Y, Song L, Li Z, Zhang T, Ma F, Wang Q, Wang J, Deng K, Zhuang Y, Wu X, Yu Y, Xu T & Cao X (2014a) Rhbdd3 controls autoimmunity by suppressing the production of IL-6 by dendritic cells via K27-linked ubiquitination of the regulator NEMO. *Nat Immunol* **15:** 612–622

Liu W, Shang Y, Zeng Y, Liu C, Li Y, Zhai L, Wang P, Lou J, Xu P, Ye Y & Li W (2014b) Dimeric Ube2g2 simultaneously engages donor and acceptor ubiquitins to form Lys48-linked ubiquitin chains. *EMBO J* **33:** 46–61

Liu Z, Gong Z, Jiang W-X, Yang J, Zhu W-K, Guo D-C, Zhang W-P, Liu M-L & Tang C (2015) Lys63-linked ubiquitin chain adopts multiple conformational states for specific target recognition. *eLife* **4:** e05767

Liu Z, Meray RK, Grammatopoulos TN, Fredenburg RA, Cookson MR, Liu Y, Logan T & Lansbury PT (2009) Membrane-associated farnesylated UCH-L1 promotes alpha-synuclein neurotoxicity and is a therapeutic target for Parkinson's disease. *Proc. Natl. Acad. Sci.* **106:** 4635–4640

Lu Y, Lee BH, King RW, Finley D & Kirschner MW (2015) Substrate degradation by the proteasome: A single-molecule kinetic analysis. *Science* **348:** 1250834–1250834

Lydeard JR, Schulman BA & Harper JW (2013) Building and remodelling Cullin-RING E3 ubiquitin ligases. *EMBO Rep.* **14:** 1050–1061

Mao Y, Senic-Matuglia F, Di Fiore PP, Polo S, Hodsdon ME & De Camilli P (2005) Deubiquitinating function of ataxin-3: insights from the solution structure of the Josephin domain. *Proc. Natl. Acad. Sci.* **102:** 12700–12705

Marcotte EM, Pellegrini M, Ng HL, Rice DW, Yeates TO & Eisenberg D (1999) Detecting protein function and protein-protein interactions from genome sequences. *Science* **285:** 751–753

Maspero E, Mari S, Valentini E, Musacchio A, Fish A, Pasqualato S & Polo S (2011) Structure of the HECT:ubiquitin complex and its role in ubiquitin chain elongation. *EMBO Rep.* **12:** 342–349

Maspero E, Valentini E, Mari S, Cecatiello V, Soffientini P, Pasqualato S & Polo S (2013) Structure of a ubiquitin-loaded HECT ligase reveals the molecular basis for catalytic priming. *Nat Struct Mol Biol* **20:** 696–701

Matos CA, de Macedo-Ribeiro S & Carvalho AL (2011) Progress in Neurobiology. *Progress in Neurobiology* **95:** 26–48

Matsumoto ML, Dong KC, Yu C, Phu L, Gao X, Hannoush RN, Hymowitz SG, Kirkpatrick DS, Dixit VM & Kelley RF (2012) Engineering and structural characterization of a linear polyubiquitin-specific antibody. *J Mol Biol* **418:** 134–144

Matsumoto ML, Wickliffe KE, Dong KC, Yu C, Bosanac I, Bustos D, Phu L, Kirkpatrick DS, Hymowitz SG, Rape M, Kelley RF & Dixit VM (2010) K11-Linked Polyubiquitination in Cell Cycle Control Revealed by a K11 Linkage-Specific Antibody. *Mol Cell* **39:** 477–484

Mattera R, Tsai YC, Weissman AM & Bonifacino JS (2006) The Rab5 Guanine Nucleotide Exchange Factor Rabex-5 Binds Ubiquitin (Ub) and Functions as a Ub Ligase through an Atypical Ub-interacting Motif and a Zinc Finger Domain. *J. Biol. Chem.* **281:** 6874–6883

McCoy AJ, Grosse-Kunstleve RW, Storoni LC & Read RJ (2005) Likelihood-enhanced fast translation functions. *Acta Crystallogr D Biol Crystallogr* **61:** 458–464

McCullough J, Clague MJ & Urbé S (2004) AMSH is an endosome-associated ubiquitin isopeptidase. *J Cell Biol* **166:** 487–492

Meas R & Mao P (2015) Histone ubiquitylation and its roles in transcription and DNA damage response. *DNA Repair* **36:** 36–42

Mevissen TET, Hospenthal MK, Geurink PP, Elliott PR, Akutsu M, Arnaudo N, Ekkebus R, Kulathu Y, Wauer T, Oualid El F, Freund SMV, Ovaa H & Komander D (2013) OTU Deubiquitinases Reveal Mechanisms of Linkage Specificity and Enable Ubiquitin Chain Restriction Analysis. *Cell* **154:** 169–184

Mevissen TET, Kulathu Y, Mulder MPC, Geurink PP, Maslen SL, Gersch M, Elliott PR, Burke JE, van Tol BDM, Akutsu M, Oualid El F, Kawasaki M, Freund SMV, Ovaa H & Komander D (2016) Molecular basis of Lys11-polyubiquitin specificity in the deubiquitinase Cezanne. *Nature* **538:** 402–405

Meyer H-J & Rape M (2014) Enhanced protein degradation by branched ubiquitin chains. *Cell* **157:** 910–921

Michel MA, Elliott PR, Swatek KN, Simicek M, Pruneda JN, Wagstaff JL, Freund SMV & Komander D (2015) Assembly and Specific Recognition of K29- and K33-Linked Polyubiquitin. *Mol Cell* **58:** 95–109

Middleton AJ & Day CL (2015) The molecular basis of lysine 48 ubiquitin chain synthesis by Ube2K. *Scientific Reports* **5:** 16793

Min M, Mevissen TET, De Luca M, Komander D & Lindon C (2015) Efficient APC/C substrate degradation in cells undergoing mitotic exit depends on K11 ubiquitin linkages. *Molecular Biology of the Cell* **26:** 4325–4332

Mizuno E, Kawahata K, Kato M, Kitamura N & Komada M (2003) STAM proteins bind ubiquitinated proteins on the early endosome via the VHS domain and ubiquitin-interacting motif. *Molecular Biology of the Cell* **14:** 3675–3689

Morris JR & Solomon E (2004) BRCA1 : BARD1 induces the formation of conjugated ubiquitin structures, dependent on K6 of ubiquitin, in cells during DNA replication and repair. *Hum Mol Genet* **13:** 807–817

Nakagawa T & Nakayama K (2015) Protein monoubiquitylation: targets and diverse functions. *Genes Cells* **20:** 543–562

Newton K, Matsumoto ML, Wertz IE, Kirkpatrick DS, Lill JR, Tan J, Dugger D, Gordon N, Sidhu SS, Fellouse FA, Komuves L, French DM, Ferrando RE, Lam C, Compaan D, Yu C, Bosanac I, Hymowitz SG, Kelley RF & Dixit VM (2008) Ubiquitin Chain Editing Revealed by Polyubiquitin Linkage-Specific Antibodies. *Cell* **134:** 668–678

Nicastro G, Menon RP, Masino L, Knowles PP, McDonald NQ & Pastore A (2005) The solution structure of the Josephin domain of ataxin-3: structural determinants for molecular recognition. *Proc. Natl. Acad. Sci.* **102:** 10493–10498

Nicastro G, Todi SV, Karaca E, Bonvin AMJJ, Paulson HL & Pastore A (2010) Understanding the role of the Josephin domain in the PolyUb binding and cleavage properties of ataxin-3. *PLoS ONE* **5:** e12430

Nuber U & Scheffner M (1999) Identification of determinants in E2 ubiquitin-conjugating enzymes required for hect E3 ubiquitin-protein ligase interaction. *J. Biol. Chem.* **274:** 7576–7582

Nucifora FC, Nucifora LG, Ng C-H, Arbez N, Guo Y, Roby E, Shani V, Engelender S, Wei D, Wang X-F, Li T, Moore DJ, Pletnikova O, Troncoso JC, Sawa A, Dawson TM, Smith W, Lim K-L & Ross CA (2016) Ubiqutination via K27 and K29 chains signals aggregation and neuronal protection of LRRK2 by WSB1. *Nat Commun* **7:** 11792

Ohi MD, Vander Kooi CW, Rosenberg JA, Chazin WJ & Gould KL (2003) Structural insights into the U-box, a domain associated with multi-ubiquitination. *Nat. Struct. Biol.* **10:** 250–255

Ohno A, Jee J, Fujiwara K, Tenno T, Goda N, Tochio H, Kobayashi H, Hiroaki H & Shirakawa M (2005) Structure of the UBA Domain of Dsk2p in Complex with Ubiquitin. *Structure* **13:** 521–532

Ohtake F, Saeki Y, Ishido S, Kanno J & Tanaka K (2016) The K48-K63 Branched Ubiquitin Chain Regulates NF-κB Signaling. *Mol Cell* **64:** 251–266

Okada M, Ohtake F, Nishikawa H, Wu W, Saeki Y, Takana K & Ohta T (2015) Liganded ERα Stimulates the E3 Ubiquitin Ligase Activity of UBE3C to Facilitate Cell Proliferation. *Mol. Endocrinol.* **29:** 1646–1657

Olsen SK & Lima CD (2013) Structure of a Ubiquitin E1-E2 Complex: Insights to E1-

E2 Thioester Transfer. *Mol Cell* **49:** 884–896

Olsen SK, Capili AD, Lu X, Tan DS & Lima CD (2010) Active site remodelling accompanies thioester bond formation in the SUMO E1. *Nature* **463:** 906–912

Ordureau A, Münch C & Harper JW (2015) Quantifying Ubiquitin Signaling. *Mol Cell* **58:** 660–676

Ordureau A, Sarraf SA, Duda DM, Heo J-M, Jedrychowski MP, Sviderskiy VO, Olszewski JL, Koerber JT, Xie T, Beausoleil SA, Wells JA, Gygi SP, Schulman BA & Harper JW (2014) Quantitative proteomics reveal a feedforward mechanism for mitochondrial PARKIN translocation and ubiquitin chain synthesis. *Mol Cell* **56:** 360–375

Palicharla VR & Maddika S (2015) HACE1 mediated K27 ubiquitin linkage leads to YB-1 protein secretion. *Cell. Signal.* **27:** 2355–2362

Pandya RK, Partridge JR, Love KR, Schwartz TU & Ploegh HL (2010) A structural element within the HUWE1 HECT domain modulates self-ubiquitination and substrate ubiquitination activities. *J. Biol. Chem.* **285:** 5664–5673

Park Y, Yoon SK & Yoon J-B (2009) The HECT domain of TRIP12 ubiquitinates substrates of the ubiquitin fusion degradation pathway. *J. Biol. Chem.* **284:** 1540–1549

Pashkova N, Gakhar L, Winistorfer SC, Yu L, Ramaswamy S & Piper RC (2010) WD40 Repeat Propellers Define a Ubiquitin-Binding Domain that Regulates Turnover of F Box Proteins. *Mol Cell* **40:** 433–443

Penengo L, Mapelli M, Murachelli AG, Confalonieri S, Magri L, Musacchio A, Di Fiore PP, Polo S & Schneider TR (2006) Crystal structure of the ubiquitin binding domains of rabex-5 reveals two modes of interaction with ubiquitin. *Cell* **124:** 1183–1195

Peng D-J, Zeng M, Muromoto R, Matsuda T, Shimoda K, Subramaniam M, Spelsberg TC, Wei W-Z & Venuprasad K (2011) Noncanonical K27-linked polyubiquitination of TIEG1 regulates Foxp3 expression and tumor growth. *J. Immunol.* **186:** 5638–5647

Peng J, Schwartz D, Elias JE, Thoreen CC, Cheng D, Marsischky G, Roelofs J, Finley D & Gygi SP (2003) A proteomics approach to understanding protein ubiquitination. *Nat. Biotechnol.* **21:** 921–926

Peterson AC, Russell JD, Bailey DJ, Westphall MS & Coon JJ (2012) Parallel reaction monitoring for high resolution and high mass accuracy quantitative, targeted proteomics. *Molecular & Cellular Proteomics* **11:** 1475–1488

Phillips CL, Thrower J, Pickart CM & Hill CP (2001) Structure of a new crystal form of tetraubiquitin. *Acta Crystallogr D Biol Crystallogr* **57:** 341–344

Pickart CM & Raasi S (2005) Controlled synthesis of polyubiquitin chains. *Meth. Enzymol.* **399:** 21–36

Pinato S, Scandiuzzi C, Arnaudo N, Citterio E, Gaudino G & Penengo L (2009) RNF168, a new RING finger, MIU-containing protein that modifies chromatin by

ubiquitination of histones H2A and H2AX. *BMC Mol. Biol.* **10:** 55

Plechanovová A, Jaffray EG, Tatham MH, Naismith JH & Hay RT (2012) Structure of a RING E3 ligase and ubiquitin-loaded E2 primed for catalysis. *Nature* **489:** 115–120

Popp MW, Artavanis-Tsakonas K & Ploegh HL (2009) Substrate Filtering by the Active Site Crossover Loop in UCHL3 Revealed by Sortagging and Gain-of-function Mutations. *J. Biol. Chem.* **284:** 3593–3602

Prag G, Lee S, Mattera R, Arighi CN, Beach BM, Bonifacino JS & Hurley JH (2005) Structural mechanism for ubiquitinated-cargo recognition by the Golgi-localized, gamma-ear-containing, ADP-ribosylation-factor-binding proteins. *Proc. Natl. Acad. Sci.* **102:** 2334–2339

Pruneda JN, Littlefield PJ, Soss SE, Nordquist KA, Chazin WJ, Brzovic PS & Klevit RE (2012) Structure of an E3:E2~Ub complex reveals an allosteric mechanism shared among RING/U-box ligases. *Mol Cell* **47:** 933–942

Qin Y, Zhou M-T, Hu M-M, Hu Y-H, Zhang J, Guo L, Zhong B & Shu H-B (2014) RNF26 Temporally Regulates Virus-Triggered Type I Interferon Induction by Two Distinct Mechanisms. *PLoS Pathog* **10:** e1004358

Raasi S, Orlov I, Fleming KG & Pickart CM (2004) Binding of Polyubiquitin Chains to Ubiquitin-associated (UBA) Domains of HHR23A. *J Mol Biol* **341:** 1367–1379

Raasi S, Varadan R, Fushman D & Pickart CM (2005) Diverse polyubiquitin interaction properties of ubiquitin-associated domains. *Nat Struct Mol Biol* **12:** 708–714

Rahighi S & Dikic I (2012) Selectivity of the ubiquitin-binding modules. *FEBS Lett.* **586:** 2705–2710

Rahighi S, Braunstein I, Ternette N, Kessler B, Kawasaki M, Kato R, Matsui T, Weiss TM, Stanhill A & Wakatsuki S (2016) Selective Binding of AIRAPL Tandem UIMs to Lys48-Linked Tri-Ubiquitin Chains. *Structure* **24:** 412–422

Rahighi S, Ikeda F, Kawasaki M, Akutsu M, Suzuki N, Kato R, Kensche T, Uejima T, Bloor S, Komander D, Randow F, Wakatsuki S & Dikic I (2009) Specific recognition of linear ubiquitin chains by NEMO is important for NF-kappaB activation. *Cell* **136:** 1098–1109

Redman KL & Rechsteiner M (1989) Identification of the long ubiquitin extension as ribosomal protein S27a. *Nature* **338:** 438–440

Ren X & Hurley JH (2010) VHS domains of ESCRT-0 cooperate in high-avidity binding to polyubiquitinated cargo. *EMBO J* **29:** 1045–1054

Reyes-Turcu FE, Horton JR, Mullally JE, Heroux A, Cheng X & Wilkinson KD (2006) The ubiquitin binding domain ZnF UBP recognizes the C-terminal diglycine motif of unanchored ubiquitin. *Cell* **124:** 1197–1208

Reyes-Turcu FE, Shanks JR, Komander D & Wilkinson KD (2008) Recognition of Polyubiquitin Isoforms by the Multiple Ubiquitin Binding Modules of Isopeptidase T. *J. Biol. Chem.* **283:** 19581–19592

Ritorto MS, Ewan R, Perez-Oliva AB, Knebel A, Buhrlage SJ, Wightman M, Kelly SM, Wood NT, Virdee S, Gray NS, Morrice NA, Alessi DR & Trost M (2014) Screening of DUB activity and specificity by MALDI-TOF mass spectrometry. *Nat Commun* **5:** 4763

Rivkin E, Almeida SM, Ceccarelli DF, Juang Y-C, MacLean TA, Srikumar T, Huang H, Dunham WH, Fukumura R, Xie G, Gondo Y, Raught B, Gingras A-C, Sicheri F & Cordes SP (2013) The linear ubiquitin-specific deubiquitinase gumby regulates angiogenesis. *Nature* **498:** 318–324

Rizzo AA, Salerno PE, Bezsonova I & Korzhnev DM (2014) NMR structure of the human Rad18 zinc finger in complex with ubiquitin defines a class of UBZ domains in proteins linked to the DNA damage response. *Biochemistry* **53:** 5895–5906

Rohaim A, Kawasaki M, Kato R, Dikic I & Wakatsuki S (2012) Structure of a compact conformation of linear diubiquitin. *Acta Crystallogr D Biol Crystallogr* **68:** 102–108

Ronau JA, Beckmann JF & Hochstrasser M (2016) Substrate specificity of the ubiquitin and Ubl proteases. *Cell Res.* **26:** 441–456

Roscoe BP, Thayer KM, Zeldovich KB, Fushman D & Bolon DNA (2013) Analyses of the Effects of All Ubiquitin Point Mutants on Yeast Growth Rate. *J Mol Biol* **425:** 1363–1377

Ross PD & Subramanian S (1981) Thermodynamics of protein association reactions: forces contributing to stability. *Biochemistry* **20:** 3096–3102

Ryabov Y & Fushman D (2006) Interdomain mobility in di-ubiquitin revealed by NMR. *Proteins* **63:** 787–796

Saeki Y, Kudo T, Sone T, Kikuchi Y, Yokosawa H, Toh-e A & Tanaka K (2009) Lysine 63-linked polyubiquitin chain may serve as a targeting signal for the 26S proteasome. *EMBO J* **28:** 359–371

Sahtoe DD, van Dijk WJ, Oualid El F, Ekkebus R, Ovaa H & Sixma TK (2015) Mechanism of UCH-L5 Activation and Inhibition by DEUBAD Domains in RPN13 and INO80G. *Mol Cell* **57:** 887–900

Sambrook J & Russell DW (2010) The Inoue Method for Preparation and Transformation of Competent E. Coli: 'Ultra-Competent' Cells. *Cold Spring Harb Protoc* **2006:** pdb.prot3944

Sato Y, Fujita H, Yoshikawa A, Yamashita M, Yamagata A, Kaiser SE, Iwai K & Fukai S (2011) Specific recognition of linear ubiquitin chains by the Npl4 zinc finger (NZF) domain of the HOIL-1L subunit of the linear ubiquitin chain assembly complex. *Proc. Natl. Acad. Sci.* **108:** 20520–20525

Sato Y, Goto E, Shibata Y, Kubota Y, Yamagata A, Goto-Ito S, Kubota K, Inoue J-I, Takekawa M, Tokunaga F & Fukai S (2015) Structures of CYLD USP with Met1- or Lys63-linked diubiquitin reveal mechanisms for dual specificity. *Nat Struct Mol Biol* **22:** 222–229

Sato Y, Yoshikawa A, Mimura H, Yamashita M, Yamagata A & Fukai S (2009a) Structural basis for specific recognition of Lys 63-linked polyubiquitin chains by

tandem UIMs of RAP80. *EMBO J* **28:** 2461–2468

Sato Y, Yoshikawa A, Yamagata A, Mimura H, Yamashita M, Ookata K, Nureki O, Iwai K, Komada M & Fukai S (2008) Structural basis for specific cleavage of Lys 63-linked polyubiquitin chains. *Nature* **455:** 358–362

Sato Y, Yoshikawa A, Yamashita M, Yamagata A & Fukai S (2009b) Structural basis for specific recognition of Lys 63-linked polyubiquitin chains by NZF domains of TAB2 and TAB3. *EMBO J* **28:** 3903–3909

Satoh T, Sakata E, Yamamoto S, Yamaguchi Y, Sumiyoshi A, Wakatsuki S & Kato K (2010) Crystal structure of cyclic Lys48-linked tetraubiquitin. *Biochem Biophys Res Commun* **400:** 329–333

Sánchez-Tena S, Cubillos-Rojas M, Schneider T & Rosa JL (2016) Functional and pathological relevance of HERC family proteins: a decade later. *CMLS, Cell. Mol. Life Sci.* **73:** 1955–1968

Scaglione KM, Basrur V, Ashraf NS, Konen JR, Elenitoba-Johnson KSJ, Todi SV & Paulson HL (2013) The ubiquitin-conjugating enzyme (E2) Ube2w ubiquitinates the N terminus of substrates. *J. Biol. Chem.* **288:** 18784–18788

Schaefer JB & Morgan DO (2011) Protein-linked ubiquitin chain structure restricts activity of deubiquitinating enzymes. *J. Biol. Chem.* **286:** 45186–45196

Schechter I & Berger A (1967) On the size of the active site in proteases. I. Papain. *Biochem Biophys Res Commun* **27:** 157–162

Scheffner M & Kumar S (2014) Mammalian HECT ubiquitin-protein ligases: biological and pathophysiological aspects. *Biochim. Biophys. Acta* **1843:** 61–74

Schreiner P, Chen X, Husnjak K, Randles L, Zhang N, Elsasser S, Finley D, Dikic I, Walters KJ & Groll M (2008) Ubiquitin docking at the proteasome through a novel pleckstrin-homology domain interaction. *Nature* **453:** 548–552

Scheuermann JC, de Ayala Alonso AG, Oktaba K, Ly-Hartig N, McGinty RK, Fraterman S, Wilm M, Muir TW & Müller J (2010) Histone H2A deubiquitinase activity of the Polycomb repressive complex PR-DUB. *Nature* **465:** 243–247

Schulman BA & Harper JW (2009) Ubiquitin-like protein activation by E1 enzymes: the apex for downstream signalling pathways. *Nat Rev Mol Cell Biol* **10:** 319–331

Schwarz SE, Rosa JL & Scheffner M (1998) Characterization of human hect domain family members and their interaction with UbcH5 and UbcH7. *J. Biol. Chem.* **273:** 12148–12154

Scott D, Oldham NJ, Strachan J, Searle MS & Layfield R (2014) Ubiquitin-binding domains: Mechanisms of ubiquitin recognition and use as tools to investigate ubiquitin-modified proteomes. *Proteomics* **15:** 844–861

Segref A, Torres S & Hoppe T (2011) A screenable in vivo assay to study proteostasis networks in Caenorhabditis elegans. *Genetics* **187:** 1235–1240

Seigneurin-Berny D, Verdel A, Curtet S, Lemercier C, Garin J, Rousseaux S & Khochbin S (2001) Identification of components of the murine histone deacetylase 6 complex: link between acetylation and ubiquitination signaling pathways. *Mol Cell Biol* **21:** 8035–8044

Shang F, Deng G, Liu Q, Guo W, Haas AL, Crosas B, Finley D & Taylor A (2005) Lys6-modified Ubiquitin Inhibits Ubiquitin-dependent Protein Degradation. *J. Biol. Chem.* **280:** 20365–20374

Sheng Y, Hong JH, Doherty R, Srikumar T, Shloush J, Avvakumov GV, Walker JR, Xue S, Neculai D, Wan JW, Kim SK, Arrowsmith CH, Raught B & Dhe-Paganon S (2012) A human ubiquitin conjugating enzyme (E2)-HECT E3 ligase structure-function screen. *Mol Cell Proteom* **11:** 329–341

Shi T, Bao J, Wang NX, Zheng J & Wu D (2012) Identification Of Small Molecule TRABID Deubiquitinase Inhibitors By Computation-Based Virtual Screen. *BMC Chem Biol* **12:** 4

Shields SB & Piper RC (2011) How Ubiquitin Functions with ESCRTs. *Traffic* **12:** 1306–1317

Shih SC, Katzmann DJ, Schnell JD, Sutanto M, Emr SD & Hicke L (2002) Epsins and Vps27p/Hrs contain ubiquitin-binding domains that function in receptor endocytosis. *Nature Cell Biology* **4:** 389–393

Silva GM, Finley D & Vogel C (2015) K63 polyubiquitination is a new modulator of the oxidative stress response. *Nat Struct Mol Biol* **22:** 116–123

Sims JJ & Cohen RE (2009) Linkage-Specific Avidity Defines the Lysine 63-Linked Polyubiquitin-Binding Preference of Rap80. *Mol Cell* **33:** 775–783

Sims JJ, Haririnia A, Dickinson BC, Fushman D & Cohen RE (2009) Avid interactions underlie the Lys63-linked polyubiquitin binding specificities observed for UBA domains. *Nat Struct Mol Biol* **16:** 883–889

Sims JJ, Scavone F, Cooper EM, Kane LA, Youle RJ, Boeke JD & Cohen RE (2012) Polyubiquitin-sensor proteins reveal localization and linkage-type dependence of cellular ubiquitin signaling. *Nat Meth* **9:** 303–309

Skaug B, Jiang X & Chen ZJ (2009) The role of ubiquitin in NF-kappaB regulatory pathways. *Annu. Rev. Biochem.* **78:** 769–796

Slagsvold T, Aasland R, Hirano S, Bache KG, Raiborg C, Trambaiolo D, Wakatsuki S & Stenmark H (2005) Eap45 in mammalian ESCRT-II binds ubiquitin via a phosphoinositide-interacting GLUE domain. *J. Biol. Chem.* **280:** 19600–19606

Smit JJ, Monteferrario D, Noordermeer SM, van Dijk WJ, van der Reijden BA & Sixma TK (2012) The E3 ligase HOIP specifies linear ubiquitin chain assembly through its RING-IBR-RING domain and the unique LDD extension. *EMBO J* **31:** 3833–3844

Song L & Rape M (2010) Regulated degradation of spindle assembly factors by the anaphase-promoting complex. *Mol Cell* **38:** 369–382

Song L, Craney A & Rape M (2014) Microtubule-dependent regulation of mitotic protein degradation. *Mol Cell* **53:** 179–192

Stamenova SD, French ME, He Y, Francis SA, Kramer ZB & Hicke L (2007) Ubiquitin binds to and regulates a subset of SH3 domains. *Mol Cell* **25:** 273–284

Stewart MD, Ritterhoff T, Klevit RE & Brzovic PS (2016) E2 enzymes: more than just middle men. *Cell Res.* **26:** 423–440

Stieglitz B, Morris Davies AC, Koliopoulos MG, Christodoulou E & Rittinger K (2012) LUBAC synthesizes linear ubiquitin chains via a thioester intermediate. *EMBO Rep.* **13:** 840–846

Stieglitz B, Rana RR, Koliopoulos MG, Morris Davies AC, Schaeffer V, Christodoulou E, Howell S, Brown NR, Dikic I & Rittinger K (2013) Structural basis for ligase-specific conjugation of linear ubiquitin chains by HOIP. *Nature* **503:** 422–426

Sundquist WI, Schubert HL, Kelly BN, Hill GC, Holton JM & Hill CP (2004) Ubiquitin recognition by the human TSG101 protein. *Mol Cell* **13:** 783–789

Swanson KA, Kang RS, Stamenova SD, Hicke L & Radhakrishnan I (2003) Solution structure of Vps27 UIM-ubiquitin complex important for endosomal sorting and receptor downregulation. *EMBO J* **22:** 4597–4606

Tan J, Wong E, Dawson VL, Dawson T & Lim KL (2008) Lysine 63-linked polyubiquitin potentially partners with p62 to promote the clearance of protein inclusions by autophagy. *Autophagy 4: 251-253*

Tasaki T, Sriram SM, Park KS & Kwon YT (2012) The N-end rule pathway. *Annu. Rev. Biochem.* **81:** 261–289

Tatham MH, Plechanovová A, Jaffray EG, Salmen H & Hay RT (2013) Ube2W conjugates ubiquitin to α-amino groups of protein N-termini. *Biochem. J.* **453:** 137–145

Teo H, Veprintsev DB & Williams RL (2004) Structural Insights into Endosomal Sorting Complex Required for Transport (ESCRT-I) Recognition of Ubiquitinated Proteins. *J. Biol. Chem.* **279:** 28689–28696

Thrower JS, Hoffman L, Rechsteiner M & Pickart CM (2000) Recognition of the polyubiquitin proteolytic signal. *EMBO J* **19:** 94–102

Tina KG, Bhadra R & Srinivasan N (2007) PIC: Protein Interactions Calculator. *Nucleic Acids Res.* **35:** W473–W476

Tokunaga F, Nakagawa T, Nakahara M, Saeki Y, Taniguchi M, Sakata S-I, Tanaka K, Nakano H & Iwai K (2011) SHARPIN is a component of the NF-κB-activating linear ubiquitin chain assembly complex. *Nature* **471:** 633–636

Tokunaga F, Sakata S-I, Saeki Y, Satomi Y, Kirisako T, Kamei K, Nakagawa T, Kato M, Murata S, Yamaoka S, Yamamoto M, Akira S, Takao T, Tanaka K & Iwai K (2009)

Involvement of linear polyubiquitylation of NEMO in NF-κB activation. *Nature Cell Biology* **11:** 123–132

Tran H, Hamada F, Schwarz-Romond T & Bienz M (2008) Trabid, a new positive regulator of Wnt-induced transcription with preference for binding and cleaving K63-linked ubiquitin chains. *Genes & Development* **22:** 528–542

Ulrich HD & Walden H (2010) Ubiquitin signalling in DNA replication and repair. *Nat Rev Mol Cell Biol* **11:** 479–489

Urbé S, Sachse M, Row PE, Preisinger C, Barr FA, Strous G, Klumperman J & Clague MJ (2003) The UIM domain of Hrs couples receptor sorting to vesicle formation. *Journal of Cell Science* **116:** 4169–4179

Vagin AA, Steiner RA, Lebedev AA, Potterton L, McNicholas S, Long F & Murshudov GN (2004) REFMAC5 dictionary: organization of prior chemical knowledge and guidelines for its use. *Acta Crystallogr D Biol Crystallogr* **60:** 2184–2195

van der Veen AG & Ploegh HL (2012) Ubiquitin-like proteins. *Annu. Rev. Biochem.* **81:** 323–357

van Wijk SJL, Fiskin E, Putyrski M, Pampaloni F, Hou J, Wild P, Kensche T, Grecco HE, Bastiaens P & Dikic I (2012) Fluorescence-Based Sensors to Monitor Localization and Functions of Linear and K63-Linked Ubiquitin Chains in Cells. *Mol Cell* **47:** 797–809

Varadan R, Assfalg M, Raasi S, Pickart C & Fushman D (2005) Structural determinants for selective recognition of a Lys48-linked polyubiquitin chain by a UBA domain. *Mol Cell* **18:** 687–698

Varadan R, Walker O, Pickart C & Fushman D (2002) Structural properties of polyubiquitin chains in solution. *J Mol Biol* **324:** 637–647

Velázquez-Campoy A, Ohtaka H, Nezami A, Muzammil S & Freire E (2004) Isothermal titration calorimetry. *Curr Protoc Cell Biol* **Chapter 17:** Unit 17.8

Verdecia MA, Joazeiro CAP, Wells NJ, Ferrer J-L, Bowman ME, Hunter T & Noel JP (2003) Conformational flexibility underlies ubiquitin ligation mediated by the WWP1 HECT domain E3 ligase. *Mol Cell* **11:** 249–259

Vijay-Kumar S, Bugg CE & Cook WJ (1987) Structure of ubiquitin refined at 1.8 A resolution. *J Mol Biol* **194:** 531–544

Virdee S, Kapadnis PB, Elliott T, Lang K, Madrzak J, Nguyen DP, Riechmann L & Chin JW (2011) Traceless and site-specific ubiquitination of recombinant proteins. *J. Am. Chem. Soc.* **133:** 10708–10711

Virdee S, Ye Y, Nguyen DP, Komander D & Chin JW (2010) Engineered diubiquitin synthesis reveals Lys29-isopeptide specificity of an OTU deubiquitinase. *Nat Chem Biol* **6:** 750–757

Vittal V, Shi L, Wenzel DM, Scaglione KM, Duncan ED, Basrur V, Elenitoba-Johnson KSJ, Baker D, Paulson HL, Brzovic PS & Klevit RE (2015) Intrinsic disorder drives N-terminal ubiquitination by Ube2w. *Nat Chem Biol* **11:** 83–89

Wang M & Pickart CM (2005) Different HECT domain ubiquitin ligases employ distinct mechanisms of polyubiquitin chain synthesis. *EMBO J* **24:** 4324–4333

Wang M, Cheng D, Peng J & Pickart CM (2006) Molecular determinants of polyubiquitin linkage selection by an HECT ubiquitin ligase. *EMBO J* **25:** 1710–1719

Wang Q, Young P & Walters KJ (2005) Structure of S5a bound to monoubiquitin provides a model for polyubiquitin recognition. *J Mol Biol* **348:** 727–739

Wang T, Yin L, Cooper EM, Lai M-Y, Dickey S, Pickart CM, Fushman D, Wilkinson KD, Cohen RE & Wolberger C (2009) Evidence for Bidentate Substrate Binding as the Basis for the K48 Linkage Specificity of Otubain 1. *J Mol Biol* **386:** 1011–1023

Waterhouse AM, Procter JB, Martin DMA, Clamp M & Barton GJ (2009) Jalview Version 2--a multiple sequence alignment editor and analysis workbench. *Bioinformatics* **25:** 1189–1191

Weissman AM, Shabek N & Ciechanover A (2011) The predator becomes the prey: regulating the ubiquitin system by ubiquitylation and degradation. *Nat Rev Mol Cell Biol* **12:** 605–620

Wertz IE, O'Rourke KM, Zhou H, Eby M, Aravind L, Seshagiri S, Wu P, Wiesmann C, Baker R, Boone DL, Ma A, Koonin EV & Dixit VM (2004) De-ubiquitination and ubiquitin ligase domains of A20 downregulate NF-kappaB signalling. *Nature* **430:** 694–699

Wiborg O, Pedersen MS, Wind A, Berglund LE, Marcker KA & Vuust J (1985) The human ubiquitin multigene family: some genes contain multiple directly repeated ubiquitin coding sequences. *EMBO J* **4:** 755–759

Wickliffe KE, Lorenz S, Wemmer DE, Kuriyan J & Rape M (2011) The mechanism of linkage-specific ubiquitin chain elongation by a single-subunit E2. *Cell* **144:** 769–781

Wilkinson CR, Seeger M, Hartmann-Petersen R, Stone M, Wallace M, Semple C & Gordon C (2001) Proteins containing the UBA domain are able to bind to multi-ubiquitin chains. *Nature Cell Biology* **3:** 939–943

Wilkinson KD, Tashayev VL, O'Connor LB, Larsen CN, Kasperek E & Pickart CM (1995) Metabolism of the polyubiquitin degradation signal: structure, mechanism, and role of isopeptidase T. *Biochemistry* **34:** 14535–14546

Wilkinson KD, Urban MK & Haas AL (1980) Ubiquitin is the ATP-dependent proteolysis factor I of rabbit reticulocytes. *J. Biol. Chem.* **255:** 7529–7532

Williamson A, Wickliffe KE, Mellone BG, Song L, Karpen GH & Rape M (2009) Identification of a physiological E2 module for the human anaphase-promoting complex. *Proc. Natl. Acad. Sci.* **106:** 18213–18218

Winborn BJ, Travis SM, Todi SV, Scaglione KM, Xu P, Williams AJ, Cohen RE, Peng J & Paulson HL (2008) The deubiquitinating enzyme ataxin-3, a polyglutamine disease protein, edits Lys63 linkages in mixed linkage ubiquitin chains. *J. Biol. Chem.* **283:** 26436–26443

Wolberger C (2014) Mechanisms for regulating deubiquitinating enzymes. *Protein Sci.* **23:** 344–353

Wu T, Merbl Y, Huo Y, Gallop JL, Tzur A & Kirschner MW (2010) UBE2S drives elongation of K11-linked ubiquitin chains by the anaphase-promoting complex. *Proc. Natl. Acad. Sci.* **107:** 1355–1360

Xu P, Duong DM, Seyfried NT, Cheng D, Xie Y, Robert J, Rush J, Hochstrasser M, Finley D & Peng J (2009) Quantitative Proteomics Reveals the Function of Unconventional Ubiquitin Chains in Proteasomal Degradation. *Cell* **137:** 133–145

Yang M, Chen T, Li X, Yu Z, Tang S, Wang C, Gu Y, Liu Y, Xu S, Li W, Zhang X, Wang J & Cao X (2015) K33-linked polyubiquitination of Zap70 by Nrdp1 controls CD8+ T cell activation. *Nat Immunol* **16:** 1253–1262

Yang W-L, Zhang X & Lin H-K (2010) Emerging role of Lys-63 ubiquitination in protein kinase and phosphatase activation and cancer development. *Oncogene* **29:** 4493–4503

Yao T & Cohen RE (2002) A cryptic protease couples deubiquitination and degradation by the proteasome. *Nature* **419:** 403–407

Yao T, Song L, Xu W, DeMartino GN, Florens L, Swanson SK, Washburn MP, Conaway RC, Conaway JW & Cohen RE (2006) Proteasome recruitment and activation of the Uch37 deubiquitinating enzyme by Adrm1. *Nature Cell Biology* **8:** 994–1002

Ye Y, Akutsu M, Reyes-Turcu F, Enchev RI, Wilkinson KD & Komander D (2011) Polyubiquitin binding and cross-reactivity in the USP domain deubiquitinase USP21. *EMBO Rep.* **12:** 350–357

Ye Y, Blaser G, Horrocks MH, Ruedas-Rama MJ, Ibrahim S, Zhukov AA, Orte A, Klenerman D, Jackson SE & Komander D (2012) Ubiquitin chain conformation regulates recognition and activity of interacting proteins. *Nature* **492:** 266–270

Ye Y, Scheel H, Hofmann K & Komander D (2009) Dissection of USP catalytic domains reveals five common insertion points. *Mol Biosyst* **5:** 1797–1808

You J & Pickart CM (2001) A HECT Domain E3 Enzyme Assembles Novel Polyubiquitin Chains. *J. Biol. Chem.* **276:** 19871–19878

Young P, Deveraux Q, Beal RE, Pickart CM & Rechsteiner M (1998) Characterization of two polyubiquitin binding sites in the 26 S protease subunit 5a. *J. Biol. Chem.* **273:** 5461–5467

Yuan W-C, Lee Y-R, Lin S-Y, Chang L-Y, Tan YP, Hung C-C, Kuo J-C, Liu C-H, Lin M-Y, Xu M, Chen ZJ & Chen R-H (2014) K33-Linked Polyubiquitination of Coronin 7 by Cul3-KLHL20 Ubiquitin E3 Ligase Regulates Protein Trafficking. *Mol Cell* **54:** 586–600

Zeng W, Sun L, Jiang X, Chen X, Hou F, Adhikari A, Xu M & Chen ZJ (2010) Reconstitution of the RIG-I Pathway Reveals a Signaling Role of Unanchored Polyubiquitin Chains in Innate Immunity. *Cell* **141:** 315–330

Zhang D, Raasi S & Fushman D (2008) Affinity Makes the Difference: Nonselective Interaction of the UBA Domain of Ubiquilin-1 with Monomeric Ubiquitin and Polyubiquitin Chains. *J Mol Biol* **377:** 162–180

Zhang L, Ding X, Cui J, Xu H, Chen J, Gong Y-N, Hu L, Zhou Y, Ge J, Lu Q, Liu L, Chen S & Shao F (2011) Cysteine methylation disrupts ubiquitin-chain sensing in NF-κB activation. *Nature* **481:** 204–208

Zhang N, Wang Q, Ehlinger A, Randles L, Lary JW, Kang Y, Haririnia A, Storaska AJ, Cole JL, Fushman D & Walters KJ (2009) Structure of the S5a:K48-Linked Diubiquitin Complex and Its Interactions with Rpn13. *Mol Cell* **35:** 280–290

Ziemba A, Hill S, Sandoval D, Webb K, Bennett EJ & Kleiger G (2013) Multimodal mechanism of action for the Cdc34 acidic loop: a case study for why ubiquitin-conjugating enzymes have loops and tails. *J. Biol. Chem.* **288:** 34882–34896

Zotti T, Uva A, Ferravante A, Vessichelli M, Scudiero I, Ceccarelli M, Vito P & Stilo R (2011) TRAF7 protein promotes Lys-29-linked polyubiquitination of IkappaB kinase (IKKgamma)/NF-kappaB essential modulator (NEMO) and p65/RelA protein and represses NF-kappaB activation. *J. Biol. Chem.* **286:** 22924–22933

Zucchelli S, Codrich M, Marcuzzi F, Pinto M, Vilotti S, Biagioli M, Ferrer I & Gustincich S (2010) TRAF6 promotes atypical ubiquitination of mutant DJ-1 and alpha-synuclein and is localized to Lewy bodies in sporadic Parkinson's disease brains. *Hum Mol Genet* **19:** 3759–3770

Zucchelli S, Marcuzzi F, Codrich M, Agostoni E, Vilotti S, Biagioli M, Pinto M, Carnemolla A, Santoro C, Gustincich S & Persichetti F (2011) Tumor Necrosis Factor Receptor-associated Factor 6 (TRAF6) Associates with Huntingtin Protein and Promotes Its Atypical Ubiquitination to Enhance Aggregate Formation. *J. Biol. Chem.* **286:** 25108–25117